SOLAR ASSISTED MULTI-EFFECT REFRIGERATION SYSTEM

BY

AYMAN JAMAL ABDEL MAJID ALAZAZMEH

A Thesis Presented to the

DEANSHIP OF GRADUATE STUDIES

KING FAHD UNIVERSITY OF PETROLEUM & MINERALS

DHAHRAN, SAUDI ARABIA

In Partial Fulfillment of the
Requirements for the Degree of

MASTER OF SCIENCE

In

MECHANICAL ENGINEERING

May 2016

KING FAHD UNIVERSITY OF PETROLEUM & MINERALS

DHAHRAN- 31261, SAUDI ARABIA

DEANSHIP OF GRADUATE STUDIES

This thesis, written by **Ayman Jamal Abdel Majid Alazazmeh** under the direction of thesis advisor and approved by his thesis committee, has been presented and accepted by the Dean of Graduate Studies, in partial fulfillment of the requirements for the degree of **Master of Science in Mechanical Engineering.**

Dr. Zuhair M. Gasem
Department Chairman

Prof. Esmail M.A Mokheimer
(Advisor)

Dr. Salam A. Zummo
Dean of Graduate Studies

Dr. Abdul Khaliq
(Member)

21/07/2016
Date

Prof. Ahmet Ziyaettin Şahin
(Member)

In the name of Allah, most gracious, most merciful

Dedicated to

My Beloved Mother, Father,

Wife, Daughters and sons.

ACKNOWLEDGEMENT

This thesis represents not only my work at the keyboard, it is a milestone in more than one decade of work and specifically within the Space Systems of air conditioning. The work presented in this thesis would not been possible without support of my family, friends, and colleagues. I would like to thanks a few people in particular.

First and foremost, I would like to thank my advisor Prof. Esmail Mokheimer and express my deepest appreciation for all time and effort he has put into helping me with my work. I really appreciate your willingness to be my mentor and to provide professional supervision that can support my journey which is a very challenging one.

I would like also to express my deep appreciation to my committee members, Prof. Ahmet Ziyaettin Şahin and Dr. Abdul Khaliq, for their constant help and encouragement.

Finally, I would like to thank my father, my wife, my son, my daughter, my brothers, and my sisters who always support me with their love, patience encouragement and constant prayers throughout my study.

TABLE OF CONTENTS

ACKNOWLEDGEMENT……....vi
TABLE OF CONTENTS……..……vii
ABSTRACT…….xii
ARABIC ABSTRACT……...…….xiii
LIST OF FIGURES……..xiv
LIST OF TABLES……..……..xxii
LIST OF ABBREVIATIONS ……..……..xxiv

CHAPTER 1: INTRODUCTION

1.1 Background. ……..……...1
1.2 Solar Cooling Technologies Classification……..2
1.3 Solar Cooling Technologies Application and Temperature ranges……..……...…….…3
1.4 Concentrated Solar Power Technologies ……..……..4
Parabolic Trough Reflector…….6
Fresnel Reflector…….7
Central Receiver System (Solar Tower)……...8
Solar Dish System……..…10
Solar Power Technologies Comparison…….……12
CSP Water Requirement……..……..…13
1.5 Solar Energy Component and Angle Definition
Direct Normal Insolation (DNI)……....13
Angle of Incidence (θ) and Declination Angle (δ)…..13
Hour Angle (ω) and Solar Time……....16
Zenith Angle (θ_z)……....…18
Incidence Angle Modifier (IAM)……..……18

CHAPTER 2: SOLAR COOLING TECHNOLOGIES DESCRIPTION and LITERATURE REVIEW

2.1 Solar Electrical Cooling System……21

Thermo-electric Cooling System……22

Vapor Compression Cooling System ……24

Stirling Refrigeration System……25

2.2 Solar Thermal Cooling System……31

Open Sorption Cycles……31

- Liquid Desiccant System……32
- Solid Desiccant System……34

Closed Sorption Cycles……37

- Absorption System……37
- Adsorption System……45
- Chemical Reaction System……50
- Energy Storage in Solar Cooling System……51
- Solar Radiation System……52
- Solar Refrigerant Cooling System……52

Thermo-mechanical System……53

- Ejector Cooling System……53
- Solar Combined Power/Cooling Systems……56
- Combined Rankine and Vapor Compression System…57
- Triple-effect Refrigeration Cycle……58

2.3 Solar Cooling Technologies Comparison Based on Driving Temperature ……59

CHAPTER 3: OBJECTIVE, METHODOLOGY and APPROACH.

3.1 Objective…….62

3.2 Approach……..63

3.3 Problem Statement ……..64

3.4 Methodology……..……65

CHAPTER 4: TRIPLE EFFECT REFRIGERATION CYCLE MODELING.

4.1 Description of The Triple Effect Refrigeration Cycle……...66

4.2 Main Assumption of The Triple Effect Refrigeration Cycle…..71

4.3 Triple-effect Refrigeration Cycle Working Fluid ……..72

4.4 Desirable Properties of Working Fluids……..73

4.5 Hot Molten Salt Properties……..74

4.6 Triple-effect Refrigeration Cycle Working Fluid Characteristic…...75

CHAPTER 5: FIRST & SECOND LAW of THERMODYNAMIC ANALYSIS.

5.1 Energy Analysis and First Law of Thermodynamics……78

5.2 Exergy Analysis and Second Law of Thermodynamics……..…81

5.3 Energy, Exergy Analysis & Mathematical Formulation…..

- Solar System (Heliostat & Central Receiver)……...…88
- **Steam Rankine Cycle**……..……..93
- HRVG……..93
- Turbine ……94
- Pump 1 ……..96
- **Ejector Refrigeration Cycle**……..……..98
- Ejector……..……98
- Entrainment Ratio……100

- Condenser-1 (C1)……112
- Throttling Valve-1(TV-1)……114
- Evaporator-1 (E1)……115
- **Absorption Refrigeration Cycle**……117
- Generator……120
- Condenser-2 (C2)……123
- Throttling Valve-2(TV-2)……125
- Evaporator-2 (E2)……126
- Absorber (A)……129
- Pump 2 ……131
- Solution Heat Exchanger (SHX)……132
- Throttling Valve-3 (TV-3)……135
- **Cascade Refrigeration Cycle** ……137
- Compressor-2 (Comp-2)……138
- Internal Heat Exchanger-2 (IHX-2)……140
- Cascade Heat Exchanger (CHX)……141
- Throttling Valve-5 (TV-5)……142
- Compressor-1 (Comp-1)……143
- Condenser-3 (C3)…… 144
- Internal Heat Exchanger-1 (IHX-1)…… 146
- Throttling Valve-4 (TV-4)……147
- Evaporator-2 (E2)……148

CHAPTER 6: RESULT and DISCUSSION.

6.1 Main Operating Parameter of the proposed Cycle……153

6.2 Result Validation……154

6.3 Power Cycle Analysis and Central Receiver Performance ……162

6.4 Central Receiver Performance Variation with Incident Solar Isolation……...…166
6.5 Central Receiver Performance Variation with Aperture Area ……..…….169
6.6 Central Receiver Performance Variation with Emissivity ……...…….171
6.7 Central Receiver Performance Variation with Reflectivity ……....…….172
6.8 Sun's Exergy Distribution for Triple-effect Refrigeration cycle……..…….……174
6.9 Variation of The Refrigeration Output and Efficiencies of the Proposed Cycle with Influential Parameter…..……..…..…..176
Hot Molten Salt Outlet Temperature ……...176
Inlet Turbine Pressure ……...179
Turbine Back Pressure ……181
Evaporator-1 (E1) Temperature ……...183
Evaporator-3 (E3) Temperature ……...184
Compressors Discharge Pressure ……....186
6.10 Variation of The Refrigeration Output of The Proposed Cycle with Changing of Average Daily and Hourly Solar Radiation……...188

CHAPTER 7: CONCLUSIONS and RECOMMENDATION.

7.1 Conclusions……..203
7.2 Recommendation and Future Work.....206
References ……209
Appendix-A.……....……223
Vitae.……..……....……229

ABSTRACT

Full Name : **Ayman Jamal Abdel Majid Alazazmeh**

Thesis Title : **Solar Assisted Multi-Effect Refrigeration System.**

Major Field : **Mechanical Engineering**

Date of Degree : **May, 2016.**

The main purpose of the present research is to investigate the thermodynamic performance (based on the first and second law analysis) of a proposed multi-effect refrigeration cycle driven by concentrated solar power (CSP) system consisting of heliostat field and central receiver which uses molten salt as heat transfer fluid.

The proposed cycle is an integration of solar energy with different cooling technologies that can supply refrigeration effect at different temperature ranges and magnitude to serve wide range of applications.

All components of exergy destruction have been analyzed and hence thermodynamic imperfection has been identified.

The effects of some influenced parameters such as pressure, temperature, fluid flow rate and fluid types were investigated.

ملخص الرسالة

الأسم الكامل : أيمن جمال عبد المجيد العزازمة.
عنوان الرسالة : نظام التبريد متعدد الأستخدام يعمل بالطاقة الشمسية.
التخصص : الهندسة الميكانيكية.
تاريخ التخرج : شعبان 1437.

الغرض الرئيسي من هذه الرسالة هو دراسة الكفاءة الديناميكية الحرارية (متمثلة بالقانون الأول والثاني) لدائرة التبريد المقترحة متعددة التأثيرات والاستخدام وتشمل هذه الدراسة كذلك استخدام الطاقة الشمسية متمثلة بالبرج الشمسي وحقول الأستقبال الحراري المركزية والتي تقوم بتسليط وعكس الاشعة الشمسية الى مستقبل مثبت اعلى البرج الذي يستخدم الملح المصهور كسائل نقل الحرارةومن ثم توفير الطاقة الحرارية اللازمة لتشغيل الدائرة المقترحة في هذه الدراسة

هذا البحث يعرض دمجا للطاقة الشمسية مع تقنيات التبريد المختلفة التي تزودنا بالتبريد المطلوب على مستويات مختلفة من درجات الحرارة والتي تخدم مجموعة واسعة من التطبيقات. ولقد تم اجراء دراسة وتحليل لجميع الاجزاء المكونة لهذة الدائرة بالتالي سيتم تحديد الاجزاء التي تقلل كفاءة هذة الدائرة ثلاثية التأثير والاستخدام.

كما تم دراسة بعض العناصر المؤثرة في هذا المشروع مثل الضغط ودرجة الحرارة ومعدل تدفق وأنواع السوائل وتأثيرها على هذة الدائرة.

List of Figures

Figure 1.1 Solar Cooling Technology……2

Figure 1.2 Solar Cooling System and Application Temperature Ranges…..…..3

Figure 1.3 Concentrated Solar Power Technologies……..…..5

Figure 1.4 Parabolic Trough Solar Collectors Schematic……..……6

Figure 1.5 Fresnel Reflector Solar Collector Schematic…….……..…7

Figure 1.6 Solar Tower Schematic……...8

Figure 1.7 Solar Dish Schematic……11

Figure 1.8 Declination angle due to Earth's Tilt……..……...14

Figure 1.9 Declination Angle Variation by Month……..……..…15

Figure 1.10 Equation of Time vs Month of the Year……...17

Figure 2.1 Peltier Cooling System……..……22

Figure 2.2 Thermoelectric Refrigeration System……23

Figure 2.3 Solar Powered Vapor Compression Cycle……..…25

Figure 2.4 Stirling Refrigerator Schematic……..26

Figure 2.5 P-V Diagram for Stirling Refrigerator……..27

Figure 2.6 Solar Thermal Cooling……..…31

Figure 2.7 Process of Moisture Transfer by Desiccant……33

Figure 2.8 Schematic of Liquid Desiccant System……34

Figure 2.9 Schematic of a Solid Descant Cooling System……35

Figure 2.10 Psychometric Chart of a Solid Desiccant System Process...37

Figure 2.11 Schematic of a Solar Absorption System.....38

Figure 2.12 Schematic of Solar Adsorption System.....45

Figure 2.13 Difference Between Absorption and Adsorption.....47

Figure 2.14 Schematic of Solar Refrigerant Cooling System.....52

Figure 2.15 Schematic of Ejector Refrigeration System.....53

Figure 2.16. Combined Rankine and Vapor Compression Cycle.....57

Figure 2.17 Solar Collector Temp. Ranges for Solar Cooling Application.....60

Figure 2.18 Solar Collector Temp. Ranges for Different Cooling Cycles.....60

Figure 2.19 COP of Different Solar Cooling Technologies and Hot Water Temperature 61

Figure 4.1 Solar Assisted Triple-effect Refrigeration Cycle.....70

Figure 5.1 Solar Tower with Steam Rankine Cycle Schematic.....86

Figure 5.2 T-S Diagram of the steam Rankine Cycle with Ejector Refrigeration Cycle.....87

Figure 5.3 Schematic Diagram for Heat Recovery Vapor Generator.....93

Figure 5.4 Schematic Diagram for Turbine.....94

Figure 5.5 Actual and Isentropic Process of the Steam Turbine.....96

Figure 5.6 Schematic Diagram for Pump (P1).....97

Figure 5.7 Schematic Diagram for Ejector.....98

Figure 5.8 Detailed Schematic Diagram for Ejector.....99

Figure 5.9 the Structure and Working Process of Ejector.....100

Figure 5.10 Variation in Stream Pressure and Velocity as a Function of Location Along The Ejector.....102

Figure 5.10 a h-s Diagram for Ejector Working Processes……....111

Figure 5.11 Schematic Diagram for Condenser (C1)……..112

Figure 5.12 T-Q Diagram for Condenser (C-1)……..…..113

Figure 5.13 Schematic Diagram for Throttling Valve (TV1)……..……...114

Figure 5.14 Schematic Diagram for Ejector Cooling Evaporator (E1)....115

Figure 5.15 T-Q Diagram for Evaporator (E1)……...116

Figure 5.16 P-T Diagram for Absorption Refrigeration Cycle (ARC).....117

Figure 5.17 Real T-S Diagram for Absorption Refrigeration Cycle.....119

Figure 5.18 Schematic Diagram for Generator…….....120

Figure 5.19 T-Q Diagram for Generator…….....122

Figure 5.20 Schematic Diagram for Condenser (C-2)…….....123

Figure 5.21 T-Q Diagram for Condenser (C-2)……..…124

Figure 5.22 Schematic Diagram for Throttling Valve (TV2)……..125

Figure 5.23 Schematic Diagram for Evaporator (E2)……...126

Figure 5.24 T-Q Diagram for Evaporator (E2)……128

Figure 5.25 Schematic Diagram for Absorber (A)……..129

Figure 5.26 T-Q Diagram for Absorber (A)……...……130

Figure 5.27 Schematic Diagram for Pump (P2)……...…..131

Figure 5.28 Schematic Diagram for Solution Heat Exchanger (SHX)…..132

Figure 5.29 Concurrent and Countercurrent Heat Exchanger Temperature Profile……...…133

Figure 5.30 Schematic Diagram for Throttling Valve (TV3)……..…..135

Figure 5.31 T-S Diagram for Cascaded Refrigeration Cycle……136

Figure 5.32 P-h Diagram for Cascaded Refrigeration Cycle……...…...136

Figure 5.33 Schematic Diagram for Compressor 2 (Comp-2)…….....138

Figure 5.34 Actual and Isentropic Process of the Compressor……..…..139

Figure 5.35 Schematic Diagram for Internal Heat Exchanger (IHX-2)…140

Figure 5.36 Schematic Diagram for Cascaded Heat Exchanger (CHX)..141

Figure 5.37 Schematic Diagram for Throttling Valve (TV5)……..……142

Figure 5.38 Schematic Diagram for Compressor 1 (Comp-1)…….....143

Figure 5.39 Schematic Diagram for Condenser-3 (C-3) ……...144

Figure 5.40 T-Q diagram for Condenser (C-3)…….....146

Figure 5.41 Schematic Diagram Internal Heat Exchanger (IHX1)……...146

Figure 5.42 Schematic Diagram Throttling Valve (TV4)……..147

Figure 5.43 Schematic Diagram for Evaporator (E3)……...148

Figure 5.44 T-Q Diagram for Evaporator (E3)……..150

Figure 6.1 Validation for CR Surface Temperature Variation with Aperture Area for Present Model and Jameel et al. Model……155

Figure 6.2 Validation for CR Surface Temperature Variation with Hot Molten Salt Outlet Temperature for Present Model and Jameel et al. Model ……156

Figure 6.3 Validation for CR Thermal Efficiency Variation with Hot Molten Salt Outlet Temperature for Present Model and Jameel et al. Model ……..156

Figure 6.4 Validation for Ejector Cycle Refrigeration Output Variation with Hot Molten Salt Outlet Temperature for Present Model and Kumar et al. model……...157
Figure 6.5 Validation for Ejector Cycle Refrigeration Output Variation with Turbine Inlet Pressure for Present Model and Kumar et al. model……..158
Figure 6.6 Validation for Absorption Cycle Refrigeration Output Variation with Hot Molten Salt Outlet Temperature for Present Model and kumar et al. model……..…159
Figure 6.7 Validation for Absorption Cycle Refrigeration Output Variation with Turbine Inlet Pressure for Present Model and kumar et al. model…….....160
Figure 6.8 Validation for Cascade Cycle Refrigeration Output Variation with Hot Molten Salt Outlet Temperature for Present Model and kumar et al. model.....…….....161
Figure 6.9 Validation for Cascade Cycle Refrigeration Output Variation with Turbine Inlet Pressure for Present Model and kumar et al. model……..161
Figure 6.10 Energy Losses in the Solar Tower and Rankine Cycle.....163
Figure 6.11 Exergy Losses in the Solar Tower and Rankine Cycle.....164
Figure 6.12 Effect of the variation of Hot Molten Salt Outlet Temperature on the Receiver Efficiency and Surface Temperature……..……...165
Figure 6.13 The Relationship between Outlet Molten Salt Temperature and Different Types of Receiver Heat Losses……...166
Figure 6.14 Effect of the Incident Solar Radiation on the Energy Efficiency and Surface Temperature of the Receiver ……...….167

Figure 6.15 Effect of the Incident Solar Radiation on the Surface Temperature of the Receiver ……...….168

Figure 6.16 Relationship between Incident Solar Radiations with Different Types of Receiver Heat Losses……..….168

Figure 6.17 Central Receiver Aperture and Surface Area……..…169

Figure 6.18 The Relationship Between CR Thermal Efficiency, Surface Temperature with CR Aperture Area……..170

Figure 6.19 the Relationship Between CR Surface Temperature with CR Aperture Area……..……...170

Figure 6.20 The Relationship between CR Heat Losses with CR Aperture Area……..……...……..171

Figure 6.21 The Relationship between CR Thermal Efficiency & Heat Losses with Emissivity……...……...…172

Figure 6.22 The Relationship between CR Thermal Efficiency and Heat Losses with Reflectivity……..……..….173

Figure 6.23 Sun's Exergy Distribution in Output and Destruction for triple-effect Refrigeration Cycle……175

Figure 6.24 Variation of Refrigeration Output for Triple-effect Refrigeration Cycle with Hot Molten Salt Outlet Temperature……..……176

Figure 6.25 Variation First and Second Law Efficiency for Triple-effect Refrigeration Cycle with Hot Molten Salt Outlet Temperature. ……...……...178

Figure 6.26 Refrigeration Output for Triple-effect Refrigeration Cycle with Turbine Inlet Pressure……...……179

Figure 6.27 First and Second Law Efficiency for Triple-effect Refrigeration Cycle with Turbine Inlet Pressure……180

Figure 6.28 Refrigeration Output for Triple-effect Refrigeration Cycle with Turbine Back Pressure……182

Figure 6.29 First and Second Law Efficiency for Triple-effect Refrigeration Cycle with Turbine Back Pressure……182

Figure 6.30 Refrigeration Output for Triple-effect Refrigeration Cycle with Evaporator-1 (E1) temperature.....183

Figure 6.31 First and Second Law Efficiency for Triple-effect Refrigeration Cycle with Evaporator-1 (E1) Temperature.....184

Figure 6.32 Refrigeration Output for Triple-effect Refrigeration Cycle with Evaporator-3 (E3) Temperature.....185

Figure 6.33 First and Second Law Efficiency for Triple-effect Refrigeration Cycle with Evaporator-3 (E3) Temperature.....185

Figure 6.34 First and Second Law Efficiency for Cascade Refrigeration Cycle with Compressors Discharge Pressure.....187

Figure 6.35 Refrigeration Output of ERC, ARC, CRC and Combined Cycle With Variation of Average Daily Solar Radiation.....191

Figure 6.36 Ejector Refrigeration Cycle Output Variation with Average Daily Solar Radiation.....191

Figure 6.37 Absorption Refrigeration Cycle Output Variation with Average Daily Solar Radiation. 192

Figure 6.38 Cascade Refrigeration Cycle Output Variation with Average Daily Solar Radiation. 192

Figure 6.39 Combined Refrigeration Cycle Output Variation with Average Daily Solar Radiation. 193

Figure 6.40 Refrigeration Output of Proposed Cycle with Variation of Average Daily Solar Radiation Annually. 194

Figure 6.41 Refrigeration Output of ERC, ARC, CRC and Combined Cycle with Variation of Average Hourly Solar Radiation-June 11. ... .196

Figure 6.42 Refrigeration output of ERC, ARC, CRC and Combined Cycle with Variation of Average Hourly Solar radiation-December 10.....196

Figure 6.43 Ejector Refrigeration Cycle Output Variation with Average Hourly Solar Radiation-June 11.....197

Figure 6.44 Absorption Refrigeration Cycle Output Variation with Average Hourly Solar Radiation-June 11. 197

Figure 6.45 Cascade Refrigeration Cycle Output Variation with Average Hourly Solar Radiation-June 11.....198

Figure 6.46 Cascade Refrigeration Cycle Output Variation with Average Hourly Solar Radiation-June 11.....198

Figure 6.47 Refrigeration Output of ERC, ARC, CRC and Combined Cycle with Variation of Average Hourly Solar Radiation-June 11. 199

Figure 6.48 Ejector Refrigeration Cycle Output Variation with Average Hourly Solar Radiation-December 10.....200

Figure 6.49 Absorption Refrigeration Cycle Output Variation with Average Hourly Solar Radiation-December 10 200

Figure 6.50 Cascade Refrigeration Cycle Output Variation with Average Hourly Solar Radiation-December 10.....201

Figure 6.51 Combined Refrigeration Cycle Output Variation with Average Hourly Solar Radiation-December 10.....201

Figure 6.52 Refrigeration output of ERC, ARC, CRC and combined cycle with Variation of Average Hourly Solar Radiation-December 10. 202

List of Tables

Table 1.1 Comparison of Solar Cooling Technology……..……12

Table 2.1 Piston Movement of the Stirling cycle…….……28

Table 2.2 Comparison between Solar Electrical Cooling System……...…..30

Table 2.3 Comparison between Vapor Absorption Refrigeration with Vapor Compression Refrigeration System……..……..……43

Table 2.4 Comparison between Absorption and Adsorption System……48

Table 2.5 Comparison between Physical and Chemical Adsorption…….50

Table 2. 6 Some Common Used Solar Cooling Technologies Efficiency and Cost Ranges for 5 TR AC units (R-22)…..61

Table 4.1 Triple Effect Refrigeration Cycle Working fluid……..……72

Table 4.2 Desirable Properties of Working Fluids…….....73

Table 4.3 Currently Available Heat Transfer Fluids for CSP Applications…….. 74

Table 5.1 General Difference between Energy and Exergy……..……78

Table 6.1 ERC Refrigeration Output with Inlet Pressure Variation Comparison between Present and Rajesh's model……158

Table 6.2 ARC Refrigeration Output with Inlet Pressure Variation Comparison between Present and Rajesh's model……160

Table 6.3 CRC Refrigeration Output with Inlet Pressure Variation Comparison between Present and Rajesh's model……162

Table 6.4 Energy analysis of the Base Case Central Receiver-Solar Tower System……....163

Table 6.5 Exergy Analysis of The Base Case Central Receiver-Solar Tower……..……164

Table 6.6 Weather Data and Average Daily Solar Radiation at Dhahran City. ……189
Table 6.7 Hourly Solar Radiation at Dhahran City on June 11 and December 10. ……190

LIST OF ABBREVIATIONS

Ah	Aperture area of heliostat [m^2]
q	Solar radiation received per unit area [W/m^2]
$\dot{E}$	Exergy rate [kJ/S]
$\dot{Q}$	Energy rate [kJ/S]
$\Delta\dot{E}$	Exergy change [kJ/S]
T	Absolute temperature [K]
$\dot{W}$	Work output [kJ/S]
h	Enthalpy [kJ/ kg]
$\dot{m}$	Mass flow rate [kg/s]
S	Entropy [kJ/kg. ^oC]
T	Temperature [^oC]
LiBr	Lithium bromide [Absorbent]
H_2O	Water [Refrigerant]
$N_2O,_1$	Nitrous oxide in Upper Cascaded Cycle
$N_2O,_2$	Nitrous oxide in Lower Cascaded Cycle
SRC	Steam Rankine Cycle
ERC	Ejector Refrigeration Cycle
ARC	Absorption Refrigeration Cycle
CRC	Cascade Refrigeration Cycle
CSP	Concentrating Solar Plant

Greek symbols

μ	Entrainment ratio
η	Efficiency [%]

Subscript

A	Absorber
E1	Evaporator-1
E2	Evaporator-2
E3	Evaporator-3
C1	Condenser-1
C2	Condenser-2
C3	Condenser-3
CR	Central Receiver
D	Destruction
GEN	Generator
HTF	Heat transfer Fluid
HRVG	Heat recovery vapor generator
T	Turbine
TV1	Throttle valve-1
TV2	Throttle valve-2

TV3	Throttle valve-3
TV4	Throttle valve-4
TV5	Throttle valve-5
P1	Pump-1
P2	Pump-2
COMP1	Compressor-1
COMP2	Compressor-2
SHX	Solution Heat Exchanger
IHX	Internal Heat Exchanger-1
IHX2	Internal Heat Exchanger-2
EJE	Ejector
d	Diffuser
n	Nozzle
m	Mixing chamber
pf	Primary flow
sf	Secondary flow
n_1	Inlet of nozzle
n_2	Outlet of nozzle
s	Solution mixture of LiBr/H_2O.

CHAPTER 1
INTRODUCTION

1.1 Background:

“Throughout the history of the human race, major advances in civilization have been measured by the increase in the rate of energy consumption. Today, energy consumption appears to be related to the life standard of the population and the degree of industrialization of the countries. However, the world today faces unfavorable condition of atmospheric pollution on a scale that has not been faced earlier in human history because of huge revolution in human use of fossil fuel in all activities, it is also Global warning for further temperature increase by 1.4 - 4.5 ^{o}K up to 2100 [1].

In order to avoid these unfavorable impact, we need to reduce the harmful emission resulting from burning fossil fuel as a source of energy. This can be achieved either by increasing energy conversion efficiency of the fossil fuel based system or using renewable source of green energy. Among these sources, solar energy is the most important and attractive source; because of the solar energy universal abundance and unlimited nature unlike many other renewable energy sources [2].

The attractive characteristic of solar energy is continues source being unending even it is intermittent source during the day and night. In addition, solar energy does not cause air pollution or affect the earth’s surface as fossil fuel. Solar energy is easy to collect unlike the extraction of fossil fuel.

In the field of solar thermal system, solar cooling has huge potential, because the cooling demand reach its peak coincides with peak solar energy availability.

1.2 Solar Cooling technologies classification:

Solar Cooling technologies can be classified in three main categories: solar electrical, thermal and combined power/cooling cycles as illustrated in Figure 1.1:

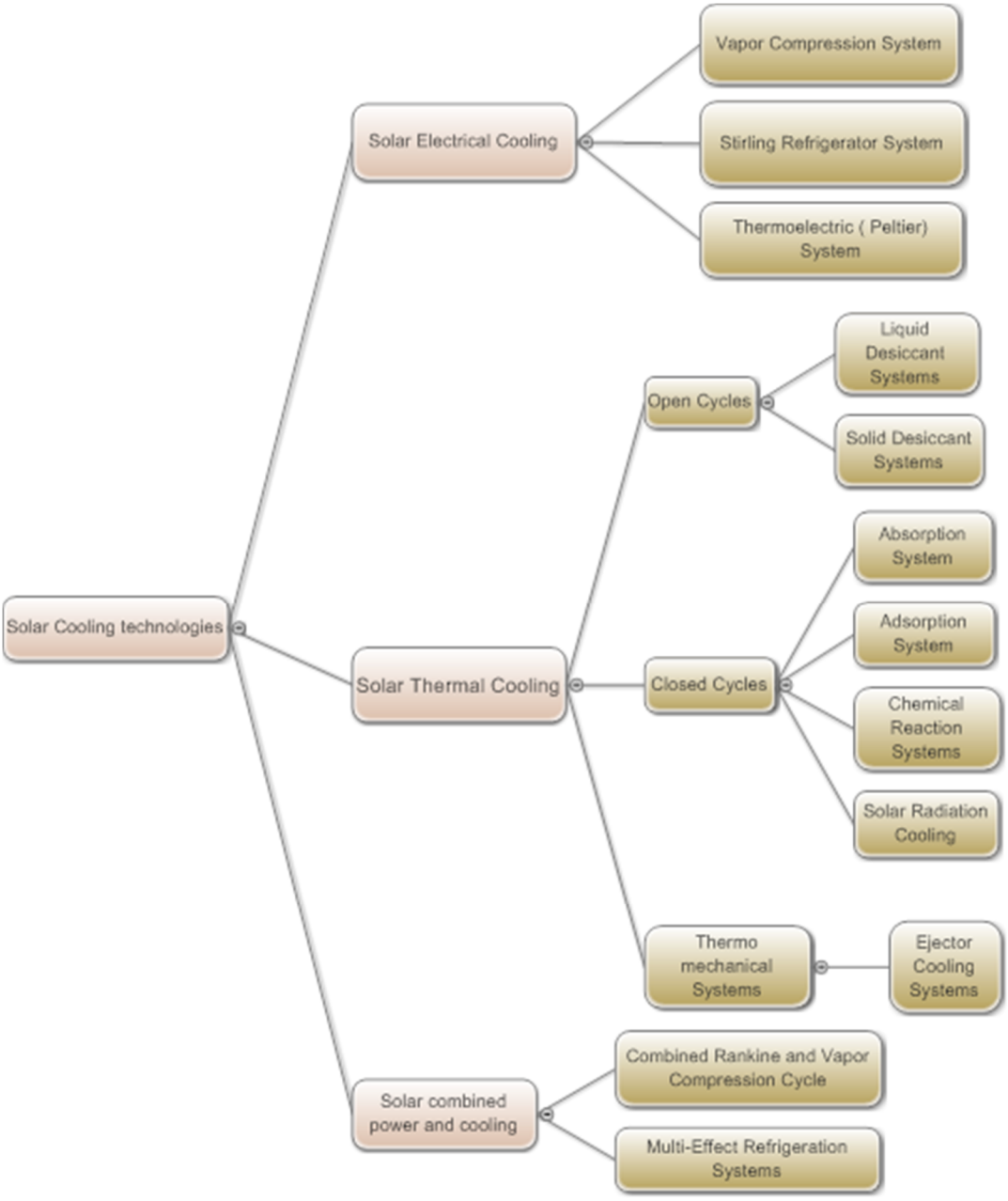

Figure 1.1 Solar Cooling technology.

1.3 Solar Cooling System and Application Temperature Ranges

The solar cooling system can be divided into three major components; solar energy collecting element, refrigeration cycles, and the application at different temperature ranges.

The proper cycle for each application mainly can be selected based on cooling demand and required temperature ranges. Figure 1.2 shows different solar cooling technologies that could produce refrigeration effect at different temperature ranges.

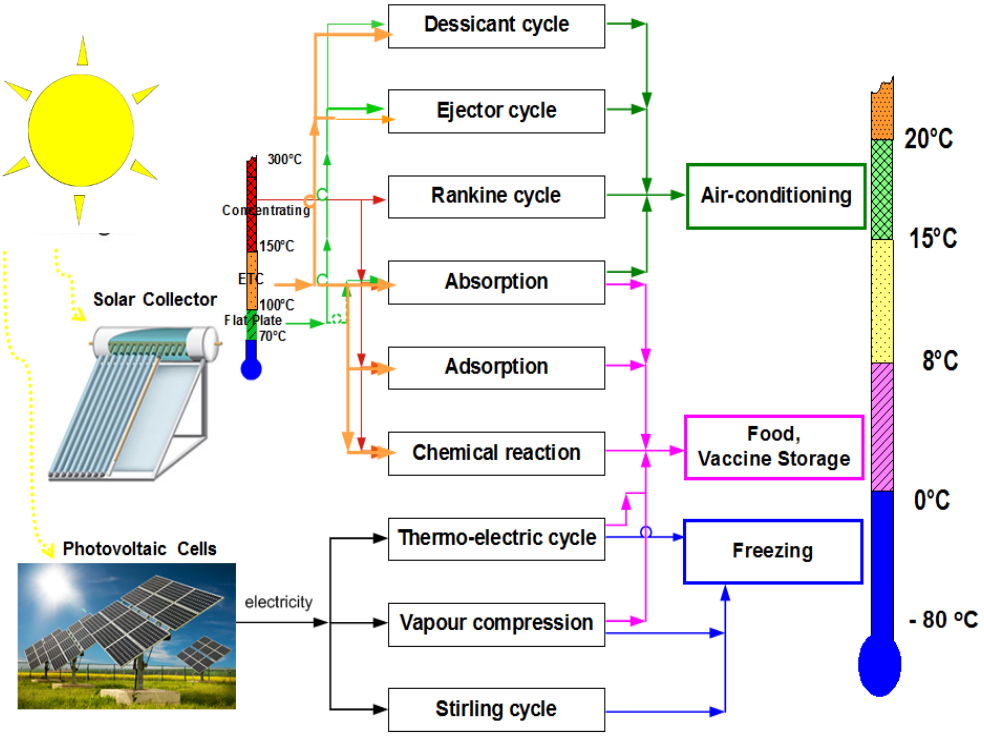

Figure 1.2. Solar Cooling System and Application Temperature Ranges.

Some applications require different range of cooling which cannot be achieved by any single refrigeration cycle. The Multi-effect system is the best way to achieve different magnitude of refrigeration effect and temperature ranges by using solar energy that helps in eliminating problems affecting the environment.

1.4 Concentrated Solar Power Technologies:

In this section, the concentrated solar power technologies will be discussed.

For applications such as air conditioning, central power generation, and numerous industrial heat requirements, flat plate collectors generally cannot provide carrier fluids at temperatures sufficiently elevated to be effective. They may be used as first-stage heat input devices; the temperature of the carrier fluid is then boosted by other conventional heating means. Alternatively, more complex and expensive concentrating collectors can be used. These are devices that optically reflect and focus incident solar energy onto a small receiving area. As a result of this concentration, the intensity of the solar energy is magnified, and the temperatures that can be achieved at the receiver (called the "target") can approach several hundred or even several thousand degrees Celsius. The concentrators must move to track the sun if they are to perform effectively [3]

Concentrating, or focusing, collectors intercept direct radiation over a large area and focus it onto a small absorber area. These collectors can provide high temperatures more efficiently than flat-plate collectors, since the absorption surface area is much smaller. However, diffused sky radiation cannot be focused onto the absorber. Most concentrating collectors require mechanical equipment that constantly orients the collectors toward the sun and keeps the absorber at the point of focus. Therefore; there are many types of concentrating collectors [4].

In Concentrating Solar Power (CSP) plants, mirrors concentrate sunlight and produce heat and steam to generate electricity via a conventional thermodynamic cycle or to drive thermal system. Unlike solar photo-voltaic (PV), CSP uses only the direct component (DNI) of sunlight and

provides heat and power only in regions with high DNI (i.e. Sun Belt regions like North Africa, the Middle East, the southwestern United States and southern Europe).

CSP plants can be equipped with a heat storage system to generate electricity even under cloudy skies or after sunset. Thermal storage can significantly increase the capacity factor and dispatch ability of CSP compared with PV and wind power. It can also facilitate grid integration

The CSP technology includes four variants, namely Parabolic Trough (PT), Fresnel Reflector (FR), Solar Tower (ST) and Solar Dish (SD). While PT and FR plants concentrate the sun's rays on a focal line and reach maximum operating temperatures between 300-550°C [5,6], ST and SD plants focus the sunlight on a single focal point and can reach higher temperatures.

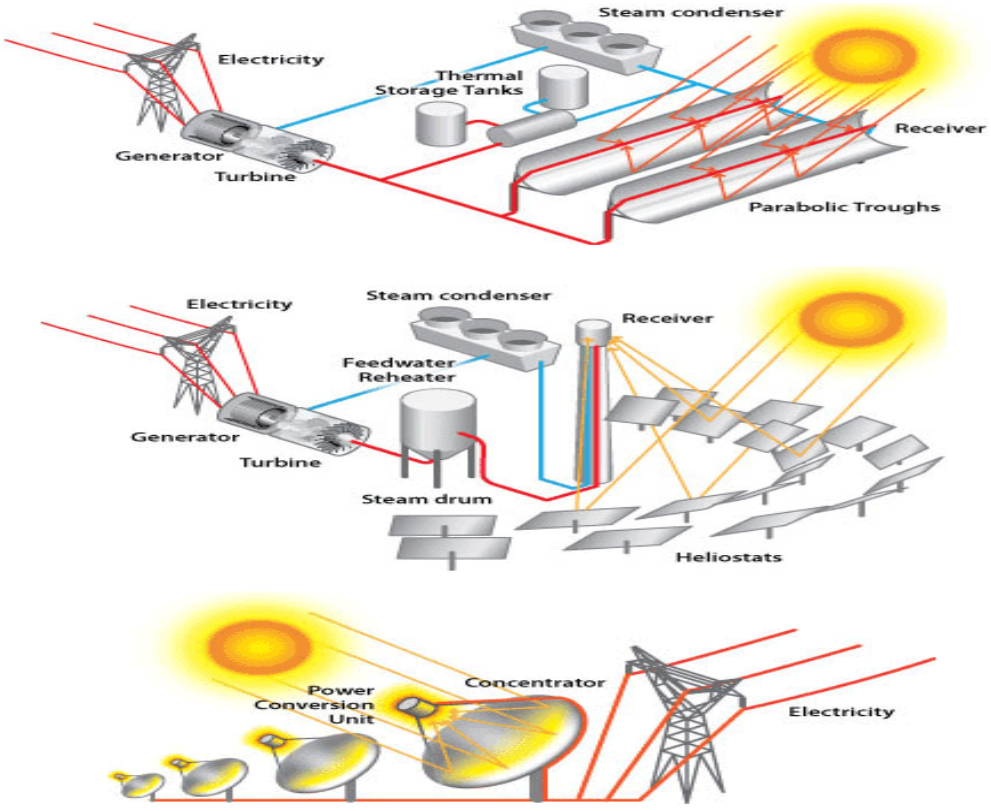

Figure 1.3. Concentrated Solar Power Technologies. [7]

1.4.1 Parabolic trough (PT)

Parabolic Trough Technology is currently the most mature and dominant CSP technology. It uses a synthetic oil, steam or molten salt are used to transfer the solar heat to a steam generator, and molten salt is used for thermal storage. It uses a single axis tracking curved mirror system to concentrate the solar radiation onto a receiver pipe which contain Heat transfer fluid. A synthetic thermal oil is most often used in a heat exchanger for steam generator. [8]

The Parabolic trough also used for direct steam generation where the fluid in the pipe is steam (working fluid) of the power cycle [9, 10, 11]. Parabolic trough can be combined with thermal storage system such as sensible storage systems, molten salt systems and latent storage system (phase change system). [12, 13, 14], Concrete (solid storage system) [15] and steam storage [16].

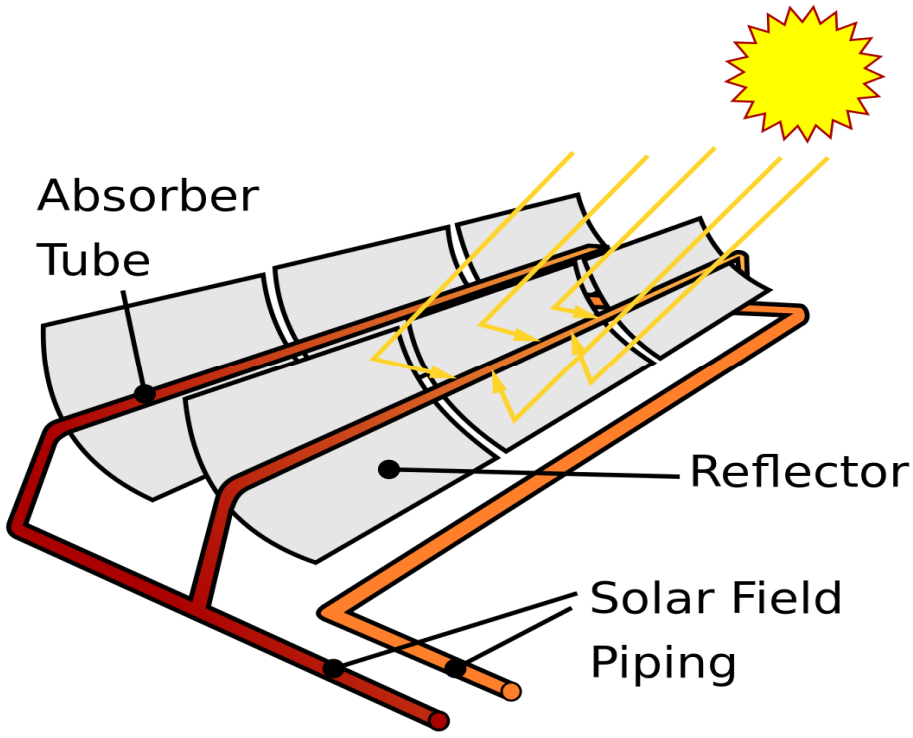

Figure 1.4. Parabolic Trough Solar Collectors Schematic. [17]

1.4.2 Fresnel Reflectors (FR)

Fresnel Reflectors are similar to parabolic troughs in that solar radiation heats a receiver pipe which contains the heat transfer fluid. In other hand, instead of parabolic shaped mirrors, Fresnel Reflector are long and narrow and have little to no curvature[18]. Fresnel reflector also differ from parabolic troughs in that the reflectors are composed of several long row segments which then focus on elevated long receivers running parallel to the rotational axis of the reflector [10].

Fresnel reflectors are cheaper than parabolic troughs (approximately 25% cheaper) and lower efficiencies (approximately percent differences 20%) [19].

Fresnel Reflectors operating temperature as high as 500 ºC [9,20]. The operating temperature of Troughs and Fresnel are relatively low and therefore may not be suited for use in hybrid cycles.

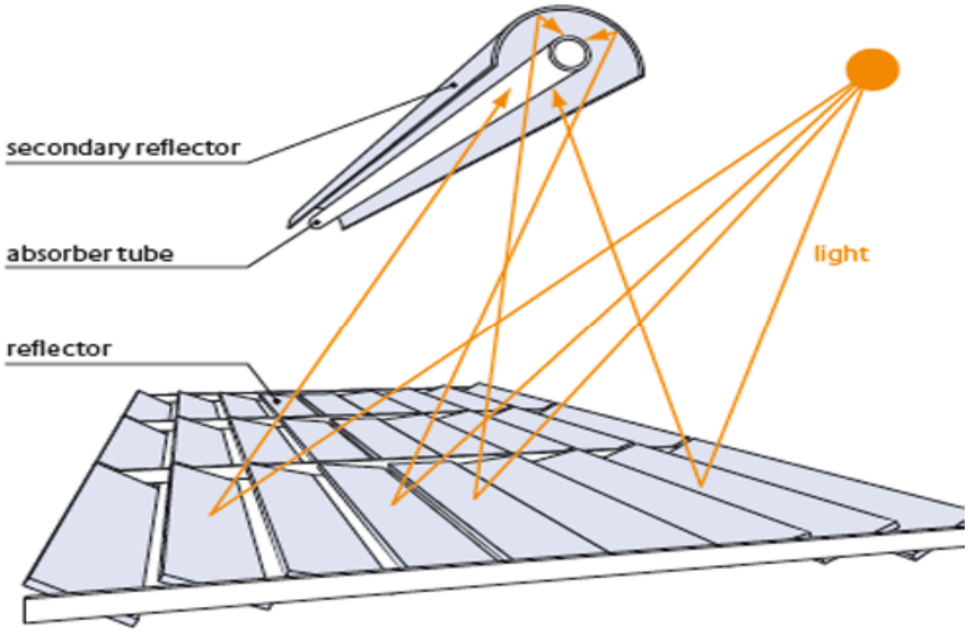

Figure 1.5. Fresnel Reflector Solar Collector Schematic. [21]

1.4.3 Central Receiver Systems (Solar Tower-ST)

Central Receiver systems uses mirrors to concentrate and reflect the sunlight on a single focal point receiver or a small number of receivers by two-axes tracking heliostat.

The most common configuration are **solar tower (ST),** where the receiver is mounted on the top of a tower positioned at the center of a heliostat field.

More advanced systems that use molten salt as the HTF can take advantage of the higher heat capacity of the fluid and can store the heat energy, which allows the system to continue to generate hot water during cloudy weather or at night. Thermal storage allows systems to continue to generate hot water for several hours longer compared to those without, which effectively increases the systems' capacity factor.[8,22]

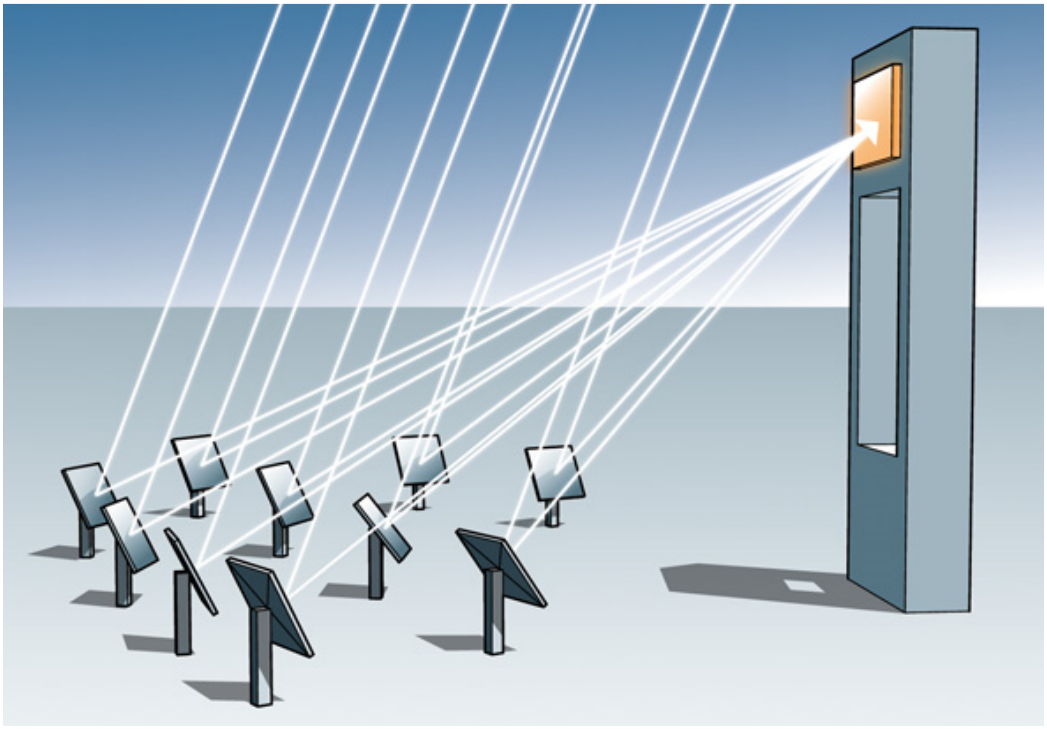

Figure 1.6. Solar Tower Schematic. [23]

The amount of solar energy collected is a function of the number of heliostats installed. However, as the number of installed mirrors increases, the height of the tower must also increase. Determining the optimal tower height and field size is driven by economies of scale. It is relatively inexpensive to increase equipment size once a project has incurred its initial fixed costs of installation.

The heliostats can be mounted in ground with up to five percent slope because they do not rely on a linear collector to heat the HTF. Like the parabolic trough systems, HTF is an integral part of the power tower system.

In principle, ST plants can achieve higher temperatures than PT and FR systems because they have higher concentration factors. The ST plants can use water-steam, synthetic oil or molten salt as the primary heat transfer fluid. The use of high-temperature gas is also being considered

Depending on the primary heat transfer fluid and the receiver design, maximum operating temperatures may range from 250-300°C (using water-steam) to 390°C (using synthetic oil) and up to 565°C (using molten salt)[5]. Temperatures above 800°C can be obtained using gases on solar air tower with pressurized volumetric receiver combined with gas turbines that can reach operating temperature between 750 ^{o}C and 950 ^{o}C [8, 24, 25, 26, and 27]. The temperature level of the primary heat transfer fluid determines the operating conditions (i.e. subcritical, supercritical or ultra-supercritical) of the steam cycle in the conventional part of the power plant.

Recent research has also been done towards designing alternative volumetric receivers that do not require a tower (i.e. all equipment including receiver are on the ground) [28, 29, 30, and 31].

ST plants can be equipped with thermal storage systems whose operating temperatures also depend on the primary heat transfer fluid.

Today's best performance is obtained using molten salt at 565°C for either heat transfer or storage purposes. This enables efficient and cheap heat storage and the use of efficient supercritical steam cycles.

High-temperature ST plants offer potential advantages over other CSP technologies in terms of efficiency, heat storage, performance, capacity factors and costs. In the long run, they could provide the cheapest CSP electricity, and thermal energy but more commercial experience is needed to confirm these expectations.

The receiver of a central solar tower power plant is located on the top of the tower. As support of the receiver the tower is commonly with a height of 80 to 100 m and is made of concrete or steel structure. A higher tower is preferable for bigger and denser heliostats fields but it should avoid the shades or objects that block the sun. At the same time, the technical factors, e.g., tracking precision and the economic factors, e.g., tower costs should also be considered in determining the height of the tower. The receiver of solar tower power plant transforms the concentrated solar energy into the thermal energy of working fluid. This working fluid could be commonly water/steam or molten salts. In further research air is applied for use in high temperature power towers. Water/steam receivers are the most used receiver in solar tower power plants.

1.4.4 Solar Dish (SD)

One of the most common solar dish systems is the dish-engine. Dish engine is the most efficient system of the receiver technologies in term of maximal achieved conversion of solar energy [8].

The solar dish system consists of a parabolic dish shaped concentrator (like a satellite dish) that reflects sunlight into a receiver placed at the focal point of the dish. SD systems require two-axis sun tracking systems and offer very high concentration factors and operating temperatures, the operating temperature of this system can reach as high as 750 ^{o}C.

The Dish engine system is also the least mature of the receiver technologies and is modular in design with a single dish limited to capacity of 10-50 kW [5]. Therefore, at least in the near term future, solar dish engine system are most likely to be used in smaller, high value application rather than large scale solar driven plants.

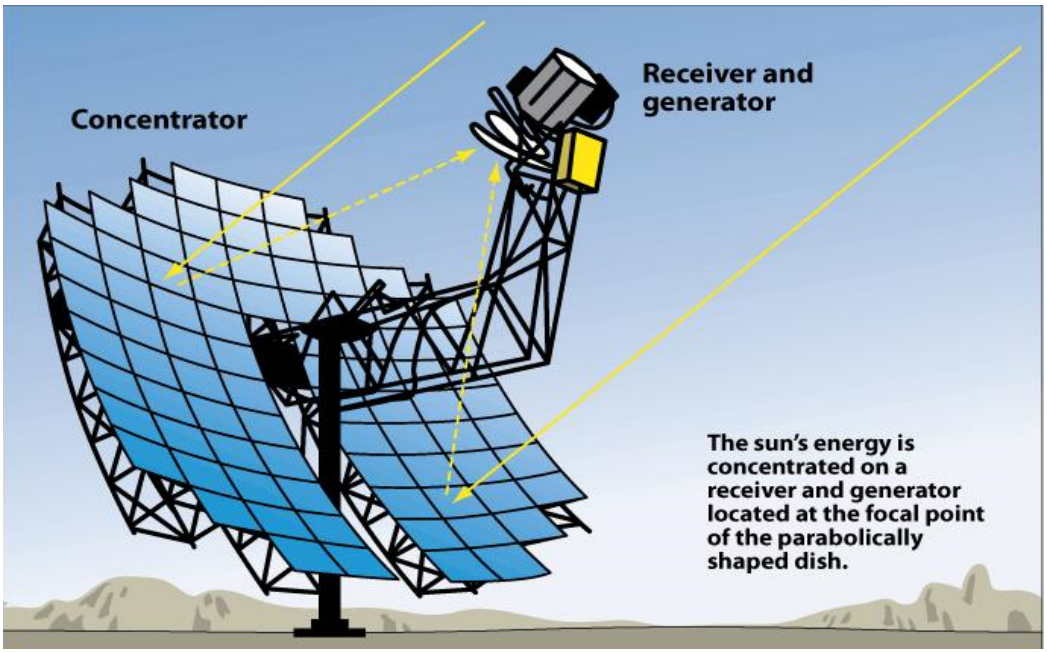

Figure 1.7. Solar Dish Schematic. [32]

The main advantages of solar dish systems include high efficiency (i.e. up to 30%) and modularity (i.e. 10-50 kW), which is suitable for distributed generation [5].

Unlike other CSP options, solar dish systems do not need cooling systems for the exhaust heat. This makes Solar dish suitable for use in water-constrained regions, though at relatively high electricity generation costs compared to other CSP options. Several Solar Dish prototypes have successfully operated over the last ten years with capacities ranging from 10-100 kW (e.g. Big Dish, Australian National University).

1.4.5 Comparison of Solar Cooling Technology

Table 1.1 Comparison of Solar Cooling Technology [33, 36]

	Parabolic Trough	Dish/Engine	Power Tower
Size	30-320 MW	5-25 kW	10-200 MW
Operating Temperature (ºC/ºF)	390/734	750/1382	565/1049
Annual Capacity Factor	23-50 %	25 %	20-77 %
Peak Efficiency	20%(d)	29.4%(d)	23%(p)
Net Annual Efficiency	11(d)-16%	12-25%(p)	7(d)-20%
Commercial Status	Commercially Scale-up Prototype	Demonstration	Available Demonstration
Technology Development Risk	Low	High	Medium
Storage Available	Limited	Battery	Yes
Hybrid Designs	Yes	Yes	Yes
Cost USD/W	2,7-4,0	1,3-12,6	2,5-4,4

(p) = predicted; (d) = demonstrated;

1.4.6 CSP Water Requirements

CSP plants using steam cycles (i.e. PT, FR and ST) require cooling (i.e. 2-3 m^3 of water per MWh) to condense exhaust steam from the turbines; the lower the efficiency, the higher the cooling needs. As water resources are often scarce in Sun Belt regions, wet or dry cooling towers are often needed for CSP installations. In general, dry (air) cooling towers are more expensive and less efficient than wet towers. [34]

1.5 Solar Energy Component and Angle Definition:

1.5.1 Direct Normal Insolation (DNI)

Extraterrestrial solar radiation follows a direct line from the sun to the Earth. Upon entering the earth's atmosphere, some solar radiation is diffused by air, water molecules, and dust within the atmosphere (Duffie and Beckman). The direct normal insolation represents that portion of solar radiation reaching the surface of the Earth that has not been scattered or absorbed by the atmosphere. The adjective "normal" refers to the direct radiation as measured on a plane normal to its direction.

1.5.2 Angle of incidence (θ) and Declination angle (δ)

Only the insolation that is directly normal to the collector surface can be focused and thus be available to warm the absorber tubes. The angle of incidence (θ) represents the angle between the beam radiation on a surface and the plane normal to that surface. The angle of incidence will vary over the course of the day (as well as throughout the year) and will heavily influence the performance of the collectors.

Figure illustrates the angle of incidence between the collector normal and the beam radiation on a solar tower. The angle of incidence results from the relationship between the sun's position in the sky and the orientation of the collectors for a given location.

The position of the sun varies throughout the year. The **declination angle** is the angular position of the sun at solar noon, with respect to the plane of the equator. If the earth rotated upright on its axis, there would be no change in declination angle as the earth revolved around the sun. However, the earth is tilted on its axis at an angle of 23.45°. As the earth rotates around the sun through the course of a year, the declination angle will change, within a range of $-23.45° \leq \delta \leq 23.45°$. See Figure for a pictorial representation of the declination angle.

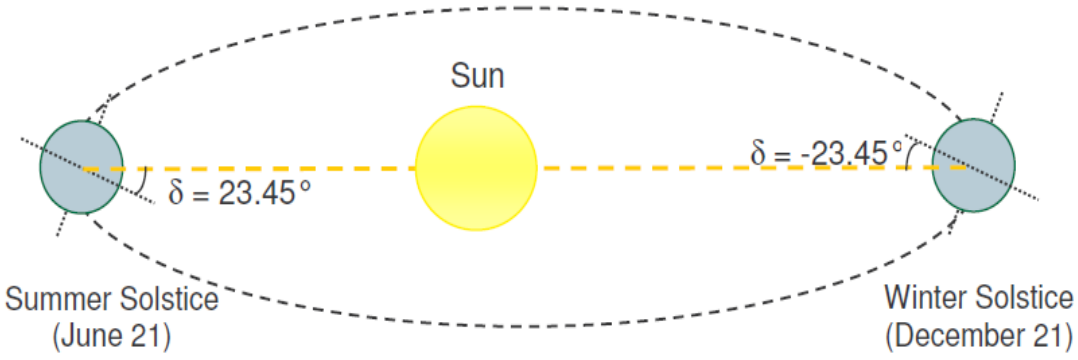

Figure 1.8. Declination angle due to Earth's tilt. [35]

The following expression for declination angle was developed by P.I. Cooper in 1969 (Cooper, as cited by Duffie and Beckman, 1991):

$$\delta = 23.45 \sin\left(360 \frac{284+n}{365}\right) \quad \text{.....1.1}$$

n = the day number of the year, from 1 (corresponding to January 1) to 365 (Corresponding to December 31).

Figure shows the variation of the declination angle throughout the year

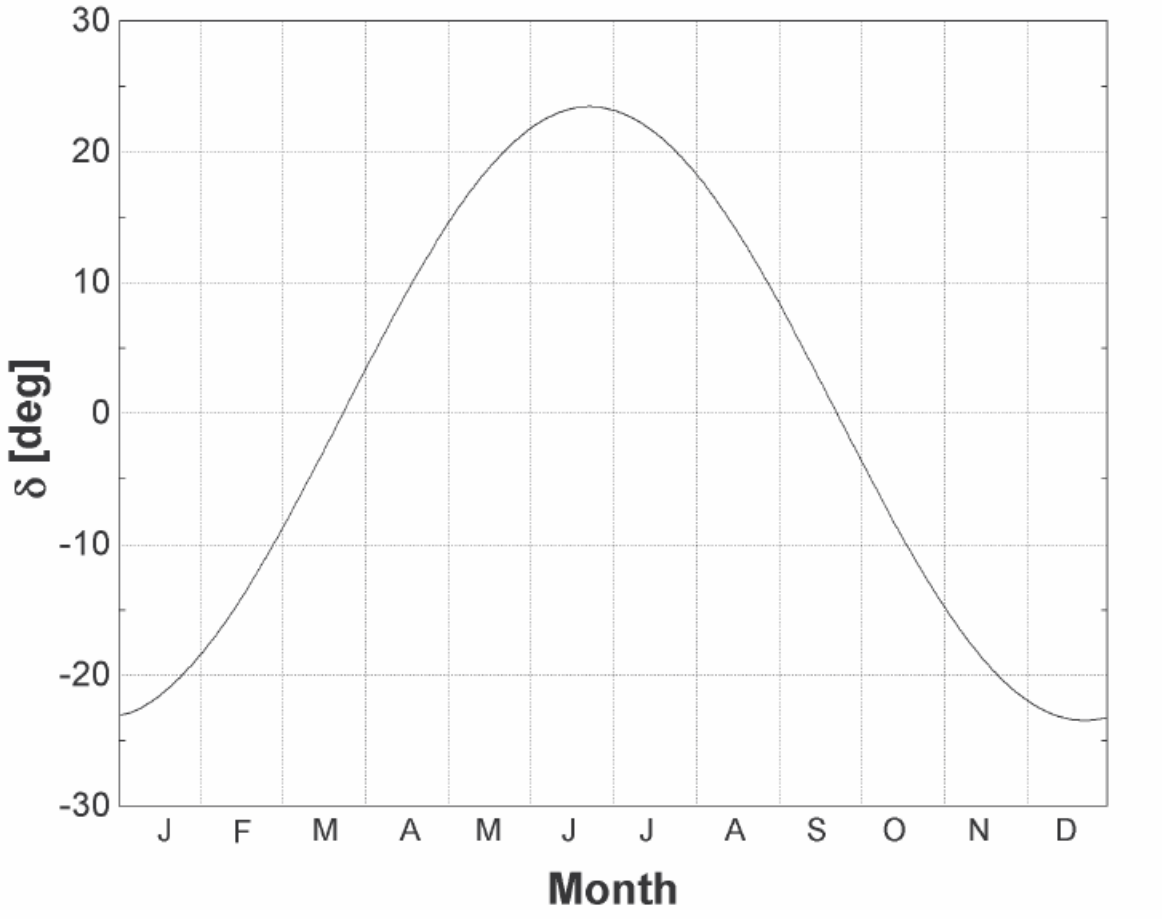

Figure 1.9. Declination angle variation by month, from Equation (1.1) [35]

1.5.3 Hour Angle (ω) and Solar Time.

The position of the sun depends on the hour angle, or the angular displacement of the sun east or west of the local meridian. The hour angle is negative when the sun is east of the local meridian (in the morning), positive when the sun is west of the local meridian (afternoon), and zero when the sun is in line with the local meridian (noon).

The hour angle comes as a result of the rotation on the earth, which spins on its axis at a rate of 15° per hour:

$$\omega = \left(Solar\ Time - 12\right).\frac{15^{o}}{hr} \quad \text{.....1.2}$$

Where ω is the hour angle [deg] and *SolarTime* is the solar time [hr].

There is an important distinction between standard time and solar time. In solar time, the sun aligns with the local meridian (ω = 0) at exactly 12:00, or "solar noon." However, standard time is based not on the local meridian, but on a standard meridian for the local time zone. The length of the solar day also varies; this variation is due primarily to the fact that the earth follows an elliptical path around the sun (Stine and Harrigan, 1985). As a result, the standard time must be adjusted to reflect the current time of day in solar time. The relationship between solar time and standard time, in hours, is:

$$Solar\ Time = Stndard\ time - 4\ (L_{st} - L_{loc}\ ) + E \text{.....1.3}$$

Where

L_{st} = standard meridian for the local time zone [deg]

L_{loc} = the longitude of the location of collector site [deg]

E = equation of time [min]

E, the equation of time, accounts for the small irregularities in day length that occur due to the Earth's elliptical path around the sun. The equation

of time used here, in minutes, comes from Spencer (as cited by Iqbal, 1983):

E = 229.18 (0.000075 + 0.001868 cos (B) – 0.032077 sin (B) – 0.014615 cos (2B) – 0.04089 sin (2B))……..……1.4

Where

$B = \frac{360}{365}$ (n-1) [Deg]……..……1.5

n = day number of the year (1 for January 1, 365 for December 31)

The variation in the equation of time over the year is given in Figure, the equation of time may offset solar time from standard time by as much as fifteen minutes during the year.

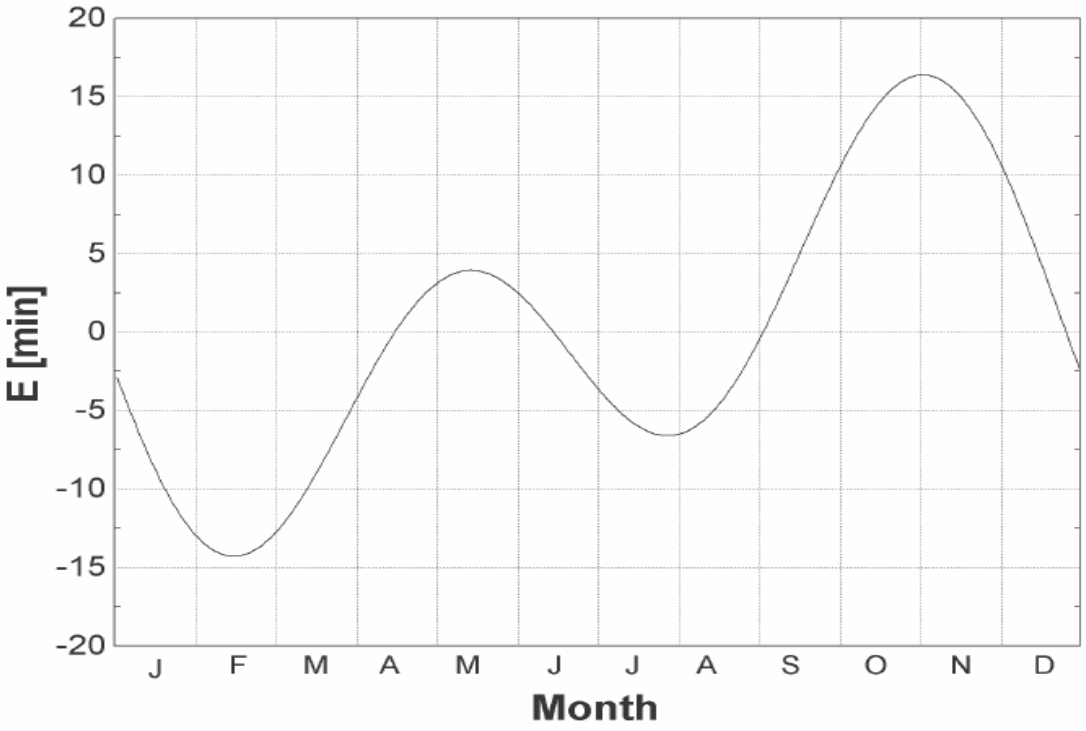

Figure 1.10. Equation of time vs month of the year (from Equation 1.4) [35]

1.5.4 Zenith Angle (θz)

The final angle required to solve for the angle of incidence is the zenith angle. The zenith angle is the angle between the line of sight to the sun and the vertical. Its complement, the angle between the line of sight to the sun and the horizon, is the solar altitude angle. The zenith angle is related to both the declination angle and the hour angle by the following relationship (Duffie and Beckman, 1991):

$$cos\theta_z = \cos(\delta)\cos(\phi)\cos(\omega) + \sin(\delta)\sin(\phi) \quad \text{.....1.6}$$

Where,

δ = declination angle (see Equation 1.1)
ω = hour angle (see Equation 1.2)
ϕ = latitude location of the plant

1.5.5 Incidence Angle Modifier (IAM)

In addition to losses due to the angle of incidence, there are other losses from the collectors that can be correlated to the angle of incidence. These losses occur due to additional reflection and absorption by the glass envelope when the angle of incidence increases [37]. The incidence angle modifier (IAM) corrects for these additional reflection and absorption losses. The incidence angle modifier is given as an empirical fit to experimental data for a given collector type.

$$\mathrm{K} = \cos(\theta) + 0.000884(\theta) - 0.0005369(\theta)^2 \quad \text{.....1.7}$$

Where θ, the incidence angle, is provided in degrees.

It is desirable to distinguish between losses in available radiation due to the angle of incidence itself and the reflection/absorption corrections empirically correlated to the angle of incidence.

For this purpose, the incidence angle modifier is defined for this work as the incidence angle modifier defined by Dudley et al, divided by the cosine of the incidence angle:

$$IAM = \frac{K}{\cos(\theta)} \quad \text{.....1.8}$$

The equation for the incidence angle modifier used in the solar field component model is:"

$$IAM = 1 + 0.000884 \,.\frac{\theta}{\cos(\theta)} - 0.00005369 \,.\frac{\theta^2}{\cos(\theta)} \quad \text{.....1.9}$$

CHAPTER 2
SOLAR COOLING TECHNOLOGIES DESCRIPTION AND LITERATURE REVIEW

Solar cooling is a clean and cost-effective technology, solar cooling offer environmental benefits including reducing main grid demand and shift the load during peak usage and reduced greenhouse gas emissions.

The main objective of this chapter is to review and analyze different solar cooling technologies that can be used to provide the required cooling and refrigeration effect from solar energy. This chapter is covering a wide range of solar cooling technologies including solar electrical refrigeration system, thermo-mechanical combined power and cooling systems and advanced triple effect refrigeration cycles [38].

This chapter includes comparisons of different technologies highlighting the advantages and disadvantages. This comparison would assist the decision makers to select the proper solar cooling technology for specific application.

Solar Cooling technologies can be classified in three main categories: solar electrical, thermal and combined power/cooling cycles.

The solar cooling system can be divided into three major components; solar energy collecting element, refrigeration cycles, and the application at different temperature ranges.
The proper cycle for each application mainly can be selected based on cooling demand and required temperature ranges.
Some applications require different range of cooling which cannot be achieved by any single refrigeration cycle.
The Multi-effect system is the best way to achieve different magnitude of refrigeration effect and temperature ranges by using solar energy that helps in eliminating problems affecting the environment.

2.1 Solar Electrical Cooling:

A solar electrical cooling system consists of photovoltaic panel and electrical refrigeration device. Photovoltaic cells transform light into electricity through photoelectric effect. Many of solar electrical refrigeration system are made for independent operation.

PV cells made of semiconductor materials, single crystalline thin films, poly-crystalline and silicon-wafers represent the solar panel materials, and the silicon is major component of PV cell in the market.
The efficiency of polycrystalline thin films is higher than that of silicon wafer, the efficiency of polycrystalline thin films in range of 10 to 17 % [39] and single crystalline thin file efficiency can reach 15 to 20 % by using multi-junction cell structure, while as silicon wafer performance is low and its cost are high compare the thin film technologies.

The produced power by solar photovoltaic cells is supplied either to the thermo-electrical system, Stirling cycle or normal vapor compression systems.

2.1.1 Thermo-Electric Cooling (Peltier Cooling System)

Thermo-electric device utilizes the Peltier effect to make a temperature gradient of two types of semiconductors materials. Peltier effect can be defined as presence of heating or cooling at junction of two different conductors due to electricity flow [40].

When a DC current is passed through one (or more pairs) of n and p-type semiconductor materials, the temperature of one conductor decreases and absorb the heat from its surrounding space. The absorbed heat from the space occurs when electrons pass from a p-type material to the n-type material (from low energy level to high energy level) [40].

When a temperature gradient is achieved between the hot and cold ends of the conductor, adverse voltage is created. [41].

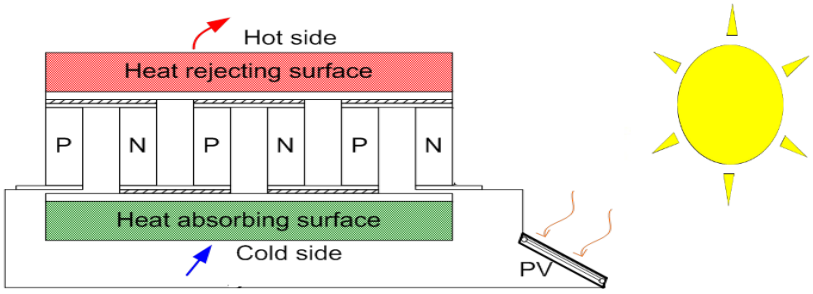

Figure 2.1. Peltier Cooling System

The heat is transferred through n and p-type semiconductor from cold side to the hot side then the heat is rejected to outside. If the direction of the current is reversed, the direction of the heat flow is reversed also, and air conditioning system operates in the heating mode [42].

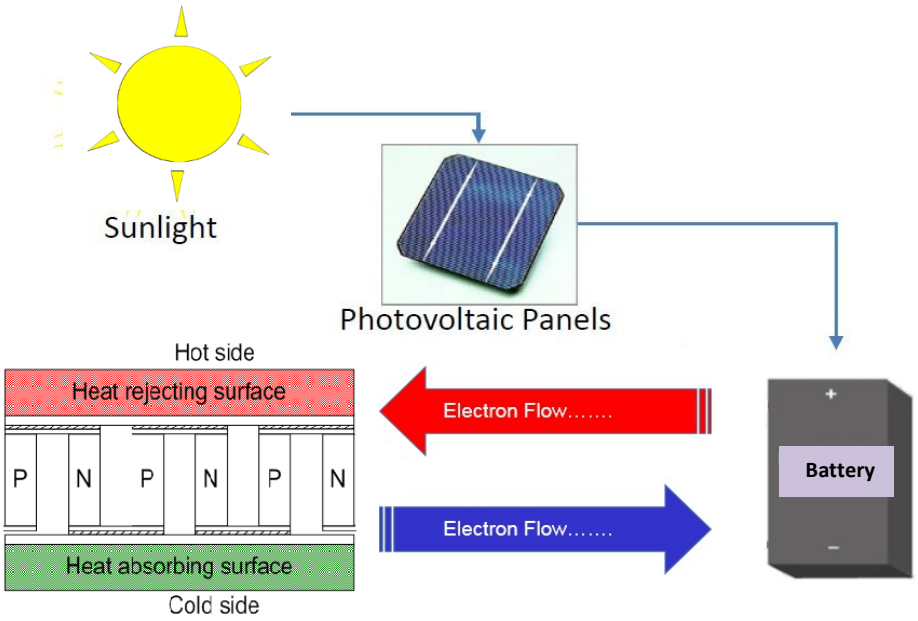

Figure 2.2. Thermoelectric Refrigeration System.

Usage of thermo-electric cooling is less compare to vapor compression cycle in the market.

The Lack of moving parts is the major feature of a Peltier cooler compared to other refrigeration cycles. In addition, the lack of circulating liquid, near-infinite life, very low potential leaks, and its small size are unique features of peltier cooler. Thermoelectric devices contain no chlorofluorocarbons, so it is environment friendly and it is fully reversible cycles, precise temperature control, and work efficiently in sensitive application.

High cost and low efficiency is the main disadvantages. Many researchers are working now to develop peltier cooler with low cost and high efficiency.

Thermoelectric can be used for cooling electronic devices, refrigerator and air conditioners. Thermoelectric equipment can be used for particular applications in military, aerospace, instruments, medicine and industrial.

Riffat et. al. [40] explained thermoelectric working principle and materials used for thermoelectric and its application. They also discussed thermoelectric devices application in refrigeration and power generation, and as sensor in thermal energy, they discussed the development of new materials that could improve the thermoelectric devices for many applications.

The main disadvantage of thermo-electric is low COP but it does have high potential in specific application, such as cooling electronic devices, where thermo-electric is preferred due to small size and consume very less electricity. [42]

2.1.2 Solar powered vapor compression cooling system

PV panel converts solar radiation to DC power which is supplied to a conventional vapor compression system. The Coefficient of performance of the system depend on the efficiency of the PV panel.
The solar radiation is intermittent source, and the solar radiation will not be available all times therefore an alternative source of power to run the system is required when the solar radiation becomes low or unavailable.
The cost of electricity supplied from photovoltaic is equal to or cheaper than grid power, is easily achieved in sunny areas and high costs for grid electricity such as in United States and Japan.

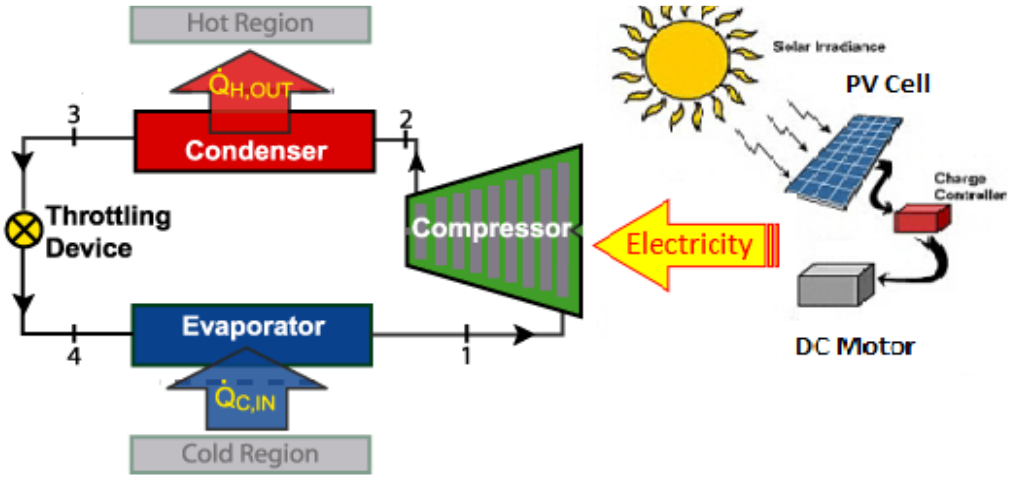

Figure 2.3. Solar Powered Vapor Compression cycle.

Klein and Reindl [43] investigated the electrical characteristics that produced from Photovoltaics cells and compare it with required characteristics of compressor motor.

The most important characteristic is the voltage that should be close to voltage producing the maximum possible power in order to run the system at highest efficiency.

This can be done by many ways to track the highest power then select electric motor with current and voltage producing maximum power of the system.

2.1.3 Solar Driven Stirling Refrigeration System:

The Stirling Cycle engine was invented by the Reverend Robert Stirling of Kilmarnock in 1812.

A Stirling system is suitable for specific applications requiring low temperatures, Stirling refrigerator can be used for cooling at very low temperatures of about 3 K.

The main field of operation of the stirling refrigerator has been in the production of low temperature on a relatively small scale. It is a standard stirling refrigerator which will produce liquid nitrogen and liquid oxygen from atmospheric air.

Hydrogen is the most often and best gas to use in a stirling refrigerator because of its low molecular weight while as nitrogen is used in commercial and standard units as it is very cheap and safe.

Stirling refrigeration cycle principle is based on volume changes caused by pistons, thus inducing changes in pressure and temperature of a gas (no phase change). On the other hand, it yields very good performance at large temperature increases [44].

The Main Concept of Stirling refrigerator is to convert mechanical energy to thermal energy (Useful Cooling).

The cooling cycle is split in four processes as shown in Figure 6, the cycle starts by isothermal compression process; compression of a gas at ambient temperature, the motive force for the compression process is provided by outside source such as electric motor that takes power either from main grid electricity or solar energy through photovoltaic cells.

The cycle starts when the compression and expansion piston at the left position.

The compression piston moves to the right while the expansion piston is fixed, the compression at the hot and compression space is isothermal.

The gas moves through hot side heat exchanger due to increase in pressure and the heat dissipated to outside at ambient temperature Ta.

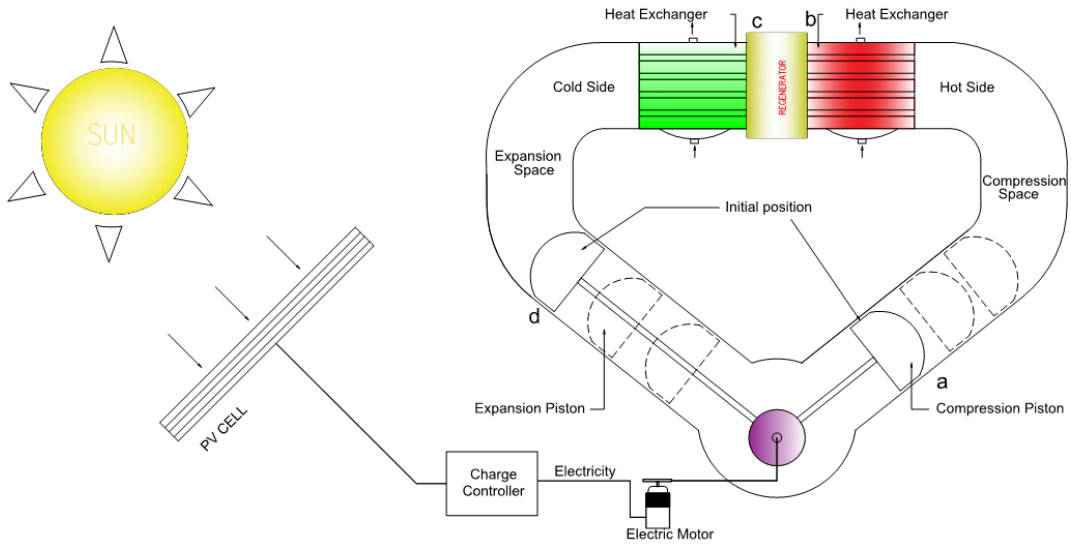

Figure 2.4. Solar Assisted Stirling Refrigerator Schematic.

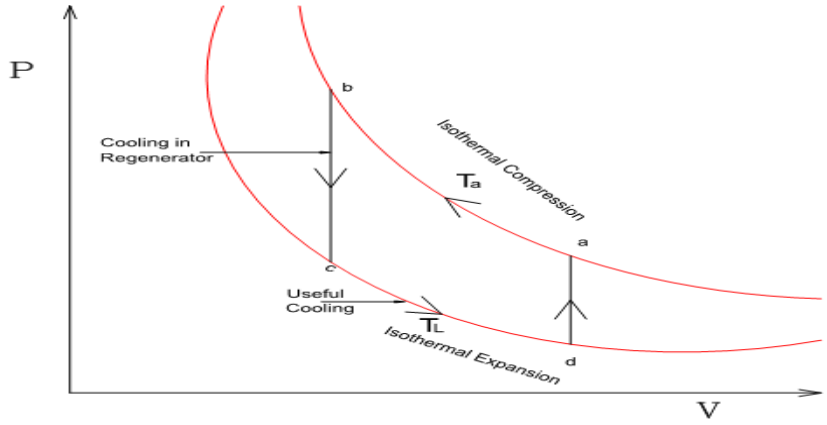

Figure 2.5. P-V Diagram for Stirling Refrigerator.

The hot gas enters regenerator as two piston moves to the right, the gas cool in the regenerator to the temperature of cold side heat exchanger, the gas give off heat to the regenerator material. This process take place at constant volume between two pistons.

The compression piston moves to the right while the expansion piston is fixed, the gas expansion take place in the expansion space (isothermal expansion) and the heat is taken up in the cold heat exchanger, and becomes cooler, it represent useful cooling.

The cold gas absorbs heat from conditioned space or machine, the gas absorb the heat and return to environment temperature.

The two pistons move to the left while the total volume remains constant.

The gas moves back to compression space at the end of expansion, during this step the gas enters the regenerator with low temperature and leaves it with high temperature so heat is taken up from the regenerator material.

Table 1 summarize the piston movement during the operation of stirling cycle.

Table 2.1 Piston movement of the Stirling cycle.

Process	Piston Movement	
	Compression Piston	Expansion Piston
a-b	Toward Right	Fixed
b-c	Toward Right	Toward Right
c-d	Fixed	Toward Right
d-a	Toward Left	Toward Left

In the ideal case the cycle is reversible so the COP (the ratio of the cooling power and the input power) is equal to the Carnot COP given by TL/ (Ta-TL), where TL is low temperature and Ta is high temperature.

Ewert et al. [45] discussed the test result of 100 watts Stirling refrigerator that showed decreasing of COP from 1.5 to 0.8 for temperature variation 13-33 K with outdoor temperature from 23-28 ^{o}C.

Berchovitz et al. [46] discussed the test result of similar machine of Ewert et.al. 1998 with 40 Watts capacity, the results showed COP decreasing from 1.65 to 1.17 with variation temperature of cold side from -1.4 to -19.1 ^{o}C and temperature of hot side from 28.4 to 30.3 ^{o}C.

Raine et. al.[47] reported test result from the Heat pump stirling cycle development programmed which showed high performance at specific condition compared to conventional vapor compression cycle. This is associated with changes of the hot / cold HEX varied from their design temperatures with a lower performance drop. Further the results obtained showed the heating COP of the Stirling-system machine at 6°C outdoor temperature is only very slightly less than that of a conventional vapor compression system. However, at 0°C outdoor temperature the vapor compression machine has considerable less COP than the Stirling

system, even the Stirling cycle machine is operating at an even lower outdoor temperature of -5°C.

There is many challenges in designing efficient Stirling refrigerator as low COP due to poor heat transfer between working fluid and ambient air [48].

Riffat et. al. [41] conducted a comparative study of the performance between vapor compression cycle, the absorption cycle and the thermoelectric refrigerator. The comparison showed that vapor compression have high COP and low cost. However, some of refrigerant used vapor compression system will be phase out due to their effect on depletion of the ozone layer like system used R-12 or R-22.

Absorption cycle generally require large space and high initial cost but consume very less electricity to run the pumps and fan as it depends on waste energy source or solar energy to provide the required thermal energy to generator, so the operational cost is very low, while as low noise or almost very less vibration due to no moving parts, small size and light weight are unique features of thermo-electric. Thermo-electric does not require refrigerant so no effect on the environment.

Table 2.2 Comparison between solar electrical cooling systems

System	Vapor Compression	Thermoelectric (Peltier)	Stirling Refrigerator
Power of 1 W of refrigeration effect (Watts)	12-50	A few W	3 - 17
COP	2-4	~0.5	~3
Working Fluid	R-134A, R407C & R410A etc.	-	He, H_2 & Air
Application	Refrigeration, Freezing, food storage & vaccine storage	Refrigeration, large LCD screen, Military communication, etc.	Cryogenic applications including: IR – Infra Red imagers.
Noise (dB)	35~48 indoor	NA	~35
Size	Medium	small	small
Life expectancy, year	10-15	~23	~15
Advantages	-High COP. -Widely Commercial Available. -Long Term Experience.	- No moving parts. - No working fluid. - Quiet. - Small Size. - Light Weight. - Near-Infinite Life. - Invulnerability to potential leaks.	- High COP for high temperature difference. - Mechanically more simple than other application for low temperature operation. - Environmentally friendly working fluid. - Mobility & Light weight.
Disadvantages	- Installation Cost is high. - PV cells cost is high. - Requires Battery for energy Backup. -Requires more space for PV cells.	- Low COP. - High Cost. - Difficult to achieve low ref. temperature. - Low Reliability.	- High Production Cost. - Complexity in Design.

2.2 Solar Thermal Cooling:

Solar energy conversion systems can be used to transform solar thermal energy to cooling or heating through chemical or physical Processes.

2.2.1 Open Sorption Cycle Solar Cooling.

It represents desiccant systems that are used in air conditioning applications for humidification or dehumidification basically transfer moisture from one air stream to another one. These cycles cab be used as pre-cooling of other system and can be used to provide cooling for specific application with special requirement.

The main operation concept of open sorption cycle is to absorb and release the moisture in three processes as follow:

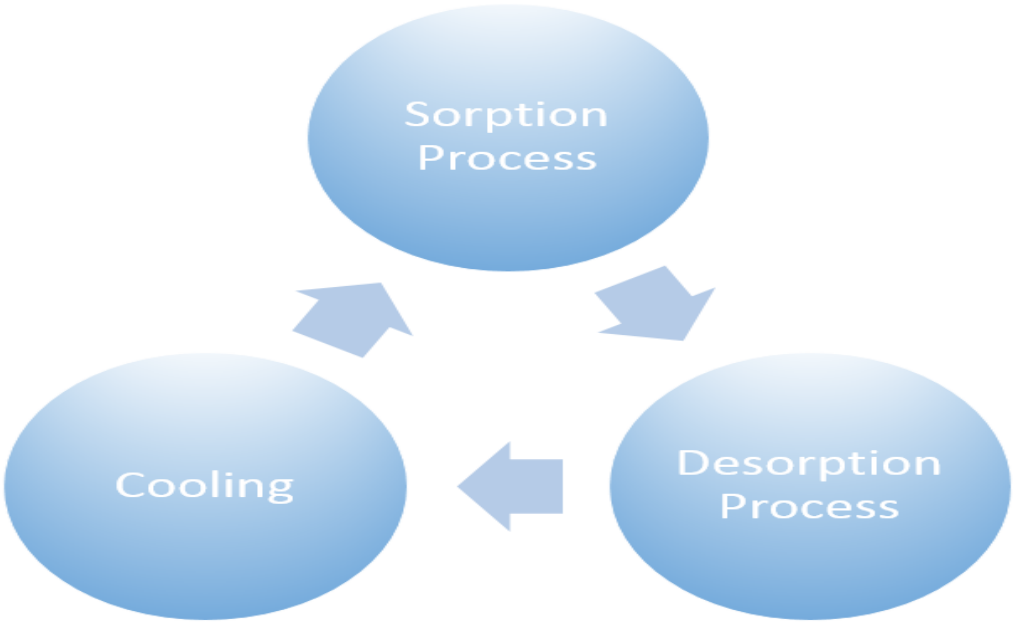

Figure 2.6. Process of Moisture Transfer by Desiccant

Description of Open Sorption Cycle Solar Cooling:

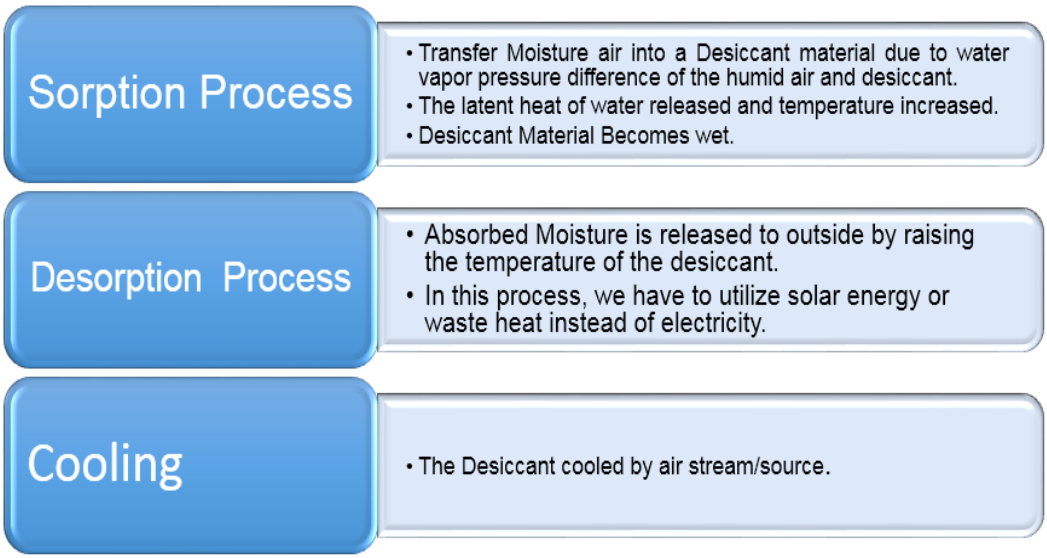

Liquid Desiccant System.

The system consists of a conditioner and regenerator, the principle operation of the system as follow:

Conditioner

The liquid desiccant is pumped and pass through nozzle that will spray the desiccant in the air to absorb the moisture from air due to difference in surface vapor pressure of the desiccant and air.
The liquid desiccant falls to the basin of conditioner and spray back in air, the desiccant temperature and pressure has increased
The water content increased due to absorption of moisture and in order to increase the concentration of desiccant small amount of the mixture of water and liquid desiccant is pumped from conditioner basin to regenerator basin.

Regenerator

The desiccant is sprayed in the air and the desiccant heated before spraying so its partial pressure increased, therefore the moisture had absorbed by regenerator's air and leave it in hot and humid condition.

The concentration of liquid desiccant increased in the basin of regenerator and its temperature and pressure increased as well.

Small amount of desiccant return to conditioner to spray again.

Finally before spraying the liquid desiccant, it must be cooled by cold water from chiller or other cooling sources.

Lithium chloride, calcium chloride, and lithium bromide are main materials used in liquid desiccant systems [49].

The advantage of liquid desiccant cycle that the desiccant can be regenerated by using low grade energy source.

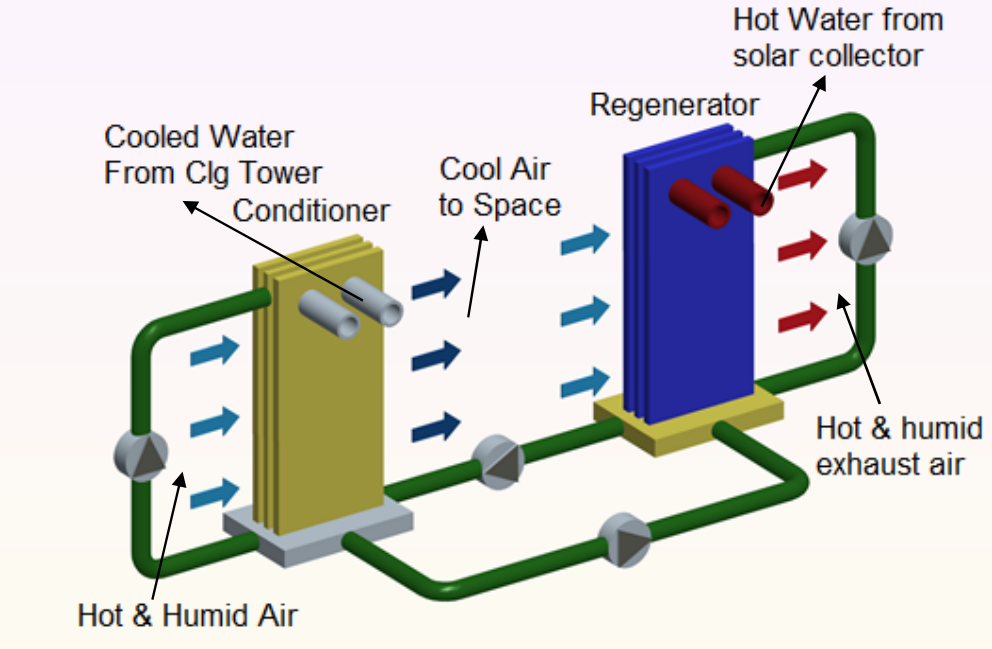

Figure 2.7. Schematic of Liquid Desiccant System.

Gommed & Grossman [50] investigated solar assisted liquid desiccant cooling system using Lithium chloride and water as working fluid, outside temperature was the influencing factor that is having high effect on the dehumidification process.

The result showed that the system supplied 16 kW of dehumidification capacity with 0.8 coefficient of performance.

Davies [51] developed the liquid desiccant system based on Abu Dhabi data weather with the solar collector for regenerative heating coil and the adiabatic cooler to reduce inside condition in greenhouses. The result revealed clearly the possibility of lower outside temperature by 5 ºC as cooling effect.

Solid Desiccant System.

The solid desiccant system used to provide air conditioned air through basic process as shown figure 2.8.

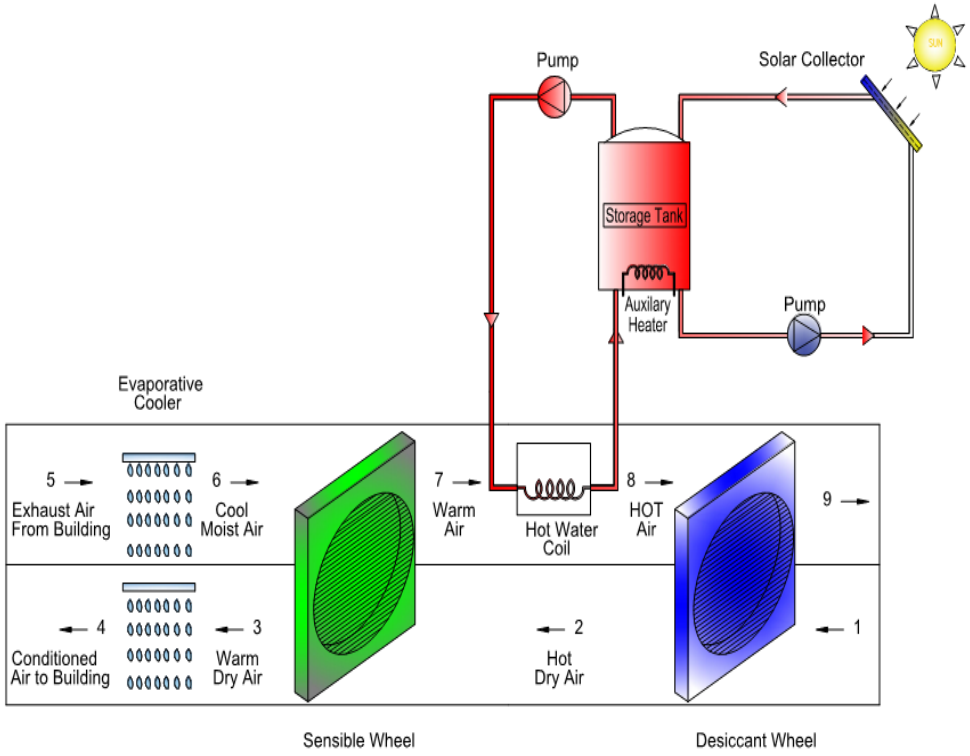

Figure 2.8 Schematic of a Solid Desiccant Cooling System

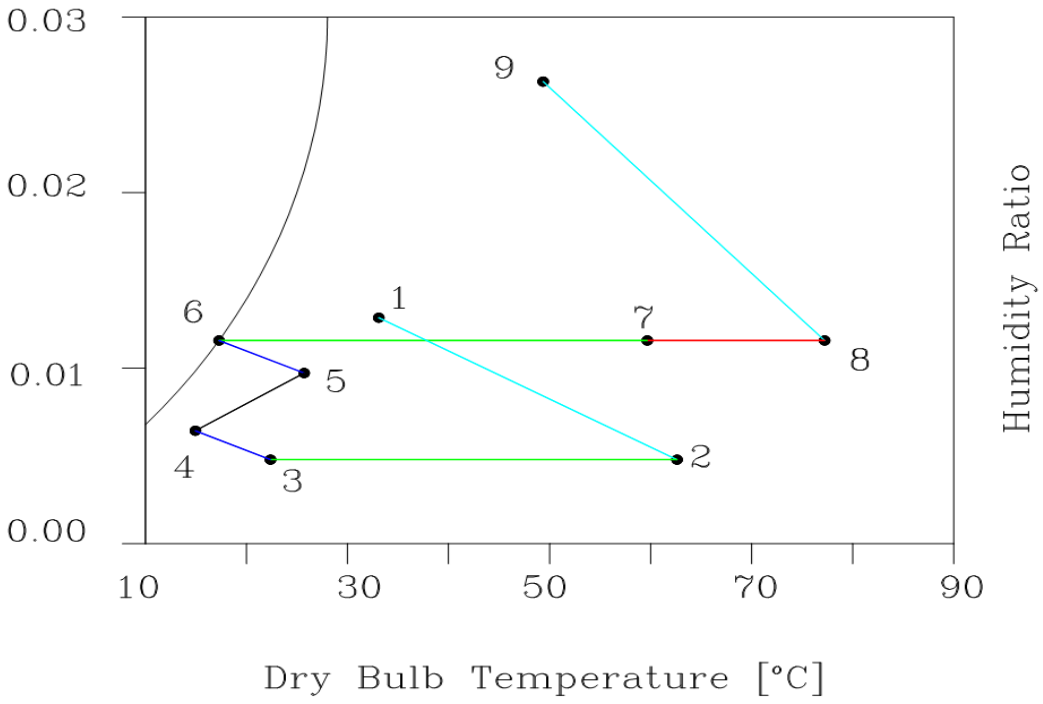

Figure 2.9. Psychometric Chart of a Solid Desiccant System Process.

Working principle of solid desiccant Wheel:

(1-2) Dehumidification process by adsorpting the water in the desiccant wheel, the air enter the wheel is Warm and humid, so the humidity ratio decreases and dry bulb temperature increase.

(2-3) Sensible cooling of the supply air in sensible wheel.

(3-4) the air is humidified and further cooled by evaporative cooler, the required room temperature and humidity can be set by using controller on supply air stream.

(5-6) the exhaust air stream from the air conditioned space is humidified by evaporative cooling to achieve the full cooling potential needed in sensible wheel

(6-7) the exhaust air is heated up in sensible wheel, the cold side of the wheel moved to supply air side to achieve the required cooling.

(7-8) the air pass through the regenerative heat coil and air temperature

increased. The hot water received from dedicated solar collector in a comparatively low temperature around 70 °C.

(8-9) the desiccant wheel has to be regenerated to keep the system operate continuously for dehumidification process, so the humidity ratio increased and dry bulb temperature decreases of the exhausted air.

The solar system consist of solar collectors and a hot water storage to maximize the utilization of the solar system. Auxiliary water heater is needed to maintain continuous operation during the night and when the solar source is not available or enough.

Standard desiccant wheel might not be efficient in coastal areas where the outdoor air is very hot and humid as the system will not be able to reduce the humidity to level which evaporative cooling can work efficiently. Therefore, more complex design can be implemented to overcome this problem.

Henning [52], Simulated a solar assisted solid desiccant system with solar collector (20 m^2 Area) and storage tank (2 m^3 volume). The results showed that a 54% collector efficiency, 0.6 COP and 76% solar fraction (auxiliary energy supplied).

Henning [53] Investigated a solid desiccant cooling system, the result showed that the maximum COP was about 0.7.

2.2.2 Closed Solar Cooling Sorption Cycle. Closed cycles are divided in two categories based on the sorption material as follow:

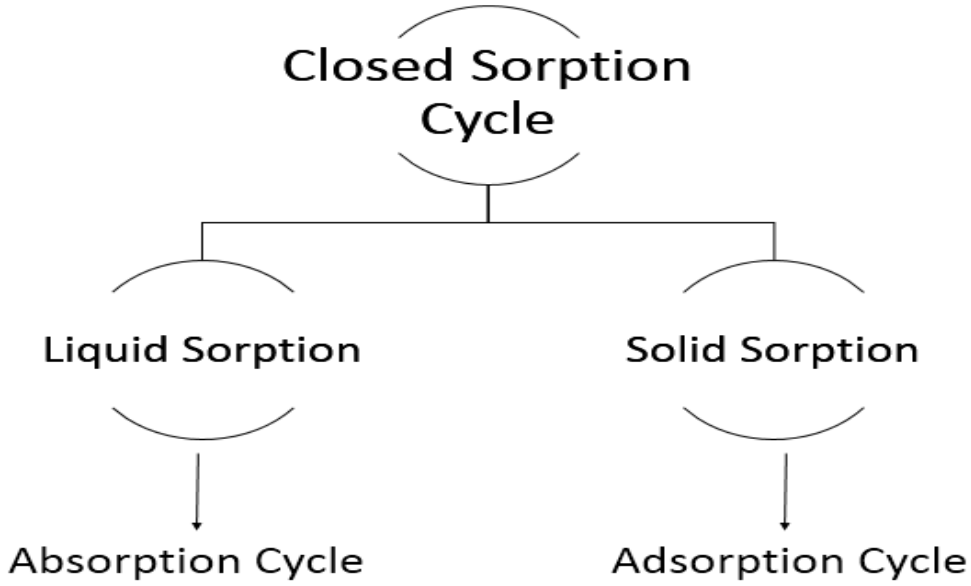

Solar Cooling Absorption systems.

Absorption refrigeration cycles require hot water from either waste heat source, solar collector or boiler to separate a water refrigerant from a mixture of LiBr/Water in the generator.

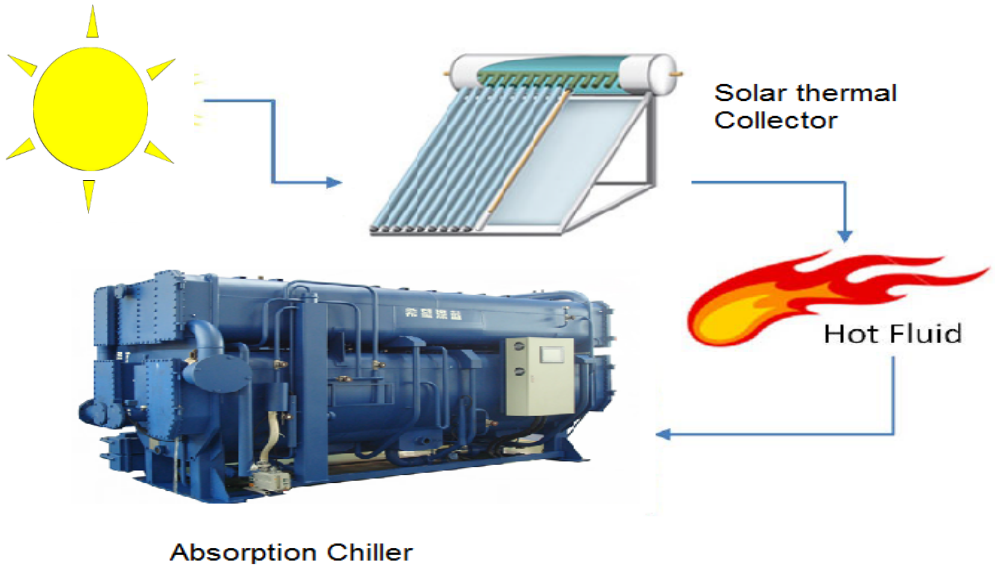

Figure 2.10 Thermal Solar Cooling Absorption System.

The history of an absorption cycle started in the 1700's. It was used to produce ice by an evaporation of pure water from a vessel placed within an evacuated container with sulfuric acid, [54, and 55].

Ferdinand Carre [56] developed machine using water/ammonia as the working Fluid in 1859 while as system using LiBr/H_2O as the working fluid was developed in 1950 .

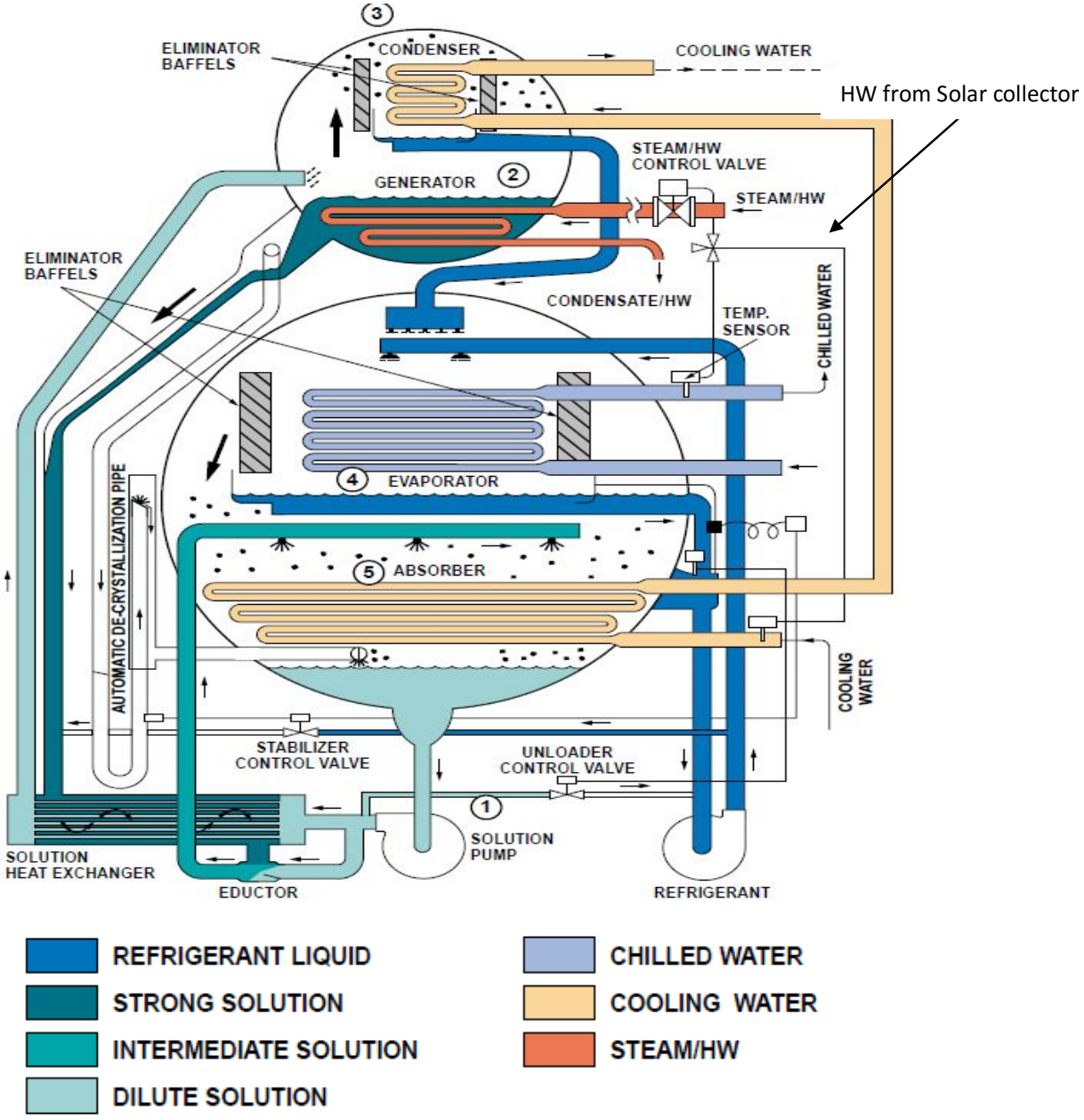

Figure 2.11. Schematic of a solar absorption system. [38]

The working principle of a solar assisted absorption refrigeration System as follow:

Solar Energy Conversion System:

The solar collector converts the solar energy from sunlight to thermal energy, The Thermal energy is then passed through high temperature energy storage tank then to the absorption system.

Evaporator:

The building load is taken in the evaporator, as the water evaporate and the water vapor will pass to absorber. Inside the evaporator, relatively warm return water from the chilled-water system flows through the tubes. An evaporator pump draws the liquid refrigerant from the bottom of the evaporator and continuously circulates it to be sprayed over the tube surfaces. This maximizes heat transfer.

As heat transfers from the water to the cooler liquid refrigerant, the refrigerant boils (vaporizes) and the resulting refrigerant vapor is drawn into the lower pressure absorber. Physically, the evaporator and absorber are contained inside the same shell

The vacuum is created by hygroscopic action due to the strong affinity lithium bromide has for water makes the refrigerant to move to absorber.

Absorber:

The Lithium bromide absorb the water and form weak solution then it is passed to the generator through intermediate heat exchanger.

Absorber types used for Lithium bromide-water system is absorption of vapor refrigerant into a falling film of solution over cooled horizontal tubes [57– 64].

Generator:

The hot water used to separate the weak solution form water vapor and form strong lithium bromide solution, then the water vapor is passed to the condenser.

The hot water provided from Low-grade heat source can be upgraded by using solar energy [65], power plant waste heat or other industrial application [66, 67]. The absorption heat source performance with various working fluids has been investigated; LiBr/water [68], Dimethyl Formamide (DMF)/R21 [69-74].

Heat Exchanger:

The strong solution of lithium bromide is passed to the absorber through heat exchanger after the separation in the generator. The weak solution from the absorber is pumped through the same heat exchanger to the generator, so the temperature of weak solution increased while as the strong solution temperature decreased.

Condenser:

The cold water from cooling tower used to remove the heat and condensate the water vapor, then the liquid water will enter the expansion valve.

Cooling water from cooling tower:

Cold water supplied from cooling tower used to remove the heat from condenser and absorber then the heat is dissipated in the cooling tower to outside.

Auxiliary heat source:

The auxiliary heat source is needed when sun is not shining or solar energy source is not enough to main continuous operation.

Performance of Absorption Solar cooling system:

$$COP = \frac{Cooling\ Capacity\ at\ evaproator}{Heat\ Input\ at\ Generator\ +\ Pump\ Required\ Power}$$

The performance of Absorption solar cooling system depends mainly on thermodynamic properties of the working fluid [38].

Working Fluid in Absorption Solar cooling system:

The most common working Fluid are LiBr/H_2O where Water is the refrigerant and LiBr is the absorbent and H_2O/ammonia are widely used in absorption systems where ammonia (NH_3) is refrigerant and Water is the absorbent.

Marcriss discussed all possible working fluids that can be used in absorption solar cooling systems, he found that there are 40 refrigerant compounds and 200 absorbent compounds available to be used in absorption refrigeration systems. [73].

H_2O / NH_3 thermodynamic properties can be obtained from [74–78].

LiBr/H_2O thermodynamic properties can be obtained from [79–83]. A corrosion inhibitor may be added to LiBr/H_2O as [84–87] or to enhance heat & mass transfer performance [88–92].

Many research has been carried out to investigate the thermodynamic properties of new working fluid like fluorocarbon refrigerant with number of organic solvents, Research on these kinds of working fluids may be obtained from the literature [93–98].

Ghaddar [99] investigated a solar assisted absorption system located in Beirut. The results showed a minimum collector Area for each ton

refrigeration is 23.3 m^2 and with best water storage tank size varied from 1,000 to 1,500 L for seven hour of operation on solar energy.

Hammed and Zurigat [100] Studied the performance of solar assisted absorption system with 1.5 ton cooling capacity, 14 m^2 solar collector and Shell and tube heat exchangers. The test carried on April and May in Jordan and the test result showed actual COP around 0.55.

Florides [101], designed a solar cooling system to handle the house load for whole year, the system consist of a solar collector storage tank, an auxiliary water heater and a LiBr/water absorption system. Selection of solar collector area can be decided through economic analysis without compromising of the system performance.

Hammad and Audi [102] simulated the performance of a non-storage solar assisted absorption system without storage tank. The results showed a maximum ideal COP of the system to be equal to 1.6 while the peak actual COP was 0.55.

Boehm [103] developed a solar assisted absorption system (single-effect with ideal cooling capacity of 10 ton) with storage tank (0.45 m^3), solar collector (63.7 m^2). Economic analysis was performed for this system and the result showed reduction from $3,448 to $1,737 annually more than the normal 8 ton vapor compression refrigeration system. The analysis showed the payback periods is 1.5 to 3 years based on the performance of the solar collector and rate of electricity difference. The system showed capability to supply more than 5.5 ton of actual cooling continuously for 8 hours on a summer day.

Table 2.3 Comparison between Vapor Absorption Refrigeration with Vapor Compression Refrigeration System:

Attribute	Vapor Absorption	Vapor Compression
Method of compression.	Absorption of the refrigerant by the absorbent like LiBr absorbed water vapor and circulating pump used to raise the system pressure.	By Compressor.
Power consumption devices	Circulation Pump, the power consuming device is very less compared to compressor.	Compressor is the major consuming of electricity.
The amount of power required	Requires very small amount.	Requires large amount.
Type of energy required	Runs mainly on the waste heat in the plant or using hot water from solar collector or hot water from boiler.	Runs by electrical power, either from main grid or any renewable energy source like solar, wind or geothermal energy.
Running cost	Relatively Very less as it depends if waste heat or renewable energy source.	Relatively Very high as it depends on electric power.
Foundations required and noise	Relatively less noisy and does not require strong foundation.	Relatively more noisy and require heavy foundation.
Maintenance	Requires little maintenance for small pumps that fails rarely.	Compressor requires a maintenance.
Capacity control	Step less capacity control and zero capacity when there is no demand.	Stepwise capacity control by compressor, it consumes power even there is no demand.

Type of refrigerant used and its cost	Ammonia and water which are cheap refrigerant.	Halocarbons refrigerants, which are very expensive refrigerant.
Leakage of refrigerant	The leakage very less.	There is leakage relatively more than absorption system as the system pressure more.
Greenhouse effect	No refrigerant produces the greenhouse effect, it is guaranteed for future use.	Most of the halocarbon refrigerants are producing greenhouse effect.
Initial capital cost	Very High compared to vapor compression.	Very less compared to vapor absorption.
Corrosive nature	LiBr is corrosive and it will reduce the life span of the system.	No corrosive material and it has longer life.
Low working pressures	Very low and no need for expansion valve.	Can work at low pressure.
Coefficient of Performance (COP)	It's relatively low, a range 0.8 ~ 1.1.	It's relatively higher a range 4~5 and can be higher if the system combined with evaporative cooling.
Heat rejection	Heat rejection factor is high and it can be around 2.5, and heat rejection will be from condenser and absorber.	Heat rejection only from the condenser, so the heat rejection factor is small, which is about 1.25
Capacity	The system can be design for capacity higher than 1,000 tons of refrigeration in a single units.	The system can produce up to 2,500 tons of refrigeration in a single unit (Centrifugal chiller).
Sound Pressure Level	Relatively Low.	Relatively high and can be more than 80 dB (A).

Adsorption cooling system:

Adsorption cooling is a one of thermal driven system. The energy source can be either solar energy or waste heat from power plant.

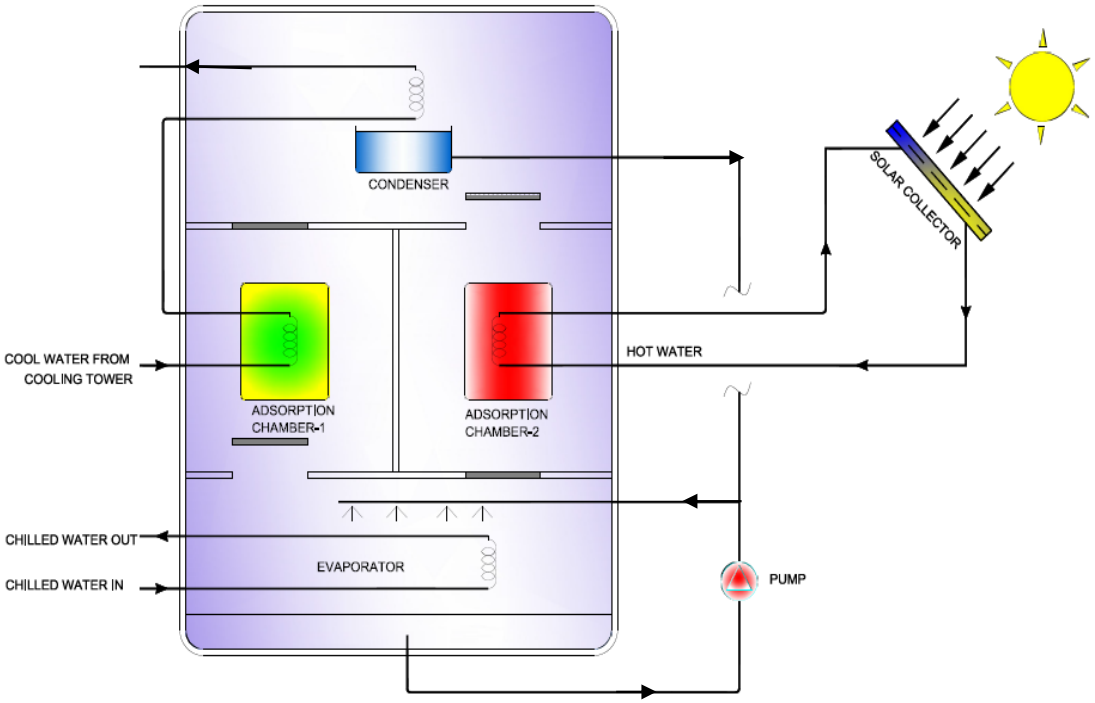

Figure 2.12. Schematic of Solar Adsorption System.

Figure 2.12 shows the major components of adsorption refrigeration system which consists of a thermal compressor, condenser, evaporator and expansion valve.

The operation principle of an adsorption cooling device can be described as follows:

Solar Heating System supply hot water to regenerate the sorbent in chamber 2, the hot water can be supplied from the external heat source like waste heat. The silica gel desorbed by hot water. The water vapor from the sorbent flows to the condenser where it is then condensed to a liquid state.

The condensed water with high pressure flows through tubes and after reaching pressure level equal to that in the evaporator, so the water enters the evaporator where a system of nozzles is spraying water on the tubes of chilled water system.

The water vapor entering from evaporator to adsorption chamber 1 through open valve at the bottom of the chamber. However to ensure vapor flow towards the reactors (adsorbers), the pressure inside the chamber should be lower than that in the evaporator, therefore the chamber precooled and the cooling required to remove the heat added by the adsorption process.

If the adsorbent in the adsorption chamber is fully saturated with water vapor, the chambers function is switched over.

The process in adsorption system can be summarized as follow:

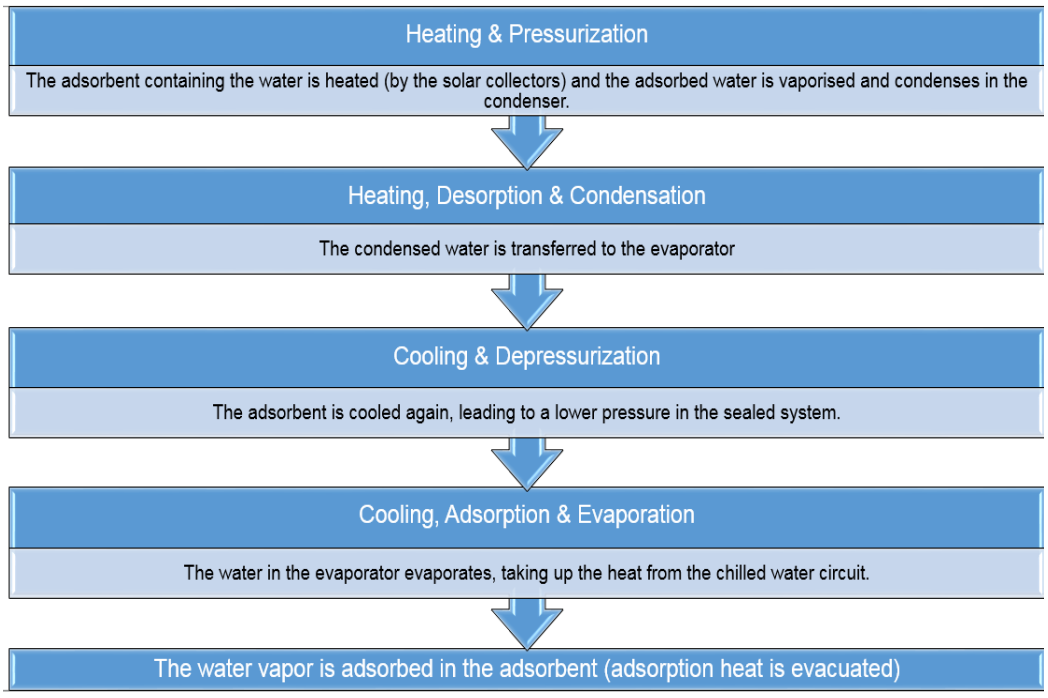

The below table and figure shows the difference between absorption and adsorption as follow:

Absorption is when one molecule completely enter inside of a volume of other molecules. It becoming a part of it. This can be a chemical (reaction) or physical process.

Absorption occurs when the physical state of the molecules have changed as a gas turns into a liquid, or a liquid into a solid.

For example, LiBr can be absorbed into water – this is an example of a chemical absorption since a reaction occurs. Another example for a physical absorption is air dissolving into water, this is since the air is entering into the water, driven by pressure difference.

Adsorption, is a surface process when one molecule not entering completely inside of a volume of other molecules, its only attracting the molecules of a substance on the surface of a liquid or a solid that increasing the concentration of the molecules on the surface.

This can be a chemical reaction (Chemisorption) chemical bonds used in sticking the adsorbate to the adsorbent or physical process (Physisorption — Van der Waals interactions).

For example, The CO_2 molecules just sit on the surface of the solid adsorbent.

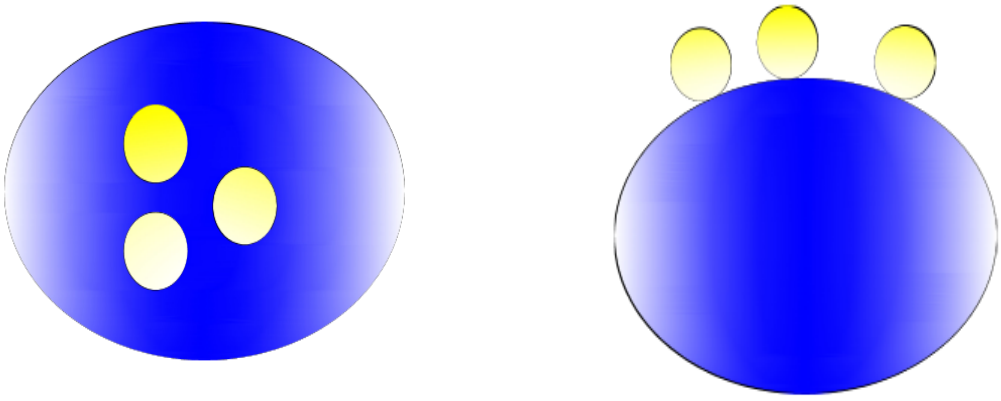

Absorption Adsorption

Figure 2.13. Difference between Absorption and Adsorption

Table 2.4 Comparison between Absorption and Adsorption systems:

Comparison Criteria	Adsorption System	Absorption System
Initial Cost	Almost similar	Almost similar
Phenomenon	It is a surface phenomenon	It is a bulk phenomenon
Heat exchange*	Exothermic process	Endothermic process
Temperature	It is favored by low temperature	It is not affected by temperature
Rate of reaction	It steadily increases and reach to equilibrium	It occurs at a uniform rate
Concentration	Concentration on the surface of adsorbent is different from that in the bulk	It is same throughout the material.
Example	(i) Water vapors adsorbed by silica gel. (ii) NH_3 is adsorbed by charcoal.	i) Water vapors absorbed by anhydrous $CaCl_2$. (ii) NH3 is absorbed in water forming NH_4OH
Continuous Operating	More than 8,000 hours per year	Require daily shutdown for dilution of lithium bromide solution.
Life Span	The silica gel up to 30 years.	10 years.
Maintenance	Replacement vacuum pump every 5 years, annual cleaning of condenser tubes.	Require more preventative maintenance for pumps, heat exchanger replacement, controls, and air leakage.
Refrigerant	Water	Water or ammonia.

Adsorbent/absorbent	Silica Gel	Lithium bromide or water
COP	0.7 ~ 0.8	0.8 ~1.1
Corrosion	None.	Lithium bromide are corrosive in nature.
Crystallization	None.	Yes, can occur in Low temperature cooled water.
Frequent Replacement Adsorbent/absorbent	Not necessary	Every 5 years.
Required Hot Water Temperature	Variable 50 to 100 ^{o}C	Variable 80 to 120 ^{o}C, Back-up heat is required if the temperature below 80 ^{o}C to prevent crystallization.
Cooling water Requirement	30 to 4 ^{o}C, lower temperature increase system capacity	It should be between 18 to 30 ^{o}C.
Chilled Water Output	3 to 9 ^{o}C.	Higher than 9 ^{o}C.

*An **endothermic** reaction occurs when energy is absorbed from the surroundings in the form of heat. Conversely, an **exothermic** reaction is one in which energy is released from the system into the surroundings.

Chemical and Physical adsorption

Adsorption and chemical reaction adsorption cycles are similar to each other. The difference between these cycles is the processes which occur in the cycles. The force causing the adsorption process is a physical adsorption force; and the force causing the chemical adsorption process is a chemical adsorption force. Differences between both types of adsorption processes are described in Table 2.5.

Table 2.5 Comparison between Physical and Chemical adsorption.

Attribute	Physical adsorption	Chemical Adsorption
Adsorption process Forces	Van Der Waals Force.	Covalent or ionic bonds, these forces are stronger than van der waals force.
The thermodynamic operation of the cycle.	Reversible process, heat is required to increase the temperature of adsorbent and complete adsorption and desorption cycle.	Very difficult to reverse. More heat is required to complete the cycle, and more heat is required to achieve high efficiency of reaction.
Working Media	Several pairs can be used: ▪ Activated carbon / methanol or ammonia. ▪ Silica gel / water.	Several pairs can be used: Ammonia Salts with alkaline compounds. Hydrogen and Methal hydrides.
Number of the adsorbers	One is enough for the base cycle, the number can be increased in order to enhance the efficiency.	Two are required.

No moving parts and low evaporation temperatures during operation is the main advantages of chemical reaction cooling system. While as low COP, high weight of adsorbent makes it not sufficient for large application.

System design complexity due to adsorber volume change through chemical reaction and difficulty to achieve system tightness during operation at low pressure and temperature, all the above demerits limiting its use.

Lemmini [104] investigated the performance of adsorptive solar assisted cooling system and compare it with normal solid adsorption system. The comparison proved that the performance of solar powered system highly depends on the absorptivity of the solar collector and the insulation on the back side of the solar collector.

Pons and Guilleminot [105] carried out a study on solar assisted solid adsorption ice maker. The result revealed clearly the system COP is 0.12 which makes this machine one of the highest efficient solar ice makers.

Wang et. al. [106] investigated a solar assisted adsorption system with activated carbon and water with solar collector (area 2 m^2), the result showed that the system are able to produce daily 10 Kg of ice with 90°C hot water (around 60 kg).

Energy Storage in Solar Cooling System:

Schweigler et al. [107] modeled solar assisted absorption system with phase change material (PCM) for latent heat storage in order to guarantee a low operating temperature of the system. In the study, the latent heat storage was based Calcium Chloride Hexahydrate, whose melting temperature starting from 27°C up to 29°C. Standard lithium bromide and water absorption system cannot provide cold chilled water at 6°C/12°C with LiBr/Water system but in this system the condenser and absorber were air cooled combined with PCM latent storage, so the

system can provide 6 /12°C of chilled water from the absorption system due to reduction of the temperature of the rejected heat by 5°C to 8°C.

Solar Refrigerant Cooling System

Refrigerant is circulated by the compressor to the condenser through water-refrigerant brazed plate heat exchanger, the hot water is supplied from the solar collector to increase the temperature of refrigerant.

The heated refrigerant is hot and at high pressure due to expansion and the further increase in the temperature and pressure reduced back pressure on the compressor, this phenomena will increase the cooling capacity of the system without increasing the power consumption resulting in high COP.

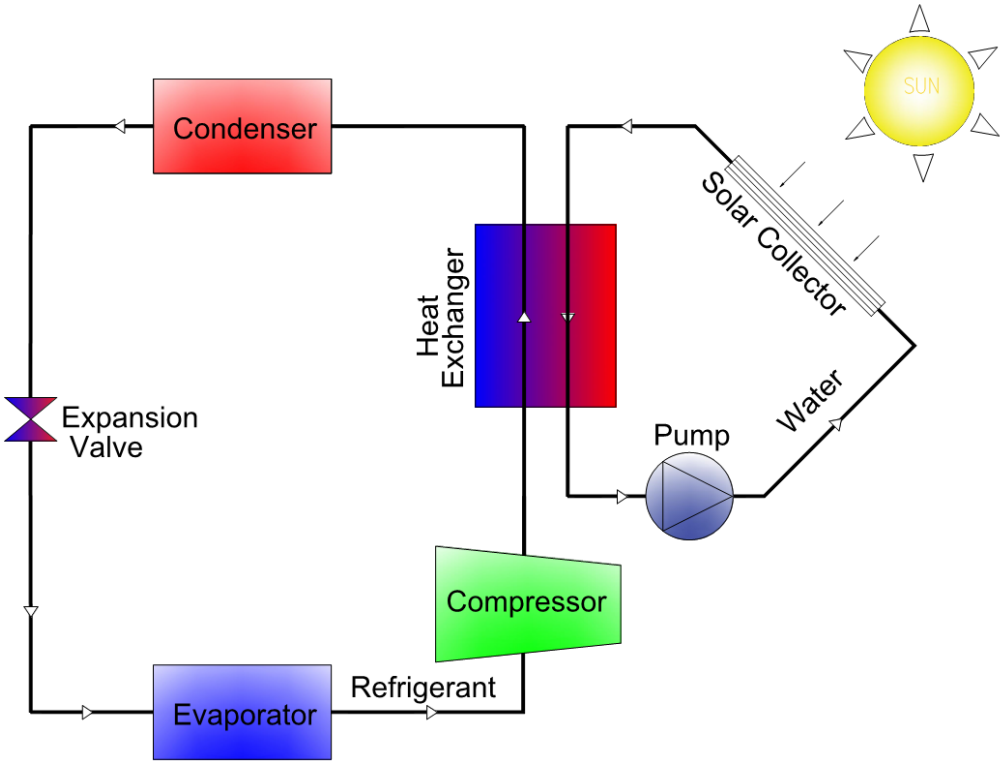

Figure 2.14. Schematic of Solar refrigerant Cooling system.

2.2.3 Thermo-Mechanical Solar Cooling.

Unlike conversion solar energy to thermal energy, in the thermo-mechanical system the solar energy converts to the thermal energy then converted to the mechanical power which can be used to provide the required cooling.

Steam Ejector Cycle.

Steam ejector cooling is one of the popular thermo-mechanical cooling system used in refrigeration and air conditioning, the system consist of solar collector, generator, condenser, evaporator, expansion valve, ejector and pump [108].

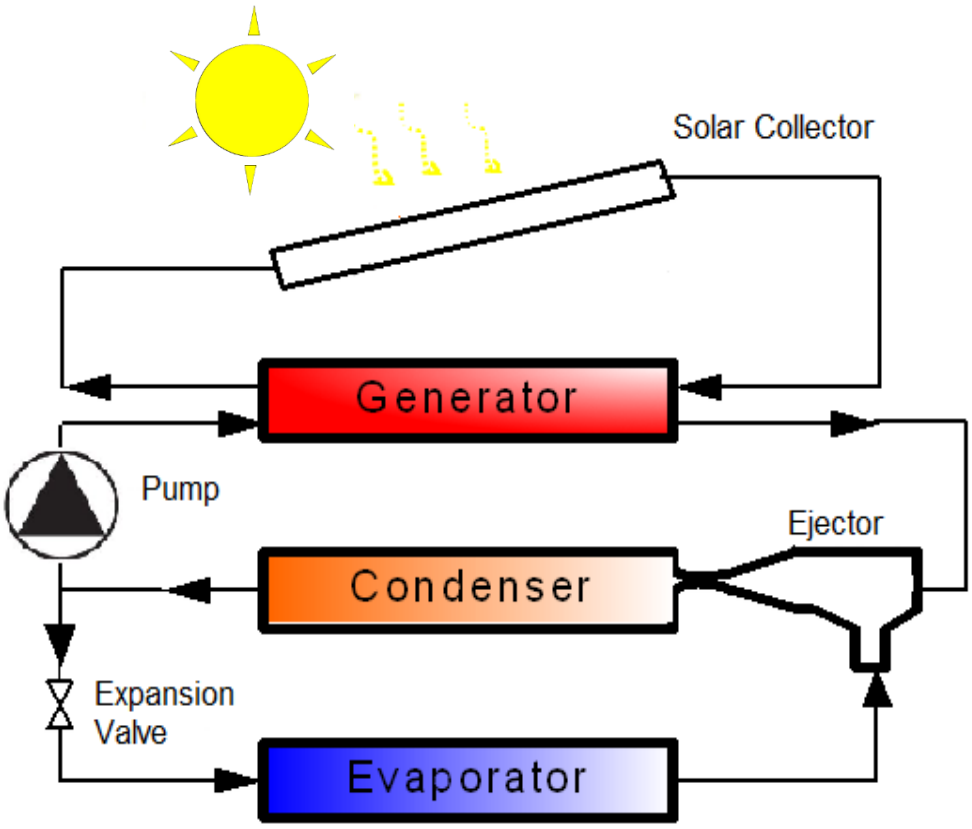

Figure 2.15. Schematic of ejector refrigeration system.

The working and operation principle of ejector cooling system are described in Figure 17. The saturated vapor primary fluid (can be water or other refrigerant) enters the nozzle of the ejector at high pressure and temperature supplied from boiler or generator.

This primary fluid expand and leaves the nozzle at a very high velocity and a low pressure which draws working fluid vapor (secondary fluid) from the evaporator and maintains the vacuum necessary for operation. When the mixing of the two streams is completed, the pressure increased in the diverging section and the mixture slow down, the ejector will be able to discharge the mixture of primary and secondary fluid at a pressure that is higher than the entering pressure. So, the ejector is boosting the pressure of the primary entering fluid.
A low energy grade energy source that can be used for this system and low cost of operation and construction are the main advantages of steam ejector solar cooling system, while as high initial cost, low COP, complicated design of the ejector and the difficulty to operate in a wide range of ambient temperatures are the challenges in this system.

Wang et. al. [109, 110] performed a study of ejector cooling system consist of multi-function generator that provides the required hot water for ejector cycle operation and can work as heat pump. In this study R141b considered as working refrigerant and the ejector design modified to work with other refrigerant like R365mfc to enhance COP of the system and R141b phased out, and R365mfc ODP was close to zero. The ejector cooling system with multifunction generator operating at full-cycle using R141b and the cooling capacity of 0.75 kW, ejector area ratio of 7.73 at 90 ^{o}C generator temperature, condenser temperature 37 ^{o}C and evaporator temperature 8.5 ^{o}C. Operating coefficient of performance can reach 0.225 at full cycle while using R141b therefore it conclude that

R365mfc can replace R141b without affecting the system overall efficiency and performance as long as the design of ejector optimized.

Pollerberg [111] investigated solar assisted steam ejector chiller for whole year in Bochum, Germany. The system includes experimental step with cooling capacity 1 kW and two types of collector a parabolic trough (PTC) and a vacuum tube collector (VTC). The effect of the operating temperatures and pressures on the efficiency of the solar collectors and the COP of the system are studied. Then, the annual mean efficiency of the solar collector, the annual mean COP of the solar ejector cooling system are determined by using simulation tools as well the annual mean total efficiency of the system for different locations worldwide are investigated. The direct horizontal solar radiation reached maximum value of 550-600 W/m^2, absorber area of 10.5 m^2, COP of the system investigated based on condenser temperature ranging from 15-35 ^oC and evaporator temperature of 7, 13 and 17 ^oC, with decreasing condenser temperature and increasing evaporator temperature COP of the system rises.

The simulation result showed that the PTC are more suitable for large application and collector fields and the ratio of direct insolation to global insolation for a particular zone had influenced on the economy aspect of the system.

Many researchers carried out experimental study [112-122] to investigate the performance of steam ejector refrigeration system with different working fluids and characteristic. A numerical study [123,124] also performed to find the optimum design condition of steam ejector refrigeration system. Good results were obtained from these numerical study such as better pressure recovery for small diffuser angle, the weight fraction recovery was higher for low angle and smaller droplet size yield to better diffuser performance.

Selvaraju et. al. [125] investigated the performance of vapor ejector refrigeration system when the ejector operates at choking-mode. When operating conditions are changed, the critical performance parameters of the system get shifted to different critical values. The effect of factors studied in this paper were a specific heat of the working fluid and friction at the constant-area mixing chamber and internal irreversibility of the ejector to validate the model, the effect of compression ratio, driving pressure ratio on the critical entrainment ratio and critical COP of the ejector system are studied. The result from simulation compared with the experimental data from the literature, the effects of operational parameters and ejector configurations of the system are studied and find out the effect in the performance. The results showed decreasing the entrainment ration and COP due to increase compression ration while as entrainment ration and COP increases with rising driving pressure. Also, comparison of performance of the system with environment friendly refrigerants, R134a, R152a, R290, R600a and R717 is made. Among working fluid considered, the system with R134a gives better performance.

Solar Combined Power/Cooling Systems:

The solar energy can be converted to thermal energy that drive power generation device therefore the produced power can be used to run refrigeration cycle which provides the required cooling and refrigeration effect.

Goswami and Lu [126] made first law efficiency analysis of the combined power and refrigeration cycles, the system includes the solar collector can supply hot water at 90°C temperature. The results showed that thermodynamic efficiency (first law) reached maximum 15.7% and minimum 10.5% based on the ambient temperature variation from 7°C-27°C.

Rankine cycle and a vapor compression cycle can be combined together. It uses the high-pressure vapor fluid to drive a turbine in the power cycle. Consequently, work from the turbine drives the compressor in the refrigeration cycle. Many option of working fluid can be used in rankine cycle.

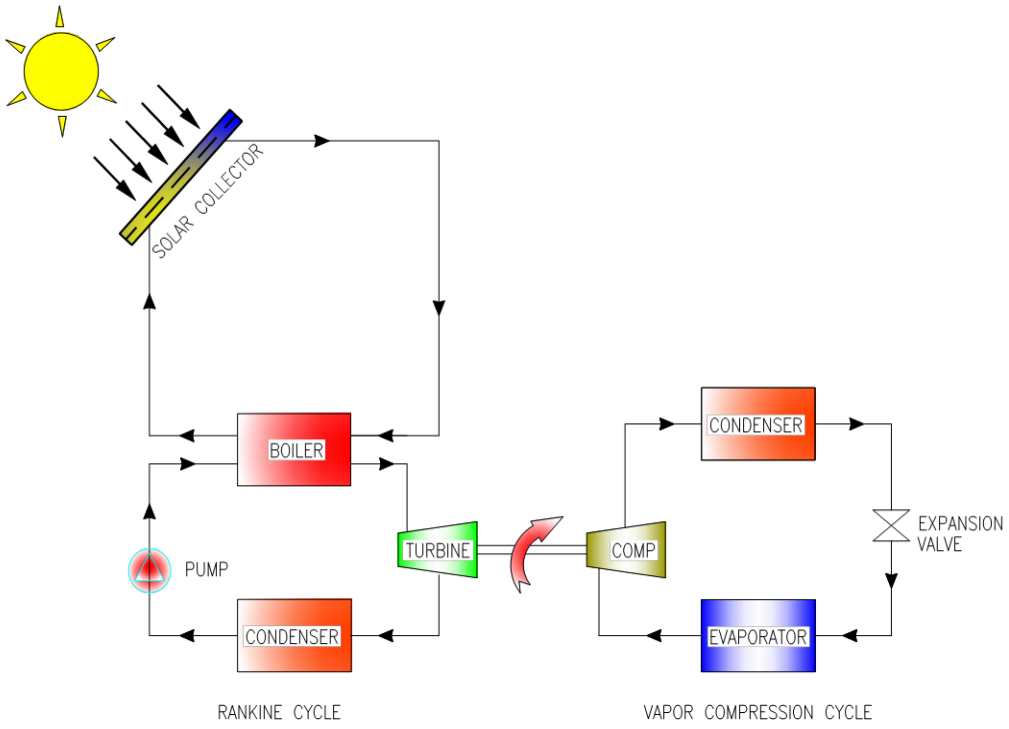

Figure 2.16. Combined Rankine and vapor compression cycle.

The COP of the refrigeration cycle is as high as that of conventional vapor compression systems powered from grid electricity but the efficiency of the power cycle is quite low (about 10%). This system is quite complex and only suitable for large air conditioning applications.

Solar Rankine air-conditioning systems were suggested in the united States in 1975-1980 during the oil crisis. Numerous efforts have been

made to develop similar solar cooling systems. The systems were not economically competitive compared with conventional systems.

Wali, [127] suggested that only halocarbon compounds and the fluorinated compounds fulfilled safety requirements. Subsequently, the working media which were previously recommended, were found not to be environmentally benign. Thus, the development of this system was detained until interest returned in the 21st century with new proposed cycles combining power and cooling cycles.

Kane, Larrain et al.,[128] proposed an Organic Rankine Cycle (ORC) including a hermetic scroll expander-generator and solar tracking equipment.

The advantages of Combined Rankine and vapor compression cycle are suitable for high capacity systems and suitable for integration into poly generation systems (heat, electricity and refrigeration).

High installation cost, large system and Regular maintenance required due to complications and many moving parts reduce the demand of this system.

Triple-Effect Refrigeration Cycle

Agrawal et. al.[129], investigated the triple effect refrigeration cycle with a cascaded vapor compression cycle (N_2O natural refrigerant), absorption cycle (LiBr/Water system) with an ejector refrigeration cycle. The main disadvantage of N_2O is its higher GWP compared to other refrigerant, however it is significantly more favorable in terms of toxicity.

The results showed that some influenced factors as waste flue gas temperature, ejector evaporator temperature, turbine inlet and outlet pressure and discharge pressure of the compressor are having significant effects on the refrigeration outputs of proposed cycles in term of exergy efficiency and thermal efficiency.

Fan et al. [130], investigated of a solar assisted ejector-absorption technologies and shows the other feature that these cycle can be used

for, not only to provide the required cooling and refrigeration effect but can be used for environmental protection.

Abdul Khaliq et al. [131], performed energy and exergy analyses of a triple effect solar assisted refrigeration system. The results clearly revealed that thermodynamic investigations based on energy analysis is not enough and the exergy analysis must be considered to find out the imperfection component and work it out to enhance the system overall performance.

Rajesh Kumar et. al. [132], performed the thermodynamic analysis of a solar assisted multi-effect refrigeration cycles. The result showed that highest irreversibility occurs in the central receiver and the heliostat field represents the second highest irreversibility. Furthermore, the first law efficiency is 11.5% while as second law efficiency is 2%, these results are another proof that the first law analysis is not accurate alone and hence, more accurate analysis shall be considered the second law analysis.

2.3 Solar Cooling Technologies Comparison based on driving temperature:

The solar thermal cooling technologies performance change based on the hot water temperature.

The Thermal-Driven system consists of three kinds of solar system types including flat plate collector, delivering output temperature of around 70 ºC to 100 ºC, evacuated tube collector, delivering temperature in the range of 100 ºC to 150 ºC, and Concentrating Solar Collector, delivering temperature of over 150 ºC. The heat generated by the panels will be transmitted into the heat transformation cycle and produce two ranges of temperature, 8 ºC fits for air conditioning system and 0 ºC to 8 ºC which is applicable for food and vaccine preservation as shown in figure 2.17.

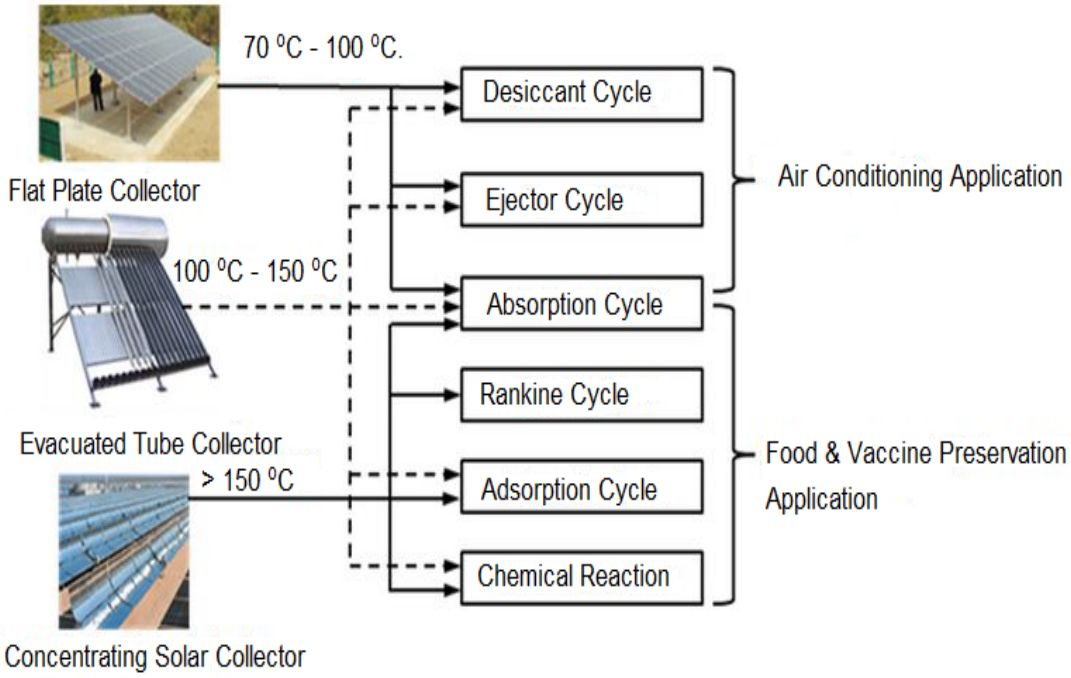

Figure 2.17. Solar Collector temperature ranges serving different Cooling application

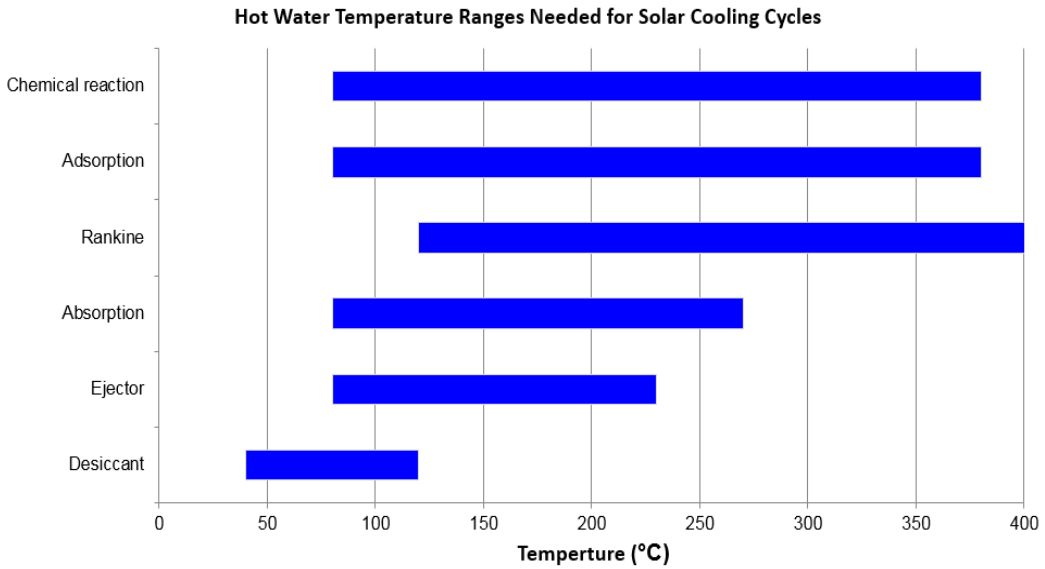

Figure 2.18. Solar Collector temperature ranges serving different Cooling Cycles

The below graph shows the serval technology COP by varying driving hot water temperature.

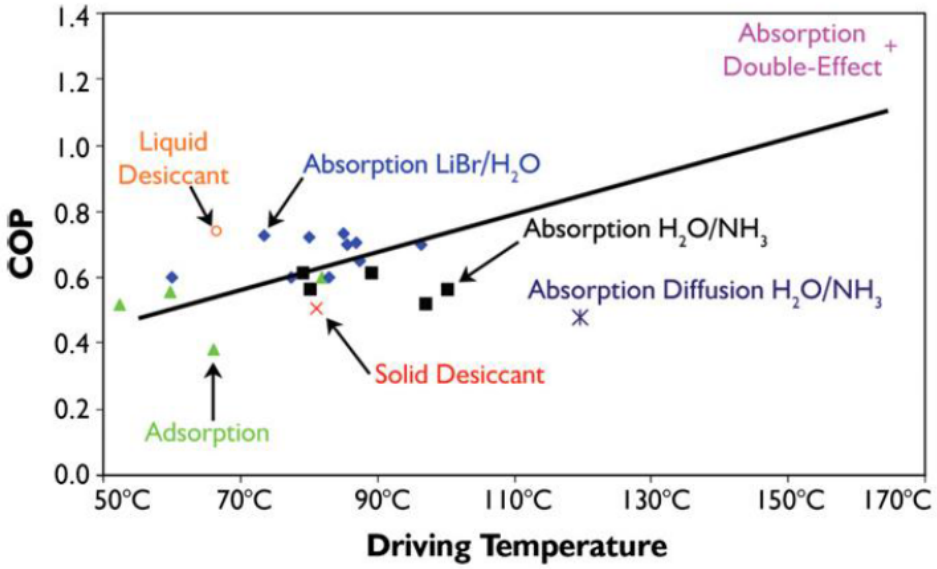

Figure 2.19. COP of Different solar cooling technologies and hot water temperature [133,134].

Table 2. 6 some common used solar cooling technologies efficiency and cost ranges for 5 TR AC units (R-22)."

Sr.	Solar Cooling Technology	Cost Range per 5 TR AC unit	COP
1	Solar Assisted Vapor Compression System	$10,503 [137]	3-6 [135-136]
2	Solar Assisted Absorption System ($LiBr/H_2O$)	$20,000 [140]	0.76–0.83 [138~142]
3	Solar Assisted Absorption System (H_2O/NH_3)	$5,000 [144]	0.57–0.62 [138,138,141,142,143,144]
4	Solar Assisted Adsorption System	$20,000 [145]	0.40–0.61 [138,145]
5	Solar Assisted Solid Desiccant System	$25,000 [146]	1.06–1.22 [138,146]

CHAPTER 3
OBJECTIVES, APPROCH AND METHODOLGY

3.1 Objective:

The main objective of the present study is to investigate the thermodynamic performance of a proposed multi-effect refrigeration cycle driven by solar energy. The proposed cycle consists of solar tower system with heliostat field and central receiver which uses molten salt as the heat transfer fluid, Ejector Refrigeration cycle, Absorption Refrigeration Cycle and cascade refrigeration cycle.

The study will consider the conservation of mass and energy along with principle of second law of thermodynamic for measuring the actual thermodynamic performance of a proposed cycle used Dhahran weather data and operating condition.

The following are the specific objectives of the thesis work:

1. To develop the mathematical model for the solar system.
2. To develop the mathematical model for the refrigeration system.
3. To develop the solar and refrigeration integrated system mathematical model.
4. To develop a software to solve mathematical model of the integrated cycle.
5. To optimize the system performance using the developed software to reach at the optimal parameter and operation condition.

3.2 Approch:

The Mathematical model is developed for each component of the proposed cycle.

To solve aforementioned mathematical model, the engineering equation solver software (EES) was used to develop a software which will be to assess different integrating models and cycles. The validation of these models had been conducted against experimental data previously published in the public literature and journal papers.

The parametric analysis conducted to reach optimal condition.

3.3 Problem Statement :

Investigation of the thermodynamic performance of a proposed multi-effect refrigeration cycle had been conducted to point out the effect of some influenced parameter on the overall efficiency of the solar assisted triple effect refrigeration cycle.

The incident solar radiation is hourly and seasonally fluctuating, and as a result the outlet energy from a solar field will also change over time. If there is a need for a stable power outlet from solar thermal power, many strategies may be used. Integrating a triple effect refrigeration cycle with the solar system to provide a compensation effect is one of these strategies.

3.4 Methodology:

A thermodynamic analysis is to be conducted to point out the effect of some influenced parameters on the overall efficiency of the solar assisted triple effect refrigeration system.
The analysis will be conducted by using EES software.

The following methodology will be followed to achieve the objective aforementioned:

1. A complete mathematical model will be developed for each individual component of the system based on first and second law of thermodynamics.
2. Heat transfer model for different components will be developed when needed.
3. A software code will be developed and used to solve the developing mathematical model using the engineering equation solver (EES)
4. The code will be validated against experimental data available in the literature.

5. Detailed parametric analysis will be performed to reach the optimal operation condition.

CHAPTER 4

TRIPLE EFECT REFRIGERATION SYSTEM MODELING

4.1 Description of the Triple-effect Refrigeration Cycle:

Solar Assisted triple effect refrigeration cycle consists of Solar Tower with central receiver connected Steam Rankine Cycle (SRC) providing thermal energy to (ERC) and (ARC), and (CRC) with only solar heat source. Figure 4.1 shows the simplified SRC, ERC, ARC, and CRC cycle.

Solar radiation reflected from the mirror of heliostat field to the aperture area of central receiver (CR) at the top of solar tower where molten salt (a mixture of 60 wt% of sodium nitrate [$NaNo_3$] and 40 wt% potassium nitrate [KNo_3]) used to absorb the solar energy.

The key advantage in using molten salt is that it is of a cheaper solution, good thermal storage and can work effectively for 24 hour operation.

The molten salt is absorbing the thermal energy at central receiver so the temperature of molten salt is increased up to 560 ^oC, then the molten salt will pass through the heat recovery vapor generator (HRVG) (1–2), the thermal energy transfer to ejector refrigeration cycle due to heat transfer in HRVG between hot molten salt in the Rankine cycle and water refrigeration in the ejector cycle.

The temperature of molten salt decreased to approximately 315 ^oC then it is flowing to generator (2–12) to provide the required heat energy to separate LiBr and water.

The molten salt reach to minimum operating temperature which is around 290 ^{o}C before freezing then it flows back to CR to absorb the solar radiation and pass again to HRVG.

The water refrigerant in ejector cycle will become superheated refrigerant vapor (4) after heat transfer take place in the HRVG with molten salt and the superheated vapor is flowing and expanded in a turbine to produce work as this work will be used to run the cascade cycle.

The exhaust (5) steam from turbine is passes through ejector, this steam will be at very high speed which create high vacuum to extract secondary vapor (11) from evaporator -1 (E-1) of ejector cycle.

The primary (5) and secondary fluid (11) are mixed in the ejector's mixing zone. The mixed fluids (6) is flowing to condenser-1(C1) where the condensation process take place as the condenser cooled by means of cold water from cooling tower, the temperature of the mixed fluid reduced.

The mixed stream leaving the condenser will be at saturated liquid (7) and will be divided in two streams (8, 9); the first stream (9) is flowing through expansion valve-1 (TV1), where pressure is reduced to evaporator pressure (10) then the low pressure fluid passes to E1, and the second stream (8) is flowing to HRVG by pump-1(P1) .

The superheated water vapor (13) leaving the generator after separation process, it will cool in condenser-2 (C2) which cooled by means of cooled water from cooling tower.

The water refrigerant leaving the condenser will be at saturated liquid (14) then it will pass through throttle valve-2 (TV2) to generate liquid (15) at low pressure, which passes to evaporator-2(E2).

The water refrigerant leaving the evaporator-2 (E2) will be saturated vapor (16) then it will flow into the absorber. The weak Solution (20), which is a mixture of LiBr-H_2O, flow through heat exchanger from

absorber to generator and due to heat transfer in solution heat exchanger the strong solution will be cooled to (21) and the weak solution will be heated then the strong solution passes through throttle valve-3 (TV3) back to absorber and the weak solution will passes to generator.

The absorber temperature will be maintained at 35 ^{o}C and the same pressure of evaporator-2. The saturated vapor (16) leaving evaporator-2 (E2) and the strong solution (22) are mixed at the absorber and formulate a new mixture (17) which flowing through pump-2 (P2) and solution heat exchanger (SHX) and then finally passes in the generator (19) for separation process.

The power produced from turbine is used to run the compressor-1(COMP-1) and compressor-2(COMP-2) of the cascaded refrigeration cycle (CRC). In order to provide low temperature refrigeration, the nitrous oxide is used as working refrigerant in high temperature cycle as well as low temperature cycle.

Superheated N_2O vapor (29) is compressed (30) in the compressor-2 so the its temperature and pressure increased and then cooled in the cascaded heat exchanger (CHX), to become saturated liquid (31).

The nitrous oxide is flowing in the internal heat exchanger-2 (IHX 2) (32) and cooled further.

The nitrous oxide is then passes in throttling valve-5(TV5) (33). The nitrous oxide is evaporating from state 33 to state 34 to get cooling effect in the evaporator-3(E3).

Nitrous oxide vapor (23) is passes and compressed in compressor 1 (24) and then after that cooled in the condenser-3(C3) (24–25).

Nitrous oxide is passes in the internal heat exchanger-1 (IHX 1) and cooled further. The nitrous oxide (26) is flowing (27) in throttling valve-4 (TV4), its heating up (27–28) in the cascade heat exchanger.

In the current project, a multi-mode thermodynamic cycle is presented for solar power cooling which could produce refrigeration output at various magnitudes at different level of temperature simultaneously.

The cycle can meet out the cooling demand for air conditioning (15^{o}C – 22^{o}C), refrigeration for food preservation (2 ^{o}C – 8 ^{o}C), deep freezing for vaccine preservation and pharmaceutical plants (-50 ^{o}C to -80 ^{o}C).

This cycle employ solar tower technology which will use molten salt as a heat transfer fluid (HTF) and integrates the heliostat field and central receiver with the Steam Rankine Cycle (SRC), ERC, ARC, and CRC.

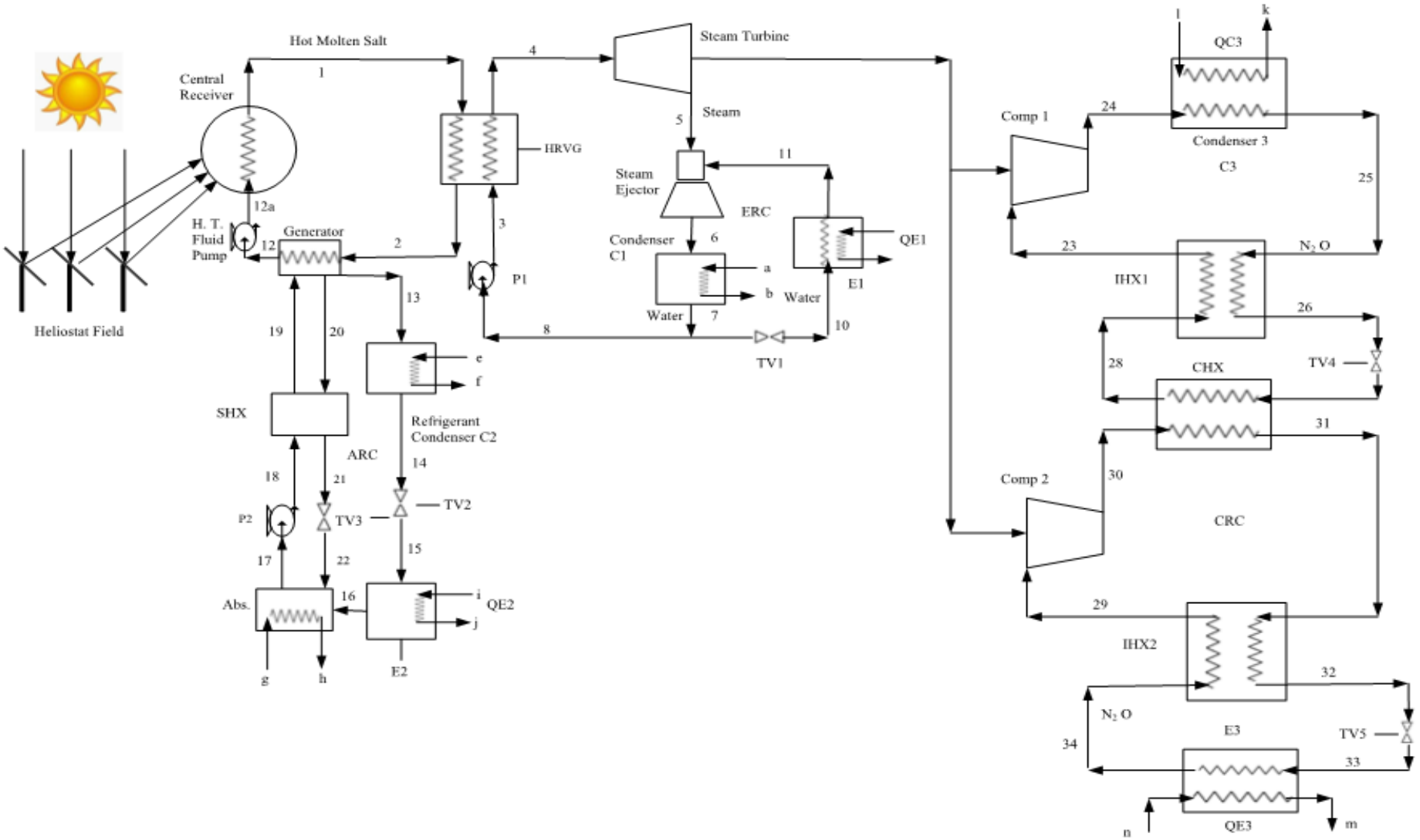

Figure 4.1 Solar Assisted Triple Effect Refrigeration Cycle.

4.2 Main assumption of the triple-effect refrigeration cycle:

Main assumptions have been as follow of the novel cycle.

(1) All components of the triple effect refrigeration cycle considered in steady state.

(2) The pipes pressure drop in in the proposed triple effect refrigeration cycle are neglected.

(3) The heat losses to the surrounding in the Heat recovery generator, steam turbine, all condensers and all evaporators are neglected.

(4) The flow through the expansion valves are isenthalpic.

(5) The condenser leaving state considered as saturated liquid.

(6) The evaporator leaving state considered as saturated vapor.

(7) Solar heat source physical exergies are used only (chemical exergy for solar heat source is negligible).

(8) Chemical exergies, Kinetic and potential of the material are not taken into account in the analysis..

(9) We considered the solution of LiBr are in equilibrium in the generator and absorber are in at standard temperature and pressure conditions.

(10) saturated condition of the solution leaving the absorber and the generator.

(11) The compression process is considered to be adiabatic

(12) Isobaric considered in evaporator, condenser and internal/cascade heat exchanger.

(13) one dimensional and steady state flow in the ejector .

(14) The ejector walls are well insulated.

(15) Saturated condition of the primary and secondary flow when entering the ejector (states 5 and 11).

(16) All flow losses are taken into account by using isentropic efficiencies in the nozzle (ηn), in the diffuser (ηd), as well as in the mixing chamber (ηm).

4.3 Triple Effect Refrigeration Cycles Working Fluids

The criteria of selecting the working fluids in the triple effect refrigeration cycle should be as follow:

- The Working Fluids are environmentally friendly, so it should be zero ozone layer depletion and low global warming potential.
- The working should have good thermodynamic properties for refrigeration.
- The Working fluid should be stable chemical composition, not toxic at certain concentration, not explosive and not corrosive with metal.
- The working fluid should available at low cost.

Table 4.1 Triple Effect Refrigeration Cycle Working Fluid.

Cycle	Working Fluid
Steam Rankine cycle With Solar tower (SRC)	Heat Transfer Fluid/Molten Salt (mixture of sodium nitrate & potassium nitrate).
Steam Rankine cycle With HRVG.	Water (H_2O).
Absorption Refrigeration Cycle (ARC)	Lithium bromide as absorbent and water as refrigerant (LiBr-H_2O).
Ejector Refrigeration Cycle (ERC)	Water (H_2O).
Cascade refrigeration cycle (CRC)	Nitrous oxide (N_2O).

The molten salt (HTF) has many merits. With Molten salt can increase solar field output temperature to 560°C, then it will increase the Rankine cycle efficiency of the power block steam turbine, Molten salts exhibit many desirable heat transfer qualities at high temperatures. They have high density, high heat capacity, high thermal stability, and very low vapor pressure even at elevated temperatures. Their viscosity is low enough for sufficient pump ability at high temperatures, and many are compatible with common stainless steels.

4.4 Desirable Properties of Working Fluids

Table-4.2 Desirable Properties of Working Fluids.

Fluid	Desirable Properties	Reason
Refrigerant	High Latent Heat.	Reduce Mass Flow Rate.
	Moderate Pressure at Condensing Temperature.	Reduce Strength Requirement for Condenser and Generator.
	Relative Low Triple Point.	Limit on evaporating Temperature
	Low Vapor Specific Volume.	Ease of Vapor Transport.
Absorbent	Negligible Vapor pressure.	Negates the vapor separation or rectification requirement.
	High Affinity for Refrigerant.	Greater Affinity means a like hood of high refrigeration capacity in the evaporator.
Solution	Low Specific Heat.	Reduce Solution Heat Exchanger Duty.
	Low Specific Volume.	Reduce Pump Work.
General Properties	Low Viscosity.	Increase Heat Transfer coefficient and reduce pipe work losses.
	Low Surface Tension.	Improve Absorber Operation.
	Low toxicity.	Safety.
	Chemically Stable.	Improves System Life.
	Low Cost.	Economy.

4.5 Hot Molten Salt Properties:

Table 4.3 shows the relevant properties of currently available high temperature heat transfer fluids relevant for CSP applications.

Table 4.3 Currently available heat transfer fluids for CSP applications.

Name	Manufacturer	Components	Melting point (liquids)	Maximum temperature
VP-1 or Dowtherm A	Solutia or Dow Chemical	biphenyl diphenyl oxide	12 °C	400 °C
Hitec XL	Coastal Chemical	sodium nitrate potassium nitrate calcium nitrate	120 °C	500 °C
Hitec	Coastal Chemical	sodium nitrate potassium nitrate sodium nitrite	142 °C	538 °C
Hitec Solar Salt	Coastal Chemical	Sodium nitrate potassium nitrate	238 °C	593 °C

Solar salt (a mixture of 60 wt% of sodium nitrate [$NaNo_3$] and 40 wt% potassium nitrate [KNo_3]) properties can be summarized as follow [147]:

- Density (kg/m^3)=2090-0.636 X T(ºC), the density at 250 ºC is 1,931 kg/m^3 . (4.1)
- Specific Heat (J/Kg K) Cp=1443+0.172 X T(ºC), Cp at 250 ºC is 1486 (J/Kg K) and 550 ºC is 1537.6 (J/Kg K). (4.2)
- The average Cp in this temperature range is 1500 (J/Kg K).
- Thermal Conductivity (W/m K) $k=0.443+1.9X10^{-4}X$ T(ºC). (4.3)

Molten Salt was considered as the most practical salt for molten-salt power tower applications due to the following reason:

- High operating temperature up to (565°C) allows the technology to be used with the most advanced Rankine cycle turbines.

- Lower cost of nitrate salts. However, while as main demerit with Solar Salt is its high freezing point of 290°C compared to other molten salt.
- Molten Salt can store thermal energy while it is in liquid state.

4.6 Triple-effect Refrigeration Cycle working fluid characteristic:

Water which has zero ODP and GWP will be used as working fluid in Steam Rankine cycle (SRC), and as refrigerant in ejector refrigeration cycle (ERC) and absorption refrigeration cycle (ARC), respectively, while N_2O which has zero ODP and moderate GWP will be used as a refrigerant in the cascaded refrigeration cycle (CRC) to produce cooling in the deep freezing range.

Nitrous oxide is selected as working fluid in cascade refrigeration cycle as it has zero ozone depletion potential as well as moderate global warming potential (GWP) in addition to that it is natural refrigerant and can produce cooling in the range of - 60 to - 80^{o}C which is necessary of for some application like vaccine storage.

The main disadvantage of N_2O its higher GWP compared to CO_2, however it is significantly more favorable in terms of toxicity.

The Lithium bromide and water ($LiBr/H_2O$) solution is used as working fluid in absorption refrigeration systems due to the following:

- It is non-volatile and non-toxic.
- Environmentally friendly.
- Low cost fluids.
- Easy handling are the advantages of using water as refrigerant (despite its high freezing point).

While as the disadvantage of $LiBr\text{-}H_2O$ that

- Restricted to applications in cooling requirements are water freezing point (0°C).

So LiBr chillers are mainly used for air-conditioning system rather than refrigeration system. Another disadvantage is that crystallization will occur if LiBr solution is of higher concentration and may damage the machine.

Many control strategies are proposed to prevent crystallization.

Control the concentration of LiBr solution is one of the most important strategy.

Increasing the chilled water temperature settings can avoid crystallization, and the byproducts include improved cooling capacity and COP.

CHAPTER 5

FIRST AND SECOND LAW OF THERMODYNAMIC ANALYSIS OF THE PROPOSED CYCLE

The thermodynamic analysis in term of energy, entropy, and exergy is provided in this chapter. The heat input and rate of exergy can be found by using mass, energy and exergy balances.

Applying exergy approach for solar assisted triple effect refrigeration cycle can provide a better understanding for each component behavior and enhanced tools for improving them.

Exergy analysis clearly indicates the location, nature and causes of energy destruction in a process and therefore can help improve a process or technology.

The primary objective of exergy balance is to provide meaningful efficiency and the magnitude of exergy losses.

Exergy balance can quantify the quality of energy during heat transfer. When exergy analysis is performed the thermodynamic imperfection can be quantified as exergy destruction which represent losses in energy quality or usefulness.

The exergy can be transported across the boundary of the system.

Important characteristic of exergy:

1. The rate of exergy in system will be raised with more relatively deviation from surrounding.
2. Rate of Exergy in definition depends not only on the state of the system or flow but also the state of the reference environment.

It is important to be aware of the difference between energy and exergy in order to make the issue clear between exergy and traditional energy

analysis. Table 5.1 summarizes the general comparison between energy and exergy.

Table 5.1 General differences between energy and exergy.

Energy	Exergy
Dependent on the properties of quantity and independent of properties of a reference environment.	Dependent on both properties of quantity and properties of reference environment.
Non-zero in values when in equilibrium with reference environment.	Zero in values when the dead state that is complete equilibrium with reference environment.
Conserved for all processes that can be neither destroyed nor produced.	Conserved for reversible process and non-conserved for real process.
Appear in many forms (e.g kinetic energy, potential energy, work and heat) and measured in that form.	Appear in many forms (e.g kinetic energy, potential energy, work and heat) and measured on the basis of work equivalent or ability to produce work.
Based on first law of thermodynamic	Based on both first and second law of thermodynamic

5.1 Energy Analysis and the First Law of Thermodynamics

An energy analysis is a conventional method for assessing the way energy is used in any operation involving the physical or chemical processing of materials.

The transfer and/or conversion of energy will be based on first law of thermodynamics while first law of thermodynamics provide no information about the inability of any thermodynamics process.

For a thermodynamic analysis, it is necessary to define some performance parameters, which will be useful for analyzing the proposed cycle.

The most relevant parameters that can characterize the usefulness of the cycle are exergy and thermal efficiency.

Exergy analysis determines the system performance based on exergy, which is defined as the maximum possible reversible work obtainable in bringing the state of the system to equilibrium with that of the environment.

In the absence of magnetic, surface tension effect, nuclear, electrical, and considering the system is at rest relative to the environment, the total exergy associated with the work can be obtainable by bringing a stream of matter from its initial state to a state that is in thermal and mechanical equilibrium with the environment.

The first law of thermodynamics is more commonly known as the law of energy Conservation.

The first law of thermodynamics indicates that energy can be neither created nor destroyed, and it can only change from one form to another form. This law defines Internal energy as a state function, and provides a formal statement of the conservation of energy.

$$\begin{bmatrix} rate\ of \\ energy\ change \\ within\ control \\ volume \end{bmatrix} = \begin{bmatrix} Net\ rate\ of \\ heat\ addition \end{bmatrix} - \begin{bmatrix} Net\ rate\ of \\ work\ out \end{bmatrix} + \begin{bmatrix} Rate\ of\ energy \\ addition\ with\ mass \end{bmatrix} - \begin{bmatrix} Rate\ of\ energy \\ removal\ with\ mass \end{bmatrix}$$

The mathematical equation for the first law of thermodynamics for an open system, or any component in an open system, is:

$$\frac{dE_{C.V.}}{dt} = \dot{Q}_{C.V.} - \dot{W}_{C.V.} + \sum \dot{m}_i(h_i + \frac{1}{2}V_i^2 + gZ_i) - \sum \dot{m}_e(h_e + \frac{1}{2}V_e^2 + gZ_e) \quad (5.1)$$

Where,

$\frac{dE_{C.V.}}{dt}$ Is the time rate of change the total energy stored within the given control volume.

$\dot{Q}_{C.V.}$ Is the net rate of heat addition.

$\dot{W}_{C.V.}$ Is the net rate of the non-flow work out;

$\sum \dot{m}_i(h_i + \frac{1}{2}V_i^2 + gZ_i$ Is the rate of the energy (h is the specific enthalpy,

$\frac{1}{2}V_i^2$ Is the specific kinetic energy,

gz Is the specific potential energy, addition or removal due to mass flowing (h).

Into (i) or out of (o) the given control volume.

For almost every typical component in an energy system, the velocity and height differences for the working fluid flows can be ignored, so that the rates of energy addition and removal are only associated with the enthalpy, such that:

An energy analysis is commonly used in evaluating the performance of a component or a system, and can be used to determine the first law efficiency (η_{th}, for a power production cycle) or the coefficient of performance (COP, for a heating or cooling cycle). The COP and η_{th} are both defined as the useful energy out, divided by the useful energy into the system.

However, an energy balance provides no information about the direction in which processes can spontaneously occur and/or the reversibility of the thermodynamic processes. The first law cannot provide information

about the inability of any thermodynamic process to convert heat fully into mechanical work, or any insight into why mixtures cannot spontaneously separate themselves.

5.2 Exergy analysis and the Second Law of Thermodynamics

The second law of thermodynamics emphasizes on the quality, rather than just the quantity, of different forms of energy, and explains the reasons that some spontaneous processes can only occur in one direction. Two well-known (and, ultimately, equivalent) statements of the second law of thermodynamics are cited below.

Clausius statement:
"It is impossible for heat to move of itself from a lower-temperature reservoir to a higher temperature reservoir. That is, heat transfer can only occur spontaneously in the direction of temperature decrease. "

Kelvin-Planck statement:

"It is impossible for a system to receive a given amount of heat from a high temperature reservoir and to provide an equal amount of work output. While a system converting work to an equivalent energy transfer as heat is possible, a device converting heat to an equivalent energy transfer as work is impossible. "

The second law of thermodynamics defines entropy as the measurement of the randomness within a system. Because entropy is a state property, an expression of the second law of thermodynamics for an open system can be developed in a similar manner to that of the first law, as below:

$$\begin{bmatrix} rate\ of \\ entropy\ increase \\ in\ control \\ volume \end{bmatrix} = \begin{bmatrix} Net\ rate\ of \\ Entropy\ Addition \\ by\ Heat \end{bmatrix} + \begin{bmatrix} Rate\ of \\ Entropy\ Addition \\ with\ mass\ flow\ in \end{bmatrix}$$

$$- \begin{bmatrix} Rate\ of \\ Entropy\ removal \\ with\ Mass\ flow\ out \end{bmatrix} + \begin{bmatrix} Rate\ of \\ Entropy\ Production \\ in\ control\ volume \end{bmatrix}$$

The mathematical equation for the second law of thermodynamics for an open system, or any component in an open system, is:

$$\frac{dS_{C.V.}}{dt} = \sum \dot{m}_i S_i - \sum \dot{m}_o S_o + \sum \frac{Q}{T} \quad (5.2)$$

Where,

$\frac{dS_{C.V.}}{dt}$ Is the time rate of change of the entropy stored in the control volume.

$\sum m\ S$ Is the rate of entropy (S) addition (i) or removal (O) from the system due mass flow.

$\sum \frac{Q}{T}$ Is the rate of entropy addition due to heat transfer.

An ideal process is a process with no entropy generation/production, so that the system would operate at its best possible performance level. Therefore, compared with the actual system performance, the second law efficiency (isentropic efficiency, for a power production process such as a turbine, for a power consumption process such as a pump) can be determined.

To better understand and quantify these restrictions on the flow and conversion of energy, it is necessary to combine the first law with the second law of thermodynamics. The exergy analysis is based on this combination and will be discussed in the next section.

Exergy is a measure of a system's ability to do useful work as it is brought into thermal mechanical and chemical equilibrium with the environment. It is derived from the combination of the first and second law of thermodynamics.

Since exergy is more valuable than energy according to the second law of thermodynamics, it is useful to consider both output and input in terms of exergy. The amount of exergy supplied in the product to the amount of exergy associated with the fuel is more accurate measure of the thermodynamic performance of the system which is defined as the ratio of exergy contained in the product to the exergy associated with the solar energy input.

$$\begin{bmatrix} rate\ of \\ exergy\ change \\ within\ control \\ volume \end{bmatrix} = \begin{bmatrix} Net\ Exergy \\ transfer \\ by\ Heat \end{bmatrix} - \begin{bmatrix} Net\ Exergy \\ Transfer \\ by\ work \end{bmatrix}$$

$$+ \begin{bmatrix} Rate\ of \\ exergy\ addition \\ with\ Mass \end{bmatrix} - \begin{bmatrix} Exergy\ Destruction \\ within\ Control \\ volume \end{bmatrix}$$

Based on the definition and equations, energy is never destroyed during a process; it only changes from one form to another. In contrast, exergy accounts for the irreversibility of process due to the increase in entropy. Exergy is always destroyed when a process involves a temperature change. The system exergetic efficiency is defined as the useful exergy out from the system, divided by the overall exergy supplied to the system.

It is important to understand the subdivision of contributions to the exergy destruction within each component. Since a conventional exergy analysis cannot provide the required information, a better approach concerning this detailed exergy analysis is needed. One approach to accomplish this is known as an advanced exergy analysis. In an advanced exergy analysis, the exergy destruction within a component can be split into unavoidable and avoidable parts. The unavoidable exergy destruction is

the exergy destruction that is not recoverable due to technological limitations, and the remaining part is the avoidable exergy destruction, which is recoverable and should be focused on by engineers to improve system efficiency. Additionally, the exergy destruction within a component can also be split into endogenous and exogenous parts.

The second law efficiency of the solar assisted triple effect refrigeration cycle may be reported as

$$\eta_{II} = \frac{\Delta\dot{E}_{E1}+\Delta\dot{E}_{E2}+\Delta\dot{E}_{E3}}{\dot{E}_{Solar}} \quad (5.3)$$

Where, $\dot{E}_{Solar}$ is incoming exergy associate with solar radiation falling on heliostat, $\Delta\dot{E}_{E1}$ is the change in exergy at ejector evaporator of ERC, $\Delta\dot{E}_{E2}$ is the change in exergy at evaporator of ARC and $\Delta\dot{E}_{E3}$ is the change in exergy at evaporator of CRC.

$$\Delta\dot{E}_{E1} = \dot{m}_{sf}[(h_{10} - h_{11}) - T_0(s_{10} - s_{11})] \quad (5.4)$$

$$\Delta\dot{E}_{E2} = \dot{m}_{r}[(h_{15} - h_{16}) - T_0(s_{15} - s_{16})] \quad (5.5)$$

$$\Delta\dot{E}_{E3} = \dot{m}_{N_2O,2}[(h_{33} - h_{34}) - T_0(s_{33} - s_{34})] \quad (5.6)$$

$$\dot{E}_{Solar} = \dot{Q}_{Solar}\left(1 - \frac{T_0}{T_s}\right) \quad (5.7)$$

Where, T_s is the apparent sun temperature (equal to 4500 K).

$$\dot{E}_1 = \dot{m}_{Molten\ Salt}[(h_1 - h_0) - T_0(s_1 - s_0)] \quad (5.8)$$

$$\dot{E}_{12} = \dot{m}_{Molten\ Salt}[(h_{12} - h_0) - T_0(s_{12} - s_0)] \quad (5.9)$$

$\dot{E}_1$ is the exergy associated with incoming Molten Salt from receiver.

$\dot{E}_{12}$ Is the exergy associated with outgoing Molten Salt from generator to the CR.

Exergy analysis determines the system performance based on exergy, which is defined as the maximum possible reversible work obtainable in bringing the state of the system to equilibrium with that of the

environment. In the absence of magnetic, surface tension effect, nuclear, electrical, and considering the system is at rest relative to the environment, the total exergy associated with the work obtainable by bringing a stream of matter from its initial state to a state that is in thermal and mechanical equilibrium with the environment.

Mathematically,

$$\dot{E} = \dot{m}[(h - h_0) - T_0(s - s_0)] \quad (5.10)$$

The First Law efficiency of the solar assisted triple effect refrigeration cycle is given by

$$\eta_I = \frac{\dot{Q}_{E1} + \dot{Q}_{E2} + \dot{Q}_{E3}}{\dot{Q}_{Solar}} \quad (5.11)$$

According to the Bejan [163], entropy generation over a control volume is given by

$$\dot{S}_{gen} = \frac{dS}{dt} - \sum_{i=0}^{n} \frac{\dot{Q}_i}{T_i} - \sum_{in} \dot{m}s + \sum_{out} \dot{m}s \geq 0 \quad (5.12)$$

According to Gouy–Stodola theorem, the exergy destruction and entropy generation are related as [161]

$$\dot{E}_{X,D} = T_0 \dot{S}_{gen} \quad (5.13)$$

Exergy for a specific state with reference to the environment is defined as follows:

$$\dot{E}_x = \dot{m}[(h - h_0) - T_o(s - s_o)] \quad (5.14)$$

The exergy destruction or irreversibility equation was defined as

$$\dot{E}_D = \sum_i Exi_{in} - \sum_i Exi_{out} - W + \sum_j (1 - \frac{T_o}{T_j}) Q_j \quad (5.15)$$

5.3 Energy, Exergy Analysis & Mathematical Formulation

The proposed system consists of Steam Rankine cycle (SRC), Ejector refrigeration cycle (ERC), Absorption refrigeration cycle (ARC), and Cascade refrigeration cycle (CRC) with solar tower heat source (STHC).

This chapter discusses the mathematical formulation for the solar assisted triple effect refrigeration cycle.

The first law efficiency of the solar assisted triple effect refrigeration cycle are obtained by energy balance approach and given as:

$$\eta_I = \frac{\dot{Q}_{E1}+\dot{Q}_{E2}+\dot{Q}_{E3}}{\dot{Q}_{Solar}} \tag{5.16}$$

Solar Tower Heat Source with Steam Rankine Cycle (SRC) and Ejector Refrigeration Cycle (ERC):

Many research has been carried out on the combined power and refrigeration cycle. In order to utilize the advantages of the ejector refrigeration cycle and recover low-grade heat effectively, a new combined power and ejector refrigeration cycle is proposed.

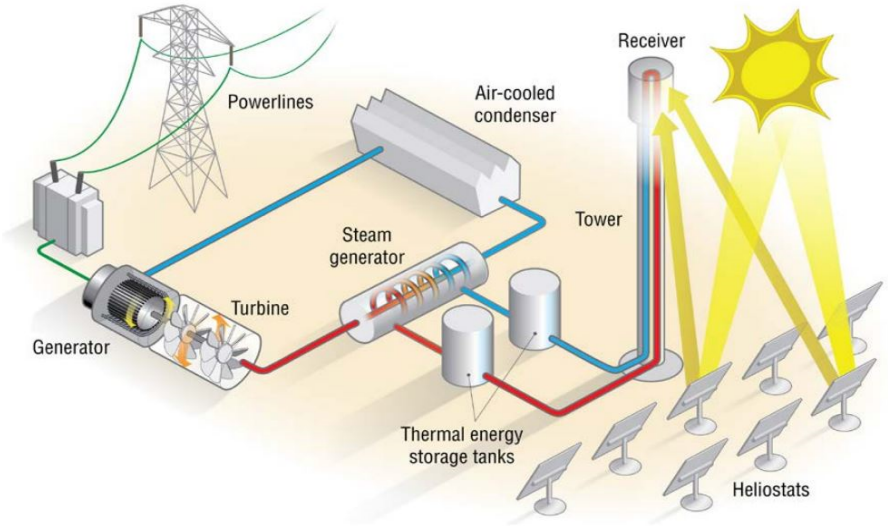

Figure 5.1 Solar Tower with Steam rankine cycle schematic.

This cycle combines the Rankine cycle and the ejector refrigeration cycle by adding a turbine between heat recovery generator and ejector. The vapor from heat recovery generator could be expanded through turbine to generate power, and the turbine exhaust can drive the ejector. This combined cycle can produce both power output and refrigeration output simultaneously.

Figure 5.2 shows the T-S diagram of the steam Rankine Cycle with Ejector refrigeration cycle.

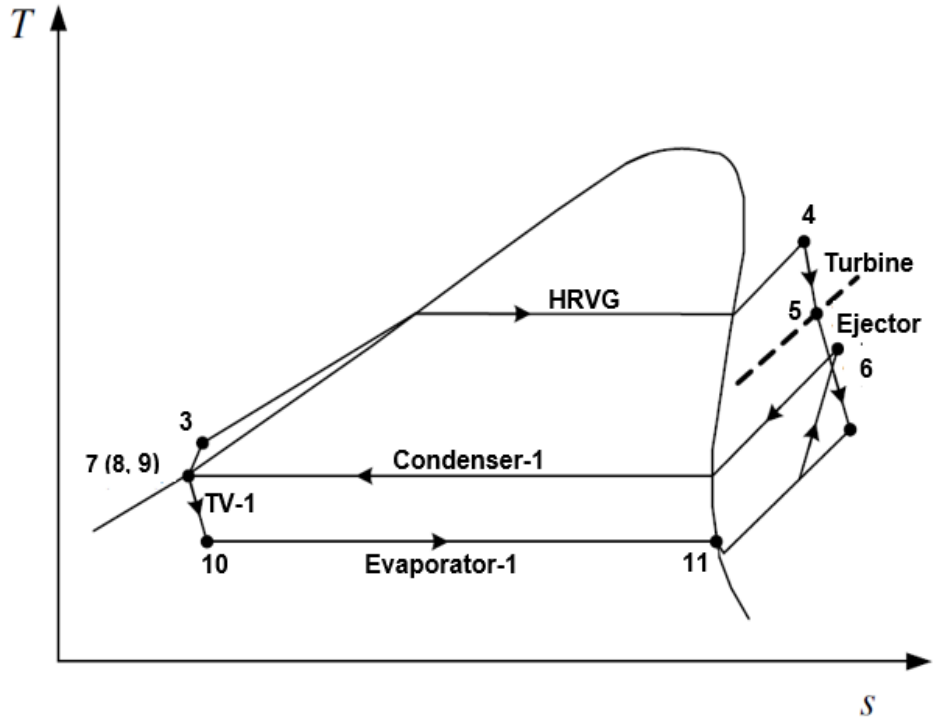

Figure 5.2 T-S diagram of the steam Rankine Cycle with Ejector refrigeration cycle.

The following assumption have been made for the analysis of the proposed cycle:

- Low Pressure in ejector refrigeration cycle P[E1]=P[10]=P[11].
- High pressure in ejector refrigeration cycle P[C1]=P[6]=P[7]=P[8]=P[9].

- Pressure of HRVG, P[HRVG]=P[3]=P[4].
- Low Temperature in ejector refrigeration cycle T[E1]=T[10]=T[11].
- High Temperature in ejector refrigeration cycle T[C1]=T[7]=T[8]=T[9].
- Isentropic process in turbine S[4]=S[5].
- Isentropic process in pump1 S[8]=S[3].
- Isenthalpic process for TV-1 h[9]=h[10]
- Mixture quality, saturated vapor (x=1) for the following state: [11]
- Mixture quality, saturated liquid (x=0) for the following state: [7],[8],[9].

For Heliostat, a part of thermal energy received by heliostat is delivered to the CR and rest is lost to environment according to Xu et al.

The thermal power output of the solar system is to be calculated from the change in enthalpy in the receiver working fluid. Across the inlet/outlet points, the delivered thermal power can be computed from:

Central Receiver Energy Balance:

$$\dot{Q}_{solar} = A_h q \tag{5.17}$$

Where A_h is aperture area and q is the solar radiation per unit area.

$$\dot{Q}_{solar} = \dot{Q}_{CR} + \dot{Q}_{lost,heliostat} \tag{5.18}$$

$$\eta_{I,heliostat} = \frac{\dot{Q}_{CR}}{\dot{Q}_{Solar}} \tag{5.19}$$

For CR, a part of thermal energy received by CR is absorbed by molten salt and rest lost to environment.

$$\dot{Q}_{CR} = \dot{Q}_{molten\ salt} + \dot{Q}_{lost,CR} = \dot{m}_{molten\ salt}(h_1 - h_{12}) + \dot{Q}_{lost,CR} \tag{5.20}$$

Where $\Delta h = \int_{T1}^{T12} C_p\, dT$, Cp=1443+0.172 T (°C) (5.20a)

Central Receiver Surface Temperature:

The central receiver surface temperature is important factor to calculate the heat losses from CR, which can be expressed as [158]:

$$T_{rec.sur} = \frac{Q_{rec}}{A_{rec.sur}}\left(\frac{d_o}{d_i h_{ms}} + \frac{d_o}{2\,k_{tube}} ln\frac{d_o}{d_i}\right) + T_{ms} \quad (5.21\text{ a})$$

$$h_{ms} = \frac{k_{ms}}{d_i}\ 0.023\ Re_{ms}^{0.8}\ Pr_{ms}^{0.4} \quad (5.21\text{ b})$$

$$Re_{ms} = \frac{d_i\ \rho_{ms} u_{ms}}{\mu_{ms}} \quad (5.21\text{ c})$$

$$Pr_{ms} = \frac{\mu_{ms}\ Cp_{ms}}{k_{ms}} \quad (5.21\text{ d})$$

Central Receiver Emissive Heat Losses:

The emissive heat losses calculated based on average receiver surface temperature and expressed by [158]:

$$Q_{rec.em} = \ \varepsilon_{avg}\ \sigma\ (T_{rec.sur}^4 - T_o^4)\ A_{rec.sur} \quad (5.21\text{ e})$$

$$\varepsilon_{avg}\ = \frac{\varepsilon_w}{\varepsilon_w + (1-\varepsilon_w)\ F_r} \quad (5.21\text{ f})$$

$\varepsilon_w : Wall\ Emissivty.$

Central Receiver convection Losses.

Forced Convection Heat Losses:

Forced Convection heat losses were considered as forced convection from a flat plate and can be expressed by equation [158]:

$$Q_{Rec.FC} = \ h_{FC.air.ins}\ \ (T_{rec.sur} - T_0)\ A_{rec.sur} \quad (5.21\text{ g})$$

$$h_{FC.air.ins}\ = \frac{k_{air}}{L}\ 0.0287\ Re_{air.ins}^{0.8}\ Pr_{air.ins}^{1/3} \quad (5.21\text{ h})$$

Where L is the aperture height, $T_{air.ins}$ is the mean temperature between the receiver temperature and ambient temperature.

Natural Convection Heat Losses:

The natural convection heat losses inside the central receiver can be expressed as [158]:

$$Q_{Rec.NC} = h_{NC.air.ins} \ (T_{rec.sur} - T_0) \ A_{rec.sur} \quad (5.21\ j)$$

$$h_{NC.air.ins} = 0.81 \ (T_{rec.sur} - T_0)^{0.426} \quad (5.21\ k)$$

Central Receiver Reflective Heat Losses:

The reflective heat losses considering surface reflectivity and view factor which can be expressed as [158]:

$$Q_{rec.ref} = Q_{rec} \ F_r \ Ref \quad (5.21\ L)$$

$$F_r = \frac{A_{ape}}{A_{rec.sur}} \quad (5.21\ m)$$

Central Receiver Conductive Heat Losses:

The conductive heat losses from the insulation layer considered and can be expressed as follow [158]:

$$Q_{rec.cond} = \frac{k_{insu}}{\delta_{insu}} \ (T_{rec.sur} - T_{insu.w}) \ A_{rec.sur} \quad (5.21\ n)$$

The combined convective heat transfer is taken into account to calculate the heat transfer coefficient of the outer receiver insulation layer and can be expressed as [158]:

$$\frac{k_{insu}}{\delta_{insu}} \ (T_{rec.sur} - T_{insu.w}) \ A_{rec.sur} =$$
$$\frac{k_{air}}{L} \ 0.0239 \ Re_{air.o}^{0.805} (0.785 \ \frac{T_{insu.w}}{T_0})^{0.2} 1.167 \ Pr_{air,O}^{0.45} \quad (5.21\ o)$$

Air Properties equations as a function of temperature [158]:

Density (Kg/m^3):

$$\rho_{air} = \frac{351.99}{T_{air}} + \frac{344.84}{T_{air}^2} \quad (5.22\ a)$$

Specific Heat for air (J/kg K):

$$Cp_{air} = 1030.5 - 0.19975\ T_{air} + 3.9734\ X\ 10^{-4}\ T_{air}^2 \quad (5.22\ b)$$

Thermal Conductivity for air (W/m K):

$$k_{air} = \frac{2.334\ X\ 10^{-3}\ T_{air}^{3/2}}{164.54 + T_{air}} \quad (5.22\ c)$$

Absolute Viscosity for air (N S/m^2):

$$\mu_{air} = \left(\frac{1.4592\ T_{air}^{\frac{3}{2}}}{109.1 + T_{air}}\right) X\ 10^{-6} \quad (5.22\ d)$$

The properties of **Molten Salt** as a function of temperature (a mixture of 60 wt% NaNO3 and 40 wt% KNO3 [158]:

Density (Kg/m^3):

$$\rho_{ms} = 2090 - 0.636\ T_{ms} \quad (5.23\ a)$$

Specific Heat for molten salt (J/kg K):

$$Cp_{ms} = 1443 + 0.172\ T_{ms} \quad (5.23\ b)$$

Thermal Conductivity for molten salt (W/m K):

$$k_{ms} = 0.443 + 1.9\ X 10^{-4}\ T_{ms} \quad (5.23\ c)$$

Absolute Viscosity for molten salt (N S/m^2):

$$\mu_{ms} = (22.714 - 0.12\ T_{ms} + 2.281\ X\ 10^{-4}\ T_{ms}^2 - 1.474\ X\ 10^{-7}\ T_{ms}^3)X\ 10^{-6} \quad (5.23\ d)$$

The optical losses, heat radiation losses, and the convection heat losses were considered for the calculation of the central receiver thermal efficiency.

$$\eta_{I,CR} = \frac{\dot{Q}_{Molten\ Salt}}{\dot{Q}_{CR}} \tag{5.24}$$

Central Receiver Exergy Balance:

For Heliostat: A part of exergy received by Heliostat is delivered to the CR and rest is lost to environment (Irreversibility),

$$\dot{E}_{Solar} = \dot{E}_{CR} + \dot{E}_{lost,heliostat} \tag{5.25}$$

So,

$$\eta_{II,heliostat} = \frac{\dot{E}_{CR}}{\dot{E}_{Solar}} \tag{5.26}$$

For CR, a part of exergy received by CR is absorbed by molten salt and rest is lost to the environment (Irreversibility),

$$\dot{E}_{CR} = \dot{E}_{Molten\ Salt} + \dot{E}_{Dest,CR} \tag{5.27}$$

$$\dot{E}_{CR} = \dot{m}_{Molten\ Salt}\,(h - T_0\,S) + \dot{E}_{Dest,CR}$$

$$= \dot{m}_{Molten\ Salt}\,c_{P,Molten\ Salt}\left[T_1 - T_{12} - T_0 \ln\frac{T_1}{T_{12}}\right] + \dot{E}_{Dest,CR} \tag{5.28}$$

$$\eta_{II,CR} = \frac{\dot{E}_{Molten\ Salt}}{\dot{E}_{CR}} \tag{5.29}$$

Heat Recovery Generator (HRVG),

The molten salt (HTF) is flowing through the pipes, which transfer the thermal energy from central receiver to the heat recovery vapor generator.

State #1, as shown in Figure 5.3, represents the hot molten salt from the solar tower and then enters generator at state#2 to be used in absorption refrigeration cycle.

Hot molten salt used to raise the temperature of saturated liquid refrigerant (state#3) and becomes superheated vapor (state#4) which is expanded in a turbine to generate work

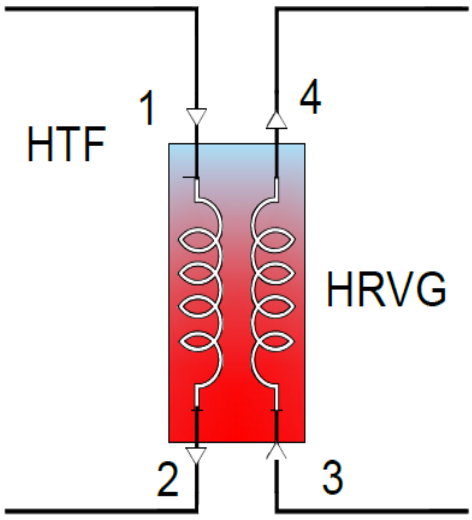

Figure 5.3 Schematic Diagram for Heat Recovery Vapor Generator

Mass Balance Equation:

$$\dot{m}_{Molten\ Salt,1} = \dot{m}_{Molten\ Salt,2} = \dot{m}_{HTF} \quad (5.30)$$

$$\dot{m}_{f,3} = \dot{m}_{f,4} = \dot{m}_f \quad (5.31)$$

Energy Balance Equation:

$$\dot{m}_{HTF}\ (h_1 - h_2) = \dot{m}_f\ (h_4 - h_3) \quad (5.32)$$

Entropy Balance Equation:

$$\dot{m}_{HTF}\,(s_1 - s_2) + \dot{s_{gen}} = \dot{m}_f\,(s_4 - s_3) \quad (5.33)$$

Exergy Balance Equation:

$$\dot{m}_{HTF}\,ex_1 + \dot{m}_f\,ex_3 = \dot{m}_{HTF}\,ex_2 + +\dot{m}_f\,ex_4 + \dot{E}x_{D,HRVG} \quad (5.34)$$

$$\dot{E}x_{D,HRVG} = T_0\left[\dot{m}_{HTF}(s_2 - s_1) + \dot{m}_f\,(s_4 - s_3)\right] \quad (5.35)$$

$$\Delta S = \int_{T1}^{T2} \frac{C_p}{T}\,dT \quad \text{, Cp=1443+0.172 T (°C)} \quad (5.35a)$$

Exergy Efficiency can be defined in general as ratio of total exergy output to exergy input and Exergy Efficiency of HRVG can be defined as exergy increase of cold stream to exergy decrease of hot stream:

$$\eta_{ex,HRVG} = \frac{\dot{m}_f\,(ex_4 - ex_3)}{\dot{m}_{HTF}\,(ex_1 - ex_2)} \quad (5.36)$$

For Turbine (T),

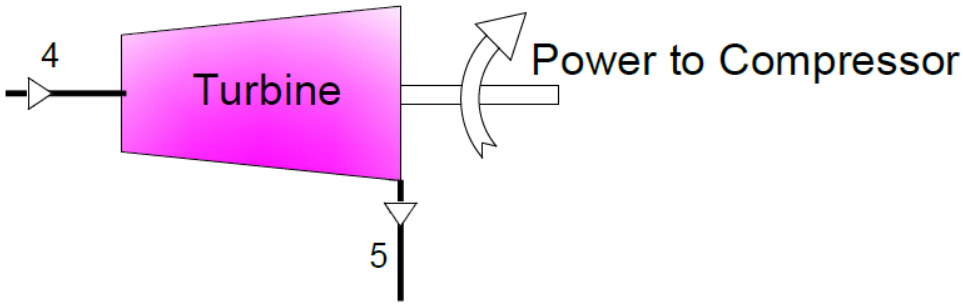

Figure 5.4 Schematic Diagram for Turbine.

The turbine exhaust at state#5 passes through converging diverging supersonic nozzle of ejector.

Mass Balance Equation:

$$\dot{m}_4 = \dot{m}_5 = \dot{m}_f \quad (5.37)$$

Energy Balance Equation:

The rate of work generated by turbine to run the compressors of cascaded refrigeration cycle is

$$\dot{W}_T = \dot{m}_f(h_4 - h_5) \quad (5.38)$$

The energy efficiency of the turbine can be defined as the ratio of the work output to the total change in energy between state 4 and 5.

$$\eta_{en,T} = \frac{\dot{W}_T}{\dot{m}_f(h_4 - h_5)} \quad (5.39)$$

The isentropic efficiency of the turbine can be defined as the ratio of the work output from turbine to the work output if the process were isentropic and can be expressed as:

$$\eta_{IS,T} = \frac{\dot{W}_{T,Act.}}{\dot{W}_{T,Isen.}} \quad (5.40)$$

$$\eta_{IS,T} = \frac{h_4 - h_5}{h_4 - h_{5s}} \quad (5.41)$$

$$h_5 = h_4 + \eta_{S,T}(h_{5s} - h_4) \quad (5.42)$$

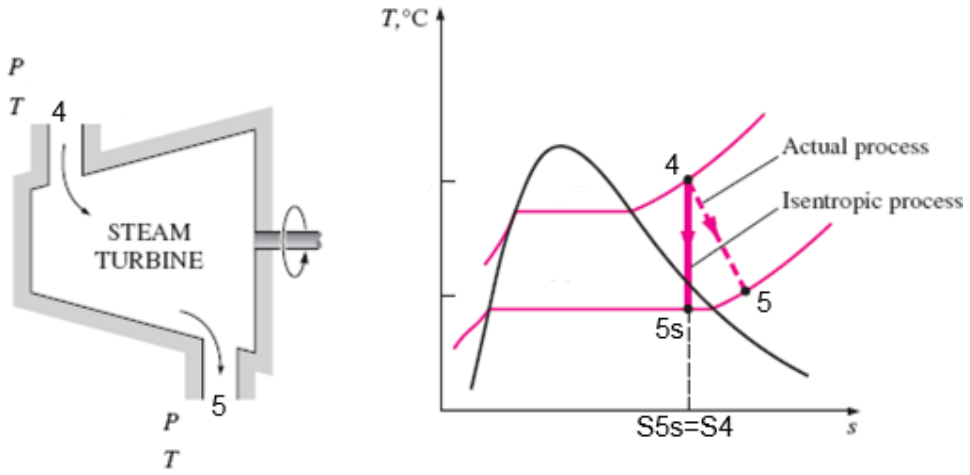

Figure 5.5 Actual and isentropic process of the steam turbine [164].

Entropy Balance Equation:

$$\dot{m}_f s_5 = \dot{m}_f s_4 + \dot{S}_{gen} \tag{5.43}$$

Exergy Balance Equation:

$$\dot{m}_f \, ex_4 = \dot{m}_f \, ex_5 + \dot{W}_T + \dot{E}x_{D,T} \tag{5.44}$$

$$\dot{E}x_{D,T} = \dot{m}_f [T_0(s_5 - s_4)] \tag{5.45}$$

The exergy efficiency of the turbine can be defined as the ratio of the work output to reversible work and can be expressed as:

$$\eta_{ex,T} = \frac{\dot{W}_{T,out}}{\dot{W}_{T,rev.}} \tag{5.46}$$

$$\eta_{ex,T} = \frac{\dot{W}_T}{\dot{m}_f \, (ex_4 - ex_5)} \tag{5.47}$$

For Pump (P1),

A pump transfer mechanical energy to fluid by raising its pressure. Saturated liquid at state#8 being pump to the heat recovery vapor generator at state#3.

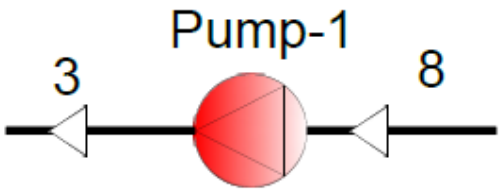

Figure 5.6 Schematic Diagram for Pump (P1)

Mass Balance Equation:

$$\dot{m}_3 = \dot{m}_8 = \dot{m}_f \tag{5.48}$$

Energy Balance Equation:

$$\dot{W}_{P1} = \dot{m}_f(h_3 - h_8) \tag{5.49}$$

The energy efficiency of the pump is defined as the ratio of the mechanical energy increase of the fluid as it is flows through the pump to mechanical energy input to pump.

$$\eta_{en,P1} = \frac{\dot{m}_f(h_3 - h_8)}{\dot{W}_{in}} \tag{5.50}$$

$$h_3 = h_8 + \frac{(h_{3s} - h_8)}{\eta_{IS,P1}} \tag{5.51}$$

Entropy Balance Equation:

$$\dot{s}_{gen} = \dot{m}_f(s_3 - s_8) \tag{5.52}$$

Exergy Balance Equation:

$$\dot{m}_f\, ex_3 + \dot{E}x_{D,P1} = \dot{m}_f\, ex_8 + \dot{W}_{P1} \tag{5.53}$$

$$\dot{E}x_{D,P1} = T_0\left[\dot{m}_f(s_3 - s_8)\right] \tag{5.54}$$

$$\eta_{ex,P1} = \frac{\dot{m}_f(ex_3 - ex_8)}{\dot{W}_{in,P1}} \tag{5.55}$$

Ejector Refrigeration Cycle (ERC):

For Ejector (EJE),

The turbine exhaust passes through converging diverging supersonic nozzle of ejector. The very high velocity refrigerant vapor at the exit of the nozzle creates a very high vacuum at the inlet of the mixing chamber and extract secondary vapor (state#11) into the chamber from the evaporator of ERC and this causes cooling effect at evaporator- 1 (E1) of ERC. The primary (state#5) and secondary vapors (State#11) are mixed in the mixing chamber.

The mixed stream (6) is cooled in condenser-1(C1) by means of cold water from cooling tower.

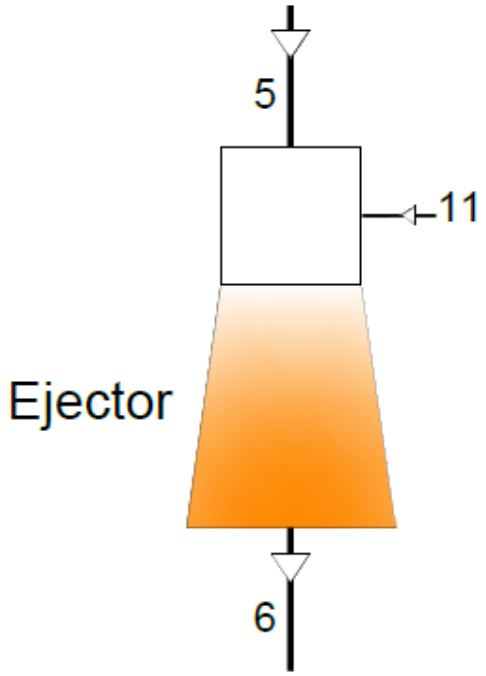

Figure 5.7 Schematic Diagram for Ejector.

Mass Balance Equation:

$$\dot{m}_{pf} + \dot{m}_{sf} = \dot{m}_6 \quad (5.56)$$

Energy Balance Equation:

$$\dot{m}_{pf} h_5 + \dot{m}_{sf} h_{11} = \left(\dot{m}_{pf} + \dot{m}_{sf}\right) h_6 \quad (5.57)$$

Entropy Balance Equation:

$$\dot{m}_{pf} s_5 + \dot{m}_{sf} s_{11} + \dot{S}_{gen} = \left(\dot{m}_{pf} + \dot{m}_{sf}\right) s_6 \quad (5.58)$$

Exergy Balance Equation:

$$\dot{m}_{pf} ex_5 + \dot{m}_{sf} ex_{11} = \left(\dot{m}_{pf} + \dot{m}_{sf}\right) ex_6 + \dot{E}x_{D,EJE} \quad (5.59)$$

$$\dot{E}x_{D,EJE} = T_0\left[\, \dot{m}_6(s_6) - \dot{m}_{pf}(s_5) - \dot{m}_{sf}(s_{11})\right] \quad (5.60)$$

$$\eta_{ex,EJE} = \frac{\dot{m}_{sf}(ex_6 - ex_{11})}{\dot{m}_{pf}(ex_5 - ex_6)} \quad (5.61)$$

An ejector is a pump-like device that uses the 'venturi effect' of a converging diverging nozzle, as shown in Fig. 4.14, to convert the pressure energy of a motive fluid to velocity energy which creates a low pressure zone that draws in and entrains a suction fluid and then recompresses the mixed fluids by converting velocity energy back into pressure energy.

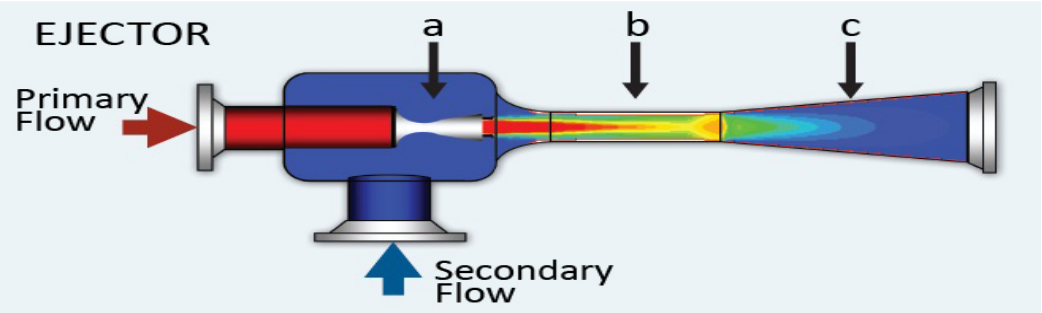

Figure 5.8 Detailed Schematic Diagram for Ejector.

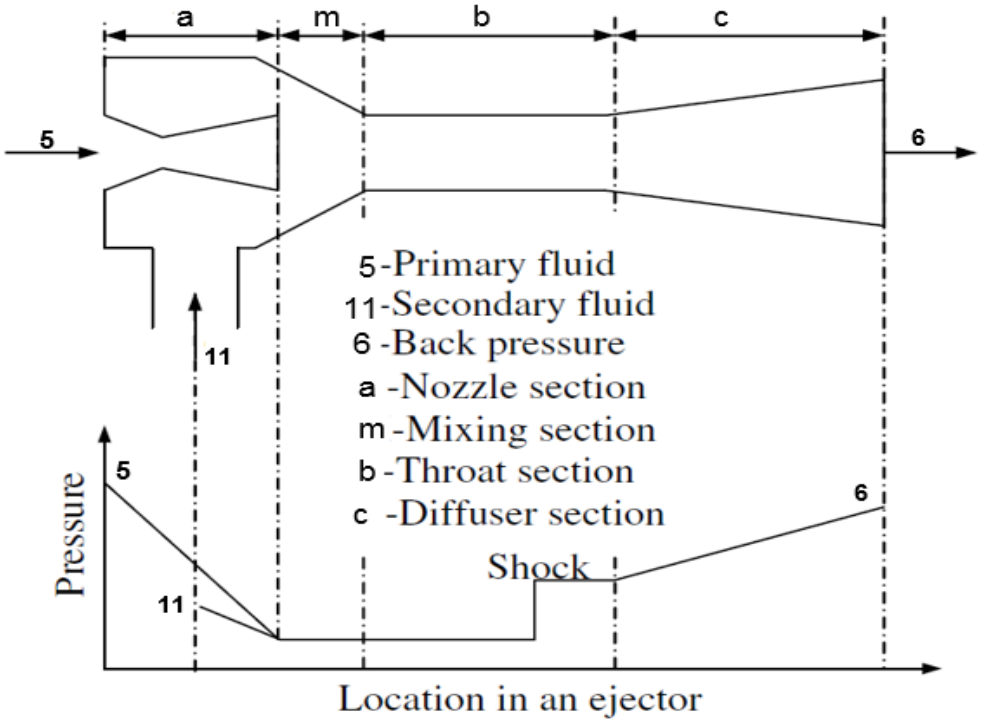

Figure 5.9 the structure and working process of ejector

Entrainment ratio

The most important aspect of ejector modeling is the determination of the entrainment ratio which is defined as the ratio of secondary mass flow rate (entrained vapor) to the primary mass flow rate (motive vapor). It is an important parameter to describe the performance of an ejector.
In order to determine the entrainment ratio, the following methodology and assumption will be followed [148~154]:

- The flow inside the ejector is steady and one-dimensional.
- The ejector walls are adiabatic.
- The primary flow and the secondary flow are saturated and their Velocities are negligible before entering the ejector (states 5 and 11).

- The velocity of the mixed flow leaving the ejector (at state 6) is also neglected.
- All flow losses are taken into account by using isentropic efficiencies in the nozzle (η_n), in the diffuser (η_d), as well as in the mixing chamber (η_m). The motive steam expands isentropically in the nozzle. Also, the mixture of the motive steam and the entrained vapor compresses isentropically in the diffuser.
- Constant isentropic expansion exponent and the ideal gas behavior.
- The mixing of motive steam and the entrained vapor takes place in the suction chamber.
- The motive steam and the entrained vapor have the same molecular weight and specific heat ratio.
- The exist of the condenser is at saturated liquid state.
- The fluid at the exist of the evaporator is at saturated vapor state.
- The exist of the generator is at saturated vapor state.

Variations in the stream velocity and pressure as a function of location inside the ejector, which are shown in Figure 5.10, are explained below:

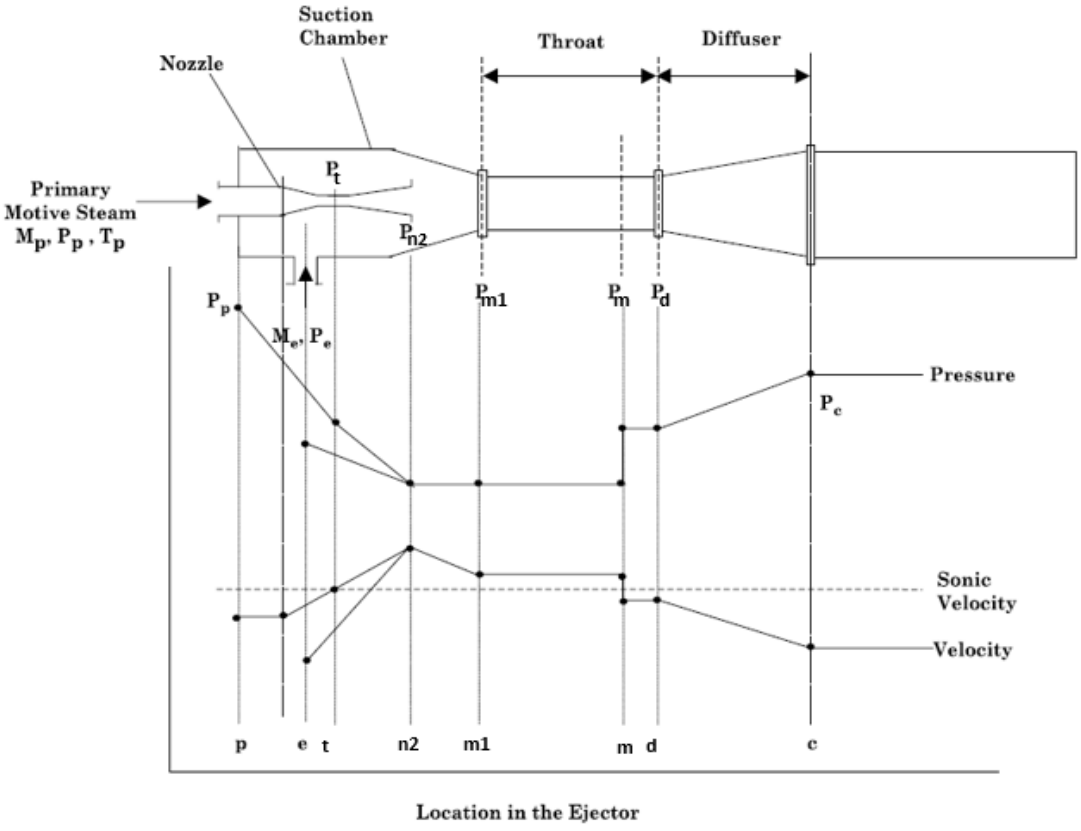

Figure 5.10 Variation in stream pressure and velocity as a function of location along the ejector

- The motive steam (Primary fluid) enters the ejector at state (5) with a subsonic velocity, as the stream flows in the converging part of the ejector, its pressure is reduced and its velocity increases.
- The stream reaches **sonic velocity** at the nozzle throat, where its Mach number is equal to one.
- The increase in the cross section area in the diverging part of the nozzle results in a decrease of the shock wave pressure and an increase in its velocity to **supersonic** conditions.
- At the nozzle outlet plane, point (n_2), the motive steam pressure becomes lower than the entrained vapor pressure and its velocity ranges between 900 and 1200 m/s.

- The entrained vapor at point (11) enters the ejector, where its velocity increases and its pressure decreases to that of point (m1).
- The motive steam and entrained vapor streams may mix within the suction chamber and the converging section of the diffuser or it may flow as two separate streams as it enters the constant cross section area of the diffuser, where mixing occurs.
- In either case, the mixture goes through a shock inside the constant cross section area of the diffuser. The shock is associated with an increase in the mixture pressure and reduction of the mixture velocity to **subsonic** conditions, point (m). The shock occurs because of the back pressure resistance of the condenser.
- As the subsonic mixture emerges from the constant cross section area of the diffuser, further pressure increase occurs in the diverging section of the diffuser, where part of the kinetic energy of the mixture is converted into pressure. The pressure of the emerging fluid is slightly higher than the condenser pressure, point (c).
- Optimum ejector operation occurs at the critical condition. The condenser pressure controls the location of the shock wave, where an increase in the condenser pressure above the critical point results in a rapid decline of the ejector entrainment ratio, since the shock wave moves towards the nozzle exit. Operating at pressures below the critical points has negligible effect on the ejector entrainment ratio.
- At the critical condition, the ejector entrainment ratio increases at lower pressure for the boiler and condenser. Also, higher temperature for the evaporator increases the entrainment ratio.

Below, the thermodynamic model and mathematical equation of the ejector processes, ideal gas behavior is assumed.

Primary flow through nozzle to m1 [165-167]:

The conservation of energy of the primary flow through nozzle n_1 to n_2:

$$\dot{m}_{pf} h_{pf,m1} + \frac{\dot{m}_{pf}\, u_{pf,m1}^2}{2} = \dot{m}_{pf} h_5 + \frac{\dot{m}_{pf} u_5^2}{2} \quad (5.62)$$

$h_{pf,m1} = c_p T_{pf,m1}$ From Ideal gas behavior, u_5=0.

Recalling from thermodynamic the relationship for perfect gas

$$c_p = R - c_v \quad (5.63)$$

Divide the above equation by c_v yields to:

$$c_p = \frac{K\,R}{K-1} \quad (5.64)$$

The speed of sound can be obtained easily for the equation of state for an ideal gas (also perfect gas as a sub set) because of a simple mathematical expression.

The pressure for an ideal gas can be expressed as a simple function of density, and a function “molecular structure” or ratio of specific heats, k namely

$$P = constant \times \rho^k \quad (5.65)$$

$$C = k\ \frac{P}{\rho} \quad (5.66)$$

Remember that P/ρ is defined for an ideal gas as RT, and equation can be written as:

$$C = \sqrt{k\,R\,T} \quad (5.67)$$

$$C^2 = K\,R\,T \quad (5.68)$$

$$T = \frac{K\,R}{C^2} \quad (5.69)$$

Perfect gas is an ideal gas with a constant heat capacity, Cp. For perfect gas equation is simplified into

$$c_p\, T_{pf,m1} + \frac{u_{pf,m1}^2}{2} = c_p T_5 + 0 \quad (5.70)$$

Dividing the above equation by $c_p\, T_{pf,m1}$ and substituting $T = \frac{K\,R}{C^2}$

And utilizing the definition of Cp as function of R & K and inserting it into equation () yields

$$1 + \frac{u_{pf,m1}^2}{2\, c_p\, T_{pf,m1}\, \eta_n} = \frac{T_5}{T_{pf,m1}} \quad (5.71)$$

$$1 + \frac{K-1}{2\eta_n} \frac{u_{pf,m1}^2}{C^2} = \frac{T_5}{T_{pf,m1}} \quad (5.72)$$

Very useful to convert equation () into a dimensionless form and denote Mach number as the ratio of velocity to speed of sound as

$$M = \frac{u}{c} \quad (5.73)$$

$$1 + \frac{K-1}{2\eta_n} {M_{m1}}^2 = \frac{T_5}{T_{pf,m1}} \quad (5.74)$$

The ratio of stagnation pressure to the static pressure can be expressed as the function of the temperature ratio because of the isentropic relationship as

$$P\, v^k = Constant \quad (5.75)$$

$$v = \frac{RT}{P} \quad (5.76)$$

$$P\, (\frac{RT}{P})^K = Constant \quad (5.77)$$

$$P_1 \left(\frac{RT_{n1}}{Pn_1}\right)^K = P_2 \left(\frac{RT_{m1}}{P_{m1}}\right)^K \quad (5.78)$$

$$\left(\frac{P_{m1}}{P_{n1}}\right)^{\frac{k-1}{k}} = \frac{T_{m1}}{T_{n1}} \quad (5.79)$$

$$1 + \frac{K-1}{2\,\eta_n} M_{m1}{}^2 = \left(\frac{P_{m1}}{P_5}\right)^{\frac{k-1}{k}} \quad (5.80)$$

$$M_{m1} = \sqrt{\frac{2\,\eta_n}{k-1}\left[\left(\frac{P_5}{P_{m1}}\right)^{\frac{k-1}{k}} - 1\right]} \quad (5.81)$$

$$h_{pf,m1,s'} = f(\mathrm{P_{m1}}, \mathrm{S_5}) \quad (5.82)$$

$$u_{m1} = \sqrt{2\,\eta_n (h_5 - h_{m1,s'})} \quad (5.83)$$

Where the isentropic efficiency in the nozzle $\eta_n$is defined a

$$\eta_n = \frac{h_5 - h_{pf,m1}}{h_5 - h_{pf,m1,s'}} \quad (5.84)$$

Secondary flow inlet from evaporator to n2 [165-167]::

The conservation of energy of the secondary flow inlet from evaporator to O:

$$\dot{m}_{sf} h_{11} + \frac{\dot{m}_{sf}\, u_{11}^2}{2} = \dot{m}_{sf} h_{n2} + \frac{\dot{m}_{sf} u_{sf,n2}^2}{2} \quad (5.85)$$

$$c_p\, T_{11} + 0 = c_p T_{n2} + \frac{u_{sf,n2}^2}{2} \quad (5.86)$$

$$1 + \frac{u_{sf,n2}^2}{2\, c_p\, T_{n2}} = \frac{T_{11}}{T_{n2}} \quad (5.87)$$

$$1 + \frac{K-1}{2}\frac{u_{sf,n2}^2}{C^2} = \frac{T_{11}}{T_{n2}} \quad (5.88)$$

$$1 + \frac{K-1}{2} M_{n2}{}^2 = \frac{T_{11}}{T_{n2}} \quad (5.89)$$

$$1 + \frac{K-1}{2} M_{e,o}{}^2 = \left(\frac{P_{11}}{P_{n2}}\right)^{\frac{k-1}{k}} \quad (5.90)$$

$$M_{n2} = \sqrt{\frac{2}{k-1}\left[\left(\frac{P_{11}}{P_{n2}}\right)^{\frac{k-1}{k}} - 1\right]} \quad (5.91)$$

$$h_{n2} = f(P_{n2}, S_{11}) \quad (5.92)$$

$$u_{n2} = \sqrt{2\,(h_{11} - h_{n2})} \quad (5.93)$$

Mixing Process before shock (n_2 & m_1 to m) [165-167]:

The primary and secondary fluid are mixed before shock generation in the mixing chamber, In the Mixing section, the momentum conservation equation is given as

$$\dot{m}_{pf} u_{pf,m1} + \dot{m}_{sf} u_{sf,n2} = \left(\dot{m}_{pf} + \dot{m}_{sf}\right) u_{mf,m,S'} \quad (5.94)$$

Dividing the above equation by $\dot{m}_{pf}$ yields to

$$u_{pf,m1} + \mu\, u_{sf,n2} = (1+\mu) u_{mf,m,S'} \quad (5.95)$$

$$u_{mf,m,S'} = \frac{u_{pf,m1} + \mu\, u_{sf,n2}}{(1+\mu)} \quad (5.96)$$

The mixing efficiency, $\eta_m = \frac{u_{mf,m,S}}{u_{mf,m,S'}}$ (5.97)

$$u_{mf,m,S} = \sqrt{\eta_m}\; u_{mf,m,S'} = \frac{u_{pf,m1} + \mu\, u_{sf,n2}}{(1+\mu)} \sqrt{\eta_m} \quad (5.98)$$

The energy conservation in mixing chamber:

$$\dot{m}_{pf} h_{pf,n1} + \frac{\dot{m}_{pf}\, u_{pf,n1}^2}{2} + \dot{m}_{sf} h_{sf,e,o} + \frac{\dot{m}_{sf} u_{sf,e,o}^2}{2} = \left(\dot{m}_{pf} + \dot{m}_{sf}\right) h_{mf,m} + \frac{u_{mf,m,S}{}^2}{2} \quad (5.99)$$

$u_{pf,n1}^2 = u_{sf,e,o}^2 = 0$ and divide the above equation $\dot{m}_{pf}$ so the equation can be simplified to

$$h_{mf,m} = \frac{h_{sf,11} + \mu\, h_{pf,n1}}{1+\mu} - \frac{u_{mf,m,S}{}^2}{2} \quad (5.100)$$

$S_m = (P_{n2}, h_{mf,m})$

The Critical Mach number (M^*), defined as the ratio of local velocity to the velocity of the sound at critical conditions, the critical Mach can be expressed as:

$$M^* = \sqrt{\frac{M^2(k+1)}{M^2(k+1)+2}} \quad (5.101)$$

The critical Mach number of the primary fluid at location m_1 can be expressed as:

$$M_{m1}^* = \sqrt{\frac{M_{m1}^2(k+1)}{M_{m1}^2(k+1)+2}} \quad (5.102)$$

The critical Mach number of the secondary fluid at location n_2 can be expressed as:

$$M_{n2}^* = \sqrt{\frac{M_{n2}^2(k+1)}{M_{n2}^2(k+1)+2}} \quad (5.103)$$

The critical Mach number of the mixed fluid at location m can be expressed as:

$$M_m^* = \sqrt{\frac{M_m^2(k+1)}{M_m^2(k+1)+2}} \quad (5.104)$$

Thus, the critical Mach number of the mixture at location m in terms of the critical Mach number for the primary and secondary fluid at m_1 and secondary fluid at point n_2 can be expressed as:

$$M_m^* = \frac{M_{m1}^2 + \mu\, M_{n2}^2 \sqrt{T_e/T_p}}{\sqrt{(1+\mu)(1+\mu T_e/T_p)}} \quad (5.105)$$

Following this, the Mach number at location m can be obtained,

$$M_4 = \sqrt{\frac{2\,(M_m^*)^2}{(k+1)-(M_m^*)^2(k-1)}} \quad (5.106)$$

Mixed Flow through the diffuser (m to C) [165-167]:

In the Diffuser section, the energy equation is given as

$$\frac{1}{2}\left(u_{mf,m}^2 - u_{mf,d,S'}^2\right) = h_{mf,d,S'} - h_{mf,m} \quad (5.107)$$

The diffuser efficiency

$$\eta_d = \frac{h_{mf,d,S'} - h_{mf,m}}{h_{mf,d} - h_{mf,m}} \quad (5.108)$$

$$h_{mf,d,S'} = f(P_c, S_m) \quad (5.109)$$

$$h_{mf,m} = h_{mf,m} + \frac{h_{mf,d,s'} - h_{mf,m}}{\eta_d} \quad (5.110)$$

$$u_{mf,m} = \sqrt{2\,\frac{h_{mf,d,s'} - h_{mf,m}}{\eta_d}} \quad (5.111)$$

Rewriting equation (5.111) using equation (5.83),(5.93),(5.108) and (5.109). The entrainment ratio can be found:

$$\mu = \frac{\sqrt{2\eta_n(h_{n1}-h_{m1})} - \sqrt{2(h_{mf,d,s'}-h_{mf,m})/(\eta_d\,\eta_m)}}{\sqrt{\sqrt{2(h_{mf,d,s'}-h_{mf,m})/(\eta_d\,\eta_m)} - \sqrt{\sqrt{2(h_{11}-h_{n2})}}} \quad (5.112)$$

Mach number and pressure of the mixed flow **after the shock wave**:

$$M_d = \sqrt{\frac{M_m^2 + 2/(k-1)}{2kM_m^2/(k-1)-1}} \quad (5.113)$$

The increase in pressure across the shock wave at location d is obtained by combining the mass and momentum equations and is expressed as

$$\frac{P_d}{P_m} = \frac{1+KM_m^2}{1+KM_d^2} \tag{5.114}$$

Moreover, further pressure recovery in the diffuser till outlet (d to c) follows the relationship below

$$\frac{P_C'}{P_m} = [\eta_d \frac{k-1}{2} M_d^2 + 1\ ]^{k/(k-1)} \tag{5.115}$$

Area Ratio [165-167]:

Once the entrainment ration for the ejector is calculated at a given set of operating pressure and temperature, the next step is to determine the area ratio.

These area ratio can be defined as the ratio of the nozzle throat area to the diffuser constant area, and the ratio of the area of the nozzle throat to the nozzle outlet.

The area of the nozzle throat can be expressed as:

$$A_t = \frac{m_p}{P_p}\sqrt{\frac{R\,T_p}{k\,\eta_n}(\frac{k+1}{2})^{k+1/k-1}} \tag{5.116}$$

The area ratio of the nozzle throat and diffuser constant area.

$$\frac{A_t}{A_{m1}} = \frac{P_c}{P_p}\ (\frac{1}{(1+\mu)(\mu(T_e/T_p)}\Big)^{1/2} \frac{((\frac{P_{n2}}{P_c})^{1/k}(1-\frac{P_{n2}}{P_c})^{k-1/k})^{1/2}}{\left(\frac{2}{k+1}\right)^{1/k-1}(1-\frac{2}{k+1})^{1/2}} \tag{5.117}$$

The area ratio of the nozzle throat and the nozzle outlet

$$\frac{A_{m1}}{A_t} = \sqrt{\frac{1}{M_{m1}^2}k + (\frac{2}{k+1}\ (1+\frac{k-1}{2}\ M_{m1}^2)^{k+1/k-1}} \tag{5.118}$$

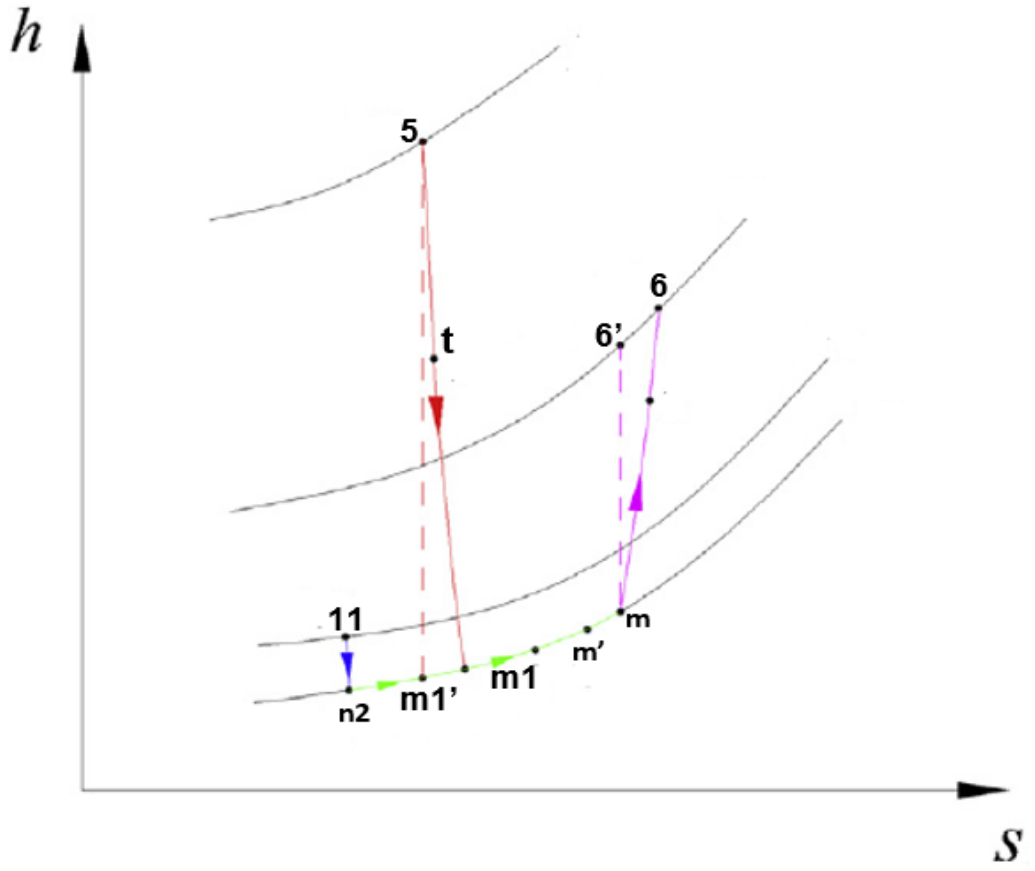

Figure 5.10 a h-s diagram for ejector working processes.

For condenser of Ejector Cooling Cycle (C1)

The saturated liquid (state#7) is divided in two parts (state#8, state#9); the first part (state#9) is passed through throttling valve-1 (TV1), where pressure is reduced to evaporator pressure (state#10) and feed to E1, and the second part (state#8) is pumped by pump-1(P1) to the HRVG of SRC cycle.

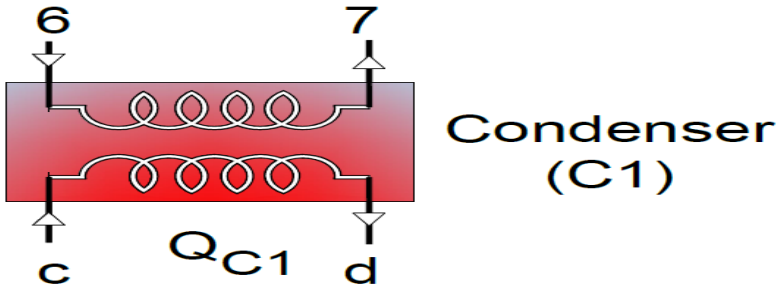

Figure 5.11 Schematic Diagram for condenser (C1)

Mass Balance Equation:

$$\dot{m}_{C1} = \dot{m}_C = \dot{m}_d \quad (5.119)$$

$$\dot{m}_6 = \dot{m}_7 \quad (5.120)$$

Energy Balance Equation:

$$\dot{Q}_{C1} = \dot{m}_{C1}(h_d - h_c) = \left(\dot{m}_{pf} + \dot{m}_{sf}\right)(h_6 - h_7) \quad (5.121)$$

Entropy Balance Equation:

$$\dot{m}_{C1}(s_d - s_c) = \left(\dot{m}_{pf} + \dot{m}_{sf}\right)(s_6 - s_7) + \dot{S}_{gen} \quad (5.122)$$

Exergy Balance Equation:

$$\dot{m}_{C1}(ex_d - ex_c) = \left(\dot{m}_{pf} + \dot{m}_{sf}\right)(ex_6 - ex_7) + \dot{E}x_{D,C1} \quad (5.123)$$

$$\dot{E}x_{\dot{Q}_{C1}} = \left[1 - \frac{T_o}{T_{c1}}\right] x\ \dot{Q}_{C1} \quad (5.123a)$$

$$\dot{E}x_{D,C1} = T_0[\left(\dot{m}_{pf} + \dot{m}_{sf}\right)(s_7 - s_6) + \dot{m}_{C1}(s_d - s_c)] \quad (5.124)$$

The exergy efficiency of heat exchanger (evaporator or condenser) can be defined as increases in the exergy of cold stream divided by decreases in the exergy of hot stream and can be expressed for C1 as:

$$\eta_{ex,C1} = \frac{\dot{m}_{C1}(ex_d - ex_c)}{(\dot{m}_{pf} + \dot{m}_{sf})(ex_6 - ex_7)} \quad (5.125)$$

T6 is the temperature for the water vapor in a **superheated state**. In the condenser, the superheated water vapor condenses to saturated water vapor, which is at a constant temperature T7. Tc represent cooled water from cooling tower, 30°C, under typical summer conditions. The temperature difference can be defined as:

$$\Delta T_{C1} = T_7 - T_c \quad (5.126)$$

Since Tc is 30°C, the lower the value of ΔT_{C1}, the more efficient the heat transfer, and the lower the exergy destruction in the condenser.

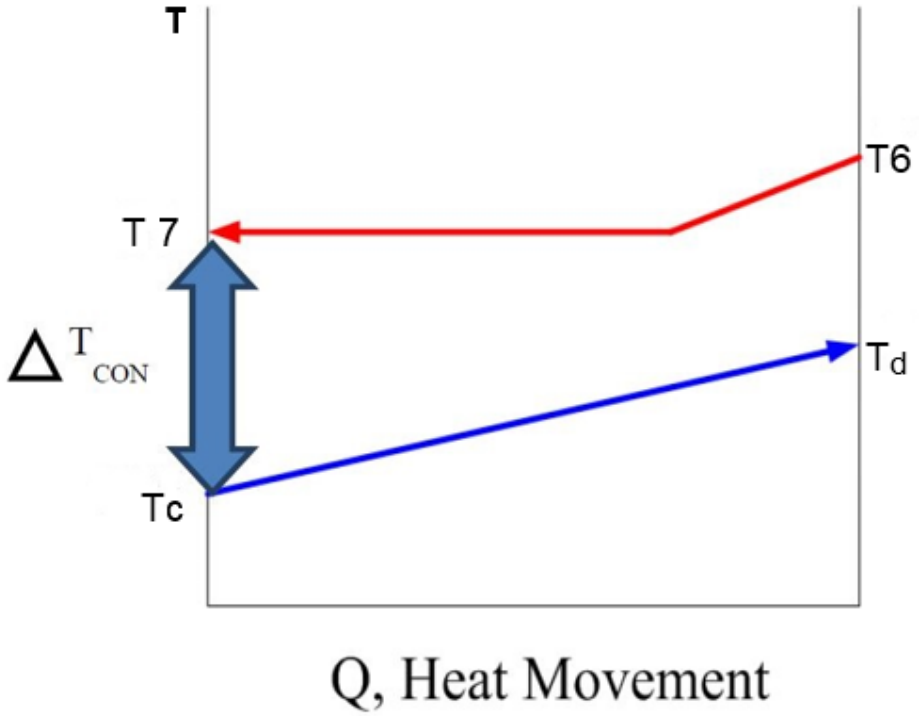

Figure 5.12 T-Q diagram for condenser (C-1).

For Throttling Valve (TV1),

Figure 5.13 Schematic Diagram for Throttling Valve (TV1)

Mass Balance Equation:

$$\dot{m}_9 = \dot{m}_{10} = \dot{m}_{sf} \tag{5.127}$$

Energy Balance Equation:

$$h_9 = h_{10} \tag{5.128}$$

Entropy Balance Equation:

$$\dot{S}_{gen} = \dot{m}_{sf}\,(s_{10} - s_9) \tag{5.129}$$

Exergy Balance Equation:

$$\dot{m}_{sf}\,ex_9 = \dot{m}_{sf}\,ex_{10} + \dot{E}x_{D,TV1} \tag{5.130}$$

$$\dot{E}x_{D,TV1} = T_0\dot{m}_{sf}\,(s_{10} - s_9) \tag{5.131}$$

The exergy efficiency of the throttling valve can be defined as the ratio of the exergy output to exergy input and can be expressed as:

$$\eta_{ex,TV1} = \frac{ex_{10}}{ex_9} \tag{5.132}$$

For Ejector Cooling Evaporator (E1),

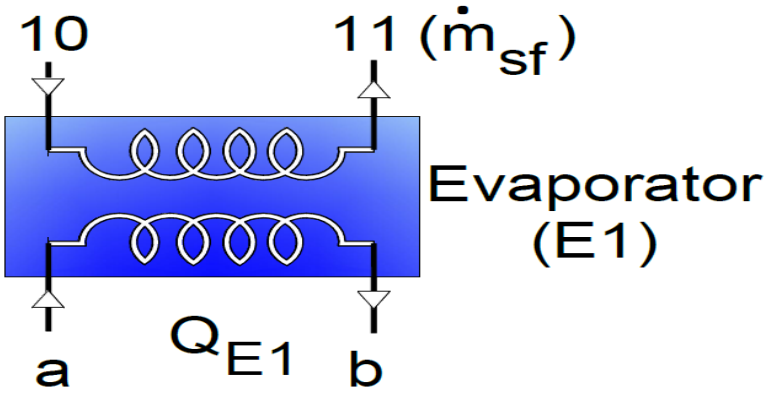

Figure 5.14 Schematic Diagram for Ejector Cooling Evaporator (E1)

Mass Balance Equation:

$$\dot{m}_9 = \dot{m}_{10} = \dot{m}_{sf} \quad (5.133)$$

$$\dot{m}_a = \dot{m}_b = \dot{m}_{E1} \quad (5.134)$$

Energy Balance Equation:

$$\dot{Q}_{E1} = \dot{m}_{E1}(h_a - h_b) = \dot{m}_{sf}(h_{11} - h_{10}) \quad (5.135)$$

Entropy Balance Equation:

$$\dot{m}_{E1}(s_a - s_b) + \dot{S}_{gen} = \dot{m}_{sf}(s_{11} - s_{10}) \quad (5.136)$$

Exergy Balance Equation:

$$\dot{m}_{E1}(ex_a - ex_b) = \dot{m}_{sf}(ex_{11} - ex_{10}) + \dot{E}x_{D,E1} \quad (5.137)$$

$$\dot{E}x_{D,E1} = T_0\left[\dot{m}_{sf}(s_{11} - s_{10}) + \dot{m}_{E1}(s_b - s_a)\right] \quad (5.138)$$

$$\eta_{ex,E1} = \frac{\dot{m}_{sf}(ex_{11} - ex_{10})}{\dot{m}_{E1}(ex_a - ex_b)} \quad (5139)$$

Ta and Tb are design conditions for the application out of the evaporator (a -9°C temperature set point) and the loop into the evaporator (0°C). T10 and T11 represent the entry and exit points for the water vaporizing inside the evaporator, and are therefore the same temperature. So, in order to provide cooling, T10 and T11 must be lower than -9°C, and a temperature difference can be defined as:

$$\Delta T_{E1} = T_b - T_{10} = -9 - T_{10} \tag{5.140}$$

It can be observed that the lower the value of ΔT_{E1}, the lower the exergy destruction inside the evaporator.

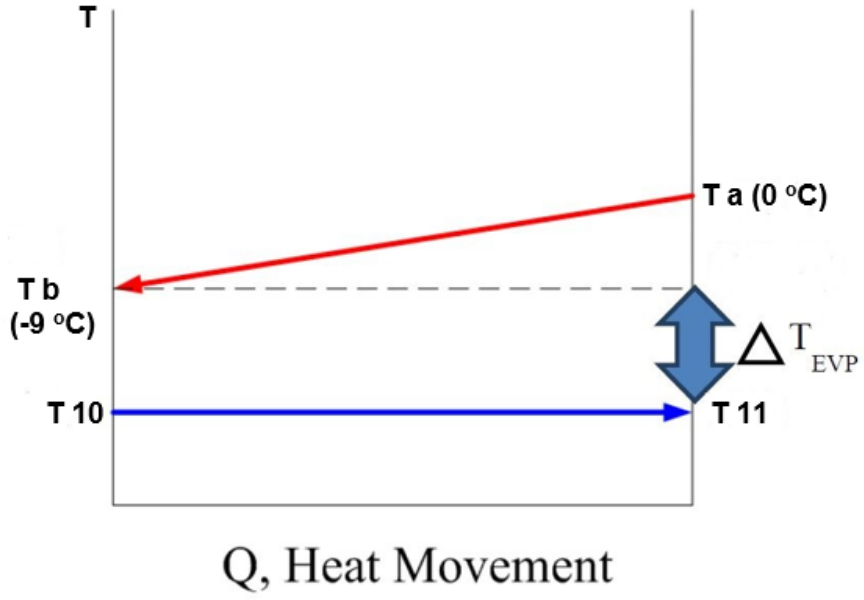

Figure 5.15 T-Q diagram for evaporator (E1).

Absorption Refrigeration Cycle (ARC):

The below diagram has been laid out on a pressure-temperature scale to emphasize the two cycle pressures and three cycle temperatures. The pressure and temperature comparison between components are indicated.

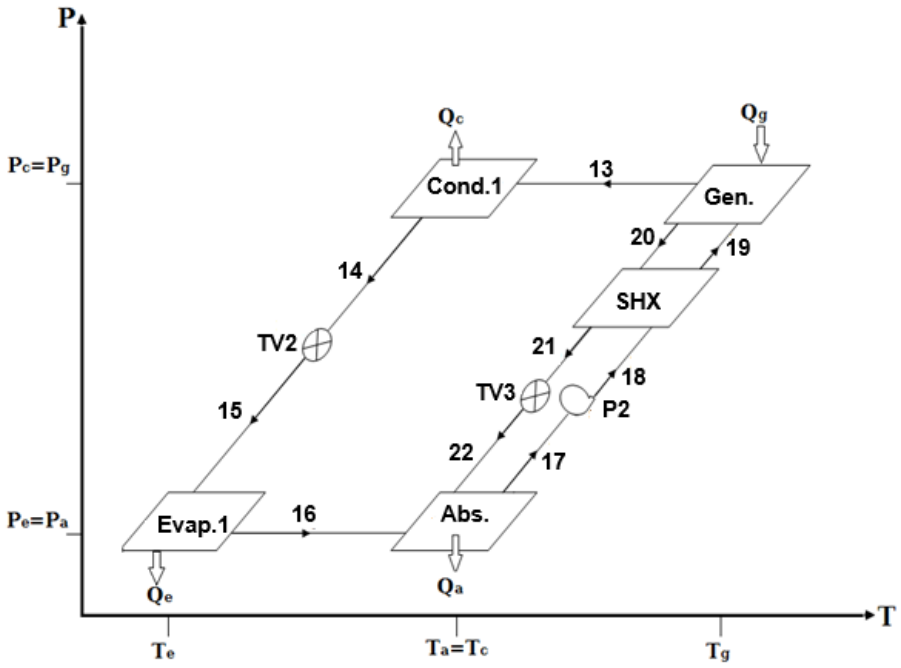

Figure 5.16 P-T diagram for absorption refrigeration cycle (ARC)

The main barrier in representing Temperature – entropy (T–S) diagrams for LiBr/water systems is that the diagram needs to represent the necessary properties of both the refrigerant (water) and of the solution (LiBr/water). The below diagram describes the use of the T–s diagram of water extended with additional curves to represent real and ideal LiBr/water absorption cycles.

Due to the different vapor pressures, no equilibrium can exist between a pure liquid refrigerant and the solution.

Therefore, mainly the refrigerant molecules in the solution are directly considered, and the solution is considered indirectly by its influence on the refrigerant. The impact of the solution heat exchanger can be evaluated separately and does not need a cycle representation.

The extended curves in the vapor region denoted Yi lines (right of saturated vapor line of the refrigerant, indicated 58% and 64%) consider the refrigerant vapor pressure in equilibrium with the solution. These points result from the intersection of the superheated vapor isobar with the superheated temperature, at which it is in pressure equilibrium with the solution.

The extended curves in the liquid region denoted Xi lines (left of saturated liquid line, indicated 58% and 64%) consider the states of liquid refrigerant in the solution. These are derived using the extended vapor curves and the difference of entropy associated with the differential heat of absorption (or generation).

The horizontal difference between the extended liquid and vapor lines indicates the difference of entropy required to reversibly expel one kg of refrigerant from a very big quantity of solution, i.e. generator heat. A real LiBr/water absorption system is represented in Fig. 5.17 (not to scale).From Fig. 5.17, two interdependent circuits can be identified, which overlap between points 8 and 1:

Refrigerant circuit: 2, 12, 13', 13, 14, 15, 16', 16, 17, 18, 19, 2.

Solution circuit: 2, 20, 21, 22, 17, 18, 19, 2.

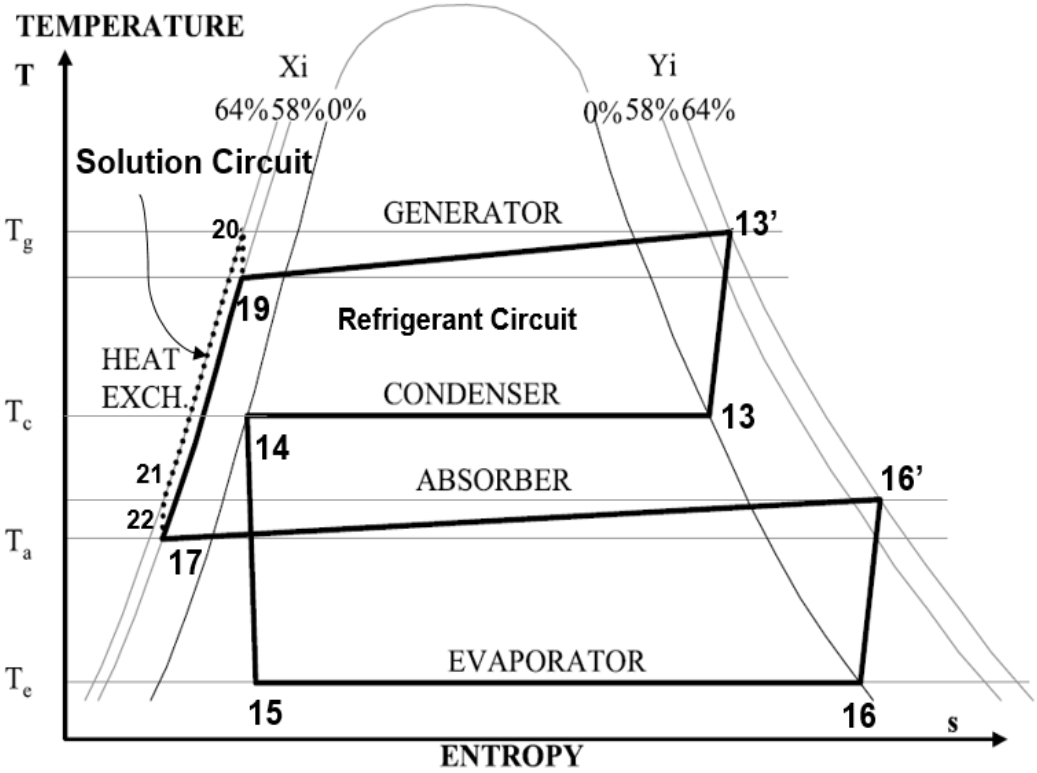

Figure 5.17 Real T-S diagram for absorption refrigeration cycle[156]

The following assumption have been made for the analysis of the proposed cycle:

- Low Pressure in the absorption cycle P[E2]=P[Abs].
- High pressure in the absorption cycle P[C2]=P[Gen.]
- Intermediate temperature in the absorption cycle T[abs]=T[C2].
- Isentropic process of the pump 2 S[17]=S[18].
- Isenthalpic process in TV-2 h[14]=h[15].
- Isenthalpic process in TV-3 h[21]=h[22]
- Mixture quality, saturated vapor (x=1) for the following state: [16].
- Mixture quality, saturated liquid (x=0) for the following state: [14].

For Generator (GEN),

The lithium bromide/water solution will be boiled off using a hot molten salt supplied from the solar tower through heat recovery vapor generator.

The hot molten salt used to separate the water and lithium bromide. State #2, as shown in Figure 5.18 represents the hot molten salt from HRVG used in separation process then leaves it in liquid form at state#12 to return to central receiver.

The mixture of water and lithium bromide enters the generator at state#19, once the weak lithium bromide and water solution is boiled, which is designed to take place at a certain operating temperature and pressure.

The mixture will release the water in vapor form at state #13 then it will be condensed and exit as liquid water at state #14. The strong solution of lithium bromide will return to solution heat exchanger at state#20.

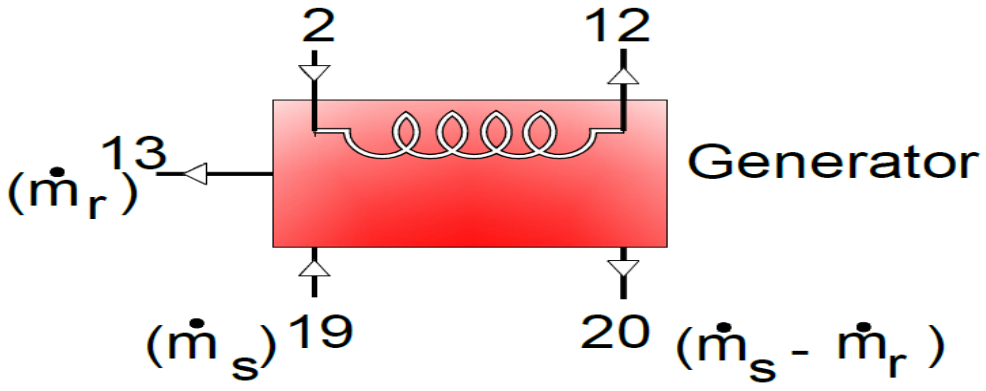

Figure 5.18 Schematic diagram for generator.

Mass Balance Equation

$$\dot{m}_2 = \dot{m}_{12} = \dot{m}_{HTF} \quad (5.141)$$

$$\dot{m}_{19} = \dot{m}_{13} + \dot{m}_{20} \quad (5.142)$$

Solute Mass Balance Equation:

$$\dot{m}_s X_{19} = (\dot{m}_s - \dot{m}_r) X_{20} \quad (5.143)$$

Where m is the mass flow rate (kg/s), X is the lithium bromide concentration, S is weak solution and *r is water* refrigerant. The circulation ratio can be defined as the ratio of the mass flow rate of the solution through the pump to the mass flow rate of the working fluid. It must be noted that *f* represents the required pumping energy. It can be expressed in terms of concentrations as follows:

$$\dot{m}_s = \frac{X_{20}}{X_{20} - X_{19}} \dot{m}_r \quad (5.144)$$

Energy Balance Equation:

$$\dot{Q}_{GEN} = \dot{m}_{HTF}(h_2 - h_{12}) \quad (5.145)$$

$$\dot{Q}_{GEN} = (\dot{m}_s - \dot{m}_r) h_{20} + \dot{m}_r h_{13} - \dot{m}_s h_{19} \quad (5.146)$$

Entropy Balance Equation:

$$\dot{m}_{HTF}(s_2 - s_{12}) + \dot{s_{gen}} = (\dot{m}_s - \dot{m}_r) s_{20} + \dot{m}_r s_{13} - \dot{m}_s s_{19} \quad (5.147)$$

Exergy Balance Equation:

$$\dot{m}_{HTF}(ex_2 - ex_{12}) = (\dot{m}_s - \dot{m}_r) ex_{20} + \dot{m}_r ex_{13} - \dot{m}_s ex_{19} + \dot{E}x_{D,GEN} \quad (5.148)$$

$$\dot{E}x_{D,GEN} = T_0[\, \dot{m}_r(s_{13} - s_{20}) + \dot{m}_s(s_{20} - s_{19}) + \dot{m}_{HTF}(s_{12} - s_2)] \quad (5.149)$$

$$\eta_{ex,Gen.} = 1 - \frac{T_0[\, \dot{m}_r(s_{13} - s_{20}) + \dot{m}_s(s_{20} - s_{19}) + \dot{m}_s(s_{12} - s_2)]}{\dot{m}_{HTF}(ex_2 - ex_{12})} \quad (5.150)$$

For the generator, from Figure 5.19, it can be seen that T2 and T12 are the temperatures for the solar loop inlet and outlet, T19 is the temperature of the dilute solution pumped into the Gen., and T20 is the temperature of the strong solution leaving the Gen. T13 is not shown in the figure, it is

the temperature for the generated water vapor leaving the Gen. where the dilute solution gets heated and reaches its saturated condition. When water volatilizes from the dilute solution, the mass fraction for the solution will increase. Plotting this heat transfer process on a T-Q diagram results in Figure 5.19.

Based on this T-Q diagram, one can define a temperature difference:

$$\Delta T_{Gen.} = T_2 - T_{20} \tag{5.151}$$

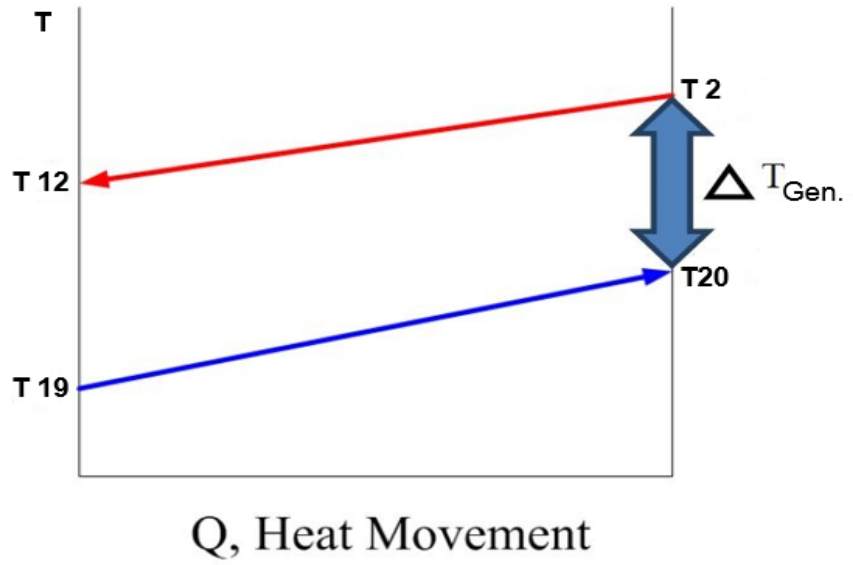

Figure 5.19 T-Q diagram for generator.

Since T2 is fixed at 165°C from the CR through HRVG, a lower value of $\Delta T_{Gen.}$ Indicates a more efficient transfer of heat, a higher strong solution outlet temperature (T20), and a lower level of exergy destruction in the high temperature regenerator.

For condenser of Absorption Refrigeration Cycle (C2),

The superheated pure water vapor at state#13 coming from generator is cooled in condenser-2 (C2) then saturated liquid at state#14 which is at

condenser pressure passes through throttle valve-2. The cooled water enters at state# e and hot water leaves it at state# f to remove the heat from condenser, this cooled water will be supplied from external source such as cooling tower.

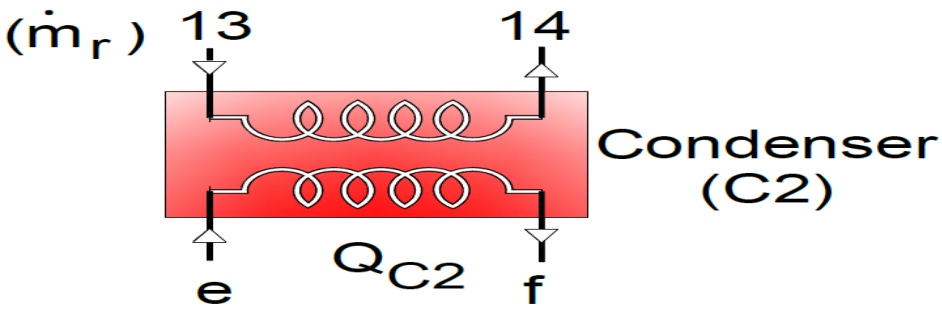

Figure 5.20 Schematic Diagram for condenser (C-2).

Mass Balance Equation:

$$\dot{m}_{13} = \dot{m}_{14} = \dot{m}_r \tag{5.152}$$

$$\dot{m}_e = \dot{m}_f = \dot{m}_{c2} \tag{5.153}$$

Energy Balance Equation:

$$\dot{Q}_{C2} = \dot{m}_{C2}(h_f - h_e) = \dot{m}_r(h_{13} - h_{14}) \tag{5.154}$$

Entropy Balance Equation:

$$\dot{m}_{C2}s_f + \dot{m}_r s_{14} = \dot{m}_r s_{13} + \dot{m}_{C2}s_e + \dot{S_{gen}} \tag{5.155}$$

Exergy Balance Equation:

$$\dot{m}_{C2}(ex_f - ex_e) = \dot{m}_r(ex_{13} - ex_{14}) + \dot{E}x_{D,C2} \tag{5.156}$$

$$\dot{E}x_{D,C2} = T_0[\dot{m}_r(s_{14} - s_{13}) + \dot{m}_{c2}(s_f - s_e)] \tag{5.157}$$

$$\eta_{ex,C2} = \frac{\dot{m}_{C2}(ex_f - ex_e)}{\dot{m}_r(ex_{13} - ex_{14})} \tag{5.158}$$

In order to reduce the exergy destruction inside the condenser, it is important to understand the heat transfer mechanisms and temperature

differences within. In the following T-Q diagrams are presented, together with the assumptions behind the resulting temperature differences.

T13 is the temperature for the water vapor in a **superheated state**. In the condenser, the superheated water vapor condenses to saturated water vapor, which is at a constant temperature T14. Ta represent cooled water from cooling tower, 30°C, under typical summer conditions. The temperature difference can be defined as:

$$\Delta T_{C2} = T_{14} - T_e \tag{5.159}$$

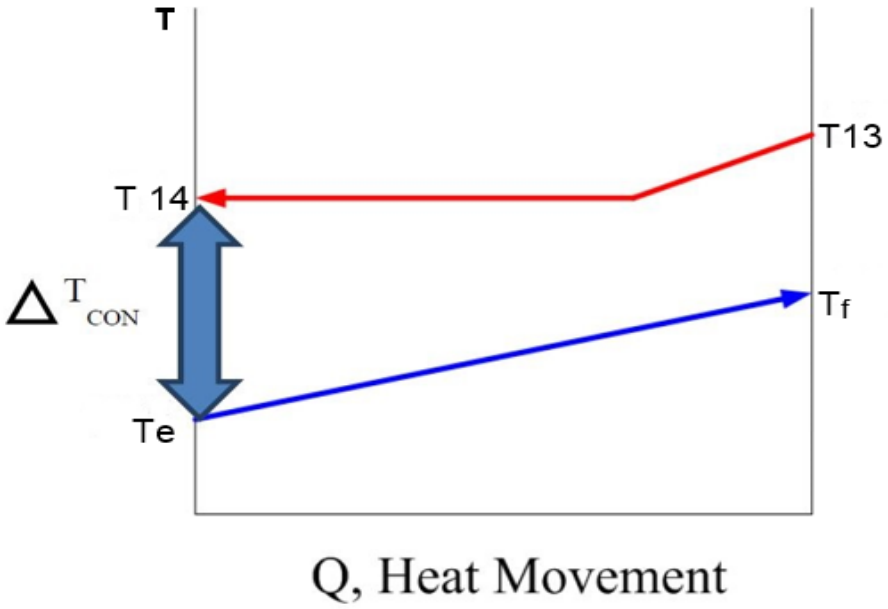

Figure 5.21 T-Q diagram for condenser (C-2).

Since Te is 30°C, the lower the value of ΔT_{C2}, the more efficient the heat transfer, and the lower the exergy destruction in the condenser.

For Throttling Valve (TV2),

Figure 5.22 Schematic Diagram for Throttling Valve (TV2).

Between the condenser and the evaporator, the refrigerant (liquid water) is forced down through the orifice due to the pressure difference from the high pressure side of the Condenser (state #14) to the low pressure region (state #15) of the evaporator. This causes the liquid refrigerant on the condenser side to flash through the orifice and also causes the temperature to decrease. The process will continue until the refrigerant reaches the saturation temperature of the evaporator pressure.

Mass Balance Equation:

$$\dot{m}_{14} = \dot{m}_{15} \tag{5.160}$$

Energy Balance Equation:

$$h_{14} = h_{15} \tag{5.161}$$

Entropy Balance Equation:

$$\dot{S}_{gen} = [\, \dot{m}_r (s_{15} - s_{14})] \tag{5.162}$$

Exergy Balance Equation:

$$\dot{m}_r \, ex_{14} = \dot{m}_r \, ex_{15} + \dot{E}x_{D,TV2} \tag{5.163}$$

$$\dot{E}x_{D,TV2} = T_0 [\, \dot{m}_r (s_{15} - s_{14})] \tag{5.164}$$

$$\eta_{ex,TV2} = \frac{ex_{15}}{ex_{14}} \quad (5.165)$$

For Absorption refrigeration Evaporator (E2),

The evaporator forms the low pressure side of the absorption cycle and its function is to produce the chilled water. The low temperature two phase (liquid-vapor) water exiting the condenser will evaporate to a low temperature water vapor due to the heat transfer from the water supply tubes at state #i & j. This heat transfer process occurs due to the heat of vaporization from the water supply then the water at vapor form at state#16 passes to absorber. The resulting is the chilled water produced in the water supply tubes at state #j, since the two phase water at state #15 is colder than the water supplied. The pressure in the evaporator is approximately 10 times smaller than the pressure in the condenser.

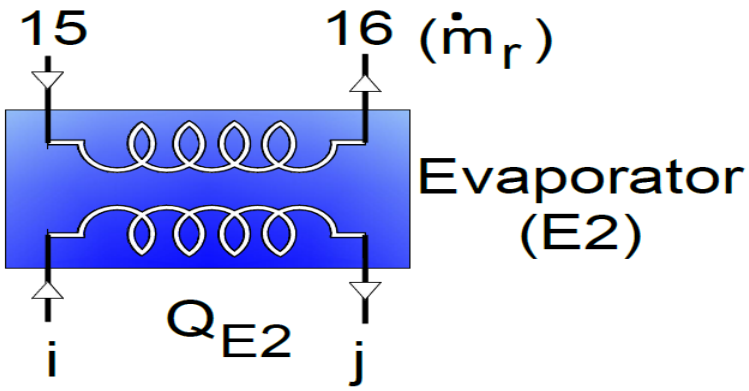

Figure 5.23 Schematic Diagram for Evaporator (E2).

Mass Balance Equation:

$$\dot{m}_{15} = \dot{m}_{16} = \dot{m}_r \quad (5.166)$$

$$\dot{m}_i = \dot{m}_j = \dot{m}_{E2} \quad (5.167)$$

Energy Balance Equation:

$$\dot{Q}_{E2} = \dot{m}_{E2}(h_i - h_j) = \dot{m}_r(h_{16} - h_{15}) \quad (5.168)$$

Entropy Balance Equation:

$$\dot{S}_{gen} = \dot{m}_r(s_{16} - s_{15}) + \dot{m}_{E2}(s_j - s_i) \quad (5.169)$$

Exergy Balance Equation:

$$\dot{m}_{E2}(ex_i - ex_j) = \dot{m}_r(ex_{16} - ex_{15}) + \dot{E}x_{D,E1} \quad (5.170)$$

$$\dot{E}x_{D,E2} = T_0\left[\dot{m}_r(s_{16} - s_{15}) + \dot{m}_{E2}(s_j - s_i)\right] \quad (5.171)$$

$$\eta_{ex,E2} = \frac{\dot{m}_r(ex_{16} - ex_{15})}{\dot{m}_{E2}(ex_i - ex_j)} \quad (5.172)$$

Ti and Tj are design conditions for the application out of the evaporator (a 5°C temperature set point) and the building loop into the evaporator (10°C). T15 and T16 represent the entry and exit points for the water vaporizing inside the evaporator, and are therefore the same temperature. So, in order to provide cooling, T15 and T16 must be lower than 5°C, and a temperature difference can be defined as:

$$\Delta T_{E2} = T_j - T_{15} = 5 - T_{15} \quad (5.173)$$

It can be observed that the lower the value of ΔT_{E2}, the lower the exergy destruction inside the evaporator.

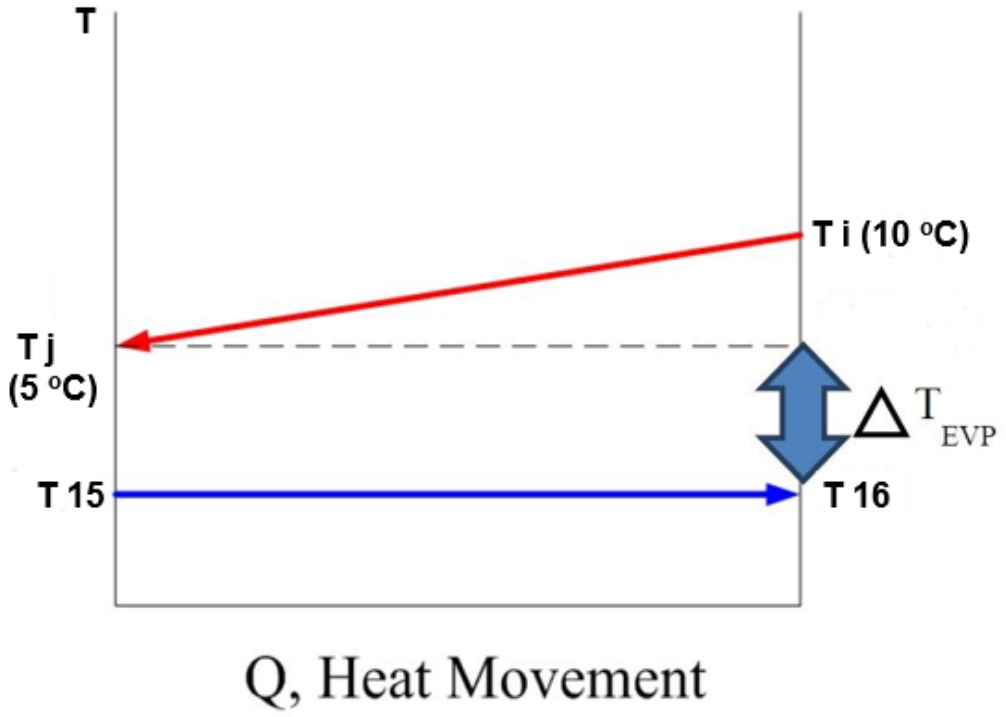

Figure 5.24 T-Q Diagram for Evaporator (E2).

For Absorber (A),

The absorber forms the lowest pressure side of the absorption cycle. Its function is to absorb the water (state #16) from the evaporator to be circulated back to the generator. The evaporation process from the evaporator causes the refrigerant to flow to the absorber (state #16). Absorption temperature is maintained at 35 °C at E2 pressure. Two streams (state#16, state#22) are mixed at the absorber and form a new mixture (state#17) which passes through pump-2 (P2) and solution heat exchanger (SHX) and then finally enters in the generator (state#19).

The refrigerant vapor also gains energy from the heat of vaporization provided by the cooling water as it passes through the tubes (state # g , state # h) at the absorber and causes the incoming vapor (state #16) from the evaporator to absorb the heat.

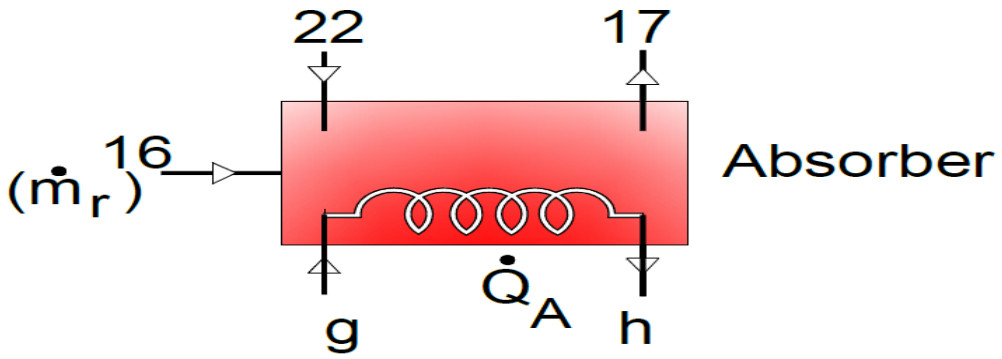

Figure 5.25 Schematic Diagram for Absorber (A).

Mass Balance Equation:

$$\dot{m}_g = \dot{m}_h = \dot{m}_A \quad (5.174)$$

$$\dot{m}_{16} + \dot{m}_{22} = \dot{m}_{17} \quad (5.175)$$

Solute Mass Balance Equation:

$$\dot{m}_s X_{17} = (\dot{m}_s - \dot{m}_{r)} X_{22} \quad (5.176)$$

$$\dot{m}_{17} X_{17} = \dot{m}_{20} X_{22} \quad (5.177)$$

Energy Balance Equation:

$$\dot{Q}_A = \dot{m}_A (h_h - h_g) \quad (5.178)$$

$$\dot{Q}_A = (\dot{m}_s - \dot{m}_r) h_{22} + \dot{m}_r h_{16} - \dot{m}_s h_{17} \quad (5.179)$$

Entropy Balance Equation:

$$\dot{m}_A (s_h - s_g) + \dot{S}_{gen} = (\dot{m}_s - \dot{m}_r) s_{22} + \dot{m}_r s_{16} - \dot{m}_s s_{17} \quad (5.180)$$

Exergy Balance Equation:

$$\dot{m}_A (ex_h - ex_g) = (\dot{m}_s - \dot{m}_r) ex_{22} + \dot{m}_r ex_{16} - \dot{m}_s ex_{17} - \dot{E}x_{D,A} \quad (5.181)$$

$$\dot{E}x_{D,A} = T_0 [\, \dot{m}_r (s_{22} - s_{16}) + \dot{m}_s (s_{17} - s_{22}) + \dot{m}_A (s_h - s_g)] \quad (5.182)$$

$$\eta_{ex,Abs.} = 1 - \frac{T_0 [\, \dot{m}_r (s_{22} - s_{16}) + \dot{m}_s (s_{17} - s_{22}) + \dot{m}_A (s_h - s_g)]}{(\dot{m}_s - \dot{m}_r) ex_{22} - \dot{m}_s ex_{17}} \quad (5.183)$$

State points g and h are the entry and exit states of the cold water from the cooling tower, whose purpose is to take away the heat generated from the solution and water vapor mixing in the absorber. State point 17 is the saturated lithium bromide solution leaving the absorber.
As before, the temperature difference is defined as:

$$\Delta T_{Abs} = T_{17} - T_g \tag{5.184}$$

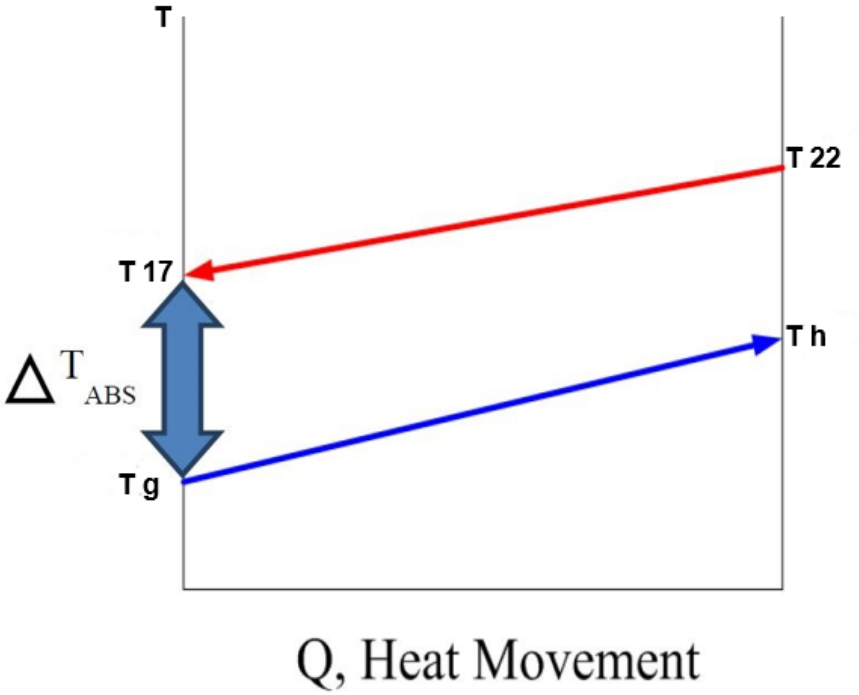

Figure 5.26 T-Q Diagram for Absorber (A).

Where Tg is the cold water temperature from cooling tower (30°C). It can be observed that the lower the ΔT_{Abs}, the more efficient the heat transfer to cool down the fluids to state point 17, and the lower the exergy destruction in the absorber.

For Pump (P2),

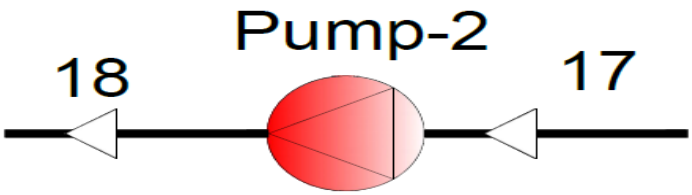

Figure 5.27 Schematic Diagram for Pump (P2).

Mass Balance Equation:

$$\dot{m}_{18} = \dot{m}_{17} = \dot{m}_s \quad (5.185)$$

Solute Mass Balance Equation:

$$\dot{m}_{17} X_{17} = \dot{m}_{18} X_{18} \quad (5.186)$$

Energy Balance Equation:

$$\dot{W}_{P2} = \dot{m}_s (h_{18} - h_{17}) \quad (5.187)$$

Entropy Balance Equation:

$$\dot{S}_{gen} = \dot{m}_s (s_{18} - s_{17}) \quad (5.188)$$

Exergy Balance Equation:

$$\dot{m}_f \, ex_{18} + \dot{E}x_{D,P2} = \dot{m}_f \, ex_{17} + \dot{W}_{P2} \quad (5.189)$$

$$\dot{E}x_{D,P2} = T_0 [\, \dot{m}_s (s_{18} - s_{17})] \quad (5.190)$$

$$\eta_{ex,P2} = \frac{\dot{m}_f (ex_{18} - ex_{17})}{\dot{W}_{in,P2}} \quad (5.191)$$

For Solution Heat exchanger (SHX),

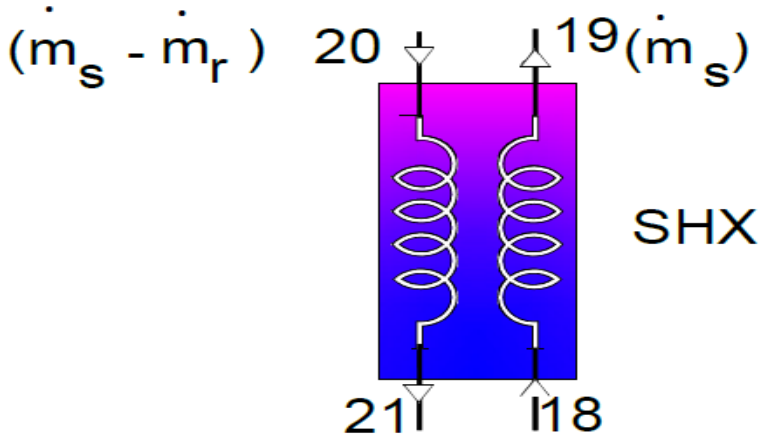

Figure 5.28 Schematic Diagram for solution heat exchanger (SHX).

Solution Heat Exchangers are used to exchange heat between the hot concentrated solution returning to the absorber (state#20, state#21) and the cool dilute solution being pump to the generator (state#18, state#19)

The solution heat exchanger is used to raise the temperature of the cold diluted solution from state 18 to state 19, before it enters the generator. This pre-heating decreases the load required from the solar heat source to evaporate the refrigerant from the solution, potentially improving system performance.

Mass Balance Equation:

$$\dot{m}_{18} = \dot{m}_{19} \tag{5.192}$$

$$\dot{m}_{20} = \dot{m}_{21} \tag{5.193}$$

Solute Mass Balance Equation:

$$\dot{m}_{19}X_{19} = \dot{m}_{18}X_{18} \tag{5.194}$$

$$\dot{m}_{20}X_{20} = \dot{m}_{21}X_{21} \tag{5.195}$$

Energy Balance Equation:

$$\dot{m}_s h_{18} + (\dot{m}_s - \dot{m}_r) h_{20} = \dot{m}_s h_{19} + (\dot{m}_s - \dot{m}_r) h_{21} \quad (5.196)$$

The effectiveness (ε) of heat exchanger can be defined as the ratio of actual heat transfer rate to maximum possible heat transfer rate, The maximum possible temperature rise is the difference between the temperatures of the two entering streams $(h_{h,in} - h_{C,in})$.

The actual heat transfer rate is given from

$$\dot{Q} = (\dot{m}\, C)_h \left(T_{h,in} - T_{h,out}\right) = (\dot{m}\, C)_c \left(T_{c,out} - T_{c,in}\right) \quad (5.197)$$

The Thermal Capacity Ratio [C], the thermal capacity of a fluid stream is the quantity of heat it can transport per unit change in temperature.

i.e. its mass flow X specific heat capacity $(m \cdot c)$

The thermal capacity ratio is defined as:-

$$C = \frac{(m \cdot C)_{min}}{(m \cdot C)_{max}} \quad (5.198)$$

We will define the effectiveness of heat exchanger for both cooling and heating model as follow:

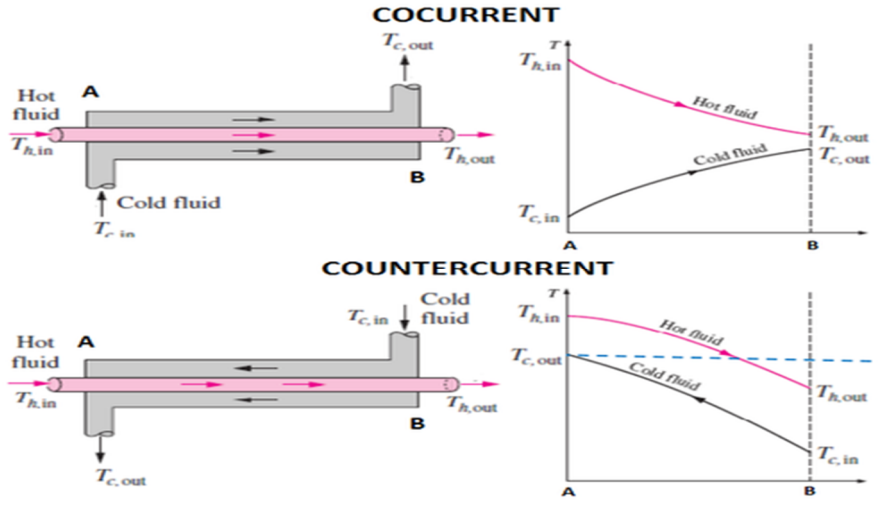

Figure 5.29 concurrent and countercurrent heat exchanger Temp. Profile [162]

If the hot fluid has the lower thermal capacity (if HE operating in cooling mode):

$$\varepsilon = \frac{T_{h,in} - T_{h,out}}{T_{h,in} - T_{c,in}} \quad (5.199)$$

If the cold fluid has the lower thermal capacity (if HE operating in heating mode):

$$\varepsilon = \frac{T_{c,out} - T_{c,in}}{T_{h,in} - T_{c,in}} \quad (5.200)$$

Effectiveness is dimensionless quantity between 0 and 1, the effectiveness of SHX can be expressed as (assumed hot fluid has the lower thermal capacity):

$$\varepsilon = \frac{T_{19} - T_{18}}{T_{20} - T_{18}} \quad (5.201)$$

Entropy Balance Equation:

$$\dot{m}_s s_{18} + (\dot{m}_s - \dot{m}_r) s_{20} + \dot{S}_{gen} = \dot{m}_s s_{19} + (\dot{m}_s - \dot{m}_r) s_{21} \quad (5.202)$$

Exergy Balance Equation:

$$\dot{m}_s ex_{18} + (\dot{m}_s - \dot{m}_r) ex_{20} = \dot{m}_s ex_{19} + (\dot{m}_s - \dot{m}_r) ex_{21} + \dot{E}x_{D,SHX} \quad (5.203)$$

$$\dot{E}x_{D,SHX} = T_0 [\, \dot{m}_s (s_{19} - s_{18}) + (\dot{m}_s - \dot{m}_r)(s_{21} - s_{20})] \quad (5.204)$$

$$\eta_{ex,SHX} = \frac{\dot{m}_s (ex_{19} - ex_{18})}{(\dot{m}_s - \dot{m}_r)(ex_{20} - ex_{21})} \quad (5.205)$$

For Throttling Valve (TV3),

Figure 5.30 Schematic Diagram for Throttling Valve (TV3).

Mass Balance Equation:

$$\dot{m}_{21} = \dot{m}_{22} = \dot{m}_s - \dot{m}_r \quad (5.206)$$

Solute Mass Balance Equation:

$$\dot{m}_{21} X_{21} = \dot{m}_{22} X_{22} \quad (5.207)$$

Energy Balance Equation:

$$h_{21} = h_{22} \quad (5.208)$$

Entropy Balance Equation:

$$\dot{S}_{gen} = [\,(\dot{m}_s - \dot{m}_r)(s_{22} - s_{21})] \quad (5.209)$$

Exergy Balance Equation:

$$(\dot{m}_s - \dot{m}_r)\, ex_{21} = (\dot{m}_s - \dot{m}_r)\, ex_{22} + \dot{E}x_{D,TV3} \quad (5.210)$$

$$\dot{E}x_{D,TV3} = T_0[\,(\dot{m}_s - \dot{m}_r)(s_{22} - s_{21})] \quad (5.211)$$

$$\eta_{ex,TV3} = \frac{ex_{22}}{ex_{21}} \quad (5.212)$$

Cascaded Refrigeration Cycle (CRC):

Figure 5.25 shows the basic cascaded vapor-compression cycle, laid out on temperature-entropy coordinates.

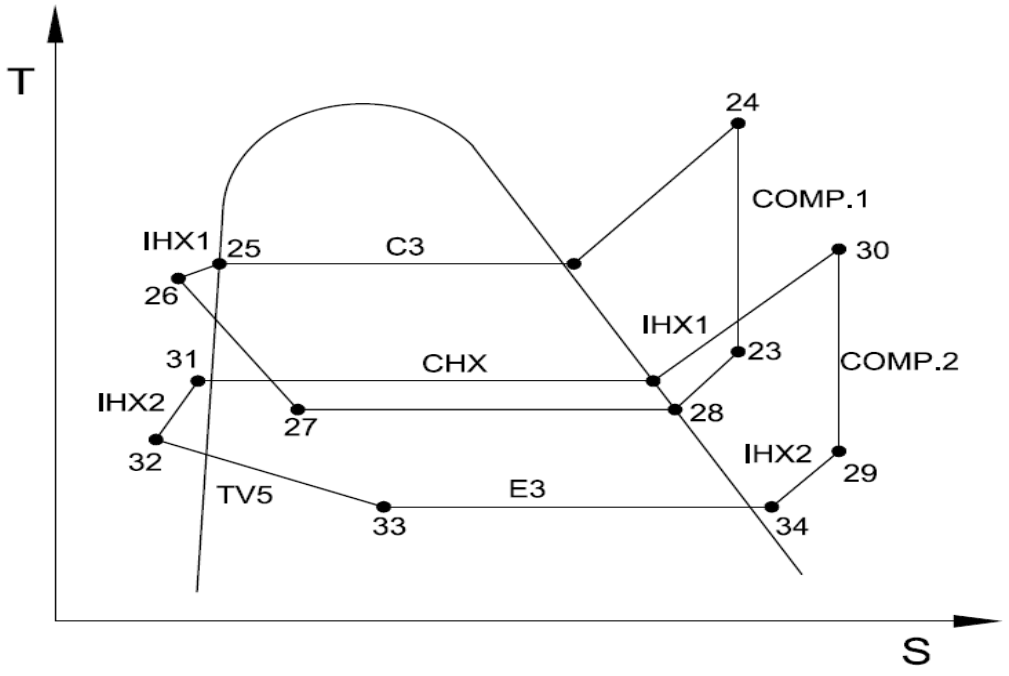

Figure 5.31 T-S diagram for cascaded refrigeration cycle

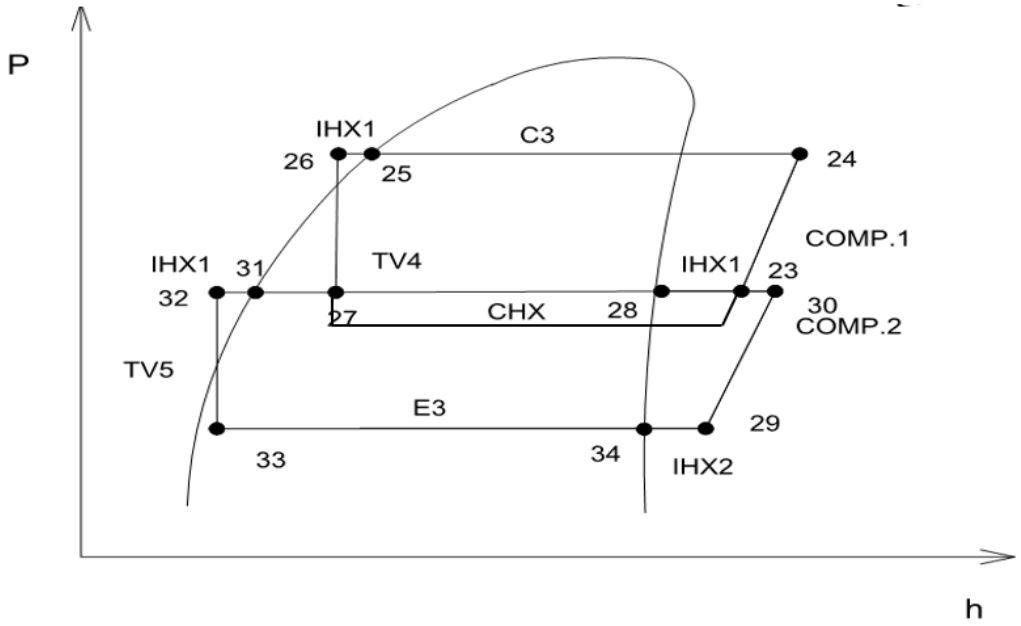

Figure 5.32 P-h diagram for cascaded refrigeration cycle

The following assumption have been made for the analysis of the proposed cycle:

- Low Pressure in cascade refrigeration cycle P [E3] =P [33] =P [34] =P [29].
- Intermediate pressure in cascade refrigeration cycle P[CHX]=P[31]=P[32]=P[27]=P[28]=P[30]=P[23].
- High Pressure in cascade refrigeration cycle P[C3]=P[26]=P[25]=P[24].
- Low Temperature in cascade refrigeration cycle T[E3]=T[33]=T[34]
- Intermediate temperature in cascade refrigeration cycle T[CHX]=T[27]=T[28]
- High Temperature in cascade refrigeration cycle T[C3]=T[25].
- Isentropic process in comp.1 S[23]=S[24]
- Isentropic process in comp.2 S[29]=S[30]
- Isenthalpic process in throttling valve TV-4 h[26]=h[27]
- Isenthalpic process in throttling valve TV-4 h[26]=h[27]
- Mixture quality X, the following state are saturated vapor (x=1): [28],[34].
- Mixture quality X, the following state are saturated liquid(x=0): [25],[31].

Unlike conventional vapor compression cycle which is taken power from main grid electricity or other electrical source, the work output from turbine is fed as inputs to compressor-1(COMP-1) and compressor-2(COMP-2) of the cascaded refrigeration cycle (CRC).

For Compressor 2 (Comp-2)

For the low temperature cycle, superheated nitrous oxide vapor (state#29) is compressed (state#30) in the COMP-2.

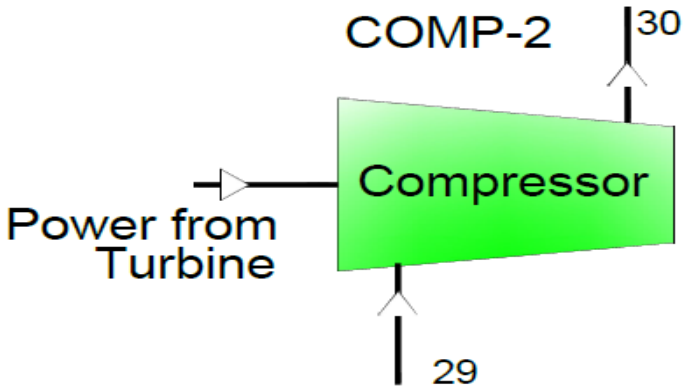

Figure 5.33 Schematic Diagram for Compressor 2 (Comp-2)

Mass Balance Equation:

$$\dot{m}_{29} = \dot{m}_{30} \tag{5.213}$$

Energy Balance Equation:

$$\dot{W}_{COMP2} = \dot{m}_{N_2O,2}(h_{30} - h_{29}) \tag{5.214}$$

The energy efficiency of the compressor can be defined as the ratio of the total energy change of the fluid passing through compressor to input compressor work

$$\eta_{en,comp.2} = \frac{\dot{m}_{N_2O,2}(h_{30}-h_{29})}{\dot{W}_{COMP2},input} \tag{5.215}$$

The isentropic efficiency of the compressor can be defined as the ratio of the work input to an isentropic process, to the work input to the actual process between the same inlet and exit pressures.

$$\eta_{S,comp.2} = \frac{\dot{W}_{COMP2},Isentropic}{\dot{W}_{COMP2},Actual} \tag{5.216}$$

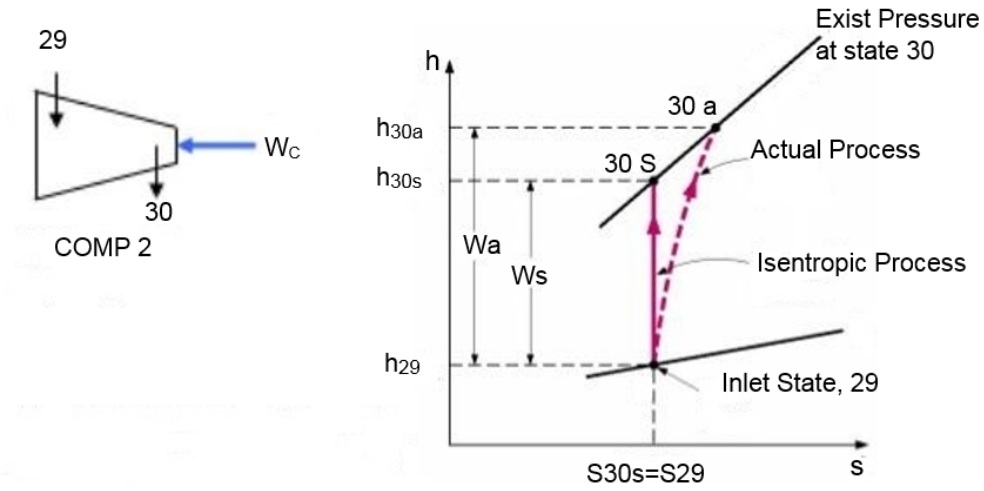

Figure 5.34 Actual and isentropic process of the compressor

$$\eta_{S,comp.2} = \frac{h_{30s} - h_{29}}{h_{30a} - h_{29}} \tag{5.217}$$

$$\mathrm{h_{30a}} = \mathrm{h_{29}} + \frac{\mathrm{h_{30s}} - \mathrm{h_{29}}}{\eta_{\mathrm{S,comp.2}}} \tag{5.218}$$

Entropy Balance Equation:

$$\dot{S}_{gen,COMP2} = \left[\, \dot{m}_{N_2O,2}(s_{30} - s_{29})\right] \tag{5.219}$$

Exergy Balance Equation:

$$\dot{W}_{COMP2} = \dot{m}_{N_2O,2}(ex_{30} - ex_{29}) + \dot{E}x_{D,COMP2} \tag{5.220}$$

$$\dot{E}x_{D,COMP2} = T_0\left[\, \dot{m}_{N_2O,2}(s_{30} - s_{29})\right] \tag{5.221}$$

$$\eta_{ex,Comp2} = \frac{\dot{m}_{N_2O,2}(ex_{30} - ex_{29})}{\dot{W}_{COMP2}} \tag{5.222}$$

For Internal Heat Exchanger-2 (IHX-2)

Nitrous oxide vapor cooled to saturated liquid (state#31) in the cascaded heat exchanger (CHX). Then, the saturated liquid is further cooled in the internal heat exchanger-2 (IHX 2) (state#32) using the lower temperature fluid from state#34 to state #29.

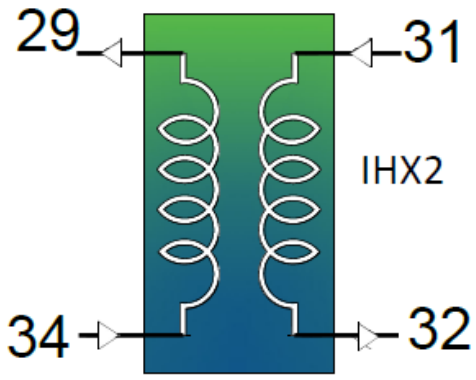

Figure 5.35 Schematic Diagram for Internal heat exchanger (IHX-2)

Mass Balance Equation:

$$\dot{m}_{29} = \dot{m}_{34} = \dot{m}_{N_2O,2} \quad (5.223)$$

$$\dot{m}_{31} = \dot{m}_{32} = \dot{m}_{N_2O,2} \quad (5.224)$$

Energy Balance Equation:

$$h_{31} - h_{32} = h_{29} - h_{34} \quad (5.225)$$

$$\varepsilon = \frac{T_{29} - T_{34}}{T_{31} - T_{34}} \quad (5.226)$$

Entropy Balance Equation:

$$\dot{S}_{gen} = [\dot{m}_{N_2O,2}(s_{29} - s_{34} + s_{32} - s_{31})] \quad (5.227)$$

Exergy Balance Equation:

$$ex_{31} - ex_{32} = ex_{29} - ex_{34} + \dot{E}x_{D,IHX2} \quad (5.228)$$

$$\dot{E}x_{D,IHX2} = T_0[\dot{m}_{N_2O,2}(s_{29} - s_{34} + s_{32} - s_{31})] \quad (5.229)$$

$$\eta_{ex,IHX2} = \frac{(ex_{31} - ex_{32})}{(ex_{29} - ex_{34})} \quad (5.230)$$

For Cascaded Heat Exchanger (CHX),

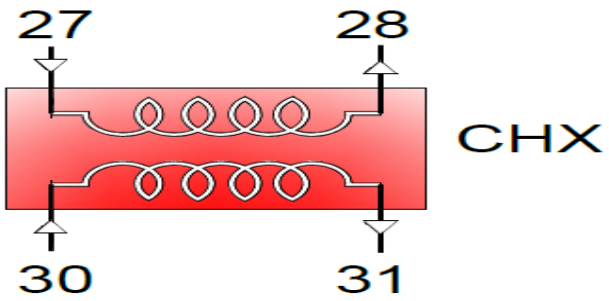

Figure 5.36 Schematic Diagram for cascaded heat exchanger (CHX)

Mass Balance Equation:

$$\dot{m}_{27} = \dot{m}_{28} = \dot{m}_{N_2O,1} \quad (5.231)$$

$$\dot{m}_{30} = \dot{m}_{31} = \dot{m}_{N_2O,2} \quad (5.232)$$

Energy Balance Equation:

$$\dot{m}_{N_2O,1}(h_{28} - h_{27}) = \dot{m}_{N_2O,2}(h_{30} - h_{31}) \quad (5.233)$$

$$\varepsilon = \frac{T_{30} - T_{31}}{T_{30} - T_{27}} \quad (5.234)$$

Entropy Balance Equation:

$$\dot{m}_{N_2O,1}(s_{28} - s_{27}) = \dot{m}_{N_2O,2}(s_{30} - s_{31}) + \dot{S}_{gen} \quad (5.235)$$

Exergy Balance Equation:

$$\dot{m}_{N_2O,1}(ex_{27} - ex_{28}) = \dot{m}_{N_2O,2}(ex_{31} - ex_{30}) + \dot{E}x_{D,CHX} \quad (5.236)$$

$$\dot{E}x_{D,CHX} = T_0\left[\dot{m}_{N_2O,1}(s_{28} - s_{27}) - \dot{m}_{N_2O,2}(s_{30} - s_{31})\right] \quad (5.237)$$

$$\eta_{ex,CHX} = \frac{\dot{m}_{N_2O,1}(ex_{27} - ex_{28})}{\dot{m}_{N_2O,2}(ex_{31} - ex_{30})} \quad (5.238)$$

For Throttling Valve (TV5),

The liquid (state#32) is then expanded in throttling valve-5(TV5) (state#33).

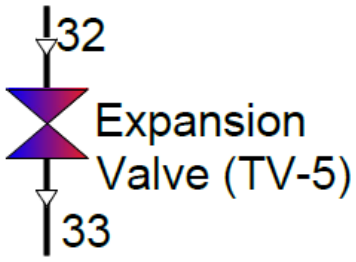

Figure 5.37 Schematic Diagram for Throttling Valve (TV5)

Mass Balance Equation:

$$\dot{m}_{32} = \dot{m}_{33} = \dot{m}_{N_2O,2} \quad (5.239)$$

Energy Balance Equation:

$$h_{32} = h_{33} \quad (5.240)$$

Entropy Balance Equation:

$$\dot{S}_{gen} = \left[\dot{m}_{N_2O,2}(s_{33} - s_{32})\right] \quad (5.241)$$

Exergy Balance Equation:

$$\dot{m}_{N_2O,2}\, ex_{32} = \dot{m}_{N_2O,2}\, ex_{33} + \dot{E}x_{D,TV1} \quad (5.242)$$

$$\dot{E}x_{D,TV5} = T_0\left[\dot{m}_{N_2O,2}(s_{33} - s_{32})\right] \quad (5.243)$$

$$\eta_{ex,TV5} = \frac{ex_{33}}{ex_{32}} \quad (5.244)$$

For the high temperature cycle, superheated nitrous oxide vapor (state#23) is compressed in COMP1 (24) and supercritical vapor is then cooled in the Gas cooler (C-3) (state#24, 25). Nitrous oxide is again cooled (state#25,26) in the internal heat exchanger-1 (IHX 1) through heating of saturated vapor (state#28,23). The nitrous oxide (state#26) is expanded (state#27) in throttling valve-4 (TV4), followed by its heating (state#27,28) in the CHX.

For Compressor 1 (Comp-1)

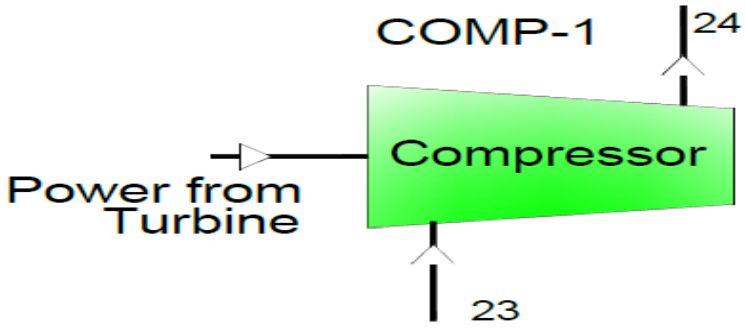

Figure 5.38 Schematic Diagram for compressor 1 (Comp-1)

Mass Balance Equation:

$$\dot{m}_{23} = \dot{m}_{24} = \dot{m}_{N_2O,1} \quad (5.245)$$

Energy Balance Equation:

$$\dot{W}_{COMP1} = \dot{m}_{N_2O,1}(h_{24} - h_{23}) \quad (5.246)$$

$$\eta_{en,comp.1} = \frac{\dot{m}_{N_2O,1}(h_{24} - h_{23})}{\dot{W}_{COMP1,input}} \quad (5.247)$$

$$\eta_{S,comp.1} = \frac{\dot{W}_{COMP1,Isentropic}}{\dot{W}_{COMP1,Actual}} \quad (5.248)$$

$$\eta_{S,comp.1} = \frac{h_{24s} - h_{23}}{h_{24a} - h_{23}} \quad (5.249)$$

$$h_{24a} = h_{23} + \frac{h_{24s} - h_{23}}{\eta_{S,comp.2}} \quad (5.250)$$

Entropy Balance Equation:

$$\dot{S}_{gen,COMP1} = [\dot{m}_{N_2O,1}(s_{24} - s_{23})] \quad (5.251)$$

Exergy Balance Equation:

$$\dot{W}_{COMP1} = \dot{m}_{N_2O,1}(ex_{24} - ex_{23}) + \dot{E}x_{D,COMP1} \quad (5.252)$$

$$\dot{E}x_{D,COMP1} = T_0\left[\dot{m}_{N_2O,1}(s_{24} - s_{23})\right] \quad (5.253)$$

$$\eta_{ex,Comp1} = \frac{\dot{m}_{N_2O,1}(ex_{24} - ex_{23})}{\dot{W}_{COMP1}} \quad (5.254)$$

For Condenser-3 in cascaded refrigeration cycle,

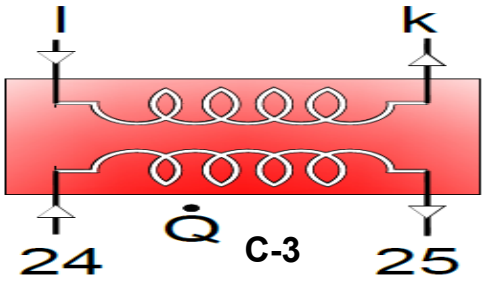

Condenser-3

Figure 5.39 Schematic Diagram for Condenser-3 (C-3)

Mass Balance Equation:

$$\dot{m}_l = \dot{m}_k = \dot{m}_{C3} \quad (5.255)$$

$$\dot{m}_{25} = \dot{m}_{24} = \dot{m}_{N_2O,1} \quad (5.256)$$

Energy Balance Equation:

$$\dot{Q}_{C3} = \dot{m}_{N_2O,1}(h_{25} - h_{24}) = \dot{m}_{N_2O,1}(h_k - h_l) \quad (5.257)$$

Entropy Balance Equation:

$$\dot{m}_{C3}(s_{25} - s_{24}) = \dot{m}_{N_2O,1}(s_l - s_k) + \dot{S}_{gen} \quad (5.258)$$

Exergy Balance Equation:

$$\dot{m}_{N_2O,1}(ex_{25} - ex_{24}) + \dot{E}x_{D,C3} = \dot{m}_{N_2O,1}(ex_l - ex_k) \quad (5.259)$$

$$\dot{E}x_{D,C3} = T_0\dot{m}_{N_2O,1}[\,(s_k - s_l) + (s_{25} - s_{24})] \quad (5.260)$$

$$\eta_{ex,C3} = \frac{\dot{m}_{C3}(ex_k - ex_l)}{\dot{m}_{N_2O,1}(ex_{24} - ex_{25})} \quad (5.261)$$

T24 is the temperature for the Refrigerant vapor in a **superheated state**. In the condenser, the superheated refrigerant vapor condenses to saturated vapor, which is at a constant temperature T25. T_L represent cooled water from cooling tower, 30°C, under typical summer conditions. The temperature difference can be defined as:

$$\Delta T_{C3} = T_{25} - T_L \quad (5.262)$$

Since T_L is 30°C, the lower the value of ΔT_{C3}, the more efficient the heat transfer, and the lower the exergy destruction in the condenser.

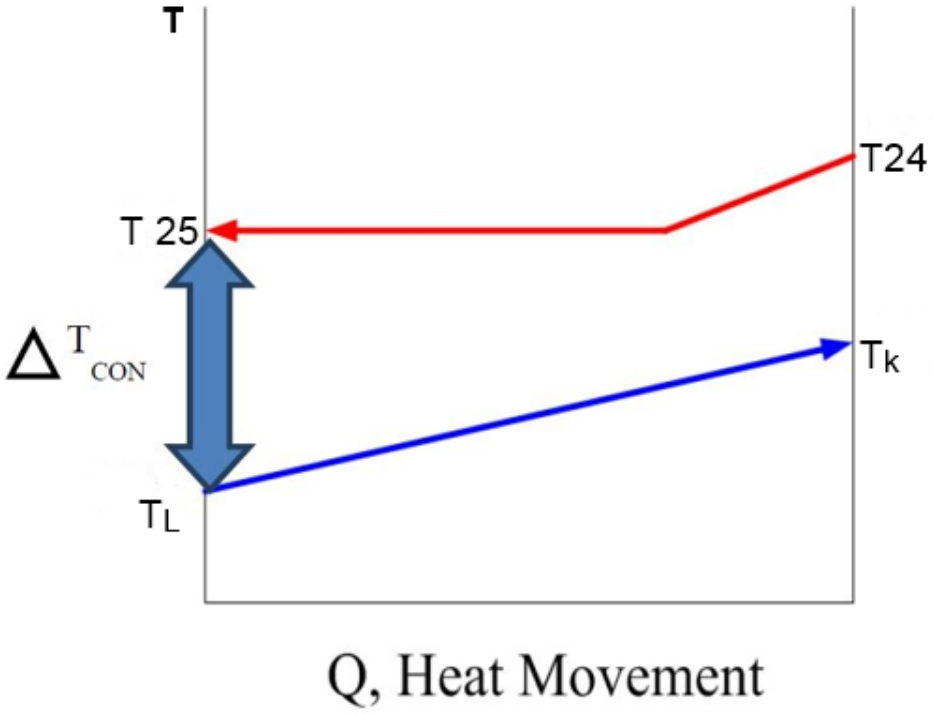

Figure 5.40 T-Q diagram for condenser (C-3).

For Internal Heat Exchanger (IHX),

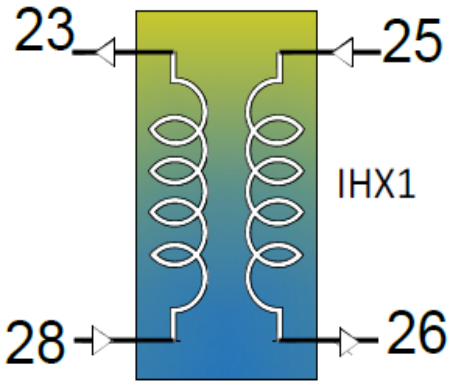

Figure 5.41 Schematic Diagram Internal Heat Exchanger (IHX1)

Mass Balance Equation:

$$\dot{m}_{23} = \dot{m}_{28} = \dot{m}_{N_2O,1} \tag{5.263}$$

$$\dot{m}_{25} = \dot{m}_{26} = \dot{m}_{N_2O,1} \quad (5.264)$$

Energy Balance Equation:

$$h_{25} - h_{26} = h_{23} - h_{28} \quad (5.265)$$

$$\varepsilon = \frac{T_{23} - T_{28}}{T_{25} - T_{28}} \quad (5.266)$$

Entropy Balance Equation:

$$\dot{S}_{gen,IHX1} = [\dot{m}_{N_2O,1}(s_{26} - s_{25} + s_{23} - s_{28})] \quad (5.267)$$

Exergy Balance Equation:

$$ex_{23} - ex_{28} = ex_{25} - ex_{26} - \dot{E}x_{D,IHX1} \quad (5.268)$$

$$\dot{E}x_{D,IHX1} = T_0[\dot{m}_{N_2O,1}(s_{26} - s_{25} + s_{23} - s_{28})] \quad (5.269)$$

$$\eta_{ex,IHX1} = \frac{ex_{23} - ex_{28}}{ex_{25} - ex_{26}} \quad (5.270)$$

For Throttling Valve (TV4),

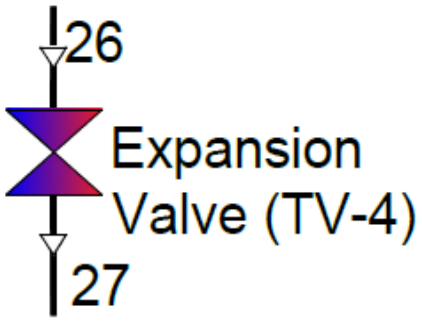

Figure 5.42 Schematic Diagram Throttling Valve (TV4).

Mass Balance Equation:

$$\dot{m}_{27} = \dot{m}_{26} = \dot{m}_{N_2O,1} \quad (5.271)$$

Energy Balance Equation:

$$h_{26} = h_{27} \tag{5.272}$$

Entropy Balance Equation:

$$\dot{S}_{gen} = \left[\dot{m}_{N_2O,1}(s_{27} - s_{26}) \right] \tag{5.273}$$

Exergy Balance Equation:

$$\dot{m}_{N_2O,1}\, ex_{26} = \dot{m}_{N_2O,1}\, ex_{27} + \dot{E}x_{D,TV4} \tag{5.274}$$

$$\dot{E}x_{D,TV4} = T_0 \left[\dot{m}_{N_2O,1}(s_{27} - s_{26}) \right] \tag{5.275}$$

$$\eta_{ex,TV1} = \frac{ex_{27}}{ex_{26}} \tag{5.276}$$

For Cascaded refrigeration cycle Evaporator (E3),

The useful cooling in the evaporator-3(E3) is achieved by evaporating nitrous oxide from state 33 to state 34.

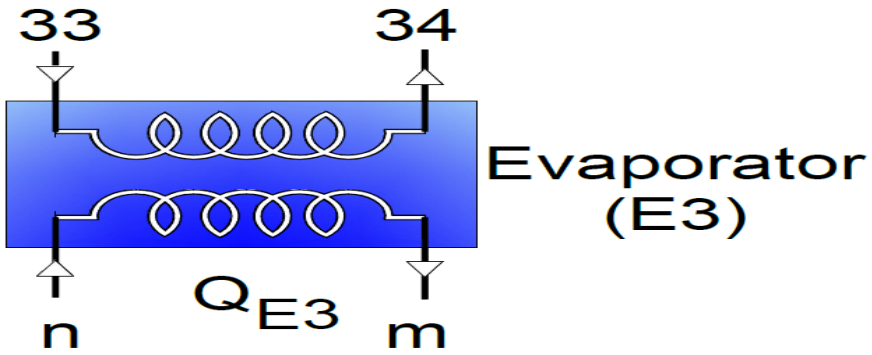

Figure 5.43 Schematic Diagram for Evaporator (E3)

Mass Balance Equation:

$$\dot{m}_n = \dot{m}_m = \dot{m}_{E3} \tag{5.277}$$

$$\dot{m}_{33} = \dot{m}_{34} = \dot{m}_{N_2O,2} \tag{5.278}$$

Energy Balance Equation:

$$\dot{Q}_{E3} = \dot{m}_{N_2O,2}(h_{34} - h_{33}) \quad (5.279)$$

$$\dot{Q}_{E3} = \dot{m}_{E3}(h_m - h_n) \quad (5.280)$$

$$\dot{m}_{N_2O,2}(h_{34} - h_{33}) = \dot{m}_{E3}(h_m - h_n) \quad (5.281)$$

Entropy Balance Equation:

$$\dot{m}_{E3}(s_m - s_n) = \dot{m}_{N_2O,2}(s_{33} - s_{34}) + \dot{S}_{gen} \quad (5.282)$$

Exergy Balance Equation:

$$\dot{m}_{E3}(ex_n - ex_m) = \dot{m}_{N_2O,2}(ex_{34} - ex_{33}) + \dot{E}x_{D,E3} \quad (5.283)$$

$$\dot{E}x_{D,E3} = T_0\left[\dot{m}_{E3}(s_m - s_n) + \dot{m}_{N_2O,2}(s_{34} - s_{33})\right] \quad (5.284)$$

$$\eta_{ex,E3} = \frac{\dot{m}_{N_2O,2}(ex_{34} - ex_{33})}{\dot{m}_{E3}(ex_n - ex_m)} \quad (5.285)$$

Tn and Tm are design conditions for the application out of the evaporator (a -80°C temperature set point) and the loop into the evaporator (-50°C). T33 and T34 represent the entry and exit points for the water vaporizing inside the evaporator, and are therefore the same temperature. So, in order to provide cooling, T33 and T34 must be lower than -80°C, and a temperature difference can be defined as:

$$\Delta T_{E3} = T_m - T_{33} = -80 - T_{33} \quad (5.286)$$

It can be observed that the lower the value of ΔT_{E3}, the lower the exergy destruction inside the evaporator.

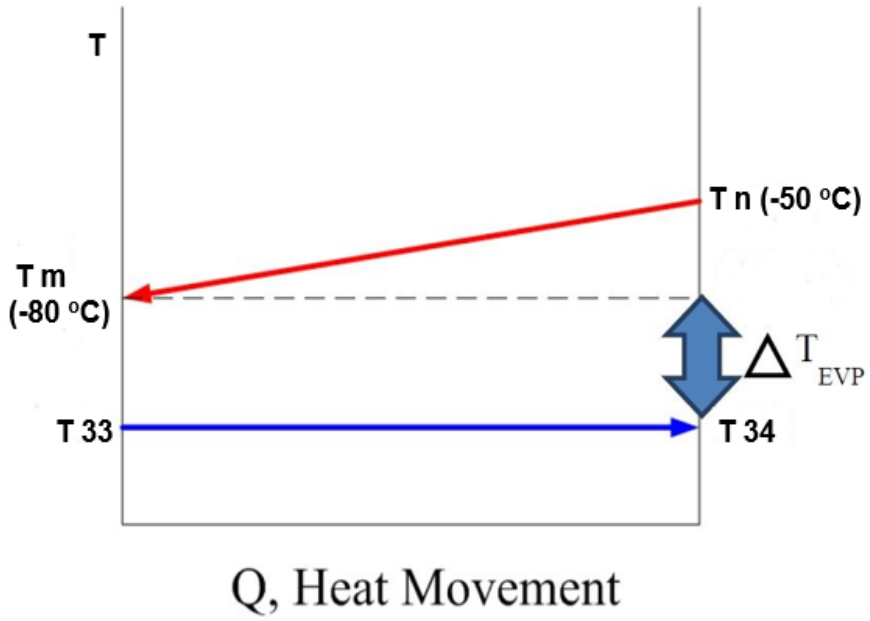

Figure 5.44 T-Q diagram for evaporator (E3).

CHAPTER 6
RESULT AND DISCUSSION

A thermodynamic analysis has been conducted to assess the performance variation of the solar assisted triple effect refrigeration system with varying some influential operating parameter.

Some of operating parameter will vary over a typical range of operation to find out its effect on the overall cycle whereas values of other parameters are kept constant at the level of base case values.

The first law efficiency and energy distribution of solar heat source are obtained by energy balance approach or the first law analysis of the cycle. However, the exergy destruction or irreversibility in each component and the second law efficiency are obtained using the exergy balance approach or the second law analysis of the cycle.

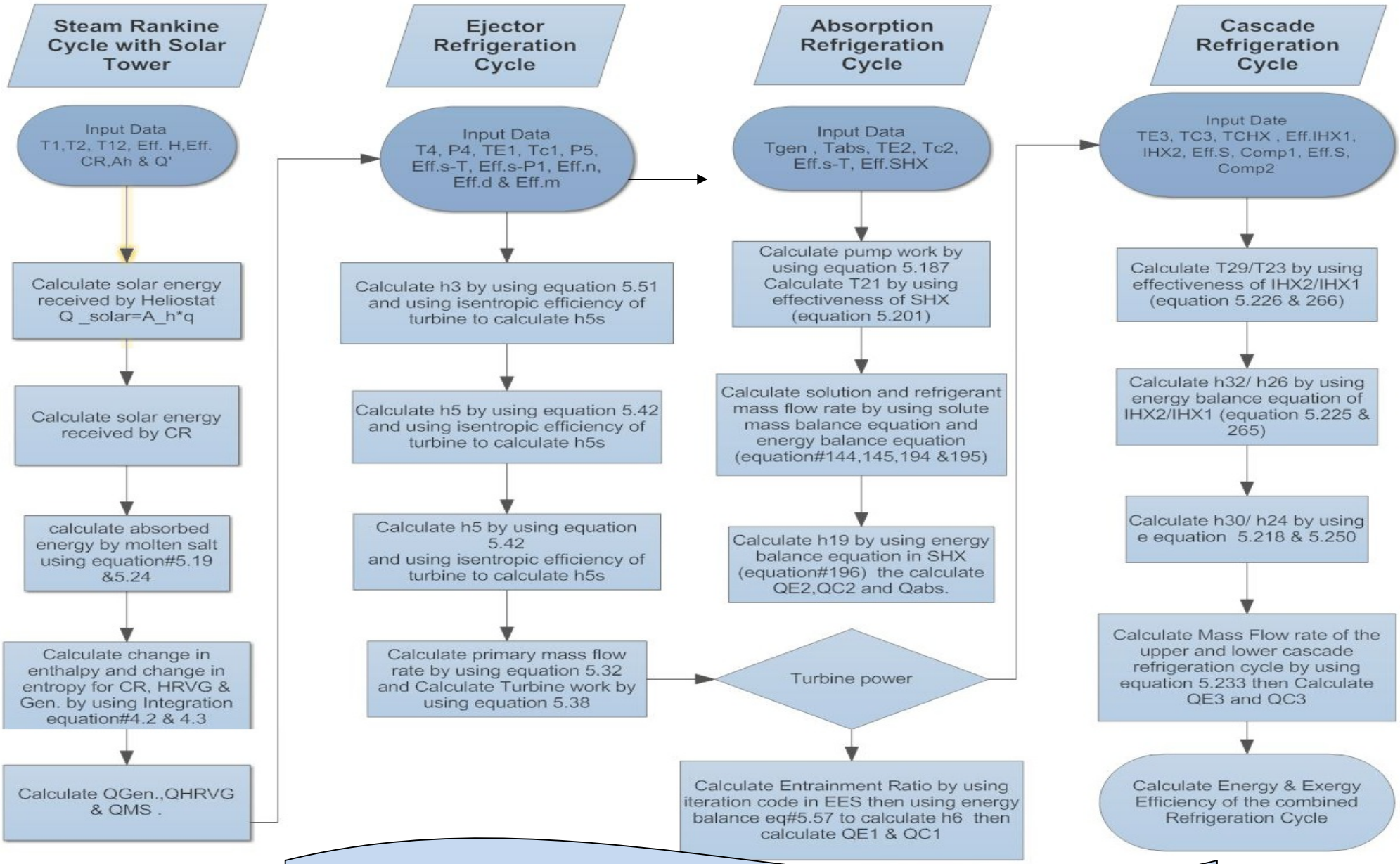

Flow Chart of Solar Assisted Triple Effect Refrigeration Cycles Calculation Algorithm

6.1 Main operating parameter considered in the proposed cycle.

Environnent Temperature (°C)	20
Environnent Pressure (MPa)	0.10135
Turbine Inlet Pressure Range (MPa)	**0.9–1.7**
Hot Molten Salt Outlet Temperature (°C)	**350-565**
Hot Molten Salt Inlet Temperature (°C)	290
Generator temperature (°C)	130
Solar Radiation Received (W/m^2)	**500-800**
Apparent Sun Temperature (K)	4,500
Heliostat Aperture Area (m^2)	10,000
Turbine Back Pressure Range (kPa)	**220–300**
Turbine Isentropic Efficiency (%)	85
ERC Evaporator Temperature (°C)	**1 to 5**
ARC Evaporator Temperature (°C)	**6 to 10**
CRC Evaporator Temperature Range (°C)	**-50 to -80**
Condenser-2 Temperature (°C)	35
Condenser-3 Temperature (°C)	35
Absorber Temperature (°C)	35
Pump Isentropic Efficiency (%)	70
HRVG Efficiency (%)	100
Upper Cascade Ref. Cycle Temperature (°C)	10.0
Lower Cascade Ref. Cycle Temperature (°C)	20.0
Nozzle Efficiency (%)	90
Mixing Chamber Efficiency (%)	85
Diffuser Efficiency (%)	85
Optical Efficiency of Heliostat Field (%)	75
First Law Efficiency of Central Receiver (%)	90
Second Law Efficiency of Heliostat Field (%)	75
Second Law Efficiency of Central Receiver (%)	30
Effectiveness of SHX, IHX1, IHX2 (%)	50
Central Receiver	
Aperture Area (m^2)	16.96
View Factor	0.80

Tube Diameter (m)	0.019
Tube Thickness (m)	0.00165
Emissivity	0.80
Reflectivity	0.04
Wind Speed (m/s)	5
Passes	20

6.2 Model Validation:

After modeling the triple effect refrigeration cycle according to the aforementioned methodology, the next step is to verify the results with the available models in the literature for each cycle individually.

The presently developed model has been validated against previously published models in the literature and excellent agreement between these models was revealed as reported hereunder.

The present model of the solar assisted triple effect refrigeration cycle was validated against Kumar et. al model [132] and Jameel et. al model [158].

6.2.1 Solar Central Receiver Model Validation:

The present solar central receiver model was compared with model of Jameel et. al [158] and the comparative result was plotted to show the differences between both models, and excellent agreements were observed.

Figure 6.1 shows the variation of central receiver surface temperatures with changing aperture area. It is observed that the difference between both models and the error percentage was less than 5%.

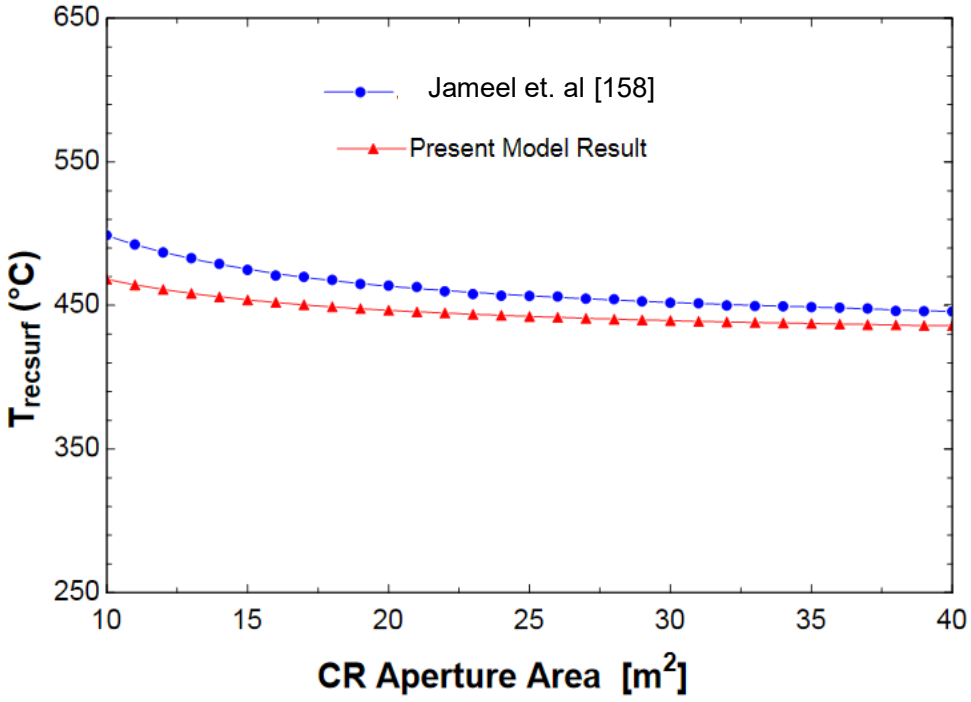

Figure 6.1 Validation for CR Surface Temperature Variation with Aperture Area for present model and Jameel et. al model [158].

Figures 6.2 and 6.3 depict validation result for variation of the central receiver thermal efficiency and surface temperature with changing the hot molten salt outlet temperature and good agreement with Jameel et. al model [158] is observed.

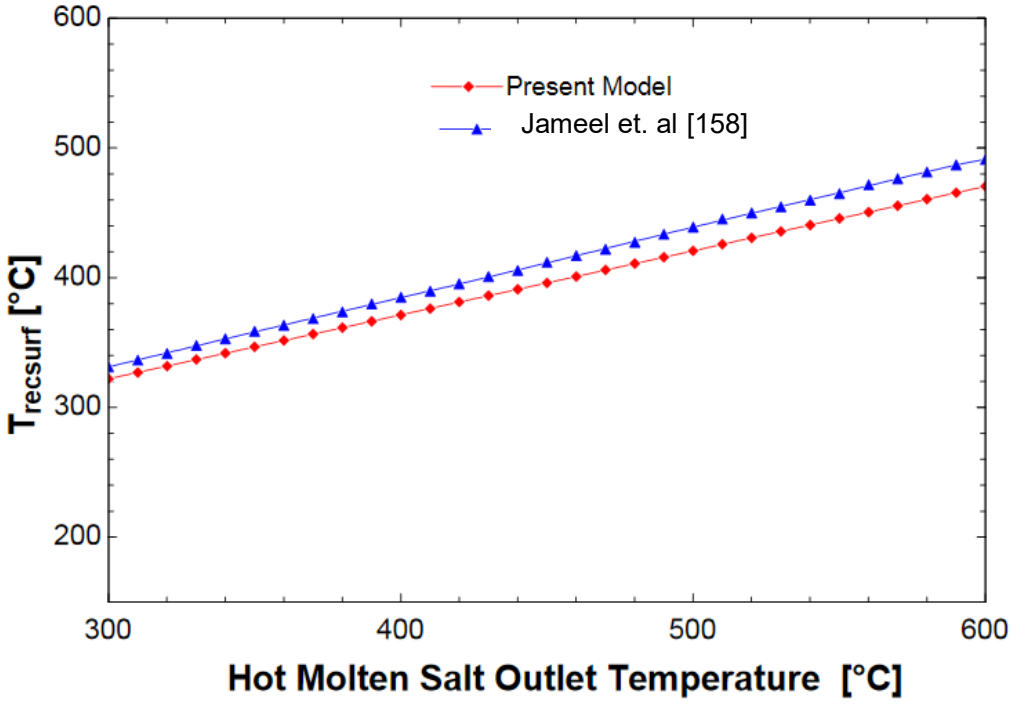

Figure 6.2 Validation for CR Surface Temperature variation with hot molten salt outlet temperature for present model and Jameel et. al model [158].

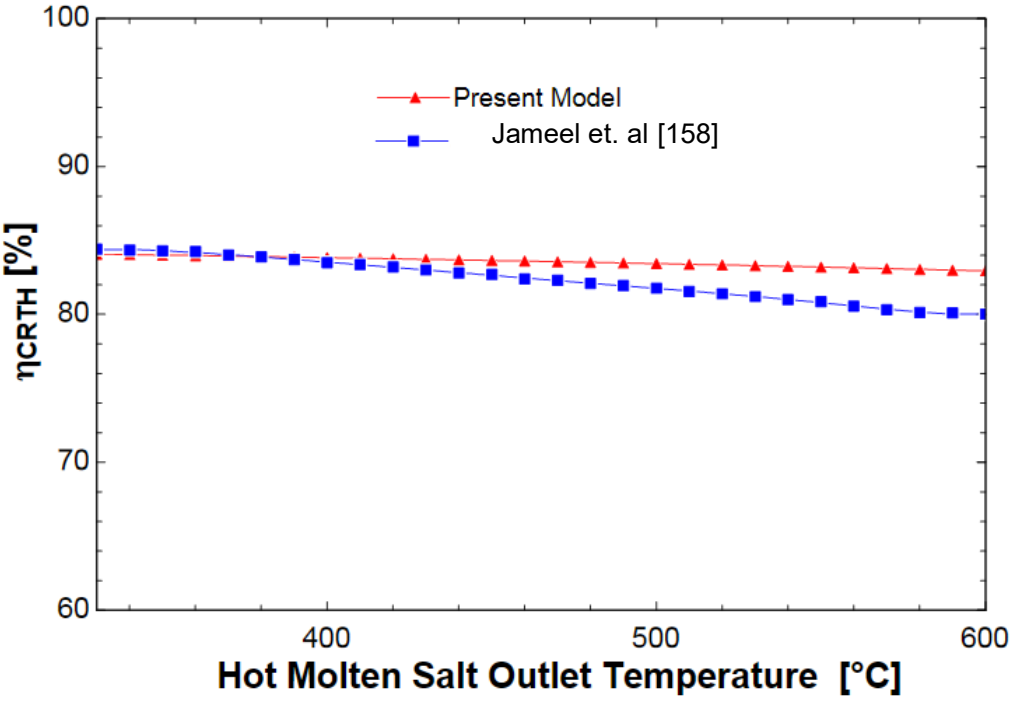

Figure 6.3 Validation for CR Thermal Efficiency Variation with hot molten salt outlet temperature for present model and Jameel et. al model[158].

6.2.2 Ejector, Absorption and Cascade refrigeration cycles Validation:

The refrigeration output for ERC and ARC had been compared with Kumar et al. model [129], the following comparison shows the difference between the present model and Kumar et al. model varied with turbine inlet pressure and hot molten salt outlet temperature:

Figures 6.4 and 6.5 show excellent agreement between the present and Kumar et al. model for refrigeration output of ERC with variation of hot molten salt temperature and turbine inlet pressure.

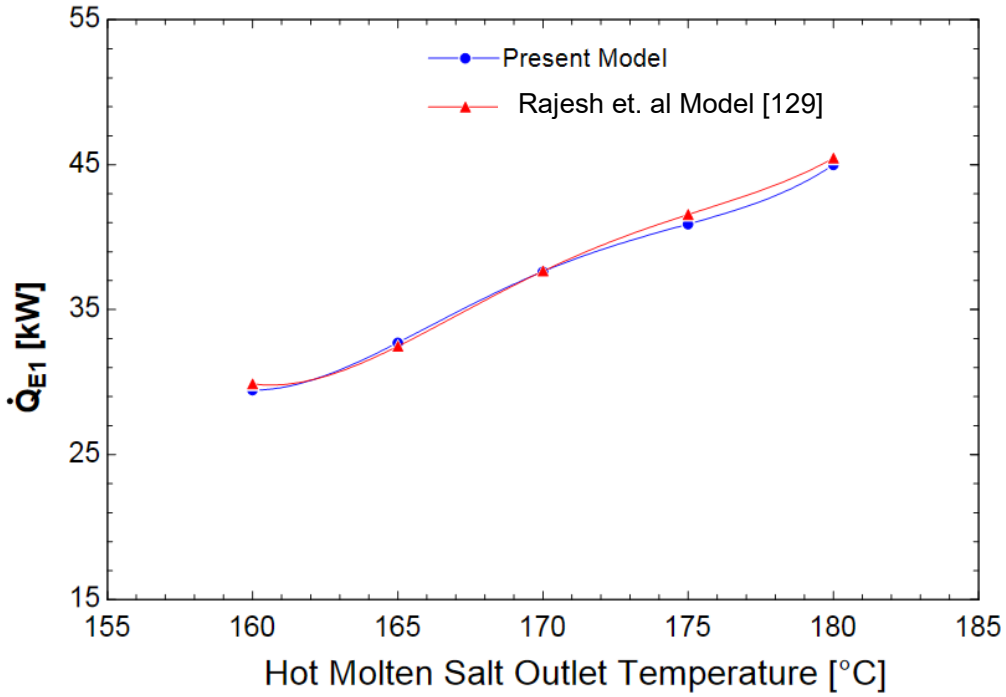

Figure 6.4 Validation for Ejector Cycle Refrigeration Output Variation with hot molten salt outlet temperature for present model and Kumar et al. model [129].

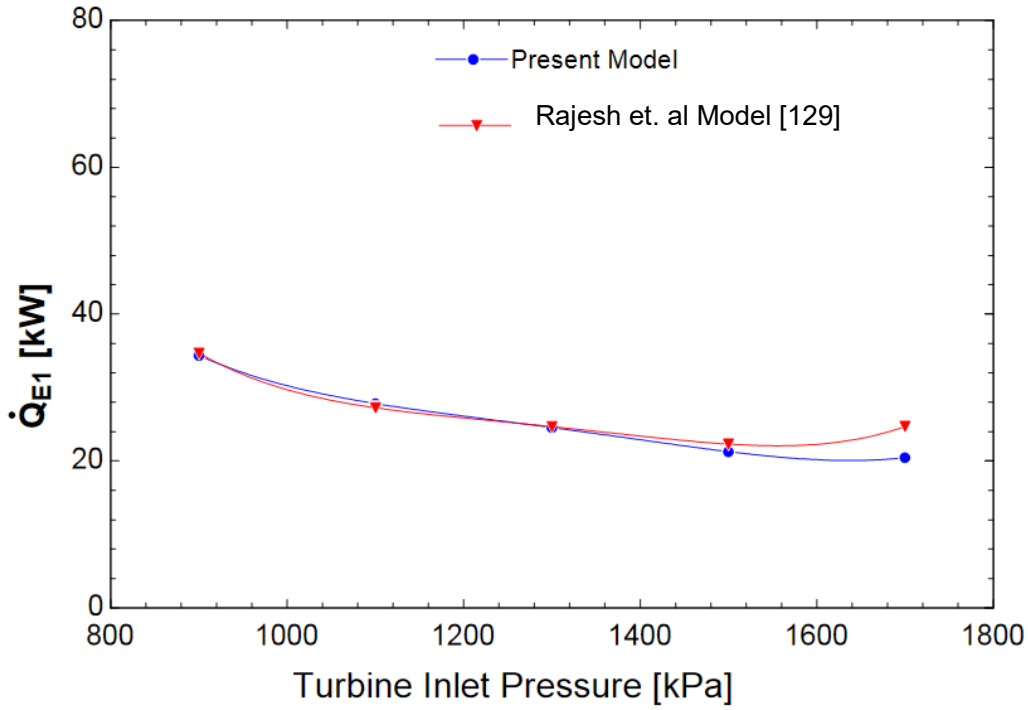

Figure 6.5 Validation for Ejector Cycle Refrigeration Output Variation with Turbine Inlet Pressure for Present Model and Kumar et al. model [129].

Table 6.1 shows the error percentage between the present model and Rajesh Kumar's model of ejector refrigeration cycle, which is less than 5%.

Table 6.1 ERC Refrigeration Output with inlet pressure variation comparison between Present and Kumar et al. Model [129].

Inlet Pressure	**ERC Refrigeration Output kW**		**Error**
kPa	**Present Model**	**Rajesh's Model**	**%**
900	34.36	34.69	0.94
1,100	27.81	27.24	2.11
1,300	24.54	24.67	0.53
1,500	21.27	22.30	4.63
1,700	20.45	20.72	1.30

Figures 6.6 and 6.7 show excellent agreement between the present and Kumar et al. model [129] for refrigeration output of absorption refrigeration cycle with changing hot molten salt outlet temperature and turbine inlet pressure.

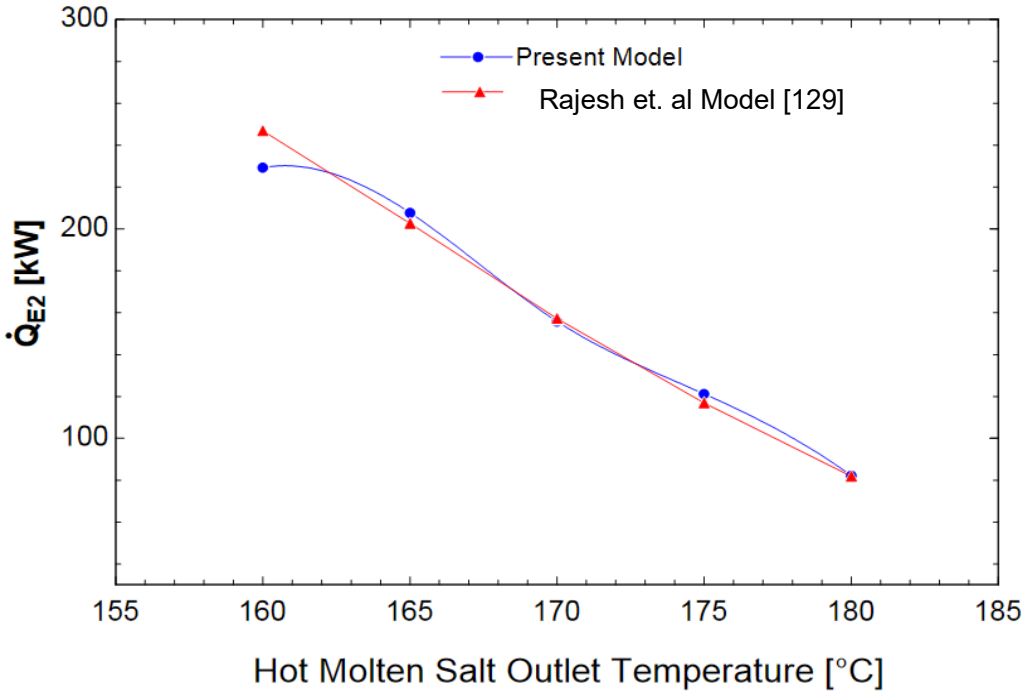

Figure 6.6 Validation for Absorption Cycle Refrigeration Output Variation with hot molten salt outlet temperature for present model and Kumar et al. model [129].

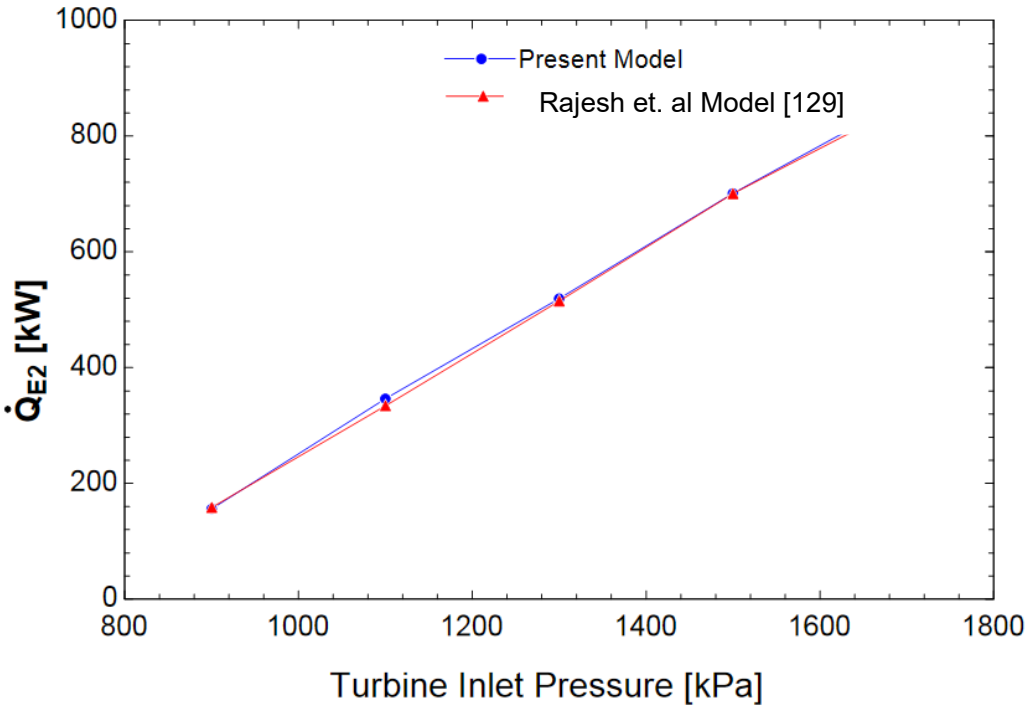

Figure 6.7 Validation for Absorption Cycle Refrigeration Output Variation with Turbine Inlet Pressure for Present Model and Kumar et al. model [129].

Table 6.2 shows the error percentage between the present model and Rajesh's model for absorption refrigeration cycle which is less than 5%.

Table 6.2 ARC Refrigeration Output with inlet pressure variation comparison between Present and Rajesh's model

Inlet Pressure	**ARC Refrigeration Output kW**		**Error**
kPa	**Present Model**	**Rajesh's Model**	**%**
900	155.8	158.45	1.67
1,100	346.1	334.17	3.57
1,300	519.2	514.83	0.85
1,500	700.9	700.49	0.06
1,700	865.3	856.44	1.04

Figures 6.6 and 6.7 show excellent agreement between the present and Kumar et al. model [129] for refrigeration output of cascade refrigeration cycle with variation of hot molten salt temperature and turbine inlet pressure.

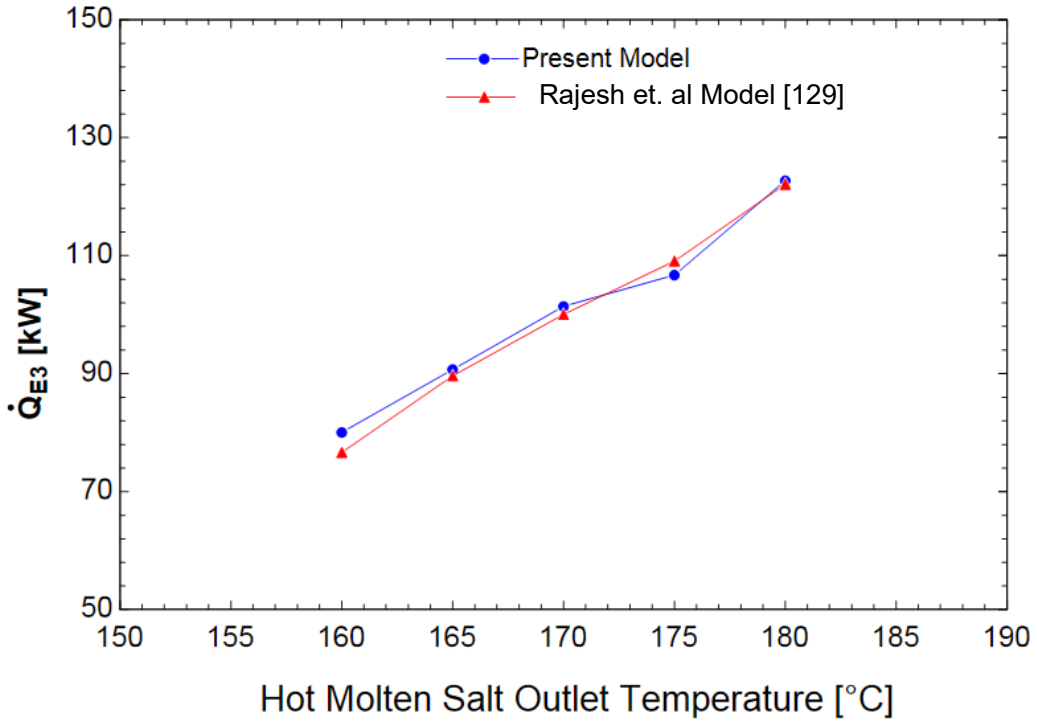

Figure 6.8 Validation for Cascade Cycle Refrigeration Output Variation with Hot Molten Salt Outlet temperature for present model and Kumar et al. model [129].

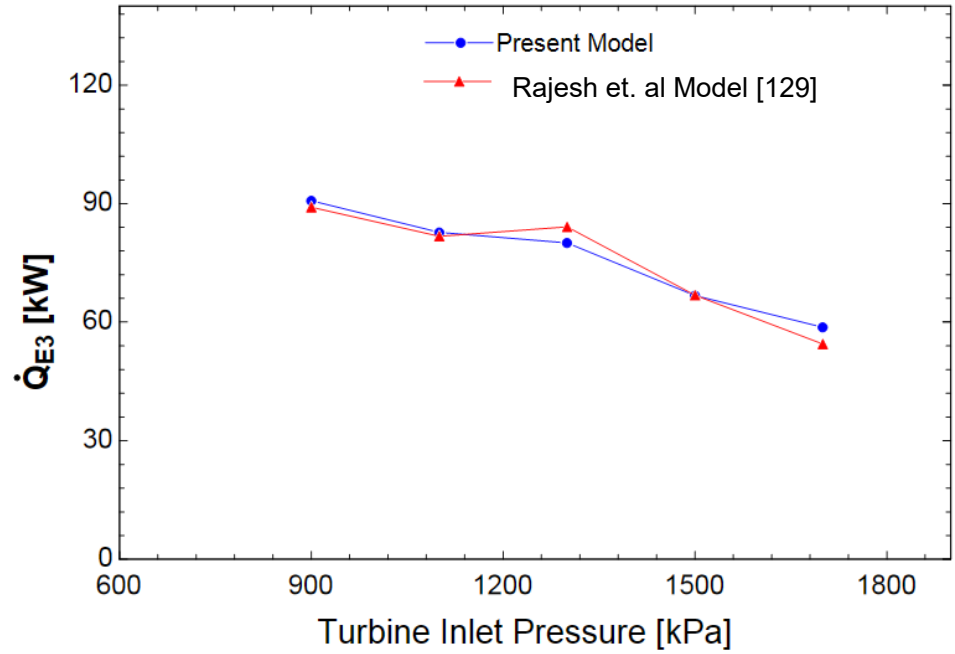

Figure 6.9 Validation for Cascade Cycle Refrigeration Output Variation with Turbine Inlet Pressure for Present Model and Kumar et al. model [129].

Table 6.3 shows the error percentage between present and RJK model of cascade refrigeration cycle which is less than 5%.

Table 6.3 CRC Refrigeration Output with inlet pressure variation comparison between Present and Kumar et al. model [129].

Inlet Pressure	CRC Refrigeration Output kW		Error
KPa	Present Model	Rajesh's Model	%
900	90.71	89.08	1.83
1,100	82.70	81.69	1.23
1,300	80.03	84.11	4.85
1,500	66.70	66.79	0.13
1,700	58.69	56.46	3.94

6.3 Power cycle analysis and central receiver performance

The power block used in the proposed solar assisted triple effect refrigeration cycle is generally a solar tower with a central receiver which provides the required thermal energy to steam rankine cycle.

The main component of steam rankine cycle consists of solar tower power plant (heliostat and central receiver) with a heat recovery generator, turbine, condenser and pump. The central receiver absorbs solar radiation and part of this energy is absorbed by molten salt. Some energy is lost to the environment due to heat losses by forced and natural convection, emission, reflection and conduction [155].

The total heat loss and the average surface temperature of the absorber are important factors to calculate the efficiency of the receiver.

Table 6.4 Energy analysis of the base case central receiver-Solar tower system.

subsystem	Energy Analysis			
	Received kW	Delivered kW	Loss kW	Efficiency (%)
Heliostat Field	8,000.0	6,000.0	2,000.0	75.0
Central Receiver	6,000.0	5,401.3	598.7	90.0
HRVG	5,401.3	5,401.3	0.0	100.0
Power Model	5,401.3	2,080.6	3,320.7	37.85
Overall Cycle	8,000.0	1,830.9	6,169.1	22.89

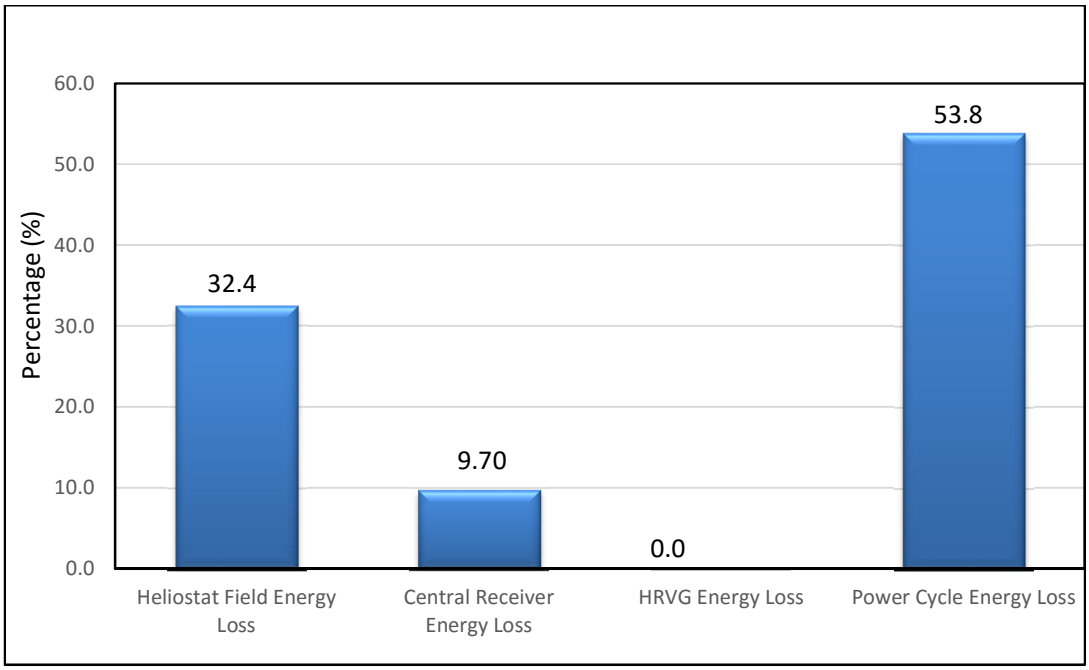

Figure 6.10 Energy losses in the solar tower and rankine cycle.

The results of energy analysis of the base case system are listed in Table 6.4. The percentages of energy losses at each subsystem are shown in Figure 6.10.

Table 6.5 Exergy analysis of the base case Central receiver-Solar tower.

subsystem	Exergy Analysis			
	Received kW	Delivered kW	Loss kW	Efficiency (%)
Heliostat Field	7,478.8	5,609.1	1,869.7	75.0
Central Receiver	5,609.1	3,111.7	2,497.9	55.48
HRVG	3,111.7	2,793.5	318.2	89.77
Power Model	2,793.5	2,080.6	712.9	74.48
Overall Cycle	7,478.8	1,830.9	5,647.9	24.48

The results of exergy analysis of the base case system are listed in Table 6.5. The percentages of exergy losses at each subsystem are shown in Figure 6.11.

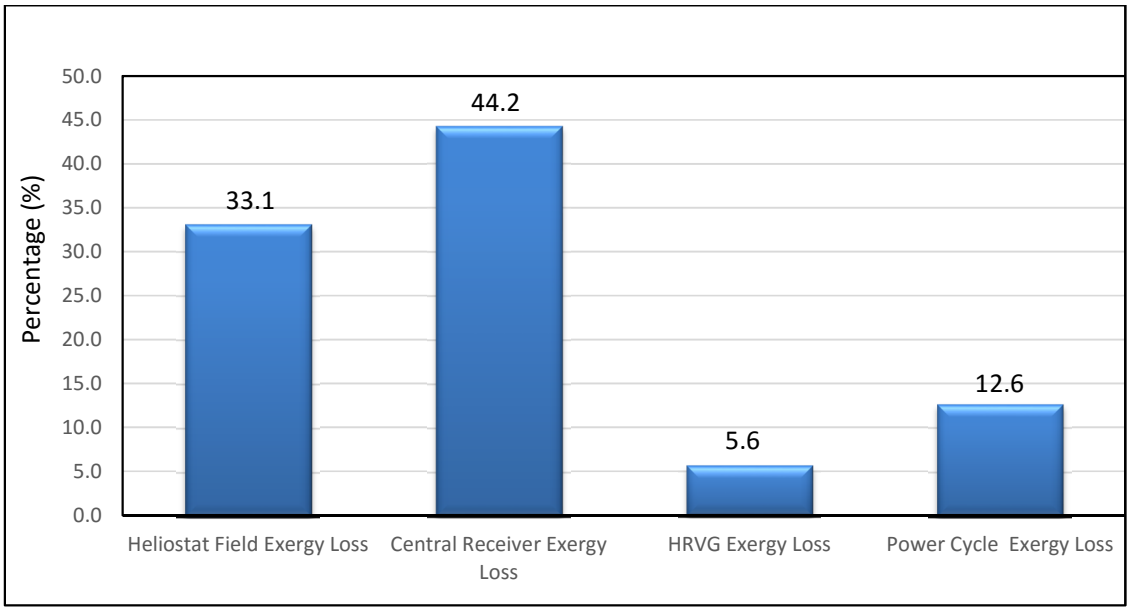

Figure 6.11 Exergy losses in the solar tower and rankine cycle.

Figure 6.12 shows central receiver energy efficiency and surface temperature variation with changing hot molten salt outlet temperature. It is observed that the energy efficiency decreased with increasing hot molten salt outlet temperature while the central receiver surface temperature is increased. The energy efficiency decrease is due to the

larger heat losses which are associated with the higher surface temperature of the central receiver.

Furthermore, there is a limitation on increasing the outlet temperature of molten salt due to material constraints of the pipes.

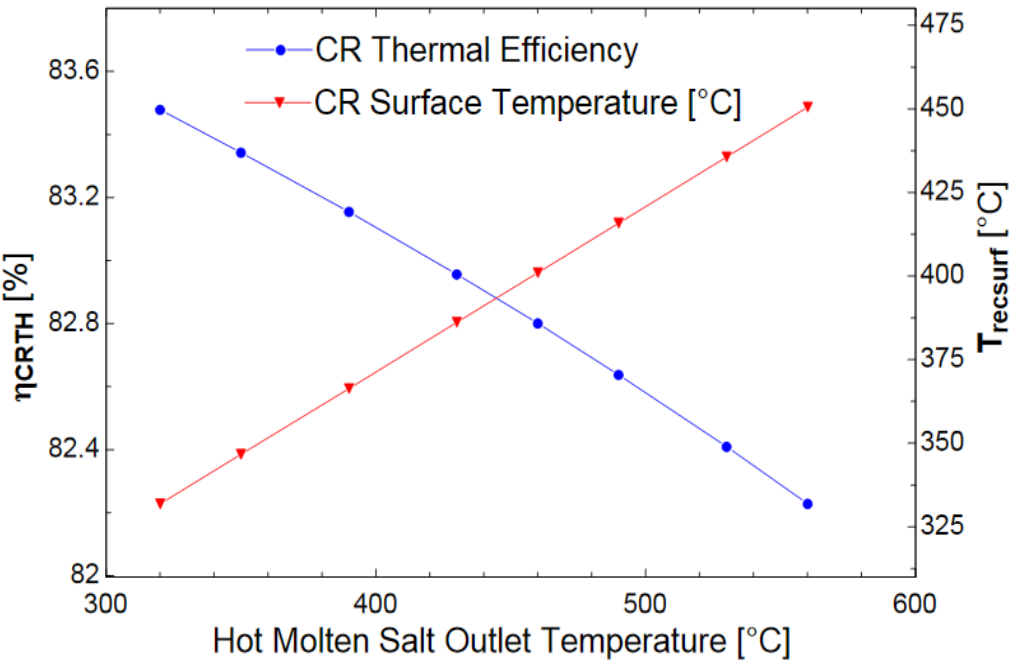

Figure 6.12 CR Thermal Efficiency and Surface Temperature variation with Hot Molten Salt Outlet Temperature.

Figure 6.13 shows the relationship between hot molten salt outlet temperatures with different types of receiver heat losses. It is observed that the total heat losses increase with increasing hot molten salt temperature.

Furthermore, a significant increase in the emissive heat losses is observed with increasing outlet temperature of the hot molten salt while a insignificant increase is observed in other types of heat losses.

It is observed from Figure 6.13 that the emissive heat losses are the lowest compared to all types of heat losses.

Forced Convection heat losses were considered as forced convection from a flat plate.

The emissive heat losses calculated based on average receiver surface temperature. The reflective heat losses calculated according to surface reflectivity and view factor.

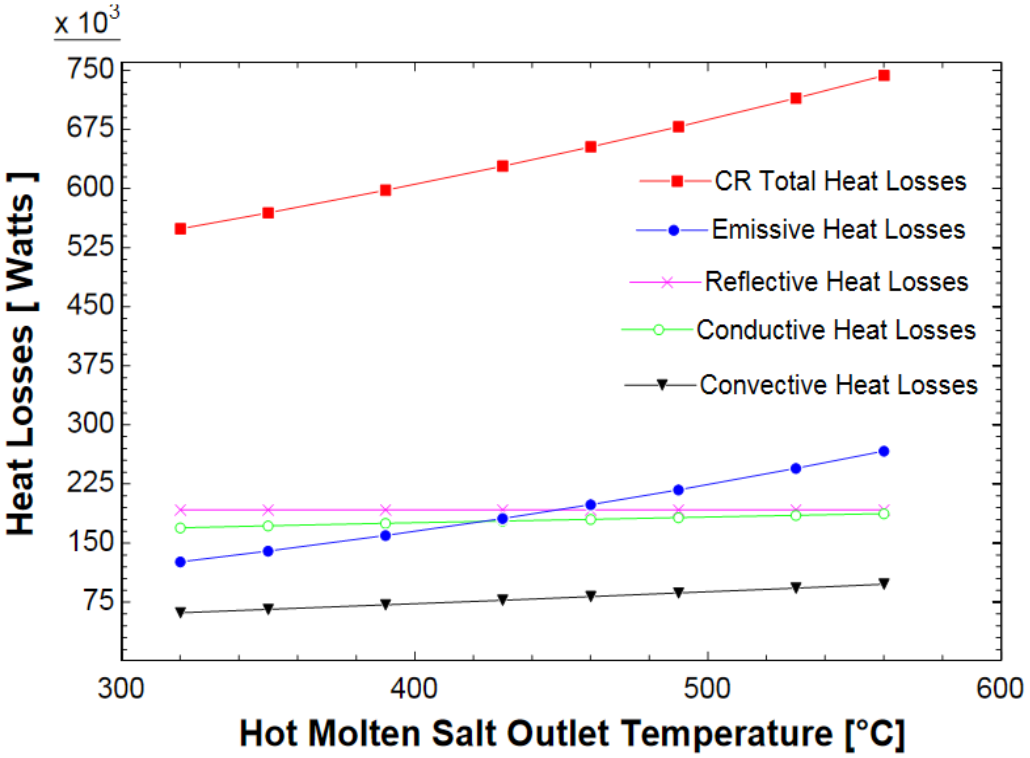

Figure 6.13 CR Heat Losses Variation with Hot Molten Salt Outlet Temperature.

6.4 Central receiver performance variation with incident solar isolation

The incident solar isolation has a significant effect on the performance of the solar tower.

Figure 6.14 indicates the variation in the energy efficiencies with variation of incident solar isolation, which varies with the geographical position.

In this research we considered the weather data of Dhahran, so in this chapter we will study the effect of average daily and hourly solar radiation on June 11 and December 10 then evaluate the effect of

incident solar radiation on the refrigeration cycle output and overall combined cycle efficiency.

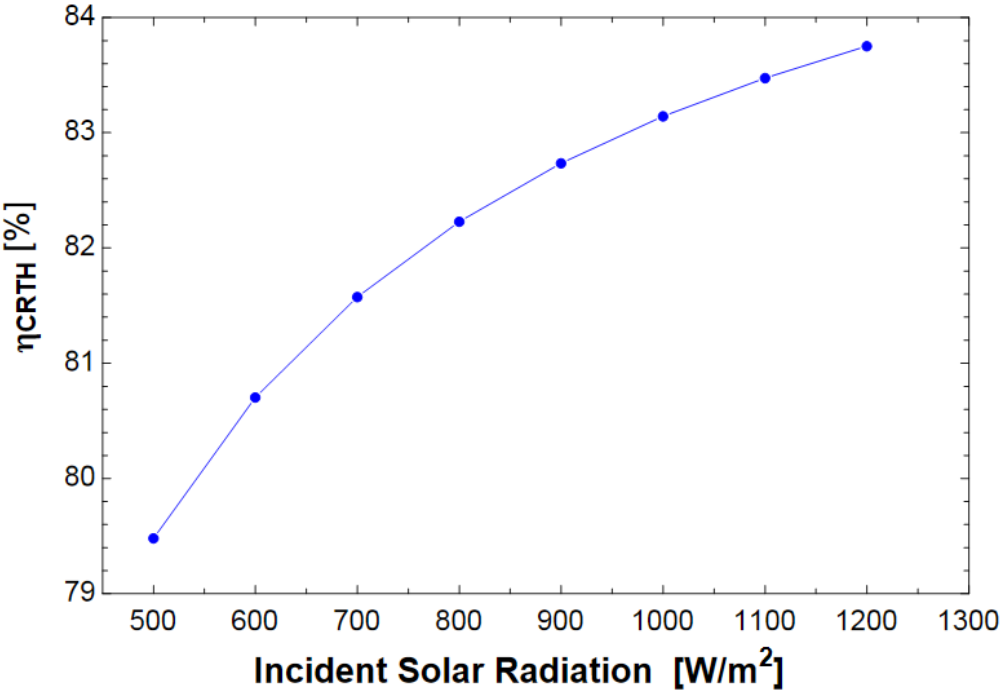

Figure 6.14 CR Thermal Efficiency Variation with Incident Solar Radiation.

It is observed from figure 6.14 that the energy efficiencies increase with the increase in the incident solar isolation. This is due to fact that the CR emissive and convective heat loss depend on the central receiver surface temperature rather than the incident solar radiation. Figure 6.15 shows the effect of incident solar radiation variation on the surface temperature of the receiver which clearly showed that with a large increase in Incident solar radiation, the surface temperature increases slightly, therefore the emissive and convective heat loss increased slightly.

When incident solar radiation increased from 500 to 1,200 [W/m^2], the central receiver surface temperature increased from 441 to 463.3 [^{o}C] which is less than 5 % (around 22 [^{o}C]).

It is observed that the CR thermal efficiency greatly increased to low incident solar radiation.

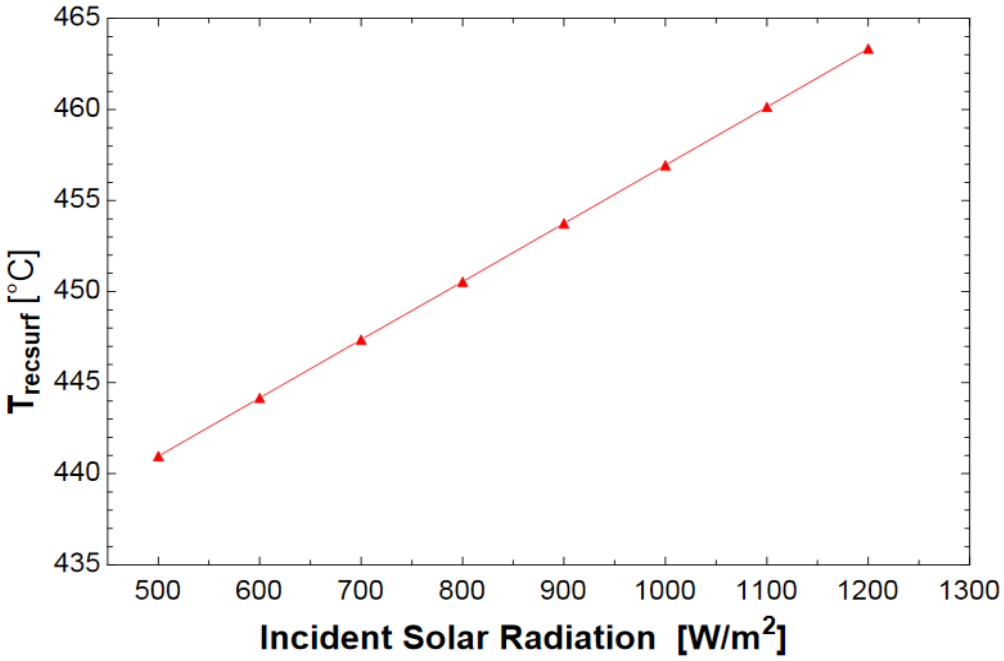

Figure 6.15 CR Surface Temperature Variation with incident Solar Radiation.

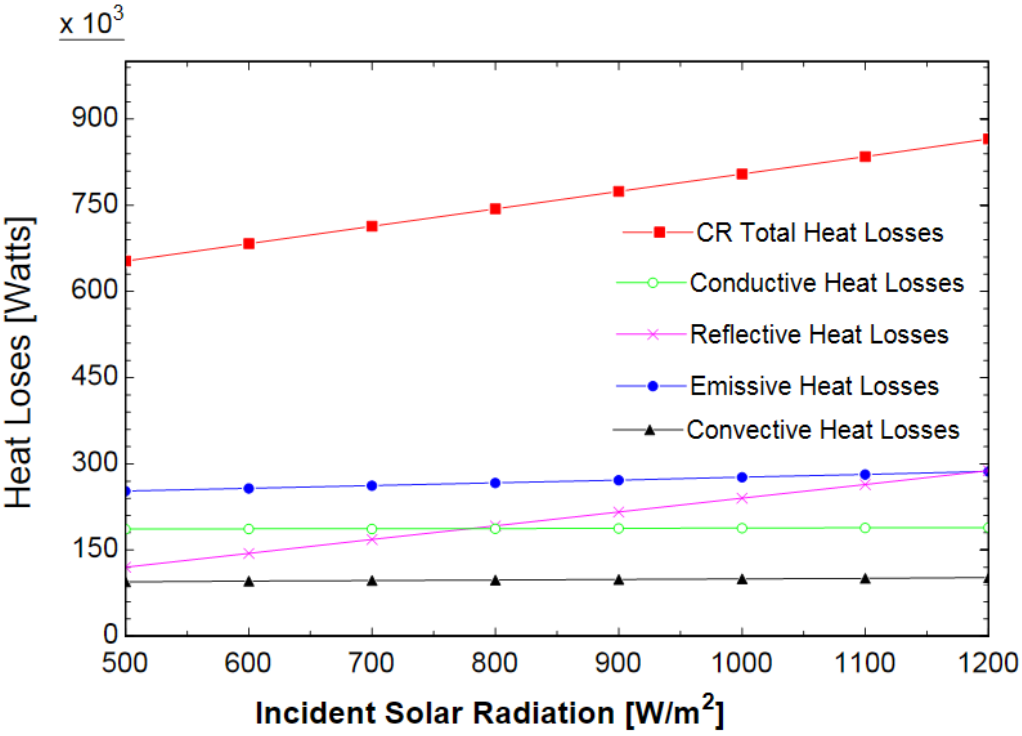

Figure 6.16 CR Surface Temperature Variation with incident Solar Radiation.

6.5 Central receiver performance variation with aperture Area:

The aperture area of the central receiver is one of the influential factors that effect on the efficiency of the central receiver. Figure 6.17 shows the difference between the aperture and surface area of the central receiver.

The larger receiver aperture area will produce more heat losses (all heat losses will be increased except reflective heat losses which depend on incident solar radiation)

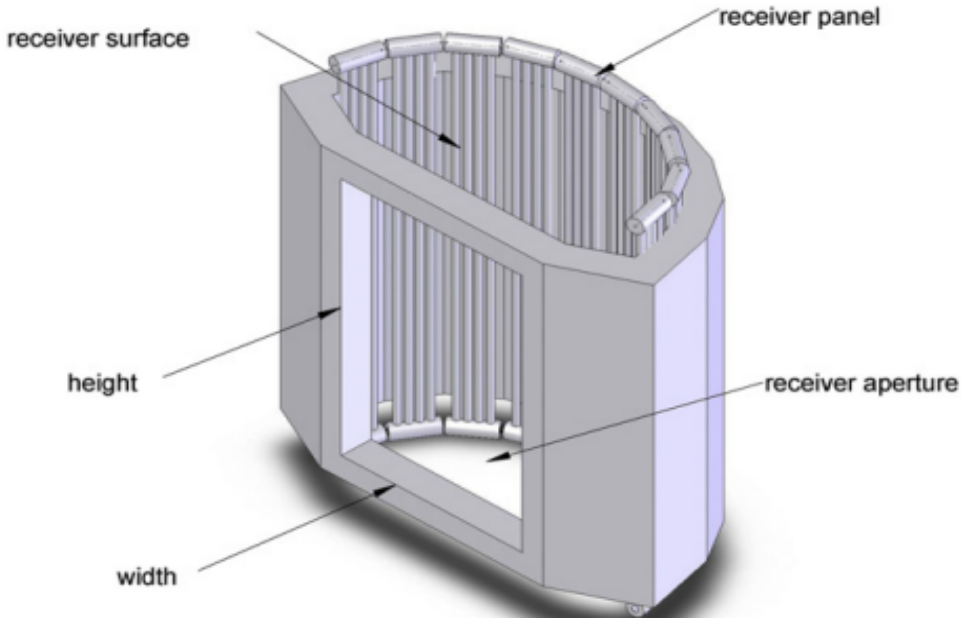

Figure 6.17 Central Receiver aperture and surface area [158].

The overall heat losses increased with an increase in the aperture area; all types of heat losses increased with an increase aperture area except reflective heat losses, which are a function of incident solar radiation.

Figure 6.18 shows the effect of increasing aperture area on the central receiver efficiency. It is observed that the central receiver efficiency decreases with increasing aperture area due to large heat losses and causes increase in the central receiver surface temperature.

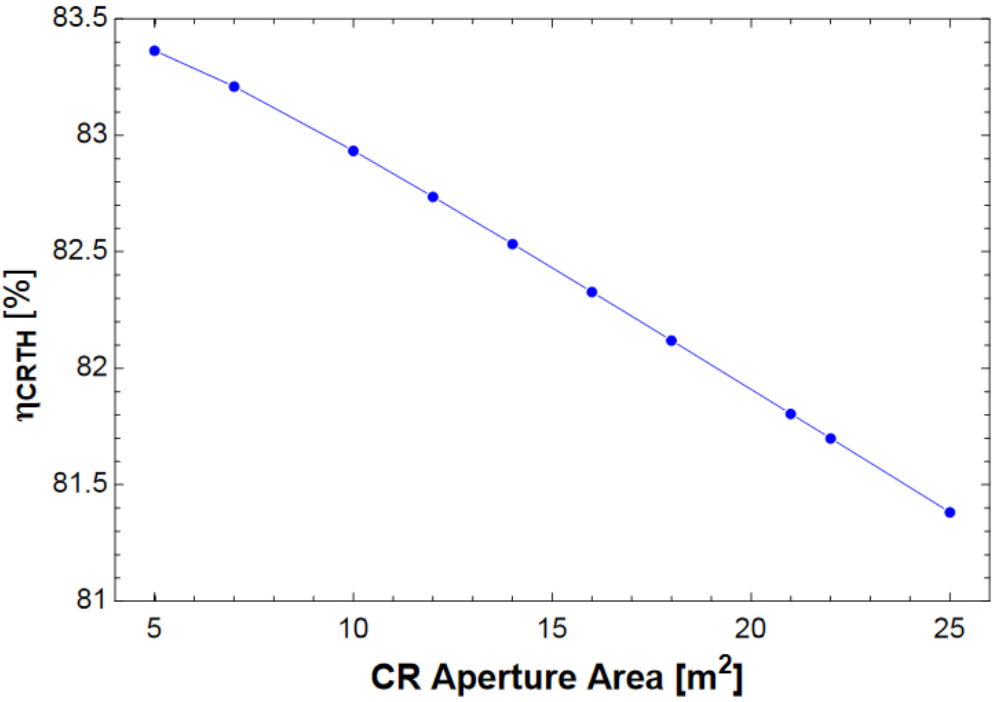

Figure 6.18 CR Thermal Efficiency Variation with CR Aperture Area.

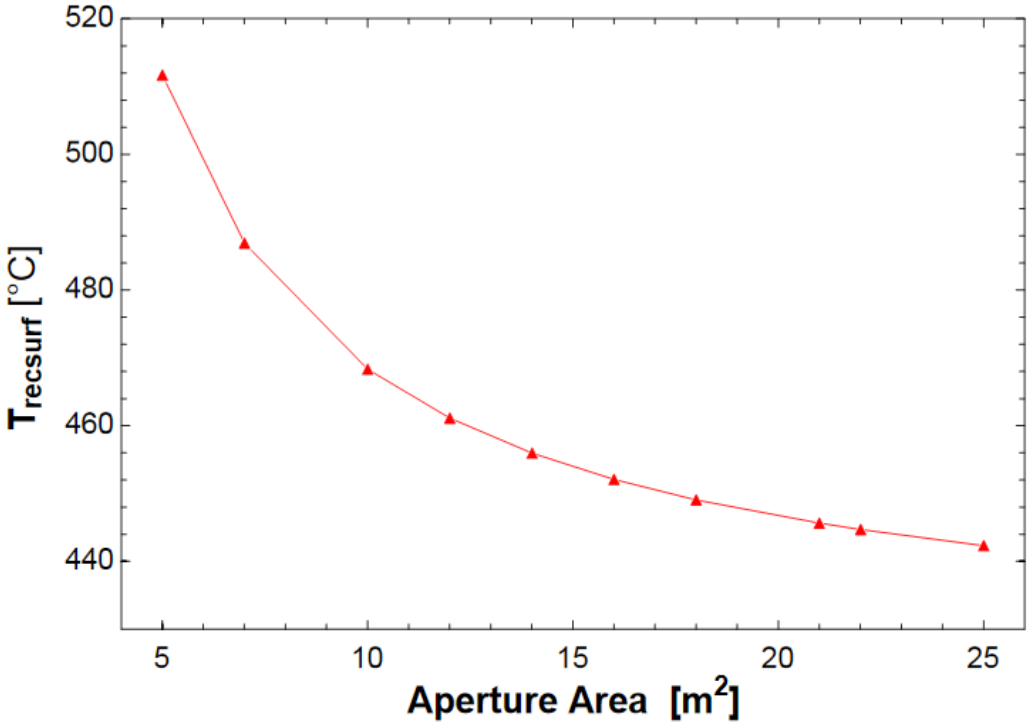

Figure 6.19 CR Surface Temperature Variation with CR Aperture Area.

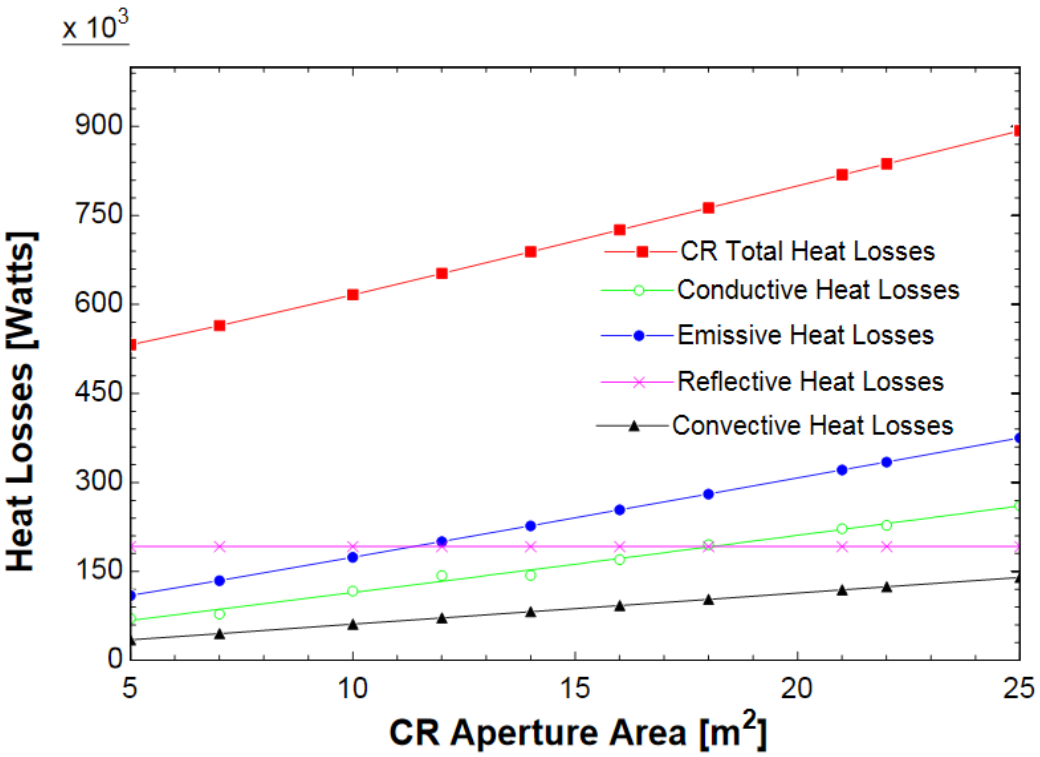

Figure 6.20 CR Heat Losses Variation with CR Aperture Area.

6.6 Central Receiver performance variation with emissivity:

Figure 6.21 shows the effect of the receiver surface emissivity on the receiver efficiency and total heat losses.

It is observed that when the emissivity increased, the total heat losses increased and then the receiver efficiency decreased.

The receiver surface emissivity had less impact on the receiver efficiency as the variation in the surface temperature had more impact on the receiver efficiency.

As shown in Figure 6.21 When the emissivity increased from 0.1 to 0.9, the receiver efficiency decreased slightly, and the heat losses increased insignificantly.

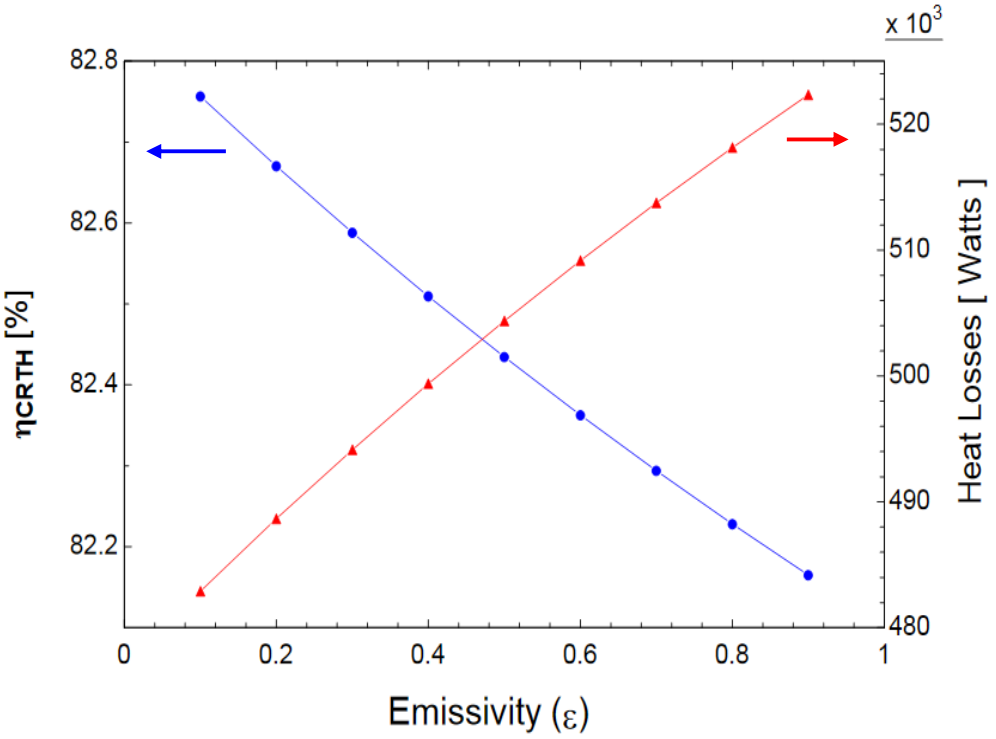

Figure 6.21 CR Thermal Efficiency and Heat Losses Variation with Emissivity.

6.7 Central Receiver performance variation with Reflectivity:

Figure 6.22 shows the effect of reflectivity on the receiver efficiency and total heat losses.

It is observed that when the reflectivity increased, the total heat losses increased and receiver efficiency decreased.

The reflectivity had a strong impact on the receiver efficiency, as shown in Figure 6.22 when the reflectivity increased from 0.01 to 0.08, the receiver efficiency decreased greatly, and the heat losses increased two times. Therefore, the reflectivity is an important factor to select the proper material of the system or adds a selective coating on the receiver surface to improve the receiver's performance.

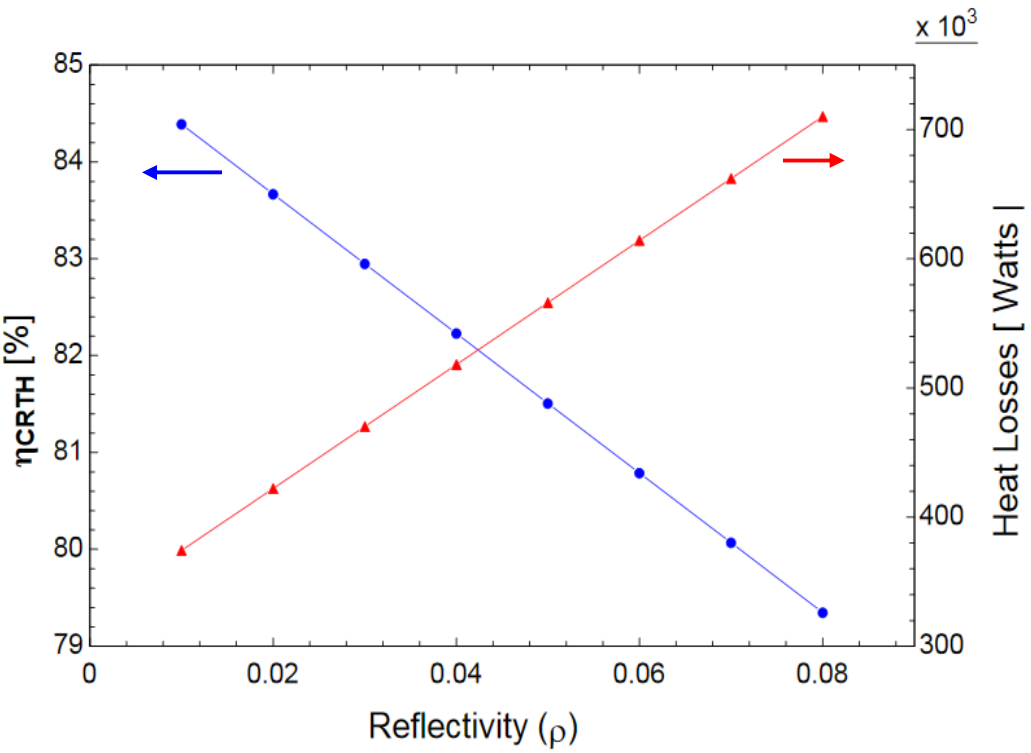

Figure 6.22 CR Thermal Efficiency and Heat Losses Variation with Reflectivity.

6.8 Sun's exergy distribution and exergy destruction for triple-effect refrigeration cycle:

The exergy distribution of the proposed cycle can be found by applying exergy balance. The result shows that 4.7% available as exergy output for ERC, ARC & CRC while the remaining part 95.3% is exergy lost from the overall refrigeration system.

The exergy analysis shows the following facts:

- The highest exergy destruction in novel cycle occurred in central receiver which is 52.5%.
- The second largest exergy destruction in the novel cycle was found in the ejector, heat recovery generator and generator, which were in the range (2-7%) as shown in figure 6.8.
- 11% of exergy destruction is found in the ejector refrigeration cycle, 6.64% in the absorption refrigeration cycle and 8.23% in the cascade refrigeration cycle.
- The second-law thermodynamic analysis shows that some component with maximum irreversibility, which are the central receiver, heliostat, Heat recovery generator and ejector, therefore these component need special care in order to enhance the performance of these component and improve overall combined refrigeration cycle efficiency.

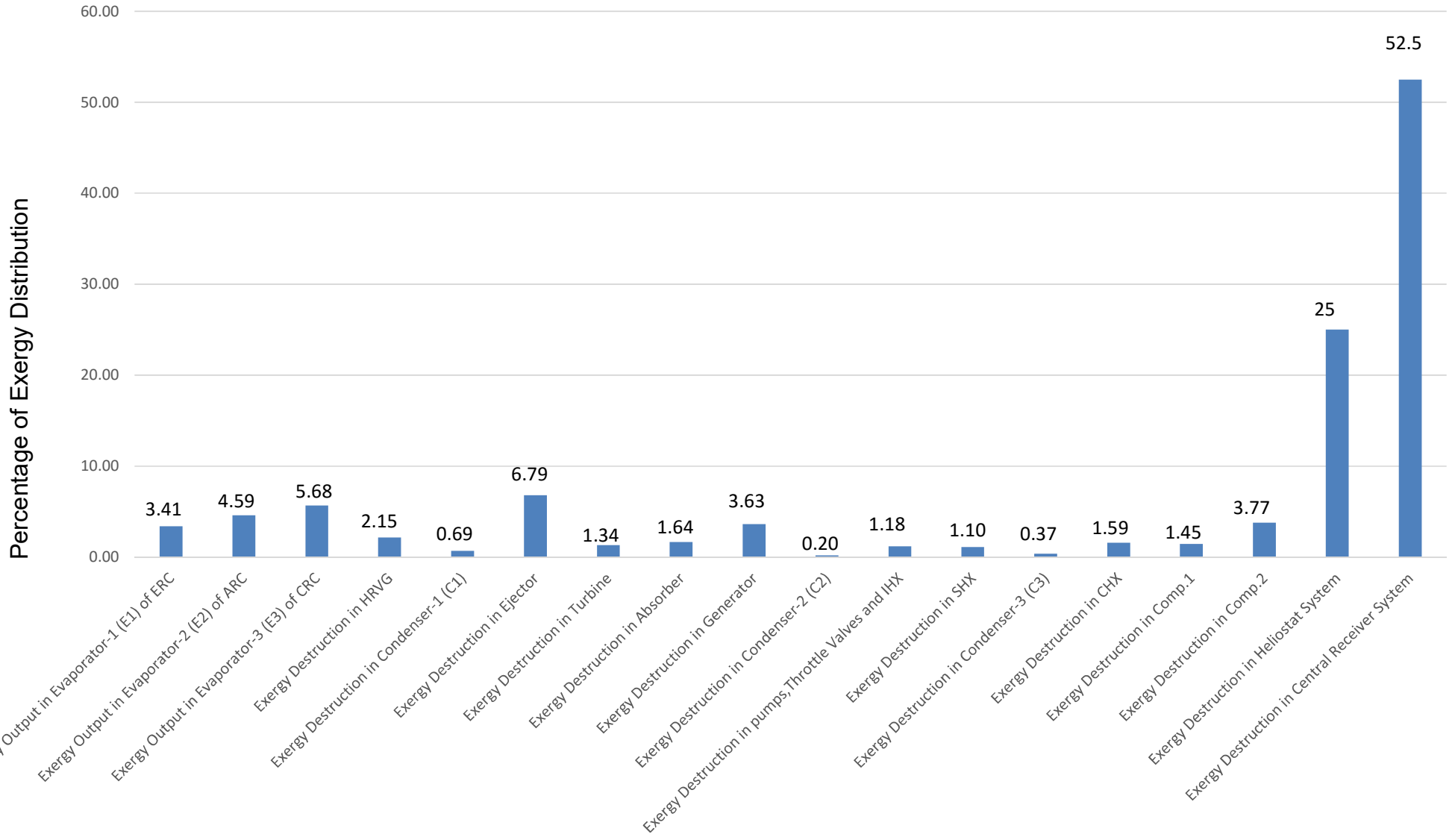

Figure 6.23 Sun's exergy distribution in output and destruction for triple-effect refrigeration cycle

6.9 Variation of the refrigeration output and efficiencies of the proposed cycle with changing of influential parameter:

Figure 6.24 shows the variation refrigeration output of each individual cycle and the overall combined refrigeration cycle of the novel solar assisted multi effect refrigeration cycle with the variation of hot molten salt outlet temperature.

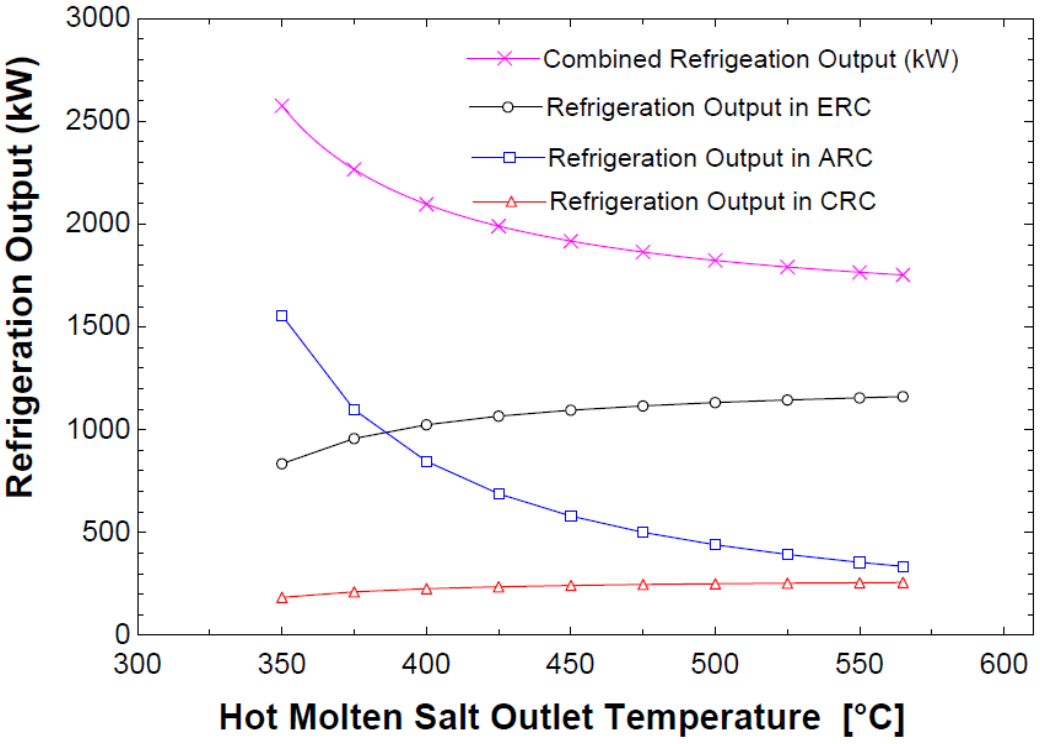

Figure 6.24 Variation of refrigeration output for triple-effect refrigeration cycle with hot molten salt outlet temperature.

Figure 6.24 shows that the refrigeration output of ERC and CRC increases with the increase in hot molten salt outlet temperature (T1). This is due to the fact that an increase in hot molten temperature results in heat transfer in HRVG and improves the thermodynamic properties of the refrigerant at turbine inlet and leaving state. Therefore turbine power output increases so the compressor will get more power which increases the mass flow rate

of N_2O in cascade refrigeration cycle and increases the cooling effect accordingly.

It is further observed that improving the thermodynamic properties of vaporized refrigerant at the turbine outlet will increase the speed of fluid leaving the nozzle of the ejector and increase the entrainment ratio which caused negative pressure (vacuum) to entrain the secondary fluid. Then, the mass flow rate of the secondary fluid in ERC will be increased accordingly and the increment in secondary mass flow will make more cooling effect in ERC.

It is further observed that increase in hot molten salt outlet temperature causes a lower refrigerating effect at the evaporator of absorption refrigeration system. This is because of the reason that an increase in hot molten salt outlet temperature results in lower temperature at the exit of HRVG that causes a low mass flow rate of water refrigerant that goes to the C2 and hence, a lower refrigerating effect at the evaporator of ARC. Because the refrigeration output of ARC is much higher than the refrigeration output of ERC and CRC cycle.

The overall combined cycle output is decreased with increasing hot molten salt outlet temperature, and this is due to the cooling output of ARC which is relatively higher than the cooling output of the ejector and cascade refrigeration cycle. Therefore, ARC has a significant effect on the total refrigeration output.

Figure 6.25 shows a significant reduction in energy efficiency with increases of the hot molten salt outlet temperature, where as the exergy efficiency increases insignificantly with increases of hot molten salt outlet temperature. This is the reason why exergy output of cascade refrigeration cycle is higher than the exergy output of absorption and ejector refrigeration cycle.

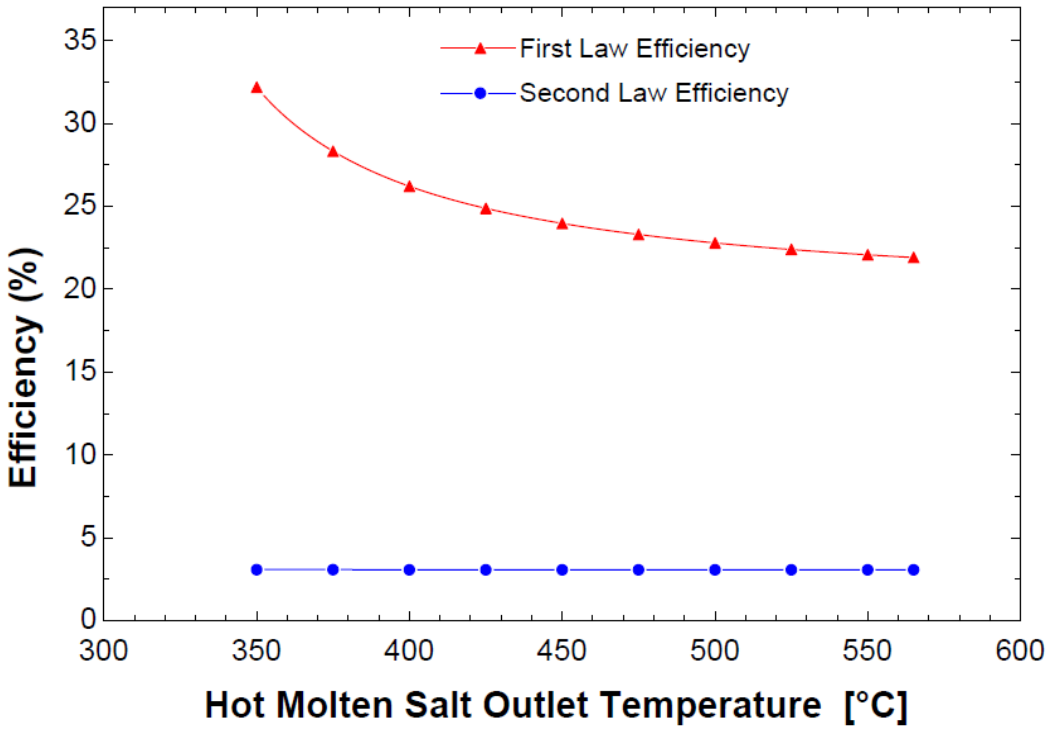

Figure 6.25 Variation first and second law efficiency for tripe effect refrigeration cycle with hot molten salt outlet temperature.

Figures 6.26 and 6.27 show variation effect of inlet turbine pressure on the refrigeration capacity of each cycle and combined refrigeration output and the variation of first and second law efficiency with varying turbine inlet pressure.

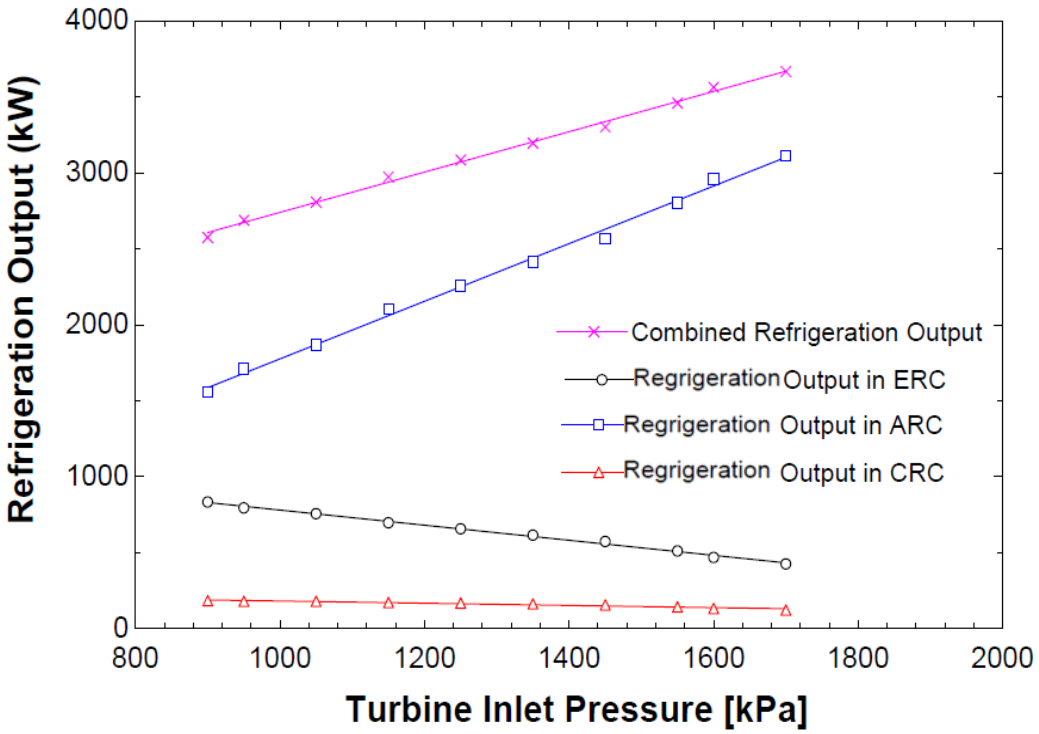

Figure 6.26 Refrigeration output for triple-effect refrigeration cycle with turbine inlet pressure.

Figure 6.26 shows the variation in the refrigeration effect of each individual refrigeration cycle and combined refrigeration cycle in the present study. It is observed that ejector and cascade evaporator refrigeration output decreases with an increase in the inlet turbine pressure while as the figure shows there is a significant increase in the absorption evaporator refrigeration output with an increase in the inlet turbine pressure.

The reason for this is that increase in turbine inlet pressure results in lower mass flow of refrigerant vapor produced in the HRVG and a lower turbine exit temperature that further results in reduction of velocity at the ejector nozzle, which causes a reduced mass flow rate of secondary refrigerant through ejector evaporator. Refrigeration capacity of ARC increases significantly because of fact that increase in turbine inlet pressure that lowers the mass flow rate of refrigerant vapor will result in a reduced absorption of heat from

the exhaust gasses through the HRVG, which leads to the higher value of HRVG exit temperature. This higher temperature at the inlet of generator causes a significant increase in the capacity of ARC due to increased mass flow rate of water refrigerant.

The decrease in refrigerating capacity of CRC cycle is observed because of the reduced mass flow rate of refrigerant (N_2O) across the compressor, which is caused by reduced mass flow rate of water across the turbine. The reduced mass flow rate will decrease the refrigerating capacity of CRC cycle due to the overall reduced mass flow rate across the cycle

The overall refrigeration output of the combined cycle increases with the increase in turbine inlet pressure. This is due to the increase in ARC capacity which is greater than the reduction in ERC and CRC.

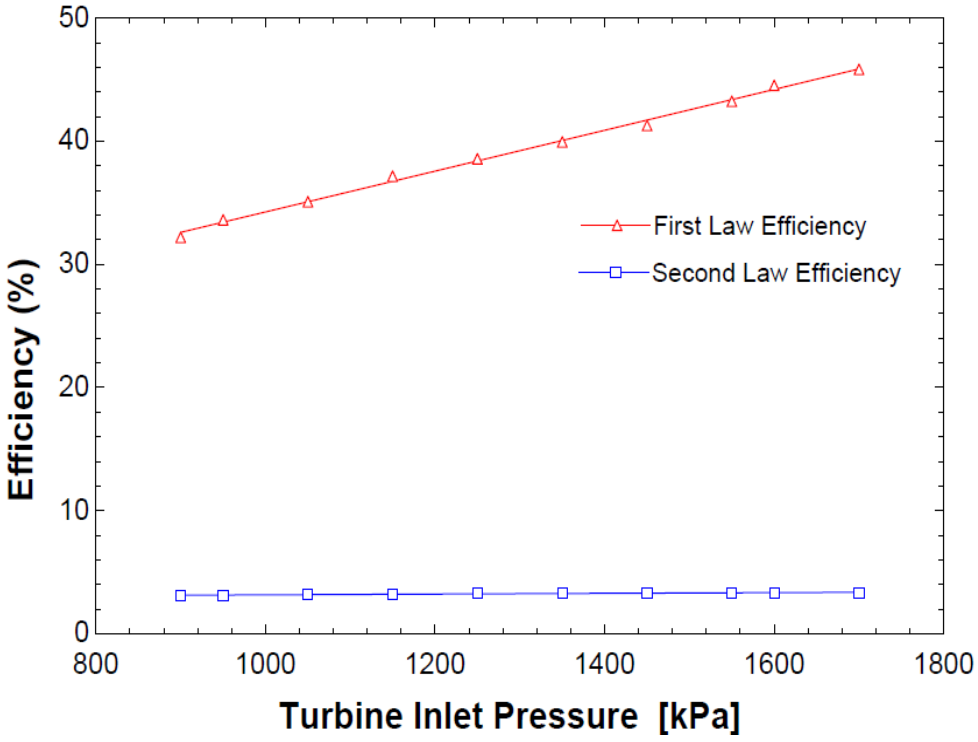

Figure 6.27 First and second law efficiency for triple-effect refrigeration cycle with turbine inlet pressure.

It is seen that the second law efficiency decreases with the increase in turbine inlet pressure whereas the first law efficiency is increased significantly with the increase in turbine inlet pressure.

Figure 6.28 shows the effect of turbine back pressure (P5) on the refrigeration outputs of CRC, ERC, ARC and combined refrigeration output. It is seen that the turbine power output decreases when turbine back pressure increases, which will lower the compressor work and cooling effect accordingly. It is also observed that the ejector cycle cooling effect will increase with an increase in the turbine back pressure. This is because, when the turbine back pressure (P5) increases, causes significant increase in primary flow velocity at the ejector nozzle and makes more vacuum, entrains more secondary fluid, and increases the cooling effect accordingly.

It is found that there is no change in the ARC cooling effect due to increase or decrease turbine back pressure (P5). This is due to the inlet and outlet state of generator which is not affected by variation of back pressure of the turbine.

The combined refrigeration outputs increase with increasing turbine back pressure.

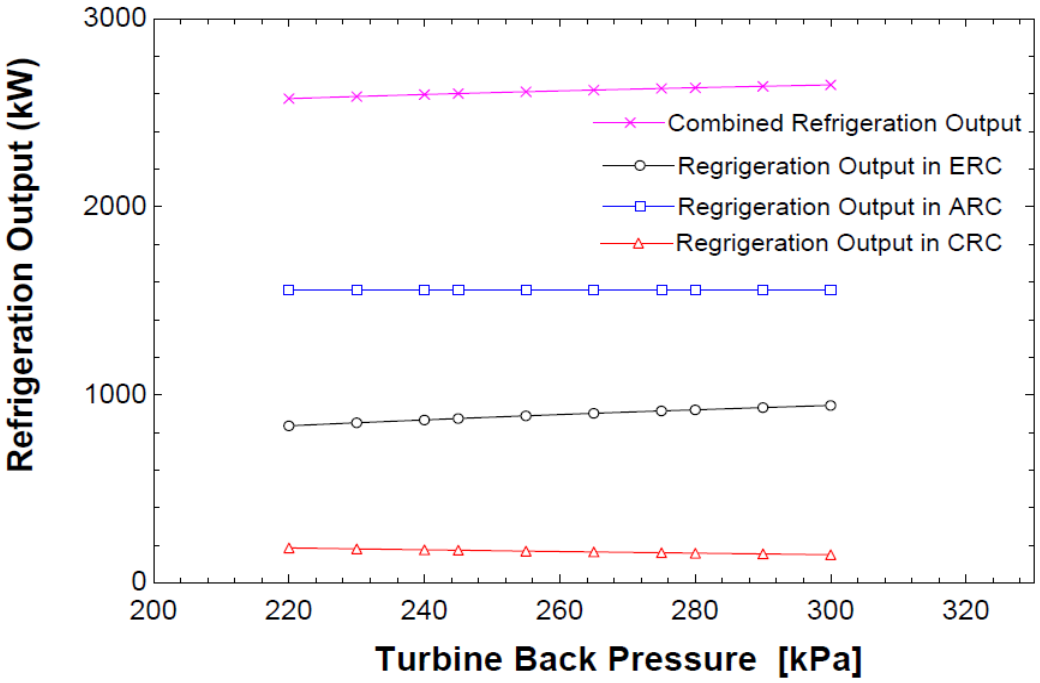

Figure 6.28 Refrigeration output for triple-effect refrigeration cycle with turbine back pressure

Figure 6.29 shows the variation of energy and exergy efficiency of novel refrigeration cycle with turbine back pressure.

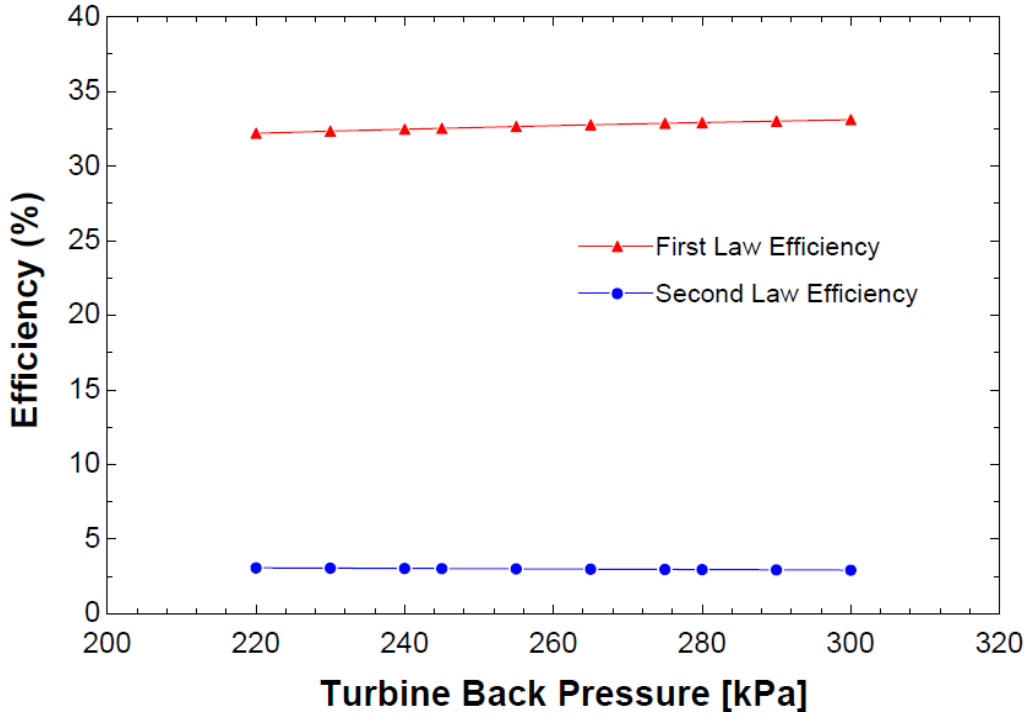

Figure 6.29 First and second law efficiency for triple-effect refrigeration cycle with turbine back pressure.

It is seen that the exergy efficiency is constant whereas a marginally increase in the first law efficiency with an increase turbine back pressure.

The refrigeration output of the ejector cycle will increase significantly with the ejector evaporator temperature increase, where as insignificant change is observed in the cascade and absorption cycle refrigeration effect as indicated in Figure 6.30.

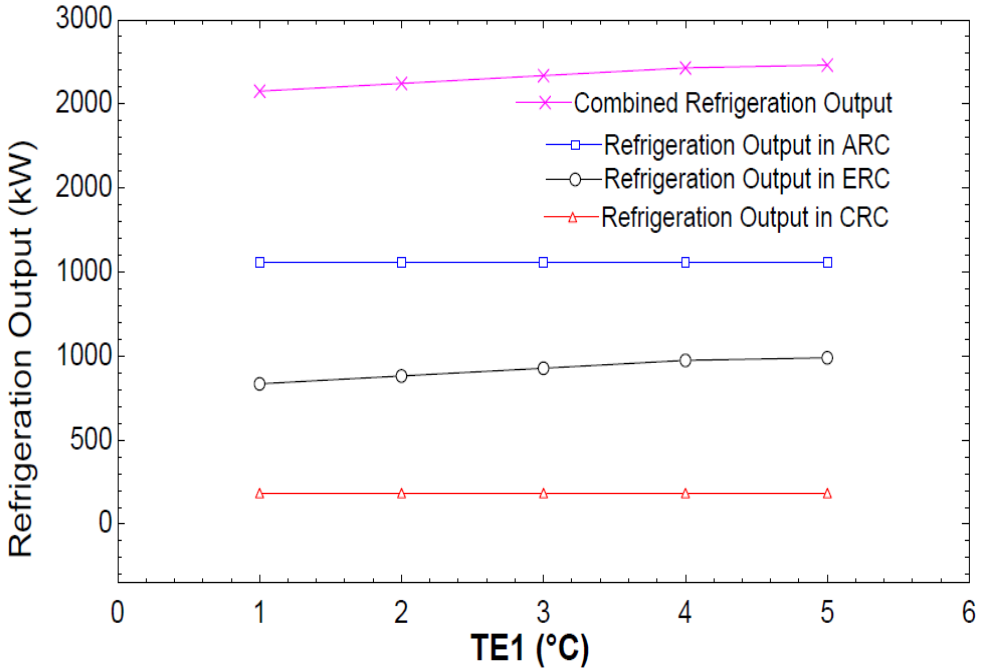

Figure 6.30 Refrigeration output for triple-effect refrigeration cycle with evaporator-1 (E1) temperature.

Figure 6.31 shows the effect of changing evaporator -1 temperature on the energy and exergy efficiency and it is observed that the energy efficiency increases considerably with the increase in ejector evaporator temperature, while the second law efficiency is slightly increased with an increase in the ejector cycle evaporator temperature.

The effect of changing evaporator-2 (E2) temperature shows an insignificant increase/decrease in refrigeration output and exergy output with increased evaporator temperature.

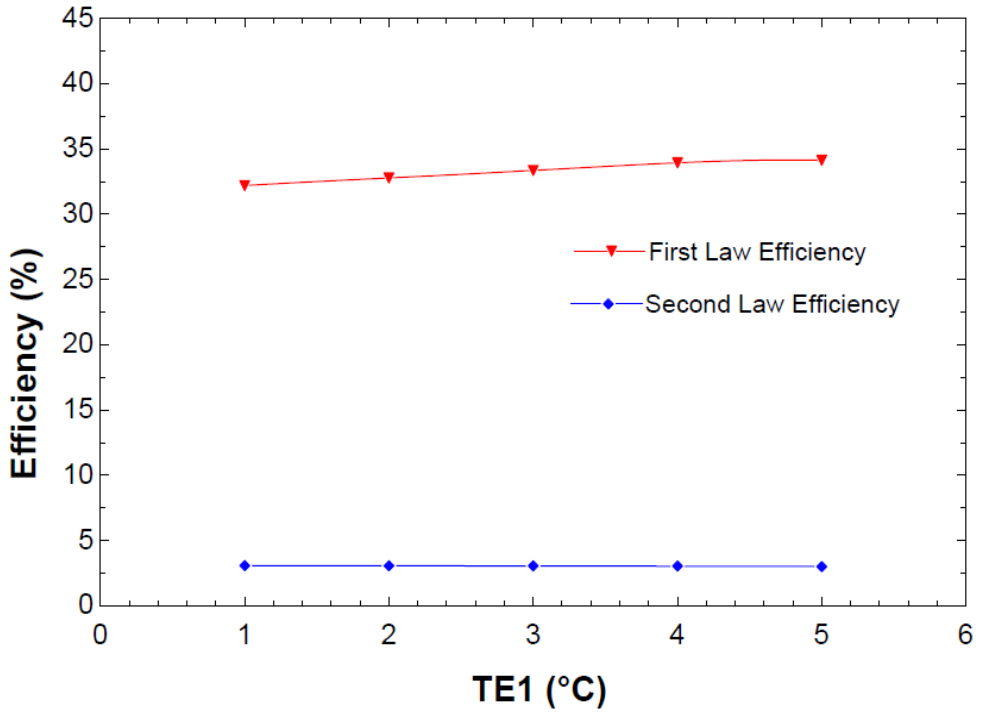

Figure 6.31 First and second law efficiency for triple-effect refrigeration cycle with evaporator-1 (E1) temperature.

It is observed that a marginal increase in refrigeration output of evaporator-3 with an increase of temperature which causes an insignificant increase in first and second law efficiency of triple effect refrigeration cycle as shown in figure 6.32 and 6.33.

The increase in the combined refrigeration output is marginal because the percentage of CRC is low compared to the absorption and ejector refrigeration cycles.

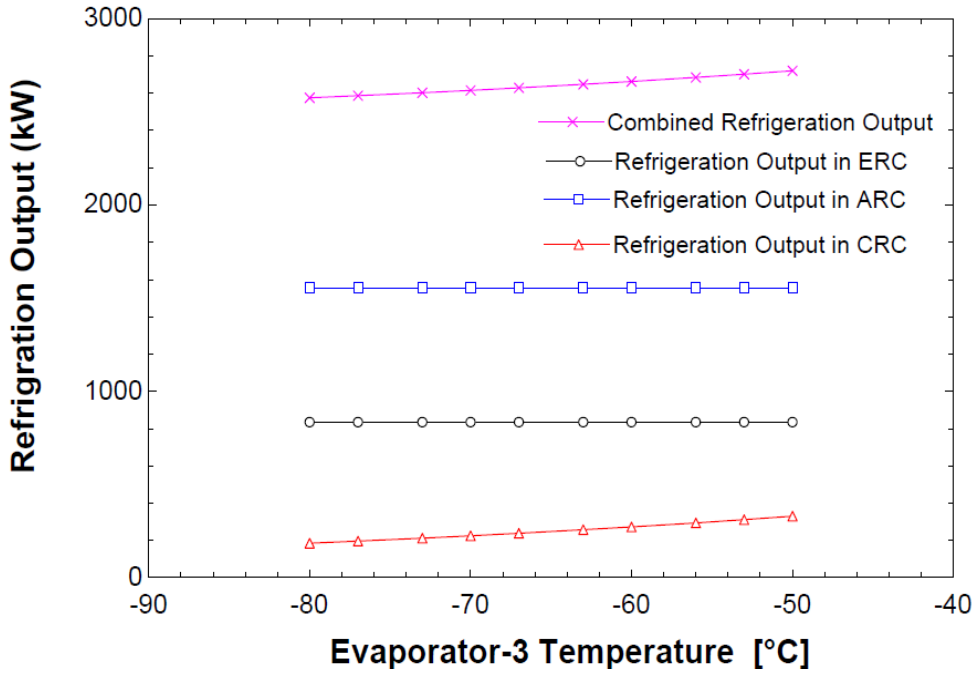

Figure 6.32 Refrigeration output for triple-effect refrigeration cycle with evaporator-3 (E3) temperature

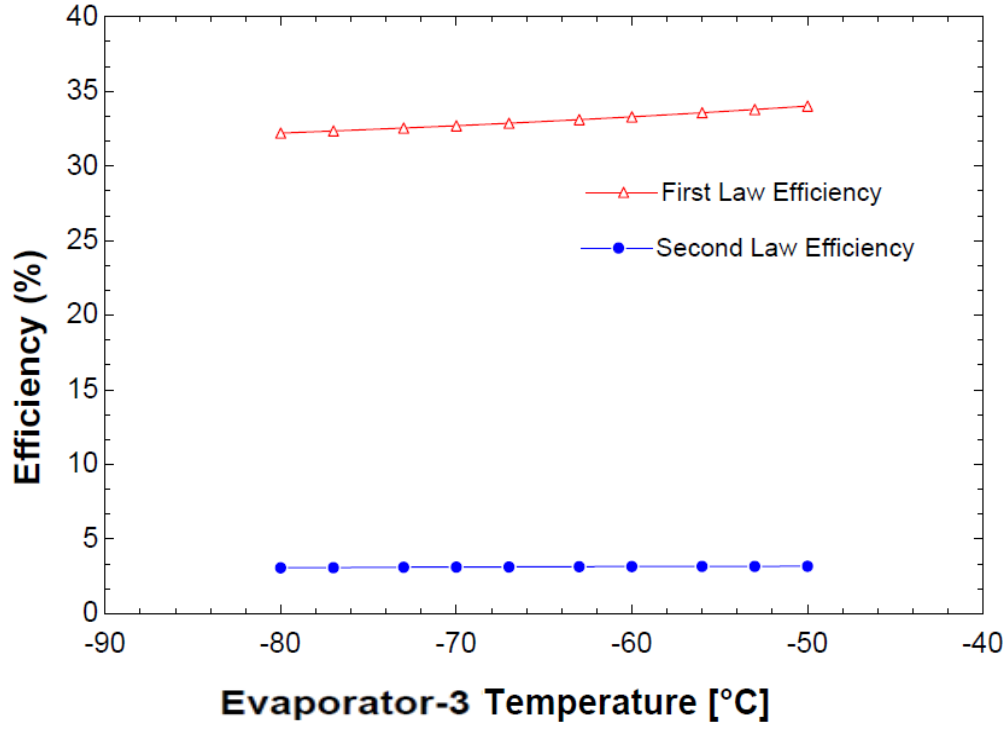

Figure 6.33 First and second law efficiency for triple-effect refrigeration cycle with evaporator-3 (E3) temperature.

Figures 6.34 shows the effect of compressor discharge pressure on the thermal and exergy efficiencies of triple effect refrigeration cycle and show the effect of compressor discharge pressure on the refrigeration outputs of CRC, ERC and ARC.

It can be observed that the refrigeration effect of CRC decreases with an increase in the compressor discharge pressure.

Further, it is seen that the variation of refrigeration effect of CRC has no effect on the refrigeration outputs of ERC and ARC.

The second law efficiency changes insignificantly with an increase in the compressor discharge pressure whereas the first law efficiency decreases as the compressor discharge pressure increases.

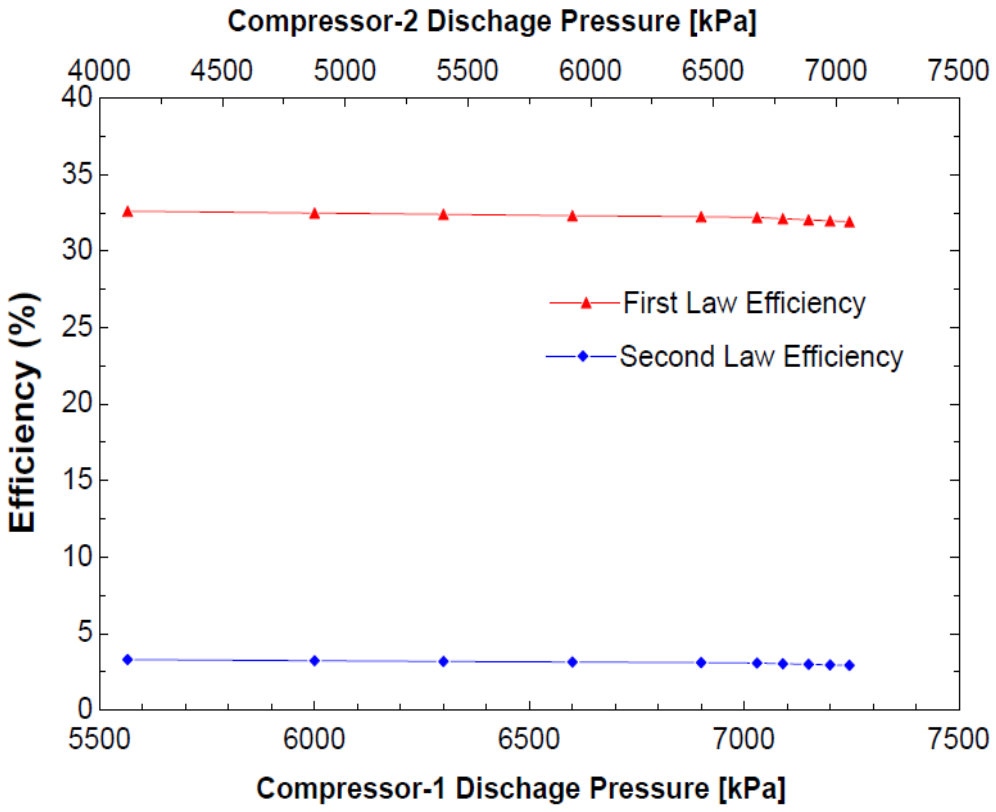

Figure 6.34 First and second law efficiency for cascade refrigeration cycle with compressors discharge pressure.

6.10 Variation of the refrigeration output of the proposed cycle with changing average daily and hourly solar radiation:

Figures 6.35 and 6.36 show the effect of average daily solar radiation on the refrigeration outputs of CRC, ERC, ARC and combined refrigeration output. It is seen that when the average daily solar radiation increases, it increases the refrigeration output in ERC, ARC, CRC and combined cycle.

The reason for the increase in the refrigeration output with increasing average daily solar radiation is due to the following facts:

- When the average daily solar radiation increases, it will increase HRVG thermal energy which will increase the mass flow rate across the turbine (primary mass flow rate) and then increase the secondary mass flow rate and the ejector cycle refrigeration output accordingly.
- When the primary mass flow rate increases across the turbine, this will increase the turbine output power, then the mass flow rate in cascade refrigeration cycle and then the refrigeration output in CRC.
- When the average daily solar radiation increases, it will increase the hot molten salt mass flow rate in the generator of absorption refrigeration cycle and the thermal energy in the generator, which will increase the mass flow rate of evaporator-2 and then increase the refrigeration output of ARC.

Weather Data and Solar Radiation Estimation:

In order to evaluate the performance of the solar field, the first step is to estimate the average daily solar radiation. Yousef [160] estimated the average daily solar radiation for Dhahran city, Saudi Arabia (Altitude 90 m, latitude 26.5°). Table 6.6 presents the average daily solar radiation for an average day in each month at Dhahran city.

Table 6.6 Weather Data and Average Daily solar radiation at Dhahran city.

Month	Average Day in the month	Day in the year	Number of Solar Hours	Average Daily Solar Radiation (W/m^2)	Average Ambient Temperature (^oC)	Average Relative Humidity (%)
January	17	17	9	568.1	19.4	46
February	16	47	9	602.1	22.1	45
March	16	75	11	638.8	25.9	45
April	15	105	11	661.8	25.9	45
May	15	135	11	669.3	37	24
June	11	162	11	669.5	39.9	22
July	17	198	11	669.5	41.7	25
August	16	228	11	665.4	39.3	36
September	15	258	11	649.0	37.8	27
October	15	288	9	617.7	32.3	42
November	14	318	9	578.5	26.9	29
December	10	344	9	555.9	20.4	43

Hourly solar Radiation Estimation at Dhahran City:

In this research we study the effect of hourly solar radiation on the performance of individual refrigeration cycles and on the performance the combined refrigeration cycle.

We selected an average day in a summer month (June 11) and the an average day in winter (December 10) to study the effect of hourly solar radiation variation on the refrigeration cycle output.

Table 6.7 Hourly solar radiation at Dhahran City on June 11 and December 10.

	June 11	**December 10**
Solar Time	Average Solar Radiation (W/m^2)	Average Solar Radiation (W/m^2)
6:00	299.7	0
7:00	564.7	184.7
8:00	713.9	390.2
9:00	796.9	584.3
10:00	843.3	685.2
11:00	868.1	733.9
12:00	875.7	748.6
13:00	868.1	733.9
14:00	843.8	685.2
15:00	796.9	584.3
16:00	713.9	390.2
17:00	564.7	184.7
18:00	299.7	0

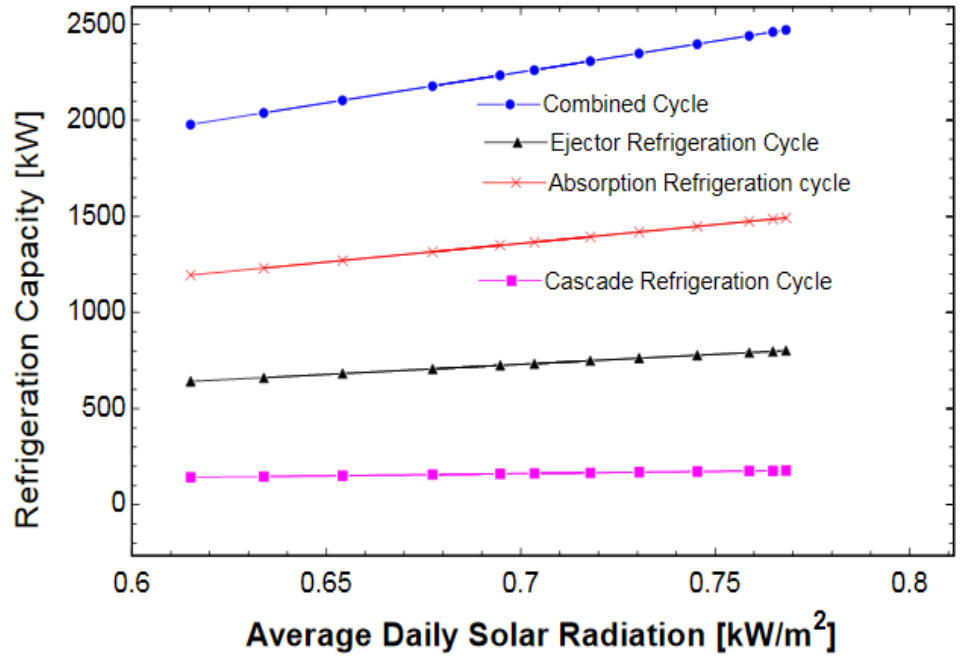

Figure 6.35 Refrigeration output of ERC, ARC, CRC and combined cycle with variation of average daily solar radiation.

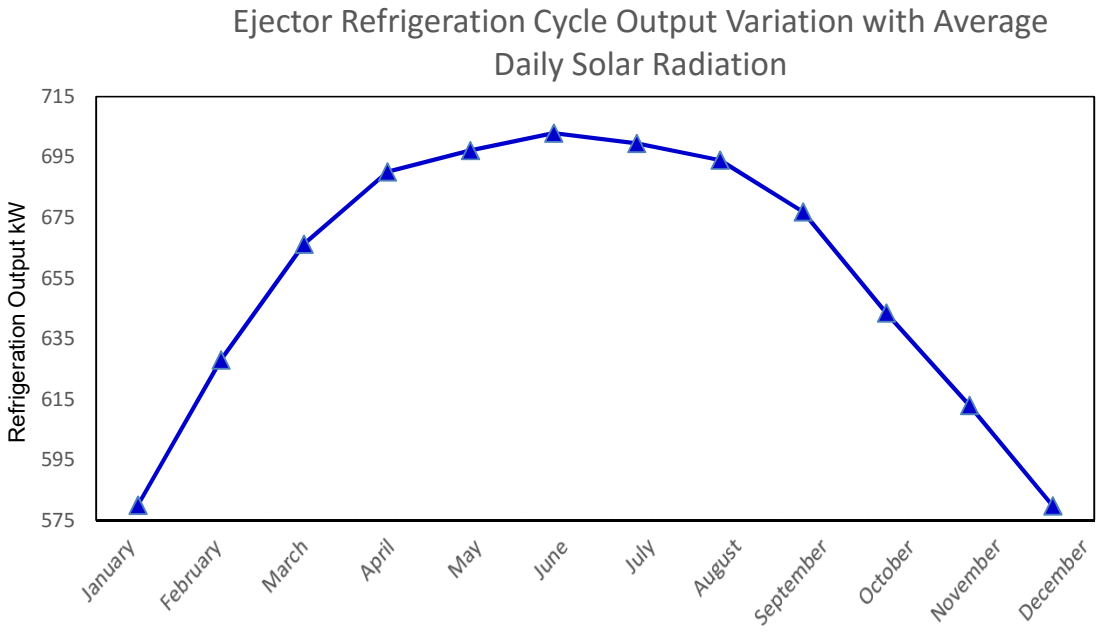

Figure 6.36 Ejector Refrigeration Cycle Output Variation with Average Daily Solar Radiation.

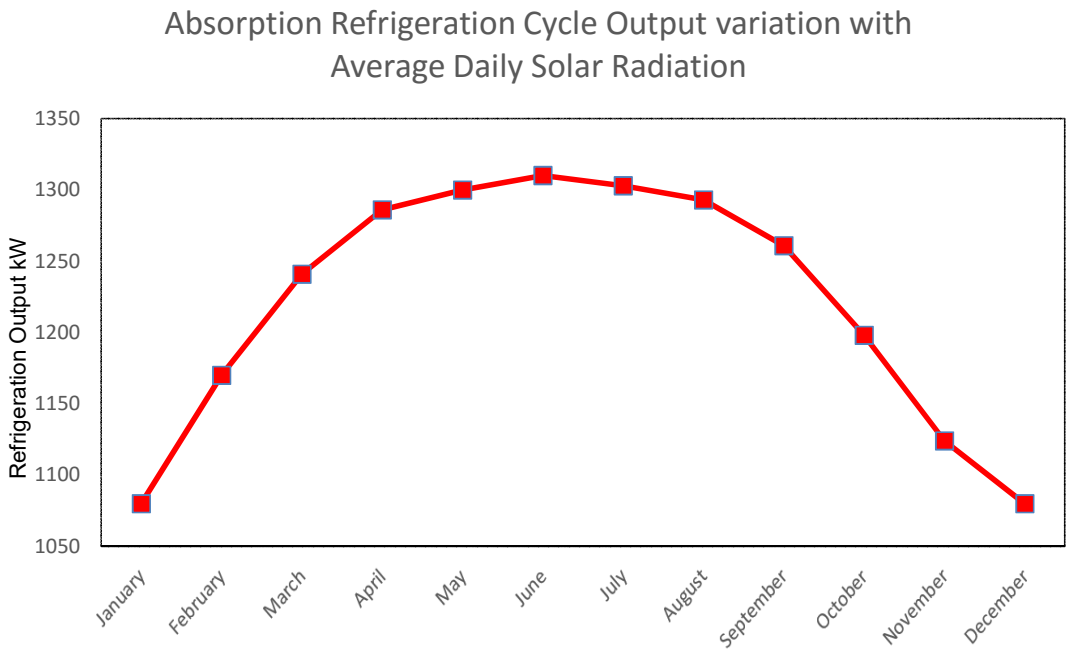

Figure 6.37 Absorption Refrigeration Cycle output Variation with Average Daily Solar Radiation.

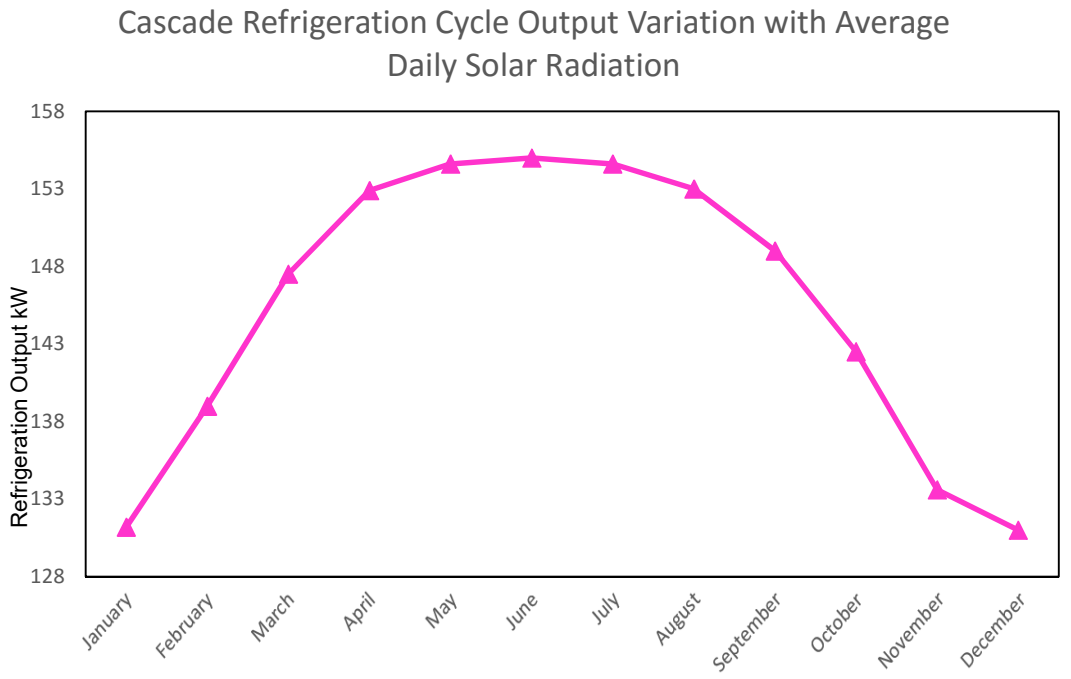

Figure 6.38 Cascade Refrigeration Cycle Output Variation with Average Daily Solar Radiation.

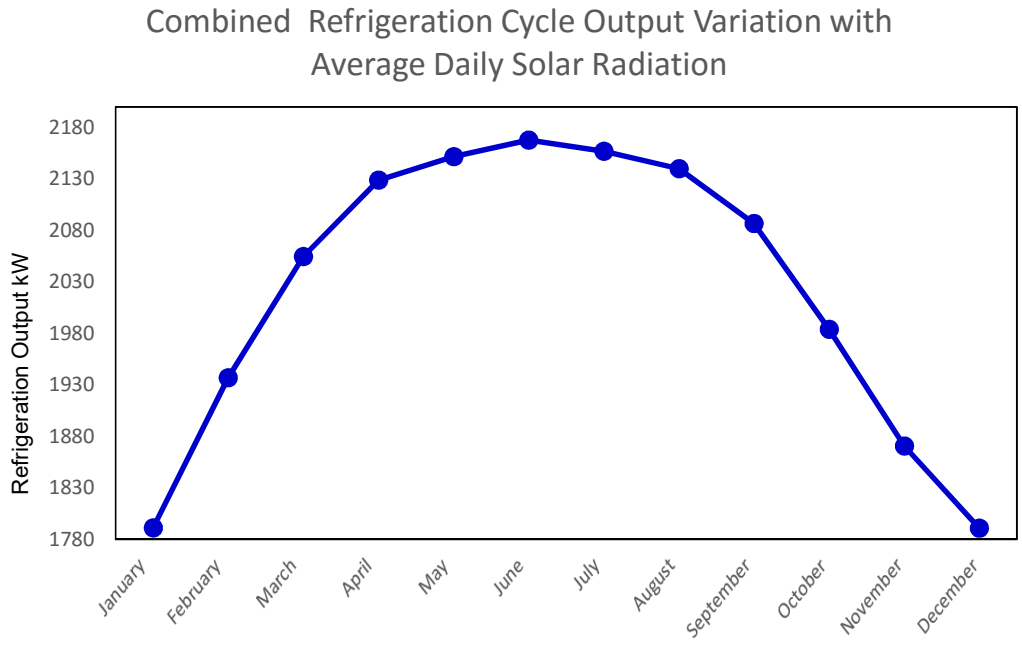

Figure 6.39 Combined Refrigeration Cycle Output Variation with Average Daily Solar Radiation.

Figures 6.36 to 6.40 shows the effect of average daily solar radiation variation on the refrigeration cycle output.

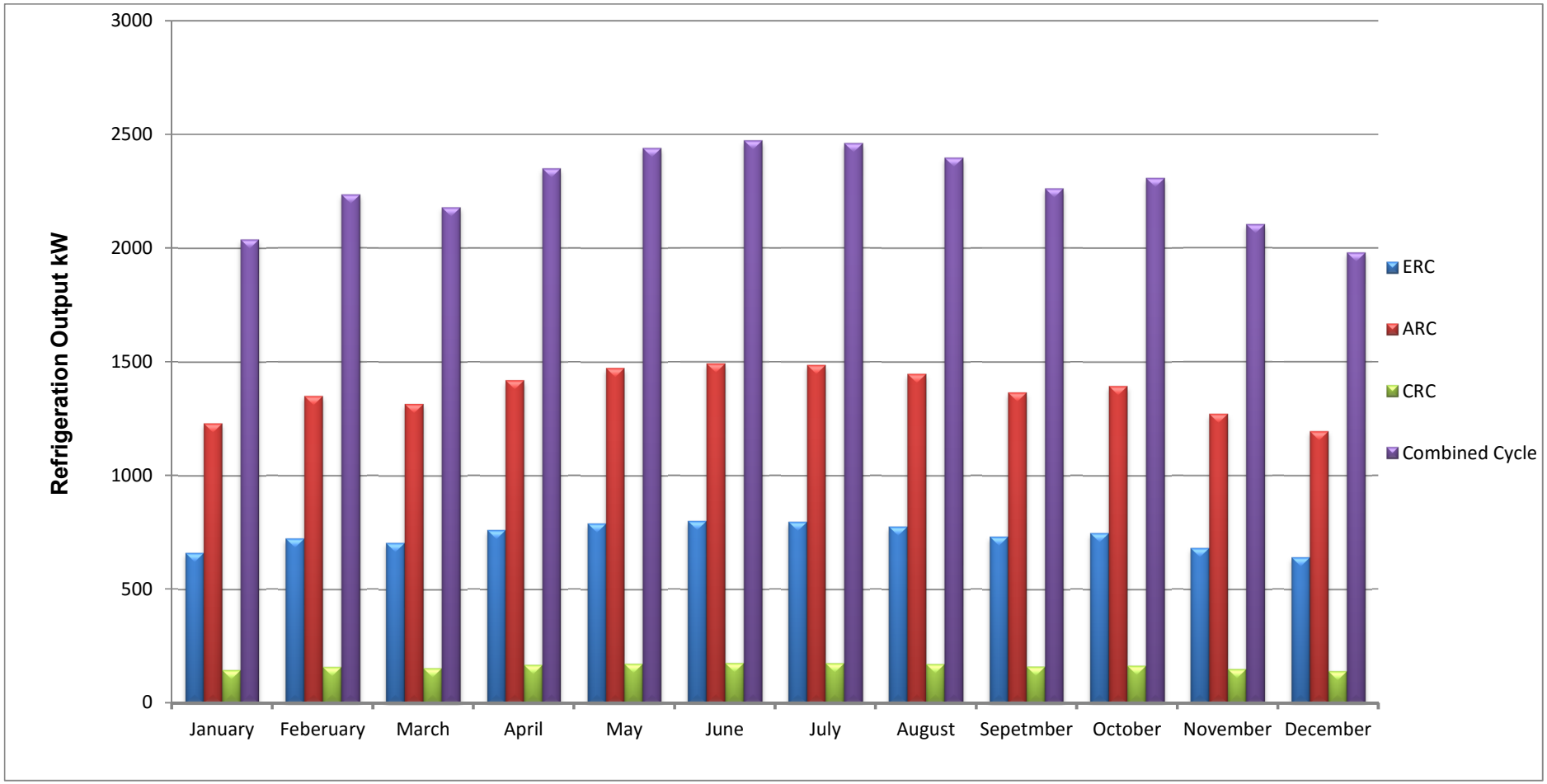

Figure 6.40 Refrigeration output of ERC, ARC, CRC and combined cycle with variation of average daily solar radiation annually.

Figures 6.36 to 6.40 are showing the refrigeration output of ERC, ARC, CRC and combined cycle with variation of average daily solar radiation for the entire year from January to December. It can be seen that the refrigeration output for all cycles reaches the maximum capacity with peak solar energy availability.

The maximum average solar radiation was in June (768.2 W/m^2) and the refrigeration output reached the maximum capacity in this month, as follows:

- 801.1 kW for Ejector refrigeration cycle.
- 1,493 kW for Absorption Refrigeration Cycle.
- 177.4 kW for Cascade Refrigeration Cycle.
- 2,471.5 kW for Combined Refrigeration Cycle.

The minimum average solar radiation was in December (615.1 W/m^2) and the refrigeration output was the minimum capacity in this month as follow:

- 641.6 kW for Ejector refrigeration cycle.
- 1,195 kW for Absorption Refrigeration Cycle.
- 142.1 kW for Cascade Refrigeration Cycle.
- 1,978.7 kW for Combined Refrigeration Cycle.

Figures 6.41 to 6.47 (excluding 6.42) show the effect of average hourly solar radiation on June 11 (11 hours from 6:00 to 18:00) on the refrigeration outputs of CRC, ERC, ARC and combined refrigeration output. It is seen that when the average hourly solar radiation increases, it increases the refrigeration output in ERC, ARC, CRC and combined cycle.

Figures 6.42 and 6.48 to 6.52 show the effect of average hourly solar radiation on December 10 (9 hours from 7:00 to 17:00) on the refrigeration outputs of CRC, ERC, ARC and combined refrigeration

output. It is seen that when the average hourly solar radiation increases, it increases the refrigeration output in ERC, ARC, CRC and Combined cycle.

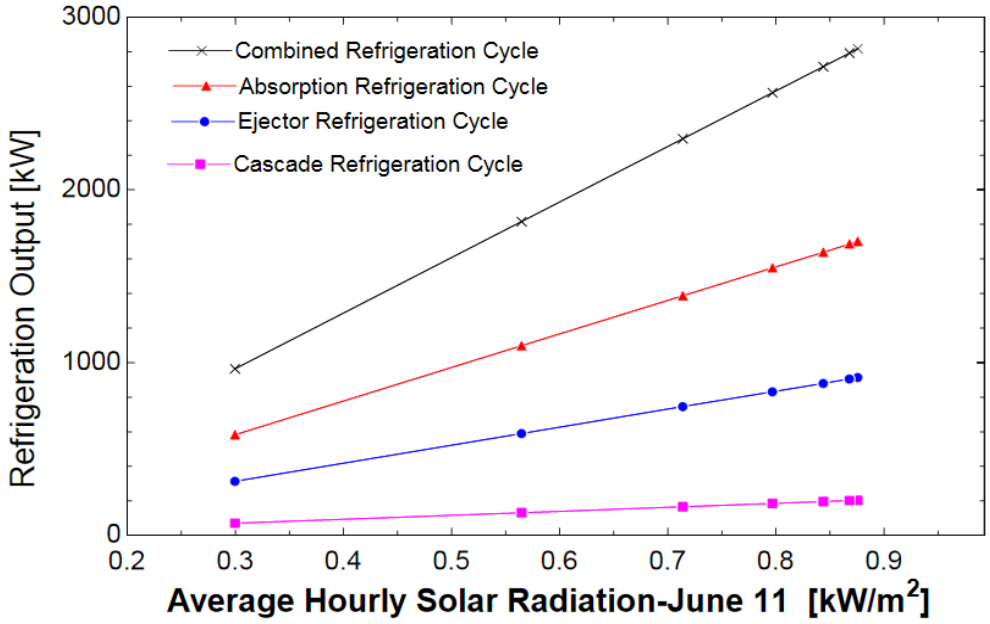

Figure 6.41 Refrigeration output of ERC, ARC, CRC and combined cycle with variation of average hourly solar radiation-June 11.

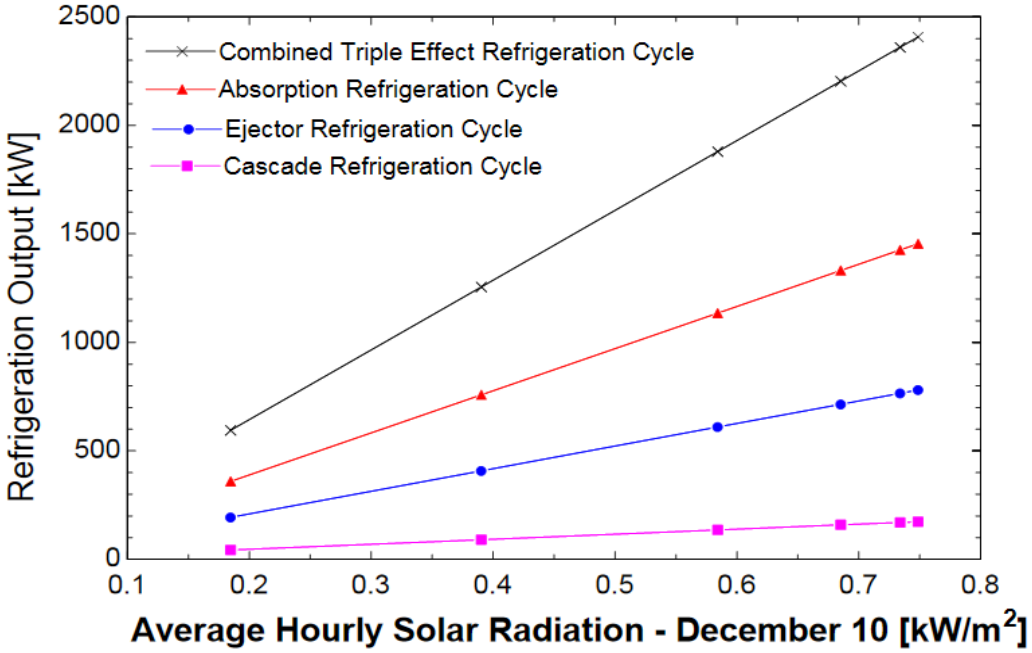

Figure 6.42 Refrigeration output of ERC, ARC, CRC and combined cycle with variation of average hourly solar radiation-December 10.

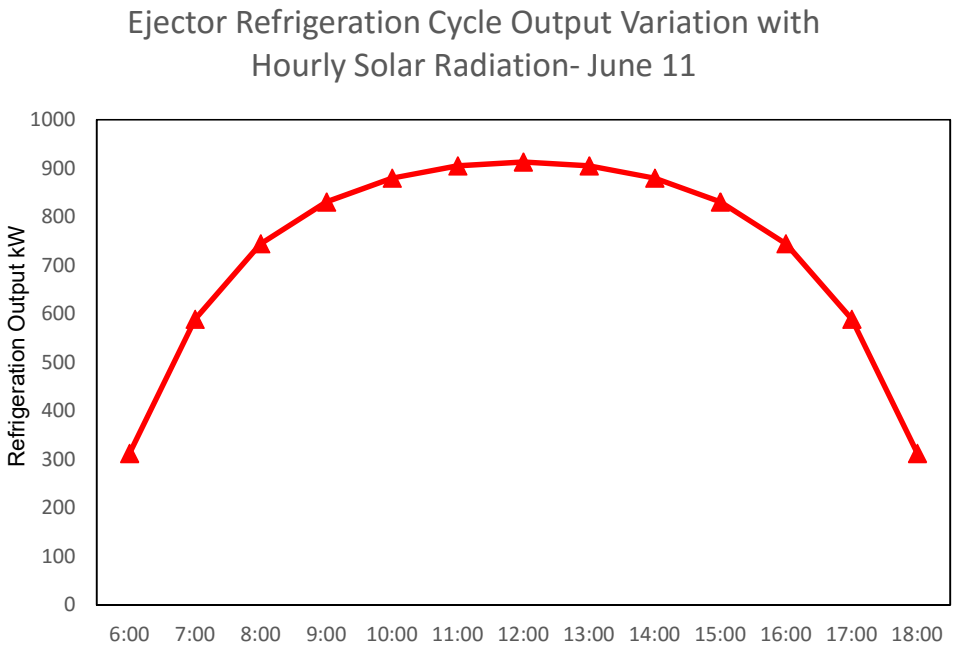

Figure 6.43 Ejector Refrigeration Cycle Output Variation with average hourly solar radiation-June 11.

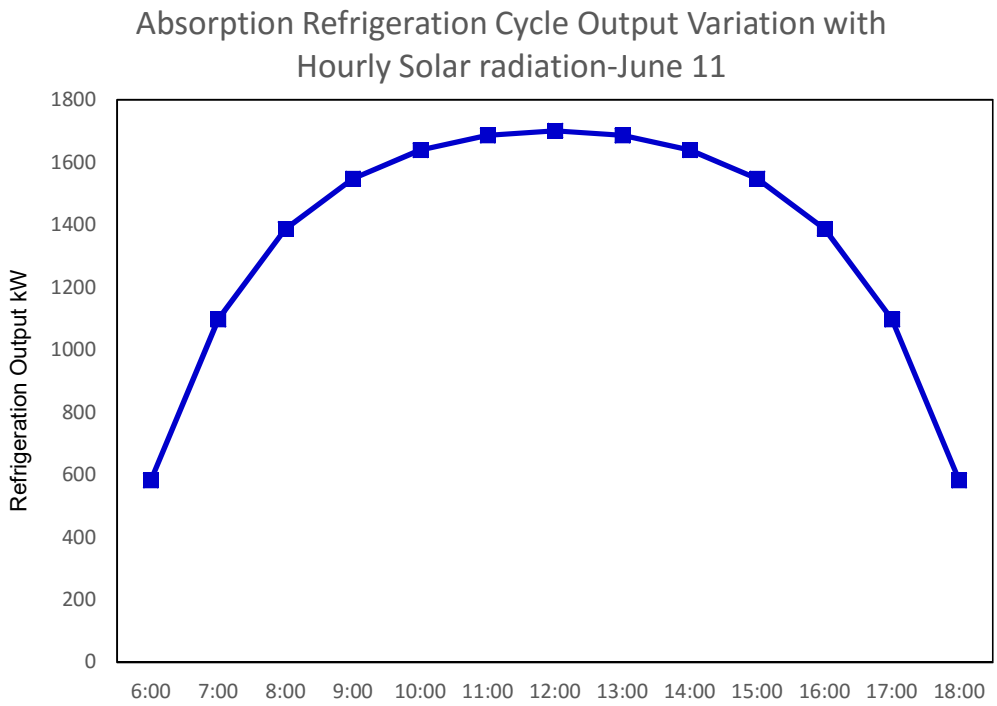

Figure 6.44 Absorption Refrigeration Cycle Output Variation with average hourly solar radiation-June 11.

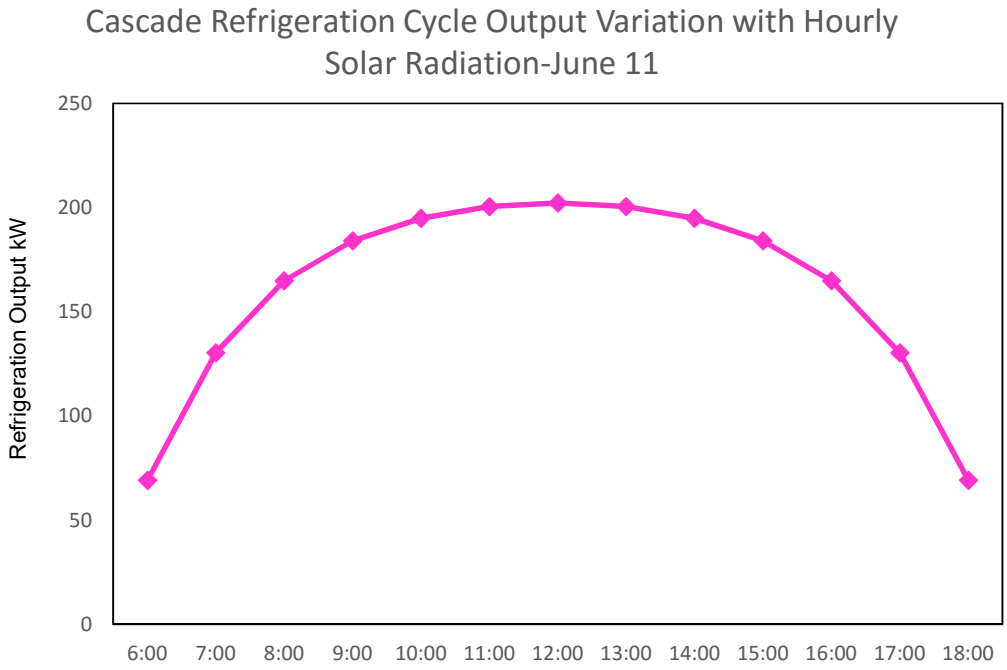

Figure 6.45 Cascade refrigeration cycle output variation with average hourly solar radiation-June 11

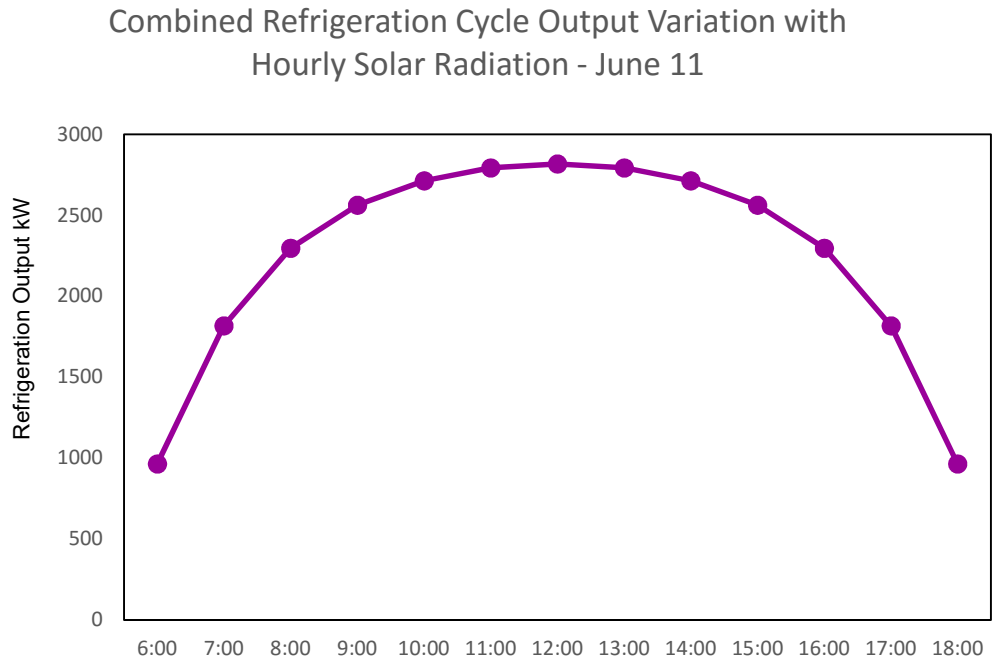

Figure 6.46 Cascade refrigeration cycle output variation with average hourly solar radiation-June 11

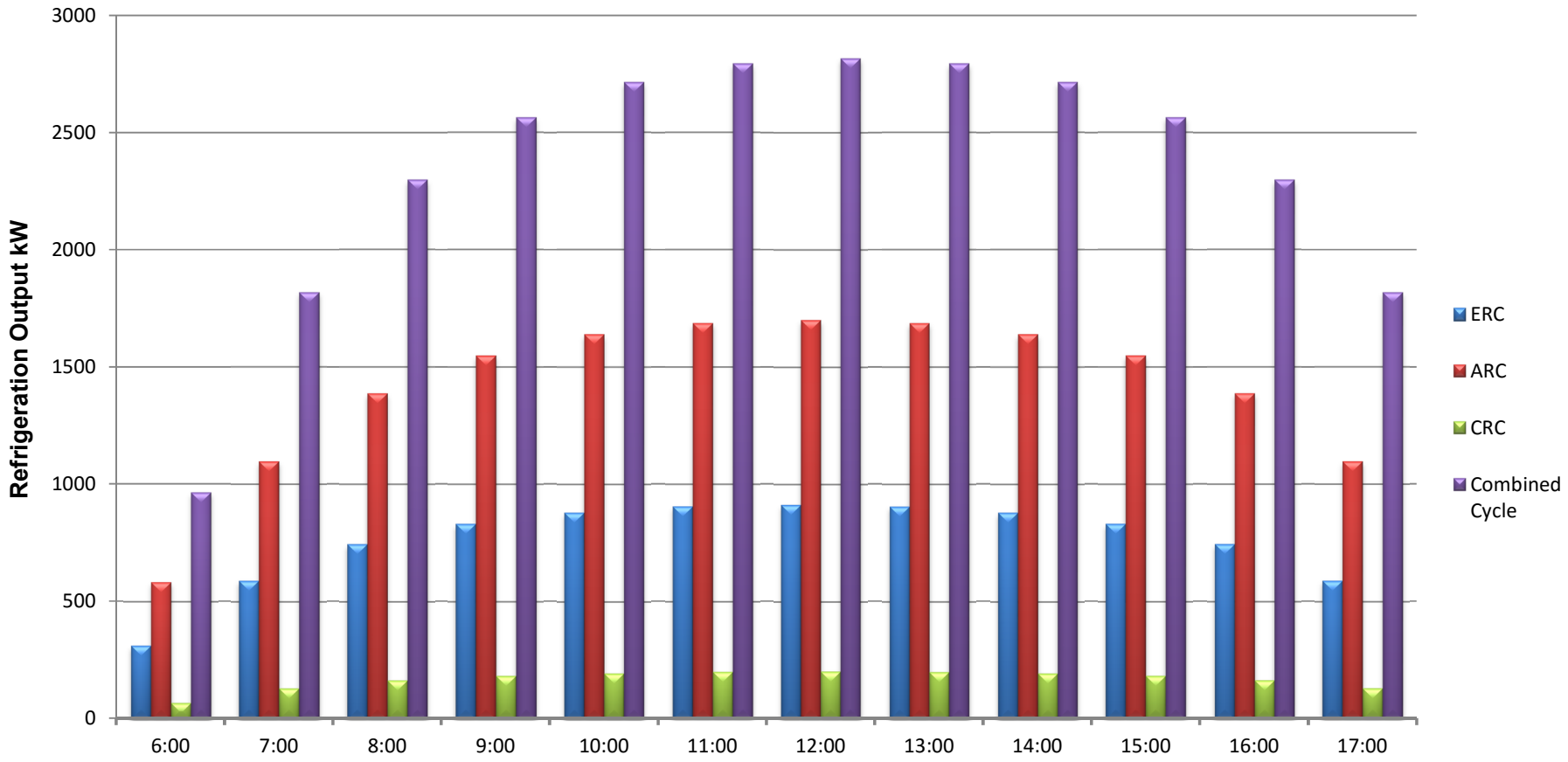

Figure 6.47 Refrigeration output of ERC, ARC, CRC and combined cycle with variation of average hourly solar radiation-June11.

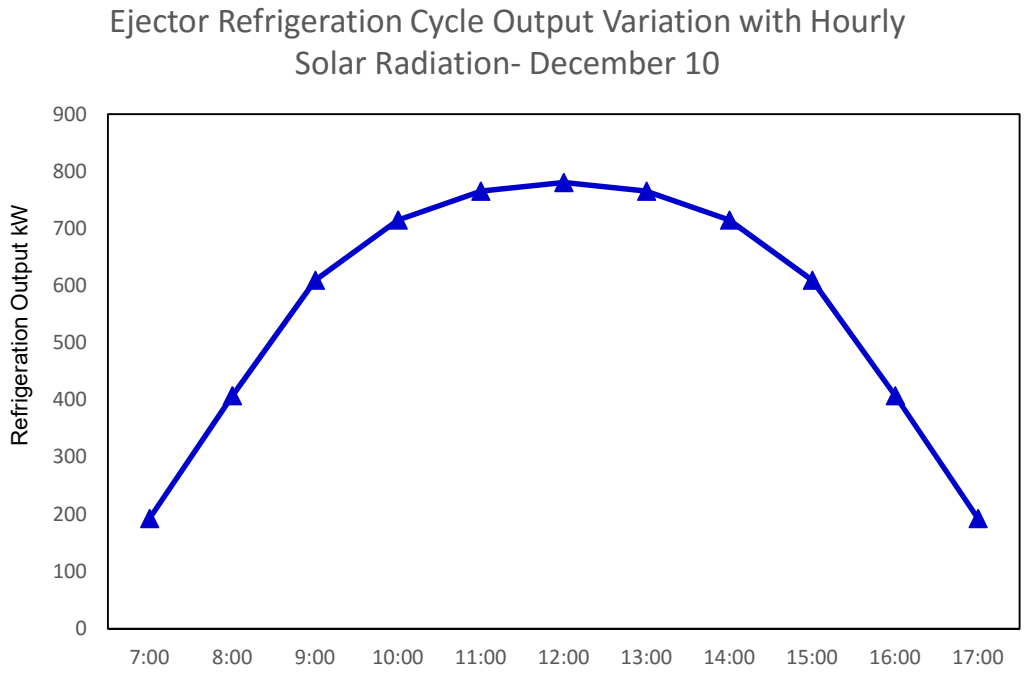

Figure 6.48 Ejector refrigeration cycle output variation with average hourly solar radiation-December 10

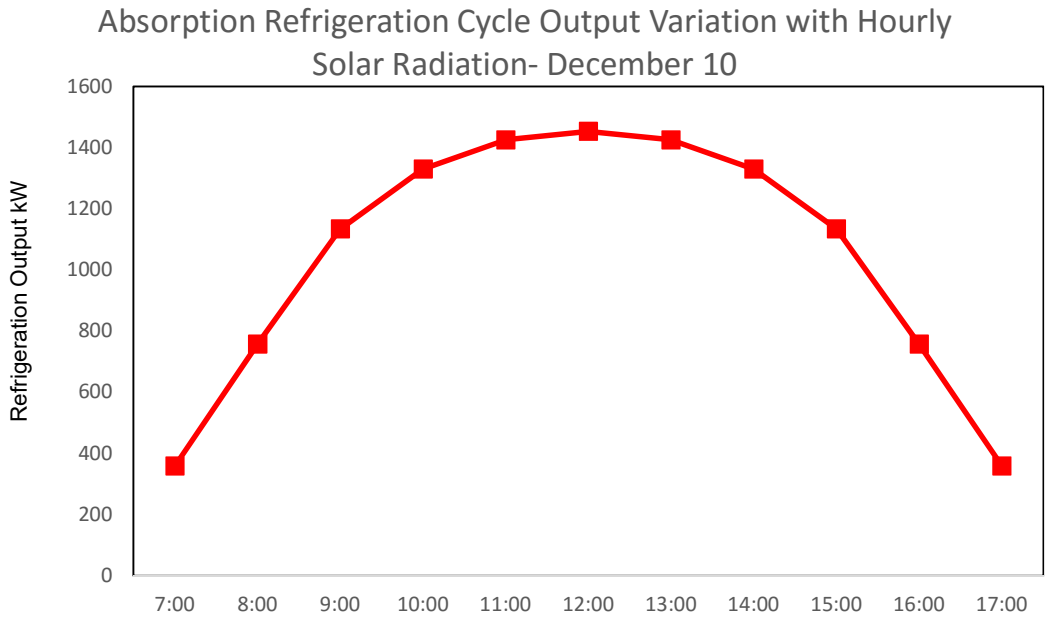

Figure 6.49 Absorption refrigeration cycle output variation with average hourly solar radiation-December 10

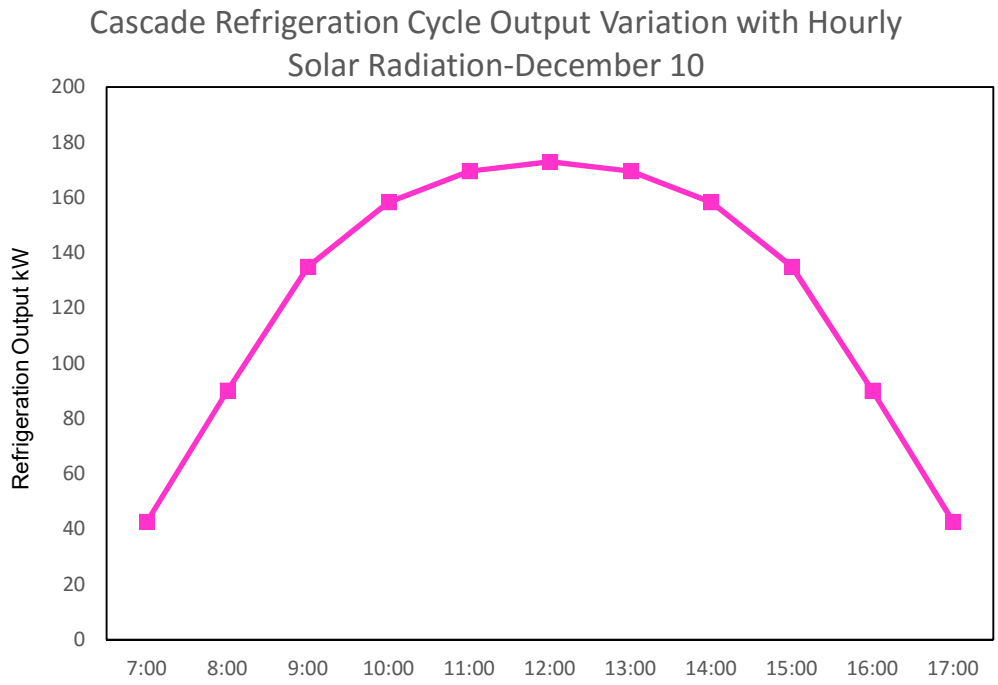

Figure 6.50 Cascade refrigeration cycle output variation with average hourly solar radiation-December 10

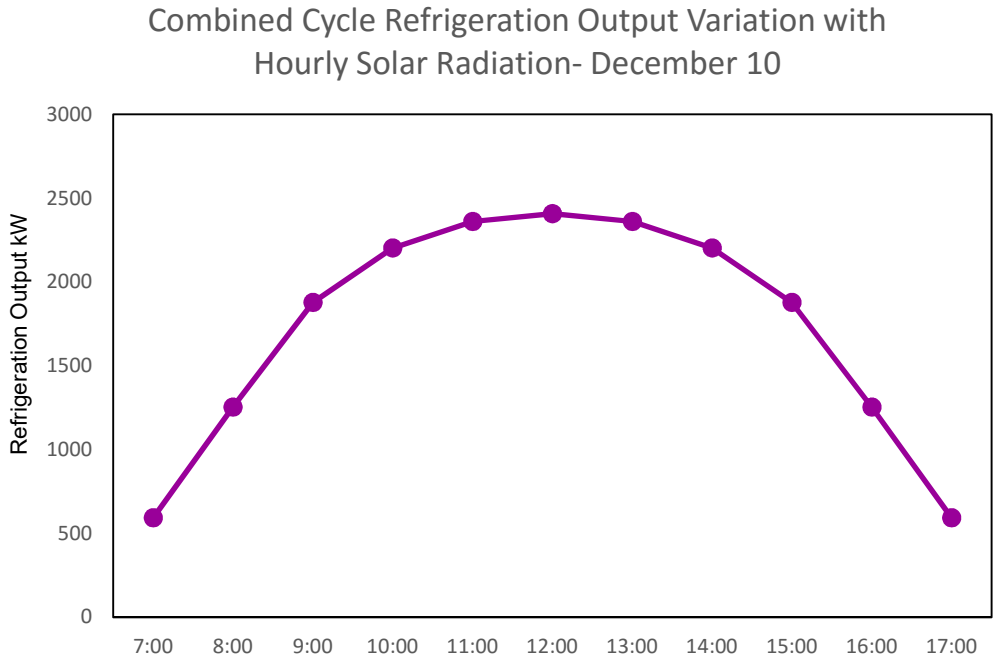

Figure 6.51 Combined refrigeration cycle output variation with average hourly solar radiation-December 10

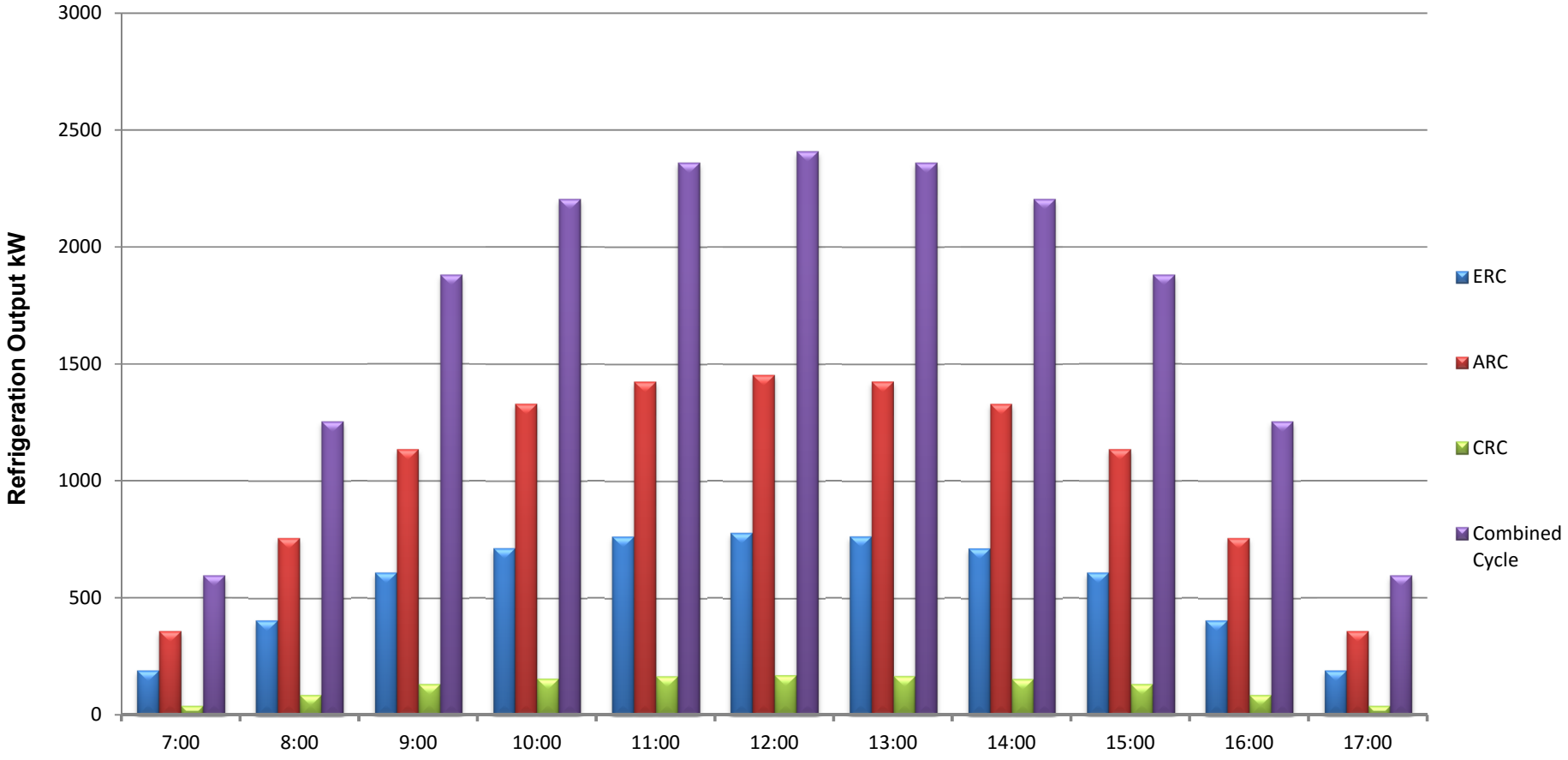

Figure 6.52 Refrigeration output of ERC, ARC, CRC and combined cycle with variation of average hourly solar radiation- December 10.

CHAPTER 7
CONCULUSION AND RECOMMENDATION

7.1 Conclusion:

Many solar energy technologies used to achieve refrigeration effect are investigated in this research. This study provides the useful indicators of these technologies performance.

A new solar driven triple-effect refrigeration cycle is proposed for the production of cooling at different temperature ranges. The main conclusion from this study can be summarized as follows:

- The largest contribution to cycle irreversibility comes from the CR and heliostat field of 52.5 and 25%, respectively. The irreversibility of the order of 2–7% is observed in the HRVG, ejector, and generator of refrigeration cycle and this could be minimized by better design consideration.
- Around 4.7% is available as useful exergy output where as 47.7% is available as useful energy output. Exergy output was low because of low temperature refrigerating effect of CRC.
- Both thermal and exergy efficiency are increased by increasing any one of the following parameters i.e. turbine back pressure, turbine inlet pressure, ejector evaporator temperature and cascade evaporator temperature, whereas both thermal and exergy efficiencies decreases with increase compressor discharge pressure, hot molten salt outlet temperature. The optimization of above parameters could be considered to improve the performance of the cycle.

- The parametric study shows that hot molten salt outlet temperature, turbine back pressure, turbine inlet pressure, and ejector evaporator temperature and compressor delivery pressure have significant effects on refrigeration outputs.
- The exergy destruction, which is happened in the generator and absorber increases with the generator temperature as the concentration difference between weak and strong solution increases.
- The condenser and evaporator exergy losses are much less than generator and absorber losses. The losses (within the condenser and evaporator) are mainly due to heat of mixing in the solution which is not present in pure fluid such as single refrigerant in vapor compression cycle. The effects of exergy losses in the solution, refrigerant pump and expansion valves on the total exergy losses are small and considered negligible.
- The performance of the absorption refrigeration cycle is strongly influenced by the operating temperatures. These results are very important in the improvement of the absorption cycle performance.

The research presented the merits and demerits of the solar cooling technologies, a number of observations can be made as follow:

- All sorption cycles including chemical sorption are in the beginning process with research laboratory to the market, but much more work is needed on cost minimization, design and packaging.
- Small-scale absorption cycles driven by solar thermal energy have been recently launched in the market by several companies.
- Adsorption and chemical adsorption cycles appear to function well in small scale applications such as small refrigerators; however, these

cycles need to solve refrigerant/ adsorbent problems due to corrosion and crystallization.

- An interesting option for the future is to integrate the desiccant cooling cycles into the ventilation system and rendering the system to become more popular.
- The combined Rankine cycle is suitable for high cooling capacities where a large number of moving parts in the cycle, and the implied regular maintenance can be accepted.
- The ejector refrigeration cycle has the benefit of being simple, reliable and feasible to operate with a low grade energy source. The cycle COP is low, but only slightly lower than other heat operated cycles.
- The Multi effect refrigeration cycles are the best way to provide cooling at different magnitude and temperature ranges using renewable energy like solar energy that could produce required refrigeration effect.
- Many researchers are working now to develop Peltier cooler with low cost and high efficiency.

It is obvious that each refrigeration cycle described has its own niche in application, advantages and disadvantages therefore a proper decision of system selection must be taken according to aforementioned solar cooling system merit and demerit.

Results obtained in the present study may be utilized by the engineers and scientists for a suitable thermodynamic design of solar-assisted triple-effect refrigeration system.

Based on the results obtained, it can be stated that the proposed cycle is a promising triple effect refrigeration cycle for the production of wide range of cooling simultaneously from thermodynamically and technical point of view.

7.2 Recommendation and Future Work:

This research presents the true fundamental life cycle solar energy and exergy analysis for triple effect refrigeration cycle, and applies exergy/ exergy analyses. The research contributions point to future research directions:

- A phase change storage device will be integrated with the current solar tower heating system for continuous operation over the year.
- In this new cycle, high temperature energy solar source like the solar tower is utilized to produce power using the high temperature availability while supplying the required thermal energy to applications that require low or medium temperature source like absorption and adsorption cycle.
- The thermal energy storage is introduced. Therefore, no auxiliary energy source is needed.
- The system includes thermal energy storage and quadruple effect refrigeration cycle which would provide cooling effect continuously when the solar radiation is not available.
- The thermal storage system of molten salt consists of hot and cold molten salt storage tank (direct type).
- An extra option of integrating waste energy heat source can be provided with a minor modification in order to achieve continuous operation in case of long periods of low solar radiation during cloudy winter days.
- An extra option can be provided to integrate the Steam Rankine cycle to an electric generator. This electric generator is to be connected to the utility grid to export electric energy to the grid in cases when, the very low temperature cooling provided by the Cascade cycle is not need or the power generated by the turbine is more than the load required by the Cascade cycle.

- An extra option can be provided to integrate the compressors of the Cascade cycle to electric motors that runs the compressors at nights and this case the sizes thermal storage tanks would be reduced.
- An extra option can be introduced via providing a control panel making proper control for the cycle exchange electric energy with the utility grade. The cycle would supply electricity to the grid when there is high solar radiation and there is a surplus in the power generated by the steam turbine compared to the required work by the compressors. And vice versa when there is low or no solar radiation and the size of the storage tanks were minimized.
- An extra option can be introduced via providing control valve at HRVG with bypass line (control valve is needed at bypass line) connected with absorption cycle generator. This is to modulate the flow of molten salt depending on the cooling demand at absorption and adsorption cycle compared to the cooling demand at the ejector and cascade refrigeration cycle. Thus, when the cooling demand is low at ejector and cascade cycle, then part of molten salt can be bypassed directly to absorption-adsorption cycle to increase the output cooling effect otherwise the control valve will be closed, and normal operation takes place.
- Improve efficiency to lower the Entropy generation

  The work gives researchers and engineers a thorough understanding of all the losses within the system. This serves as the first step for the improvement of the energy efficiency. The components with the highest exergy destruction should be focused upon first, and the Lowering entropy generation techniques should be applied to reduce the entropy generation in those components.

  That techniques includes reducing temperature difference for a heat exchanger , and reducing the pressure drop and friction in pipes, this is based on Bejan's work (1995).

- Thermoeconomic optimization for the overall system.
- Change the type of molten salt in order to improve the cycle efficiency.
- Change the type of refrigerant in cascade refrigeration cycle in order to replace it with safe refrigerant.
- Improve the performance of absorption cycle and considering triple effect refrigeration cycle.
- Study the performance of other mixture can be used in solar absorption cooling system and this mixture should be high performance, safe, non-toxic, environmentally friendly, non-corrosive, non-explosive, cheap and available in the market.

References

1. M.M.EL-WAKIL., Power Plant Technology, McGraw-Hill.
2. Zekai Sen., 2002, Solar energy in progress and future research trends, Istanbul, Turkey.
3. http://aloisiuskolleg.www.de/schule/fachbereiche/comenius/charles/solar.html
4. http://www.tpub.com/utilities/index.html
5. E.A. Demeo and J.F. Galdo. Renewable energy technology characterization. Technical report , electrical power research institute (EPRI) and US dept of energy, 1997.
6. H. Price, E.Lupfert, and D.Kearney . Advances in parabolic trough solar power technology. Journal of solar energy engineering-Transaction of the ASMe,124(2):109-125, 2002.
7. U.S. Department of Energy.http://www1.eere.energy.gov/solar.
8. F.Cavallaro. Multi-criteria descision aid to assess concentrated solar thermal technologies. Renewable energy, 34(7):1678-1685, 2009.
9. J. Birnbaum, M. Eck, M. Fichtner, T. Hirsch, D.Lehmann, and G. Zimmermann. A direct steam generation solar power plant with integrated storage. Journal of solar energy engineering-Transaction of the ASME, 132(3):310-314, 2010.
10. D.Mills. Advances in solar thermal electricity technology. Solar energy 76(1-3:19-31, 2004.
11. E. Zarza, M.E. Rojas, L. Gonzalez, J. Caballero , and F.Rueda. INDITEP: The first pre- commercial DSG solar power plant. Solar energy, 80 (10):1270-1276, 2006.
12. M. J. Hale. Survey of thermal storage for parabolic trough power plants. Technical report, NREL, 2000.
13. H. Herrmaan and D.W.Kearney. Survey of thermal storage for parabolic trough power plants. Technical report, NREL, 2000. Journal of solar engineering – transaction of the ASME,124 (2):145-152, 2002.

14. J.E. Pacheco, S. K. Showalter, and W. J. Kolb. Development of molten salt thermocline thermal storage system for parabolic trough plants. Journal of solar energy engineering transaction of the ASME, 124(2)153-159, 2002.
15. D. Laing, W.D. Steinmann, M. Fib, R. Tamme, T. Brand, and C. Bahl, Solid Media thermal storage development and analysis of a modular storage operation concept for parabolic trough power plant. Journal of solar energy engineering transaction of the ASME, 130(1):011005-1-011005-5, 2008.
16. V.Mirisson, M.rady, E.Palomo, and E.Arquis. Thermal energy storage system for electricity production using solar energy direct steam generation technology. Chemical engineering and processing: Process intensification 47(3):499-507, 2008.
17. http://www.photofileit.com/Collection.htm
18. D.R. Mils and G.L. Morrison. Compact Linear Fresnel reflector Solar thermal power plants. Solar energy, 68(3):263-283, 2000.
19. A. Lewandowski and D.Simms. An assessment of linear Fresnel lens concentrator for thermal application. Energy, 12(3-4):333-338, 1987.
20. Novatec solars Fresnel collector generates superheated steam above 500c. http://www.novatecsolar.com/86-1-novatec-solar-fresnel-collector-generates-superheated-steam-above-500C.html
21. http://usmanali-views.blogspot.com
22. H. E. Reilly and G.J. Kolb. An evaluation of molten-salt power towers including results of the solar two project. Technical report, sandia National Labs, 2001.
23. http://www.energy.siemens.com/co/en/fossil-power-generation/power-plants/csp-power-block/
24. R. Buck, M. Abele, J. Kunberger, T.Denk, P.Heller, and E.Lupfert. Receiver for solar-hybrid gas turbine and combined cycle system. Journal de physique,9(3):537-544,1999.
25. R.Buk,T.Brauning, T.Denk,M.Pfander, P.Schwarzbozl, and F.Telles. Solar Hybrid gas turbine based power systems (REFOS). Journal of solar energy engineering transaction of the ASME,124(1):2-9, 2002.

26. M.Horn, H.Fuhring, and J. Rheinlander. Economic analysis of integrated solar combined cycle power plants: A sample case: the economic feasibility of an ICCS power plant in Egypt. Energy,29(5-6):935-945, 2004.
27. M. Romero, R. Buck, and J.Pacheco. an update on solar central receiver systems, projects, and technologies. Journal of solar energy engineering – Transaction of the ASME,124(2):98-108, 2002.
28. A. Chobeity, C.J. Noone, C.N. Papanicolas, and A. Mitsos. Optimal time invariant operation of a power and water cogeneration solar thermal plant. Solar energy,85(9):2295-2320,June 20, 2011.
29. C.J. Noone, A.Ghobeity, A.H. Slocum, G.Tzarntzis and A.Mitsos. Site Selection for hillside central receiver solar thermal plant. Solar energy, 85(5):839-848, 2011.
30. A. H. Slocum, J. Buongiorno, C. W. Forsberg, D. S. Codd, and A. T. Paxson. Concentrated solar power system. PCT patent Application PCT/US10/49474, 2009.
31. A. H. Slocum, D. S. Codd, J. Buongiorno, C. Forsberg, T. Mckrell, J. C. Nave, C. N. Papanicolas, A.Ghobeity, C.J. Noone, S. Passerini, F. Rojas, and A.Mitsos. Concentrated solar power on demand. Solar, 85(7):1519-1529, 2011.
32. http://www.boem.gov/Renewable-Energy-Program/Renewable-Energy-Guide/Offshore-Solar-Energy.aspx .
33. http://www.geocities.com/dieret/re/Solar/solar.html
34. Nicole T. Carter, Richard J. Campbell, 2009. Water Issues of Concentrating Solar Power (CSP) Electricity in the U.S. Southwest, Congressional Research Service 7-5700 www.crs.gov R40631.
35. Solar Engineering of Thermal Processes, 4th Edition John A. Duffie, William A. Beckman.
36. J.Dersch, M.geyer, U.Herrmann, S.Jones, B.Kelly, R.Kistner, W.ortmannas,R. Pitz-Paal, and H.Price. Through integration into power plants – A study on the performance and economy of in integrated solar combined cycle system. Energy, 29(5-6):947-959, 2004.

37. S. A. Kalogirou. Solar energy engineering: Process and Systems. Elsevier, 2009.
38. Alazazmeh AJ, Mokheimer EM (2015) Review of Solar Cooling Technologies. J Appl Mech Eng 4: 180. doi:10.4172/2168-9873.1000180
39. Wu, X., 2004. High-efficiency polycrystalline CdTe thin-film solar cells. Solar energy 77(6):803-14.
40. Riffat, S. and Xiaoli, M., 2003. Thermoelectrics: a review of present and potential applications. Applied Thermal Engineering 23 913–935.
41. Zemansky, M. and Dittman, R., Heat and Thermodynamic, Sixth ed., McGraw-Hill Book Company, 1981, pp.431-442.
42. Riffat, S. and Xiaoli, M., 2004. Comparative investigation of thermoelectric air-conditioners versus vapor compression and absorption air-conditioners. Applied Thermal Engineering 24 1979–1993.
43. Klein, S. and Reindl, D., 2005 Solar refrigeration. ASHRAE Journal 47(9):S26-S30.
44. Lundqvist, P., (1993). Stirling Cycle Heat Pumps and Refrigerators. Applied Thermodynamics and Refrigeration. Stockholm, Royal Institute of Technology: 284.
45. Ewert, M., Agrella, M., DeMonbrun, D., Frahm, J., Bergeron, D., and Berchowitz, D., 1998. Experimental evaluation of a solar PV refrigerator with thermoelectric, Stirling, and vapour compression heat pumps. In: Proceedings of ASES Solar 98 Conference, Albuquerque, USA.
46. Berchovitz, D., McEntee, J. and Welty, S., 1999. Design and testing of a 40W free-piston Stirling cycle cooling unit. In: Proceedings of 20th International Congress of Refrigeration, Sydney, Australia.
47. Haywood, D., Raine, J. and Gschwendtner, M. Stirling-Cycle Heat-Pumps and Refrigerators – a Realistic Alternative, Stirling Cycle Research Group, Department of Mechanical Engineering, University of Canterbury, New Zealand. http://www.mech.canterbury.ac.nz/research/stirling/stirling.htm
48. Kribus, A., 2002. Thermal integral micro-cogeneration systems for solar and conventional use. Journal of Solar Energy Engineering 124, 189–197.

49. Ameel, T., Gee, K., and Wood, B., 1995. Performance predication of alternative, low cost absorbents for open-cycle absorption solar cooling. Solar engineering (2):65-73.
50. Gommed, K. and Grossman, G. 2007. Experimental investigation of a liquid desiccant system for solar cooling and dehumidification solar energy 81(1) 131-38.
51. Davies, P., 2005. A solar cooling system for greenhouse food production in hot climate. Solar energy 79 (6):661-68.
52. Henning, H., T.Erpenbeck, C. Hindenburg and I.S.Santamaria. 2001. The potential of solar energy use in desiccant cooling cycles. International journal of refrigeration. 24 (3)220-29.
53. Henning, H., 2004. Solar-assisted Air-conditioning Handbook in Buildings: A Handbook for Planners. Springer-Verlag, Wien, ISBN 3-211-00647-8.
54. Herold, K. and Radermacher, L. Absorption heat pump, Mech. Eng., Aug, 1989;68–73.
55. Gosney, W., Principle of refrigeration. Cambridge Uni. Press, 1982.
56. Srikhirin,P. and Aphornratana,S., Chungpaibulpatana,S., 2001. A review of absorption refrigeration Technologies, Renewable and Sustainable Energy Review 343–372.
57. Murphy, K. and Phillips, B. Development of residential gas absorption heat pump. Int J Refrig 1984;7(1):56–8.
58. Choudhury, S., Hisajima, D., Ohuchi, T., Nishiguchi, A., Fukushima, T. and Sakaguchi, S., Absorption of vapors into liquid films flowing over cooled horizontal tubes. ASHRAE Trans 1993; 99:81–9.
59. Matsuda, A., Choi, K., Hada, K. and Kawamura, T., Effect of pressure and concentration on performance of a vertical falling-film type of absorber and generator using lithium bromide aqueous solutions. Int J Refrig 1994; 17(8):538–42.
60. Cosenza, F. and Vliet, G., Absorption in falling water/LiBr films on horizontal tubes. ASHRAE Trans 1990; 96:693–701.

61. Morioka, I. and Kiyota, M., Absorption of water vapor into a wavy film of an aqueous solution of LiBr. JSME Int J, Series II 1991;34(2):183–8.
62. Kim, K., Berman, N., Chau, D. and Wood, B. Absorption of water vapour into falling films of aqueous lithium bromide. Int J Refrig 1995; 18(7):486–94.
63. Benzeguir, B., Setterwall, F. and Uddholm, H., Use of wave model to evaluate falling film absorber efficiency. Int J Refrig 1991;14:292–6.
64. Fujita, T., Falling liquid films in absorber machines. Int J Refrig 1993;16(4):282–94.
65. Andberg, J.and Vliet, G., A simplified model for absorption of vapors into liquid films flowing over cooled horizontal tubes. ASHRAE Trans 1987;93:2454–66.
66. Grossman, G., Absorption heat transformer for process heat generation from solar ponds. ASHRAE Trans 1991;97:420–7.
67. Ikeuchi, M., Yumikura, T., Ozaki, E. and Yamanaka, G., Design and performance of a high-temperature boost absorption heat pump. ASHRAE Trans 1985;90:2081–94.
68. Nakanishi, T., Furukawa, T. and Sato, N., Industrial high-temperature heat pump. Hitachi zosen Tech Rev 1981;42(1):7–12.
69. Siddig, M., Performance studies on a reversed absorption heat pump. PhD thesis, University of Salford, UK, 1982.
70. George, J. and Murthy, S., Influence of heat exchanger effectiveness on performance of vapour absorption heat transformers. Int J Energy Res 1989; 13:455–7.
71. George, J. and Murthy, S., Influence of absorber effectiveness on performance of vapour absorption heat transformers. Int J Energy Res 1989; 13:629–38.
72. Perez-Blanco, H. Absorption heat pump performance for different types of solution. Int J Ref 1984; 7(2):115–22.
73. Marcriss, R., Gutraj, J. and Zawacki, T. Absorption fluid data survey: final report on worldwide data, ORLN/sub/8447989/3, Inst. Gas Tech., 1988.
74. Park, Y. and Sonntag, R. Thermodynamic properties of ammonia-water mixtures: a generalized equation-of-state approach. ASHRAE Trans 1990; 96:150–9.

75. El-Sayed, Y. and Tribus, M. Thermodynamic properties of water-ammonia mixtures: theoretical implementation for use in power cycle analysis. ASME Pub AES 1985; 1:89–95.
76. Ziegler, B. and Trepp, C., Equation of state for ammonia-water mixtures. Int J Refrig 1984; 7(2):101–6.
77. Herold, K., Han, K. and Moran, M., a computer program for calculating the thermodynamic properties of ammonia and water mixtures using a Gibbs free energy formulation. ASME Pub AES 1988; 4:65–75.
78. Patek, J. and Klomfae, J., Simple function for fast calculations of selected thermodynamic properties of ammonia-water system. Int J Refrig 1995; 18(4):228–34.
79. McNeely, L., Thermodynamic properties of aqueous solutions of lithium bromide. ASHRAE Trans 1979; 85(2):413–34.
80. Patterson, M. and Perez-Blanco, H., Numerical fits of properties of lithium-bromide water solutions. ASHRAE Trans 1988; 94(2):2059–77.
81. Lee, R., DiGuilio, R., Jeteter, S. and Teja, A., Properties of lithium bromide-water solutions at high temperatures and concentrations-part II: density and viscosity. ASHRAE Trans 1990; 96:709–14.
82. Jeter, S., Moran, J. and Teja, A., Properties of lithium bromide-water solutions at high temperatures and concentrations-part III: specific heat. ASHRAE Trans 1992; 98:137–49.
83. Lenard, J., Jeter, S. and Teja, A. Properties of lithium bromide-water solutions at high temperatures and concentrations-part IV: vapor pressure. ASHRAE Trans 1992; 98:167–72.
84. Modahl, R. and Lynch, P., Arsenic trioxide corrosion inhibitor for absorption refrigeration system, US Patent No. 3609086, 1971.
85. Iyoki, S. and Uemura, T., Studies on corrosion inhibitor in water-lithium bromide absorption refrigerating machine. Reito 1978; 53(614):1101–5.
86. Wen, T., Lin, S., Corrosion inhibitors the absorption system. J Chin Inst Chem Eng 1992; 22:311–6.

87. Verma, S., Mekhjian, M., Sandor, G., Nakada, N., Corrosion inhibitor in lithium bromide absorption fluid for advanced and current absorption cycle machines. ASHRAE Trans 1999; 105(1):813–5.
88. Albertson, C. and Krueger R., Heat transfer additives for absorbent solution, US Patent No.3580759, 1971.
89. Chang, W., Marcriss, R. and Rush, W., Secondary alcohol additives for lithium bromide-water absorption refrigeration system, US Patent No. 3609087, 1971.
90. Elkassabgi, Y., Perez-Blanco, H., Experimental study of the effects of alcohol additives in lithium bromide/water pool absorber. ASHRAE Trans 1991; 97:403–5.
91. Daiguji, H., Hihara, E. and Saito, T., Mechanism of absorption enhancement by surfactant. Int J Heat and Mass transfer 1997;40(8):1743–52.
92. Hihara, E. and Saito, T., Effect of surfactant on falling film absorption. Int J Refrig 1993; 16(5):339–46.
93. Aphornratana, S., Research on absorption refrigerators and heat pumps. Reric Int Energy J 1995; 17(1):1–19.
94. Agarwal, R. and Bapat, S., Solubility characteristics of R22-DMF refrigerant-absorbent combination. Int J Refrig 1985; 8:70–4.
95. Ando, E. and Takeshita, I., Residential gas-fired absorption heat pump based on R22-DEGDME pair part I: thermodynamic properties of the R22-DEGDME pair. Int J Refrig 1984; 7:181–5.
96. Bhaduri, S., Verma, H., P-T-X behavior of R22 with five different absorbents. Int J Refrig 1986; 9:362–6.
97. Bhaduri, S., Verma, H., Heat of mixing of R22-absorbent mixture. Int J Refrig 1988; 11:92–5.
98. Fatouh, M., Murthy, S., Comparison of R22-absorbent pairs for vapour absorption heat transformers based on P-T-X-H data. Heat Recovery Systems and CHP 1993; 13(1):33–48.
99. Ghaddar, N., Shihab, M., Bdeir, F., Modeling and simulation of solar absorption system performance in Beirut. Renewable Energy 1997; 10(4):539–58.

100. Hammad, M., Zurigat, Y., Performance of a second generation solar cooling unit. Solar Energy 1998; 62(2):79–84.
101. Florides, G., Kalogirou, S., Tassou, S., Wrobel, L., Modeling and simulation of absorption solar cooling system for Cyprus. Solar Energy 2002; 72(1):43–51.
102. Hammad, M., and Audi, M., (1992) Performance of a solar LiBr–water absorption refrigeration system. Renew. Energy 2(3), 275–282.
103. Boehm, R., “The Development of a Model for a Solar-Fired, Single-Effect, Absorption Chiller”, (ES2008-54186), 2008, ASME.
104. Lemmini, F., Buret Bahraoui, J., Pons, M., Meunier, F., Simulation des performances d’un refrigerator solaire a adsorption: comparison des performances pour deux types de charbonactif. Rev Int Froid 1992; 15(3):159.
105. Pons, M., Guilleminot, J., 1986. Design of experimental solar powered, solid-adsorption ice maker. Journal of Solar Energy Engineering 108, 332–337.
106. Wang, R., Li, M., Xu, Y., Wu, J., 2000. An energy efficient hybrid system of solar powered water heater and adsorption ice maker. Solar Energy 68, 189–195.
107. Schweigler, C., Hiebler, S., Keil, C., kren, C., Kobel, H. and Mehling, H., 2007. Low temperature heat storage for solar heating and cooling application, ASHRAE Transaction 113 (1).
108. Chunnanond, K. and Aphornratana, S., "Ejectors: applications in refrigeration technology," Renewable and sustainable energy reviews, vol. 8, pp. 129-155, 2004.
109. Wang,J., Wu,J., Hu,S. and Huang,B. "Performance of ejector cooling system with thermal pumping effect using R141b and R365mfc," Applied Thermal Engineering, Vol. 29, No. 10, pp. 1904-1912, 2009.
110. Huang,B., Chang,J., Petrenko,V. and Zhuk, K. "A solar ejector cooling system using refrigerant R141b," Solar Energy, vol. 64, pp. 223-226, 1998.
111. Pollerberg, A., Ali,H. and Dotsch,C. "Solar driven steam jet ejector chiller," Applied Thermal Engineering, Vol. 29, No. 5-6, pp. 1245-1252, 2009.
112. George, J., Murthy, S., Influence of generator effectiveness on performance of vapour absorption heat transformers. Int J Energy Res 1989;13:687–99.

113. Eames, I., Aphornratana, S., and Haider,H., "A theoretical and experimental study of a small-scale steam jet refrigerator," International Journal of Refrigeration, vol. 18, pp. 378-386, 1995.
114. Sun, W. "Experimental investigation of the performance characteristics of a steam jet refrigeration system," Energy Sources, vol. 19, pp. 349-367, 1997.

115. Sankarlal, T. and Mani, A. "Experimental investigations on ejector refrigeration system with ammonia," Renewable Energy, vol. 32, pp. 1403-1413, 2007.
116. Ma, X. , Zhang,W., Omer, S. and Riffat,S. "Performance testing of a novel ejector refrigerator for various controlled conditions," International Journal of Energy Research, vol. 35, pp. 1229-1235, 2011.
117. Sankarlal, T. and Mani, A. "Experimental studies on an ammonia ejector refrigeration system," International communications in heat and mass transfer, vol. 33, pp. 224-230, 2006.
118. Sriveerakul,T., Aphornratana,S. and Chunnanond,K. "Performance prediction of steam ejector using computational fluid dynamics: Part 1. Validation of the CFD results," International Journal of Thermal Sciences, vol. 46, pp. 812-822, 2007.
119. Aphornratana, S., and Chunnanond, K. "Steam Ejector Refrigeration Cycle."
120. Aphornratana, S., and Chunnanond, K. and Srikhirin,P., "Experimental investigation of an ejector refrigerator: effect of mixing chamber geometry on system performance," International journal of energy research, vol. 25, pp. 397-411, 2001.
121. Aphornratana, S., and Chunnanond, K., "An experimental investigation of a steam ejector refrigerator: the analysis of the pressure profile along the ejector," Applied Thermal Engineering, vol. 24, pp. 311-322, 2004.
122. Ma,X., Zhang,W., Omer, S. and Riffat,S. "Experimental investigation of a novel steam ejector refrigerator suitable for solar energy applications," Applied Thermal Engineering, vol. 30, pp. 1320-1325, 2010.

123. Khattab, N., "Optimum design conditions of farm refrigerator driven by solar steam-jet system," International Journal of Sustainable Energy, vol. 24, pp. 1-17, 2005.

124. Levy,A. Jelinek, M. and Borde,I., "Numerical study on the design parameters of a jet ejector for absorption systems," Applied Energy, vol. 72, pp. 467-478, 2002.

125. Selvaraju,A. and Mani,A., "Analysis of a vapour ejector refrigeration system with environment friendly refrigerants," International Journal of Thermal Sciences, vol. 43, pp. 915-921, 2004.

126. Lu,S., and Goswami,D., 2003. Optimization of a novel combined power/refrigeration thermodynamic cycle, transaction of the ASME 125:212-17.

127. Wali, E. (1980). "Optimum Working Fluids for Solar Powered Rankine Cycle Cooling of Buildings." Solar Energy 25(3): 235-241.

128. Kane, M., Larrain, D., Favrat, D. and Allani, Y. (2003). "Small Hybrid Solar Power System." Energy 28(14): 1427-1443.

129. Agrawal, B., Karimi, M. .2012. Thermodynamic performance assessment of a novel waste heat based triple effect refrigeration cycle. International journal of refrigeration 35 1647-1656.

130. Fan, Y., Luo, L., and Souyri, B., 2007, “Review of Solar Sorption Refrigeration Technologies: Development and Applications,” Renewable Sustainable Energy Rev., 11, pp. 1758–1775.

131. Abdul Khaliq, A., Kumar,R., Dincer.I. and Khalid,F. 2014. Energy and Exergy Analyses of a New Triple-Staged Refrigeration Cycle Using Solar Heat Source. Journal of Solar Energy Engineering, Vol. 136 / 011004.

132. Agrawal, B., Kumar, R. and Abdul Khaliq, A., .2014. First and second law investigations of a new solar-assisted thermodynamic cycle for triple effect refrigeration, International Journal of energy research, 38:162–173.

133. Choudhury, B., Baran Saha, B., Chatterjee, P., and Prakas Sarkar, J. An overview of developments in adsorption refrigeration systems towards a sustainable way of cooling. Applied Energy 104(2013), 554-567. 11-19-2012.

134. Kalkan, N., Young, E., and Celiktas, A. Solar thermal air conditioning technology reducing the footprint of solar thermal air conditioning. Renewable & Sustainable Energy Reviews 16(2012), 6352-6383. 7-15-2012.

135. Anyanwu,E., Review of solid adsorption solar refrigerator II: an overview of the principles and theory Energy Conversion and Management, 45 (2004), pp. 1279–1295.

136. Critoph, R., Performance limitations of adsorption cycles for solar cooling.

137. Ayyash,S., Sartawi,M., Economic comparison of solar absorption and photovoltaic-assisted vapour compression cooling systems International Journal of Energy Research, 7 (1983), pp. 279–288.

138. Gordon, J.M., Ng, K.C., 2000. High-efficiency solar cooling. Solar Energy 68, 23–31.

139. Kim, D.S., Ferreira, C.A.I., 2008. Solar refrigeration options – a state-of the art review. International Journal of Refrigeration 31, 3–15.

140. Ton, D., Peek, G.H., Hanley, C., BOyes, J., 2008. Solar Energy Grid Integration Systems – Energy Storage (SEGIS–ES). Sandia National Laboratories.

141. Itron, 2007. CPUC Self-generation Incentive Program – Solar PV Costs and Incentive Factors.

142. Duffie, J.A., Beckman, W.A., 2006. Solar Engineering of Thermal Processes, third ed. Wiley.

143. Choudhury, B., Chatterjee, P.K., Sarkar, J.P., 2010. Review paper on solar-powered air-conditioning through adsorption route. Renewable and Sustainable Energy Reviews 14, 2189–2195.

144. EnergyStar, Savings Calculator, 2010. Energy Star. <http://www.energystar.gov/index.cfm?c=cac.pr_central_ac>.

145. Joshi, A.S., Dincer, I., Reddy, B.V., 2009. Performance analysis of photovoltaic systems: a review. Renewable and Sustainable Energy Reviews 13, 1884–1897.

146. AET, 2011. Flat Plate Solar Thermal Collector Technical Information. Alternative Energy Technology. http://www.aetsolar.com/ AEseries.html>.

147. Xu C, Wang Z, Li X, Sun F. Energy and exergy analysis of solar power tower plants. Applied Thermal Engineering 2011; 31:3904–3913.

148. E.E. Ludwig, Applied Process Design for Chemical and Petrochemical Plants, vol. 1, second ed, Gulf, Houston, TX, 1977.
149. R.B. Power, Hydrocarb. Proc. 43 (1964) 138.
150. H.T. El-Dessouky, H.M. Ettouney, Single effect thermal vapor compression desalination process: thermal analysis, Heat Trans. Eng. 20 (1999) 52–68.
151. J.T. Munday, D.F. Bagster, A new ejector theory to steam jet refrigeration, IEC 16 (1977) 442–449.
152. D.W. Sun, I.W. Eames, Recent developments in the design theories and applications of ejectors—a review, J. Inst. Energy 68 (1995) 65–79.
153. I.W. Eames, S. Aphornaratana, H. Haider, A theoretical and experimental study of a small-scale steam jet refrigerator, Int. J.Refrig. 18 (1995) 378–385.
154. S. Aphornratana, I.W. Eames, A small capacity steam-ejector refrigerator: experimental investigation of a system using ejector with moveable primary nozzle, Int. J. Refrig. 20 (1997) 352–358.
155. X. Li, W.Q. Kong, Z.F. Wang, C. Chang, F.W. Bai, Thermal model and thermodynamic performance of molten salt cavity receiver, Renewable Energy 35 (2010) 981e988.
156. R. Tozer, A.Syed, G. Maidment, Extended temperature–entropy (T–S) diagrams for aqueous lithium bromide absorption refrigeration cycles, International Journal of Refrigeration 28 (2005) 689–697.
157. N.E. Bergan, An external molten salt solar central receiver test, Solar Engineering (1987).
158. M.S Jamel, Performance evaluation of molten salt cavity tubular solar central receiver for future integration with existing power plants in Iraq, Australian Journal of basic and applied sciences , 7(8):399-410, 2013.
159. B. J. Huang, J. M. Chang, C. P. Wang, and V. A. Petrenko, "A 1-D analysis of ejector performance," International Journal of Refrigeration, Vol. 22, No. 5, pp. 354-364, 1999.
160. Development and Assessment of Solar-Assisted Gas Turbine Cogeneration Systems in Saudi Arabia, Yousef Naji, 2013.

161. Irreversibility and Gouy-Stodola Theorem - Kostic-www.kostic.niu.edu
162. Çengel, Y. A and A. J. Ghajar, Heat and Mass Transfer: Fundamentals and Applications, 4th edition, McGraw-Hill, 2011.
163. Adrian Bejan, Entropy Generation Minimization: The Method of Thermodynamic Optimization of Finite-Size Systems and Finite-Time Processes.
164. https://www.ohio.edu/mechanical/thermo/Intro/Chapt.1_6/Chapter6a.html.
165. B.J. Huang, J.M. Chang, C.P. Wang, V.A. Petrenko, A 1-D analysis of ejector performance. International Journal of Refrigeration 22 (1999) 354–364.
166. A.S. Hanafi, G.M. Mostafa, A. Waheed , A. Fathy 1-D Mathematical Modeling and CFD Investigation on Supersonic Steam Ejector in MED-TVC. Energy Procedia Volume 75, August 2015, Pages 3239-3252 Clean, Efficient and Affordable Energy for a Sustainable Future: The 7th International Conference on Applied Energy (ICAE2015).
167. W. Chen, C. Shi, S. Zhang, H. Chen, D. Chong, J. Yan. Theoretical analysis of ejector refrigeration system performance under overall modes. Applied Energy (2015)

Appendix A

CLIMATE DATA FOR DHAHRAN CITY

These measurement provided from Research institute of KFUPM – Dhahran - Saudi Arabia

	January				Feb.		
Hr	Ambient Temp. Deg C.	Wind Speed Deg. C	Solar Irradiance-I_T (W/m^2)	Hr	Ambient Temp. Deg C.	Wind Speed Deg. C	Solar Irradiance-I_T (W/m^2)
12:00 AM	11.3	7.5	0	12:00 AM	12.8	2.1	0
1:00 AM	11	6.7	0	1:00 AM	12.6	2.3	0
2:00 AM	10.6	6.3	0	2:00 AM	12.3	2.8	0
3:00 AM	10.3	3.9	0	3:00 AM	12.2	2.7	0
4:00 AM	10.4	3.6	13.1	4:00 AM	12.3	3	13.1
5:00 AM	10.4	4	13.1	5:00 AM	12.2	2.1	13.1
6:00 AM	10.1	3.3	14	6:00 AM	12	1.4	29.6
7:00 AM	10.7	4	21.3	7:00 AM	12.7	1.3	148.7
8:00 AM	11.9	4.6	54.3	8:00 AM	15.9	0.4	507.9
9:00 AM	12.8	4.3	69	9:00 AM	17.5	1	610.5
10:00 AM	13.8	4.8	176.2	10:00 AM	18.4	1.5	660
11:00 AM	14.7	5	124	11:00 AM	18.9	2.2	656.4
12:00 PM	16.6	6.1	91.9	12:00 PM	20.3	1.5	586.7
1:00 PM	16.3	5.7	106.6	1:00 PM	20.5	2	472.2
2:00 PM	15.8	5.8	148.7	2:00 PM	19.3	3	299
3:00 PM	15.7	5.5	62.6	3:00 PM	17.8	2.6	122.1
4:00 PM	15.2	5.4	31.4	4:00 PM	16.4	2.6	23.2
5:00 PM	14.7	4.6	14	5:00 PM	15.3	2.7	13.1
6:00 PM	14.6	4.5	13.1	6:00 PM	15	3.1	0
7:00 PM	14	5.2	0	7:00 PM	14.9	3.3	0
8:00 PM	12.9	6	0	8:00 PM	15	3.8	0
9:00 PM	12.7	5.6	0	9:00 PM	15.1	4.4	0
10:00 PM	11.9	6	0	10:00 PM	14.8	4.7	0
11:00 PM	10.9	7	0	11:00 PM			

Appendix A

CLIMATE DATA FOR DHAHRAN CITY

These measurement provided from Research institute of KFUPM – Dhahran - Saudi Arabia

	Mar.				April		
Hr	Ambient Temp. Deg C.	Wind Speed Deg. C	Solar Irradiance-I_T (W/m^2)	Hr	Ambient Temp. Deg C.	Wind Speed Deg. C	Solar Irradiance-I_T (W/m^2)
12:00 AM	16	6.1	0	12:00 AM	22.9	2.9	0
1:00 AM	15.5	5.4	0	1:00 AM	23.5	3.7	0
2:00 AM	15.5	4.6	0	2:00 AM	23.2	4.5	0
3:00 AM	15.7	4.4	0	3:00 AM	23.3	4.9	0
4:00 AM	15.4	4.5	13.1	4:00 AM	23	5	13.1
5:00 AM	15	4.9	14.9	5:00 AM	24	5.2	31.4
6:00 AM	15.9	4.7	75.4	6:00 AM	25.5	3.8	174.4
7:00 AM	17.2	4.8	258.7	7:00 AM	29.5	0.5	387
8:00 AM	18.5	6.2	474	8:00 AM	31	1.2	602.3
9:00 AM	19.7	7.5	666.4	9:00 AM	34.3	0.1	774.6
10:00 AM	20.7	8.1	804.8	10:00 AM	34.9	1.5	883.6
11:00 AM	21.5	9.7	901.9	11:00 AM	33.1	2.8	935.8
12:00 PM	21.7	8.5	872.6	12:00 PM	31.8	5	938.8
1:00 PM	21.5	6.9	775.5	1:00 PM	31.8	4	845.1
2:00 PM	21.2	6.8	623.4	2:00 PM	31.8	3.3	690.3
3:00 PM	20.8	5.4	411.7	3:00 PM	30.5	3.7	480.4
4:00 PM	20	4.8	195.4	4:00 PM	29.5	3.3	250.4
5:00 PM	18.8	5.5	43.3	5:00 PM	27.5	3	58.9
6:00 PM	18.2	4.2	13.1	6:00 PM	25.2	2.8	13.1
7:00 PM	18	3.1	0	7:00 PM	26.2	3.2	0
8:00 PM	17.5	3.8	0	8:00 PM	25.6	3.5	0
9:00 PM	16.8	5	0	9:00 PM	24.4	3.1	0
10:00 PM	16.7	5.7	0	10:00 PM	24.8	3.8	0
11:00 PM	16.8	5.8	0	11:00 PM	24.1	3.8	0

Appendix A

CLIMATE DATA FOR DHAHRAN CITY

These measurement provided from Research institute of KFUPM – Dhahran - Saudi Arabia

	May				June		
Hr	Ambient Temp. Deg C.	Wind Speed Deg. C	Solar Irradiance-I_T (W/m^2)	Hr	Ambient Temp. Deg C.	Wind Speed Deg. C	Solar Irradiance-I_T (W/m^2)
12:00 AM	30.3	6	0	12:00 AM	31.5	5.4	0
1:00 AM	29.7	6.4	0	1:00 AM	31	5.3	0
2:00 AM	29.8	7	0	2:00 AM	31	5.7	0
3:00 AM	29	7.3	0	3:00 AM	31.1	6.4	0
4:00 AM	29.3	6.9	13.1	4:00 AM	31	6.2	14
5:00 AM	29.6	6.7	62.6	5:00 AM	30.7	7	65
6:00 AM	29.6	5.3	221.1	6:00 AM	31	5.7	209.2
7:00 AM	32.5	6.8	435.5	7:00 AM	32.8	4.4	394.3
8:00 AM	34	7	640.8	8:00 AM	34.5	1.1	584.9
9:00 AM	35.5	6.9	864.4	9:00 AM	35.7	2.5	725.1
10:00 AM	35.8	5	792.9	10:00 AM	36.5	2.8	814.9
11:00 AM	36.7	5.9	986.2	11:00 AM	37.4	2.2	853.4
12:00 PM	37.5	6.4	967	12:00 PM	37.7	5	882.7
1:00 PM	37.7	5.4	878.1	1:00 PM	37.6	6.3	784.6
2:00 PM	37.1	6.7	715	2:00 PM	37.1	8.3	649
3:00 PM	36.9	6.5	513.4	3:00 PM	35.7	7.5	451.1
4:00 PM	36	5.9	293.5	4:00 PM	34.6	6.3	257.8
5:00 PM	34.8	5.1	100.1	5:00 PM	33.5	5.7	101.1
6:00 PM	33.9	3.5	14.9	6:00 PM	32.9	4.2	19.5
7:00 PM	33.2	3	0	7:00 PM	32.2	3.2	0
8:00 PM	33.6	3.2	0	8:00 PM	31.7	1.9	0
9:00 PM	34.1	3.5	0	9:00 PM	31.8	1.4	0
10:00 PM	34.5	3.8	0	10:00 PM	31.1	2.3	0
11:00 PM	34.4	4.2	0	11:00 PM	29.1	3.1	0

Appendix A

CLIMATE DATA FOR DHAHRAN CITY

These measurement provided from Research institute of KFUPM – Dhahran - Saudi Arabia

	July				August		
Hr	Ambient Temp. Deg C.	Wind Speed Deg. C	Solar Irradiance-I_T (W/m^2)	Hr	Ambient Temp. Deg C.	Wind Speed Deg. C	Solar Irradiance-I_T (W/m^2)
12:00 AM	32.9	4	0	12:00 AM	32	3.9	0
1:00 AM	33.6	4.4	0	1:00 AM	31.2	3.9	0
2:00 AM	34.7	4.6	0	2:00 AM	30.6	4.2	0
3:00 AM	34.8	6.1	0	3:00 AM	31.7	5	0
4:00 AM	34.4	6.9	13.1	4:00 AM	32.3	5.4	13.1
5:00 AM	33.6	7	39.7	5:00 AM	32.1	5.3	36
6:00 AM	34.4	7.4	153.3	6:00 AM	33.5	5.7	173.5
7:00 AM	35.7	6.7	313.7	7:00 AM	35.8	3.6	380.5
8:00 AM	36.6	6.9	467.6	8:00 AM	38.6	3.9	595
9:00 AM	37.7	5.9	617.9	9:00 AM	39.8	5.6	775.5
10:00 AM	38.3	6.6	770	10:00 AM	41.3	3.4	892.8
11:00 AM	38.7	6.9	831.4	11:00 AM	41.7	2.8	943.2
12:00 PM	39.2	7.3	833.2	12:00 PM	41.4	4.2	906.5
1:00 PM	39.5	6.8	767.2	1:00 PM	39.8	3.7	805.7
2:00 PM	38.9	8.2	638.9	2:00 PM	39.1	3	648.1
3:00 PM	38.3	8	459.3	3:00 PM	38.7	3.5	446.5
4:00 PM	38.2	6.4	272.4	4:00 PM	37.4	3.1	236.7
5:00 PM	37.7	6.2	100.1	5:00 PM	35.8	3	68.1
6:00 PM	37.2	5.4	18.6	6:00 PM	34.4	2.9	13.1
7:00 PM	37.4	6	0	7:00 PM	34	2.4	0
8:00 PM	37.7	5.8	0	8:00 PM	33.8	3.3	0
9:00 PM	36.9	5.1	0	9:00 PM	33.2	2.3	0
10:00 PM	36.8	4.7	0	10:00 PM	33.1	3.2	0
11:00 PM	37.4	6.5	0	11:00 PM	32.3	2.4	0

Appendix A

CLIMATE DATA FOR DHAHRAN CITY

These measurement provided from Research institute of KFUPM – Dhahran - Saudi Arabia

	Sep.				October		
Hr	Ambient Temp. Deg C.	Wind Speed Deg. C	Solar Irradiance-I_T (W/m^2)	Hr	Ambient Temp. Deg C.	Wind Speed Deg. C	Solar Irradiance-I_T (W/m^2)
12:00 AM	26.2	2.8	0	12:00 AM	27.4	3.8	0
1:00 AM	25.4	3.3	0	1:00 AM	27.7	3.9	0
2:00 AM	25.2	3.5	0	2:00 AM	27.5	4	0
3:00 AM	24.8	3.8	0	3:00 AM	27.1	4.5	0
4:00 AM	25.9	3.8	13.1	4:00 AM	26.8	4.2	13.1
5:00 AM	27.4	2.9	25	5:00 AM	25.9	4.7	18.6
6:00 AM	29	1.1	149.6	6:00 AM	26	4.4	115.7
7:00 AM	32	0.9	364	7:00 AM	27.3	3.7	256.8
8:00 AM	34.5	2.2	568.4	8:00 AM	29.2	4.1	397
9:00 AM	32.5	5.8	748.9	9:00 AM	31.6	4.6	614.2
10:00 AM	35.2	4.8	869.9	10:00 AM	33.5	3.7	687.5
11:00 AM	36.7	5.1	900.1	11:00 AM	35	3.9	784.6
12:00 PM	38.1	4.1	860.7	12:00 PM	34.5	4.5	671
1:00 PM	38.7	3	759	1:00 PM	34.2	4.4	618.8
2:00 PM	37.6	5.3	593.1	2:00 PM	33.4	3.5	446.5
3:00 PM	36.7	6.5	390.6	3:00 PM	32.9	3.2	247.7
4:00 PM	35.6	6.2	170.7	4:00 PM	30.6	2.9	66.2
5:00 PM	33.4	5	26.8	5:00 PM	30	3.3	13.1
6:00 PM	32.6	4.7	13.1	6:00 PM	29.5	3.5	13.1
7:00 PM	31.6	3.8	0	7:00 PM	29.4	4.5	0
8:00 PM	30.6	2.9	0	8:00 PM	29.3	4.5	0
9:00 PM	30.7	2.3	0	9:00 PM	29.2	4.6	0
10:00 PM	31.7	3.3	0	10:00 PM	29	4.3	0
11:00 PM	31.7	3	0	11:00 PM	28.7	3.8	0

Appendix A

CLIMATE DATA FOR DHAHRAN CITY

These measurement provided from Research institute of KFUPM – Dhahran - Saudi Arabia

	Nov.				Dec.		
Hr	Ambient Temp. Deg C.	Wind Speed Deg. C	Solar Irradiance-I_T (W/m^2)	Hr	Ambient Temp. Deg C.	Wind Speed Deg. C	Solar Irradiance-I_T (W/m^2)
12:00 AM	20	3.2	0	12:00 AM	23	4.4	0
1:00 AM	20	2.9	0	1:00 AM	23	3.2	0
2:00 AM	18.7	2.4	0	2:00 AM	23	2.6	0
3:00 AM	18.5	2.3	0	3:00 AM	23.3	1.9	0
4:00 AM	18.5	3.2	13.1	4:00 AM	24.1	2.2	14
5:00 AM	18.8	2.8	14	5:00 AM	24.8	2.8	13.1
6:00 AM	19.7	2	62.6	6:00 AM	23.5	3.1	31.4
7:00 AM	20.4	2.1	227.5	7:00 AM	22.5	3.8	130.4
8:00 AM	21.8	1.6	398	8:00 AM	22.4	4.4	218.4
9:00 AM	25.4	1.1	540	9:00 AM	23.5	5.7	430.9
10:00 AM	26.4	1	584	10:00 AM	24.3	7.2	409.9
11:00 AM	25.6	1.9	633.4	11:00 AM	23.7	8.1	379.6
12:00 PM	25.8	2.3	591.3	12:00 PM	23.2	7.7	317.3
1:00 PM	26	2.3	474	1:00 PM	23.8	5.9	371.4
2:00 PM	26.1	2.2	381.5	2:00 PM	23.7	5.2	239.4
3:00 PM	25.3	2.7	155.1	3:00 PM	23.2	5	136.8
4:00 PM	23.6	1.8	25	4:00 PM	22.9	4.1	29.6
5:00 PM	22.5	0.5	13.1	5:00 PM	22.3	3.7	13.1
6:00 PM	21.4	0.5	13.1	6:00 PM	22.6	4.8	13.1
7:00 PM	20.2	0.2	0	7:00 PM	22.2	4.5	0
8:00 PM	20.5	0.9	0	8:00 PM	21.3	6.3	0
9:00 PM	21.1	2.4	0	9:00 PM	19.3	6.2	0
10:00 PM	21.7	1.8	0	10:00 PM	18.6	2.7	0
11:00 PM	21.6	1.5	0	11:00 PM	18.4	3.9	0

Vitae

Name : Ayman Jamal Abdel Majid Alazazmeh

Nationality : Jordanian.

Date of Birth : June 19, 1985.

Email : aiman_hu@yahoo.com

ajalazazmeh@zamilac.com

Address : Jordan - Amman

Academic Background : B.S (Mechanical Engineering)
August 2007
Hashemite University
Alzarqa, Jordan.

Journal publications:

Alazazmeh AJ, Mokheimer EM (2015) Review of Solar Cooling Technologies. J Appl Mech Eng .

Patent “Pat. Applied For":

EVAPORATIVE CONDENSER COOLING SYSTEM, Alazazmeh AJ, Mokheimer EM (2015).